Surface Ligand Controlled Photophysics and Photopatterning with InP/ZnS Quantum Dots

A Thesis

Submitted in Partial Fulfilment of the Requirements

for the Degree of

Doctor of Philosophy

By

Devatha Gayathri
(20153379)

IISER PUNE

Department of Chemistry,

Indian Institute of Science Education and Research (IISER),

Pune, India – 411008

November 2020

__Dedicated to__

Amma, Nanna and

My little Kannu

Certificate

This is to certify that this dissertation entitled "**Surface Ligand Controlled Photophysics and Photopatterning with InP/ZnS Quantum Dots**" submitted by Devatha Gayathri has been carried out by the candidate at the Indian Institute of Science Education and Research (IISER), Pune, under my supervision. The work presented here or any part of it has not been included in any other thesis submitted previously for the award of any degree or diploma from any other university or institution.
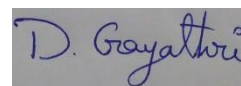
Date: 06/11/2020   **Dr. Pramod P. Pillai**

Place: Pune   **(Research Supervisor)**

Declaration

I, hereby declare that the thesis entitled "**Surface Ligand Controlled Photophysics and Photopatterning with InP/ZnS Quantum Dots**" submitted for the degree of Doctor of Philosophy in Chemistry at Indian Institute of Science Education and Research (IISER), Pune has not been submitted by me to any other University or Institution. This work was carried out at the Department of Chemistry, Indian Institute of Science Education and Research (IISER), Pune, India under the supervision of Dr. Pramod P. Pillai.

Date: 06/11/2020

Place: Pune

Ms. Devatha Gayathri

(Reg. No: 20153379)

Acknowledgements

Table of Contents

3. *FRET Assisted Multicolor Photopatterning from Single Quantum Dot Nanohybrid Films*

4. *Multicolor Luminescent Patterning via Photoregulation of Electron and Energy Transfer Processes in Quantum Dots*

Thesis Synopsis

Light-matter interaction is one of the most fascinating phenomena in nature, which has inspired researchers to accomplish significant breakthroughs in the past, as well as the present. For instance, a thorough understanding on the process of *photosynthesis* has led researchers to tackle the challenges of energy crisis. The progress made in the area of modern energy research is highly commendable, and solar harvesting has emerged as one of the most practical alternatives to meet our energy demands. A closer examination of the phenomenon of *photosynthesis* reveals the presence of two fundamental photophysical processes: light induced energy, and electron transfer. Mimicking the above mentioned light induced processes in artificial materials, in an efficient fashion, continues to be a subject of intense research. Among various classes of materials available, semiconductor nanoparticles or quantum dots (QDs) have achieved a special feat due to their unique size and shape-tunable optoelectronic properties. Additionally, QDs offer a unique opportunity, where the core can act as the primary light harvester, and the surface ligands can be engineered for controlling the various interparticle forces. Although the effects of QD core (like size, shape, composition etc.) have been well documented in literature, the role of surface ligands on various optoelectronic properties is still in its infancy. A proper and precise tuning of the surface chemistry of QDs has the potential to not only improve, but also impart newer properties to QD based nanohybrid systems. Thus, the present thesis is mainly focused on studying the effect of surface ligands on the optoelectronic and photophysical properties of QD based light harvesting systems. In this direction, **Chapter 1** gives a brief summary of how ligands on the surface of QDs can control the interactions in a donor-acceptor system and summarizes their impact on various photophysical processes.

In **Chapter 2,** we have developed a place exchange protocol to impart a permanent positive charge on the surface of eco-friendly and less toxic indium phosphide/zinc sulfide (InP/ZnS) cores/shell QDs. Our ability to craft permanent positive charges on the surface of InP/ZnS QDs represents a fundamental and practically important advance in the area of environmentally friendly QDs. Next, the two important properties of QDs, namely bioimaging and light induced resonance energy transfer, were successfully demonstrated with cationic InP/ZnS QD. The low cytotoxicity compared to traditional [+] CdSe QDs and stable photoluminescence of [+] InP/ZnS QDs inside the cells make them ideal candidates as optical probes for cellular imaging applications. Furthermore, an efficient Förster resonance energy

transfer (FRET) process was demonstrated with [+] InP/ZnS QDs as the donor and negatively charged merocyanine-540 dye (MC) as the acceptor, both in solution and solid states. A large bimolecular quenching constant along with a linear Stern-Volmer plot confirms the formation of a strong ground state complex between [+] InP/ZnS QD and [-] MC dye. The key point is the decisive role of electrostatics in controlling the light induced energy transfer, which can rightfully form the basis for future nanobio studies between [+] InP/ZnS QDs and negatively charged biomolecules.

In **Chapter 3,** the interaction driven FRET process with [+] InP/ZnS QDs was efficiently explored in the area of QD photopatterning. We have developed a robust technique for the creation of reusable multicolor luminescent photopatterns from a single QD-nanohybrid system, as opposed to the common practice of using different colored QDs. Our photopatterning approach relies on the photoregulation of FRET process in a InP/ZnS QD – MC dye agarose film. The superior photostability of the QDs over organic dyes was smartly used to form multicolor luminescent patterns in QD nanohybrid film. The photoirradiation causes the controlled degradation of organic dye molecules, and modulates the composition of donor-acceptor pair in the QD-dye agarose film. Consequently the efficiency of FRET in QD – dye agarose film was regulated between completely ON and OFF states, through a moderately efficient state. This led to the generation of high contrast reusable multicolor luminescent patterns comprising of at least three distinctly different colors: orange (corresponding to FRET ON state, E_{FRET} ~85 %), yellow (corresponding to moderately FRET ON state, E_{FRET} ~50 %) and green (corresponding to FRET OFF state, E_{FRET} = 0%). The creation of luminescent patterns by the photoregulation of FRET is conceptually unique, and cost effective for the manufacturing of luminescent nanocrystal based multicolor display devices.

In **Chapter 4,** we investigated the potency of [+] InP/ZnS QDs as a donor in the photoinduced electron transfer (PET) process with oppositely charged Indocyanine green (ICG). A strong electrostatic attraction resulted in a highly efficient electron transfer (~95 %) from [+] InP/ZnS QD to [-] ICG dye, leading to a completely non-fluorescent QD nanohybrid system. Furthermore, we could successfully couple and regulate light induced electron and energy transfer processes in a single QD nanohybrid film, which by itself is a significant advancement in the area of QD light harvesting. Additionally, the ability to generate non-emissive (due to efficient electron transfer) and luminescent states (due to energy transfer)

from a single QD – dye nanohybrid system was then used to create high contrast multicolor luminescent patterns. The dominance of electron transfer over the energy transfer process generates a non-luminescent QD nanohybrid film, which provides the black background for multicolor patterning. A selective photodegradation of the electron acceptor dye triggered the onset of energy transfer process, thereby imparting a luminescent color to the QD nanohybrid film. Finally, a controlled photoregulation of energy transfer process paved the way for multicolor luminescent patterning. Apart from enhancing the color contrast, our approach offers the option of creating luminescent images that have inherent black regions, at a multicolor level.

In summary, the present Thesis helped in introducing environmentally friendly InP/ZnS QDs to the family of cationic nanoparticles as a practical alternative to toxic metal ion based QDs, for future interaction driven light-harvesting and biological studies.

Cationic InP/ZnS QDs

FRET – Förster resonance energy transfer   PET– Photoinduced electron transfer

Electrostatically Driven Photophysics

Photoregulated High-Contrast Multicolor QD Patterning
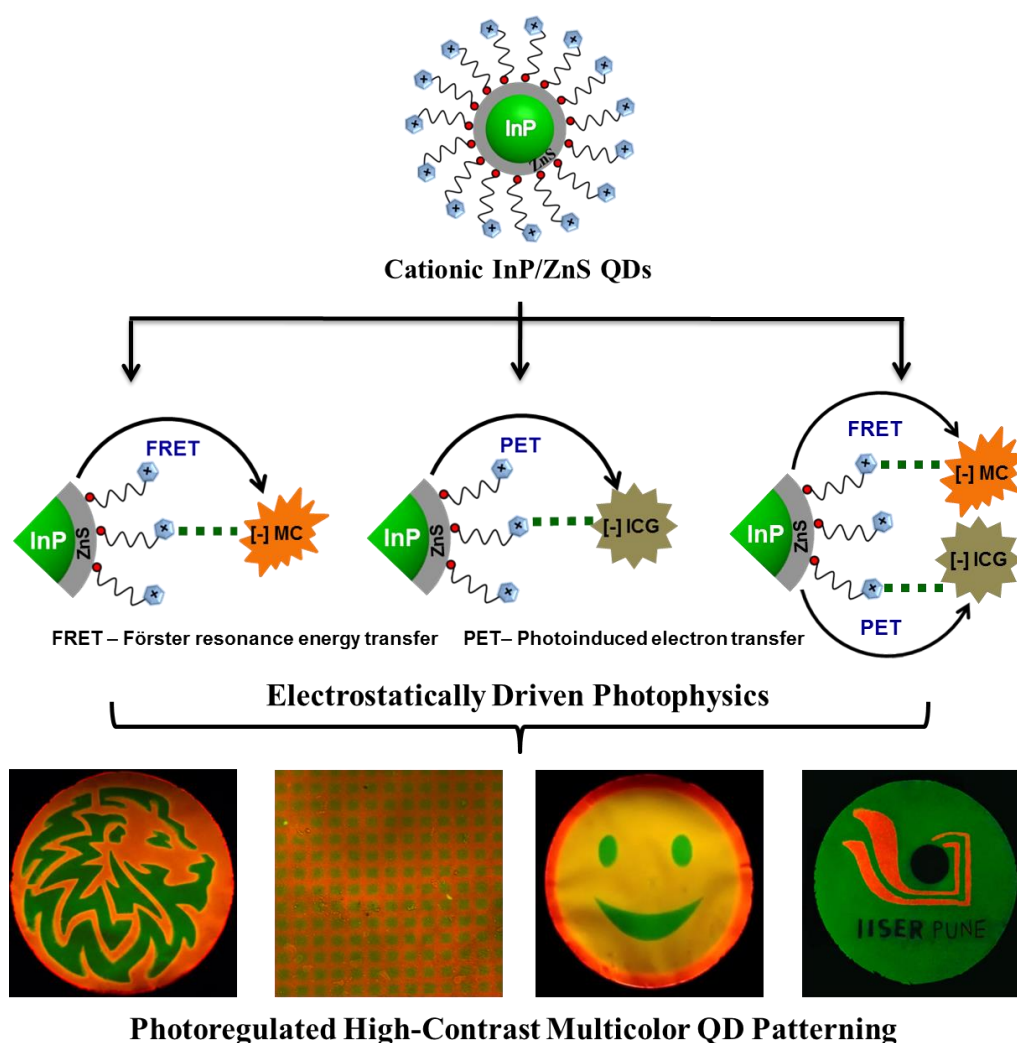
Chapter 1

Introduction on Surface Ligand Directed Light Harvesting by Quantum Dots

1.1 Introduction

Nature has always been an inspiration, as well as a puzzle for scientists! Out of the many, the interaction of light with matter is one of the most fascinating phenomena, which leads to a variety of exciting application in the areas of both medical and energy research.[1] The demand and significance of light harvesting research, perhaps, may have reached its top in our present day to day life.[2-4] Relentless efforts from the researchers over the past two decades have brought us to a stage, where solar energy harvesting strategies have become the prime alternative to meet our future energy demand.[5] For instance, Bloomberg New Energy Finance has predicted solar power to cost less than coal, and even other natural gases, by 2021 (**Figure 1.1**).[6]
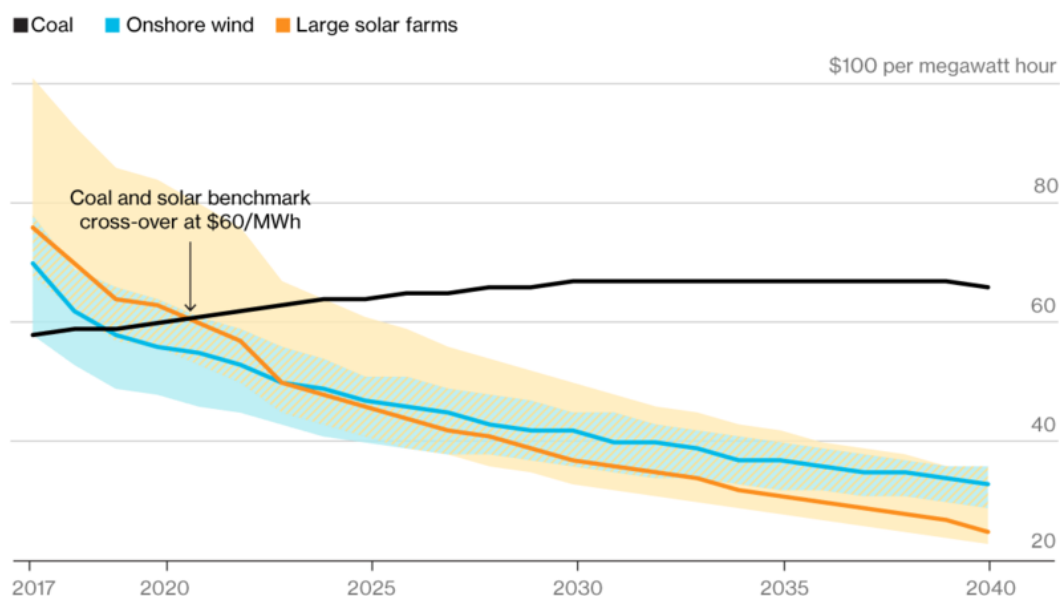
Figure 1.1: A plot predicting the cost of power production between coal and solar/ wind powers. (Reproduced in part with permission from reference 6. Copyright 2016 American Association for the Advancement of Science).

Photovoltaics forms an integral part of modern energy research, and has played a crucial role in the emergence of light harvesting as an affordable means of energy source.[5,7] Active research in the area of photovoltaics has led to the development of materials that can yield efficiencies close to the Shockley-Queisser limit of 33.7 % (**Figure 1.2**).[8]
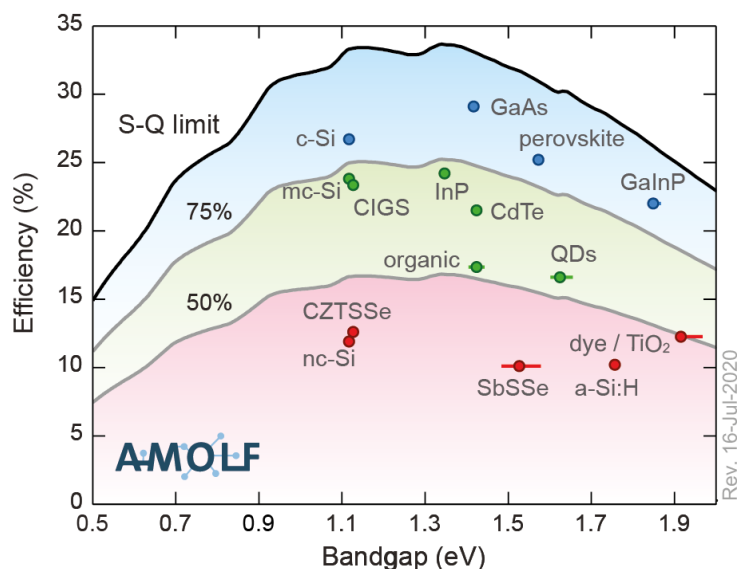
Figure 1.2: A plot showing the Shockley-Queisser detailed-balance efficiency limit as a function of band gap (black line). The record efficiencies for different materials are plotted for the corresponding band gaps. (Reproduced in part with permission from reference 8. Copyright 2020 AMOLF Physics of functional complex matter).

The key, for the present success achieved in energy research, is the improved understanding of various photophysical processes involved in the phenomenon of light-matter interaction.[1] The credit for this again goes to nature, for gifting one of the most elegant processes known to mankind so far – *photosynthesis*.[9-15] The process of photosynthesis involves a combination of light and dark reactions, where sunlight is used for the conversion of toxic carbon dioxide into value added products like oxygen and glucose.[9] This is achieved through the design of a photosynthetic light harvesting assembly, one of the finest pieces of molecular machinery that nature has ever created. Photosynthetic light harvesting assembly primarily utilizes photoinduced energy transfer, followed by well-organized sequence of electron transfer reactions in the photosynthetic reaction centre (RC).[10,11,13,14] A Z-scheme is developed by the researchers to visualize the molecular architecture and various steps involved in the process of photosynthesis (**Figure 1.3**).[12] Specifically, the Z-scheme represents various steps involved in the light reaction, and mainly shows the pathway of light induced electron transfer from water to $NADP^+$.[9,11] The y-axis is the energy scale showing each molecule's ability to reduce the next one from left to right, by transferring the photogenerated electrons.[12] In short, Z-scheme represents the pathway used by the plants to transform light energy to electrical energy (electron flow through oxidation and reduction steps), and finally to chemical energy (stored in the form of reduced NADH and ATP).[9,11]
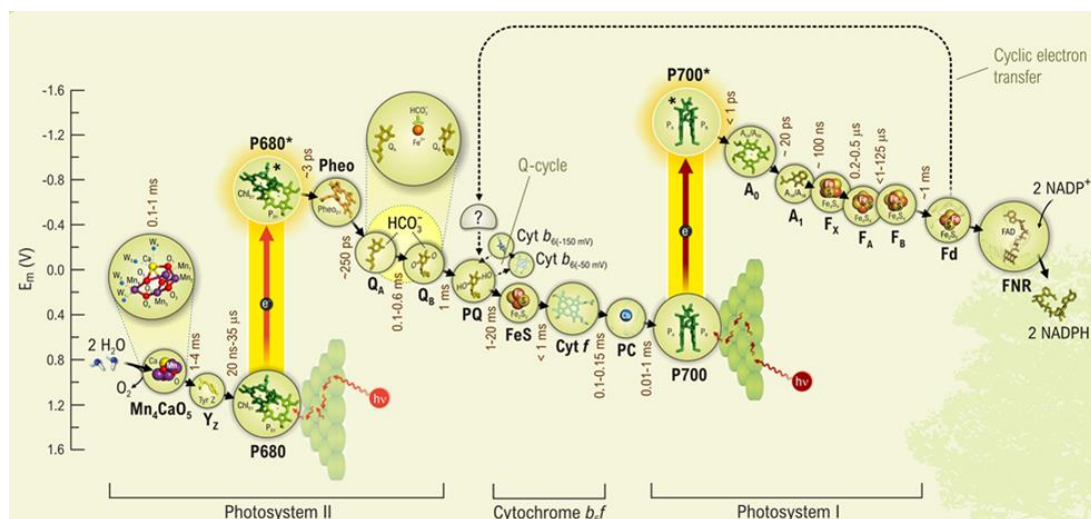
Figure 1.3: Schematic representation of z-scheme. Abbreviations used from left to the right of the diagram: Mn - manganese complex, Tyr - tyrosine; P680 - reaction centre chlorophyll (Chl) in photosystem (PS) II (the primary electron donor of PSII); Pheo - pheophytin (the primary electron acceptor of PSII); QA, QB –and PQ are plastoquinone molecules; FeS - iron sulfur protein; Cyt. - cytochrome; PC - copper protein plastocyanin; P700 - reaction centre chlorophyll; A_o - special chlorophyll a molecule; A_1 - phylloquinone (Vitamin K) molecule; FX , FA , and FB - three separate iron sulfur Centres; FD - ferredoxin; FNR - ferredoxin NADP oxido reductase. (Reproduced in part with permission from reference 12. Copyright 2015 Springer).

A closer examination of the phenomenon of photosynthesis reveals the presence of two fundamental photophysical processes: light induced energy and electron transfer processes. Mimicking the light induced energy as well as electron transfer processes, efficiently, continues to be a major challenge and a subject of intense research.[14,15] Among different mechanisms proposed for light induced energy transfer process, Forster resonance energy transfer (FRET) remains to be one of the well-studied one. FRET is a non-radiative transfer of energy from an excited state donor to a ground state acceptor, through a long range dipole-dipole interaction (typically operates in a range of 1-10 nm; **Figure 1.4a,b**).[16] Some of the important factors influencing the efficiency of FRET process include spectral overlap integral between the emission of the donor and the absorption of the acceptor, donor-acceptor distance, and orientation factor (dipole-dipole interaction) (**Figure 1.4c**).[16] For a given system, the process of FRET is highly sensitive to the distance between the donor and acceptor, r (Efficiency α $1/r^6$), and for this reason, FRET is often used as a spectroscopic ruler in many areas of research ranging from biology to energy science.[16-25]
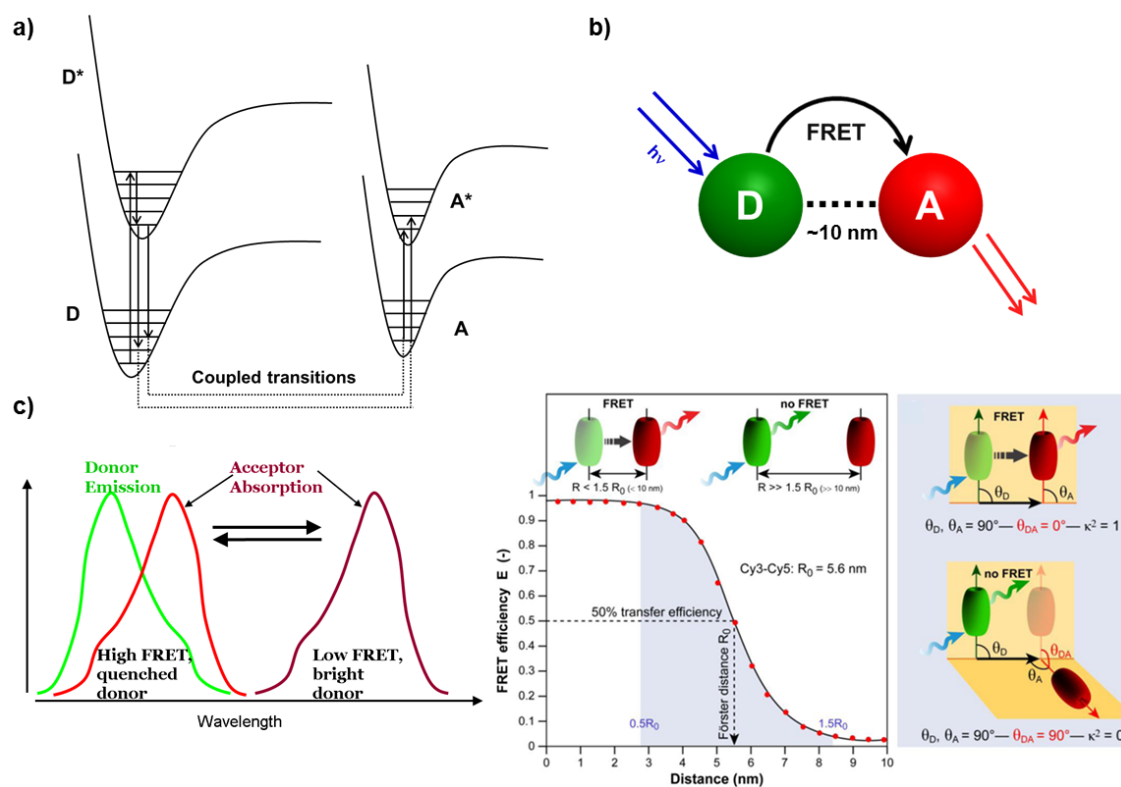
Figure 1.4: a) Schematic representation of the energy transfer process based on FRET formalism. b) Schematic representation showing the process of FRET in a donor-acceptor system. c) Various factors influencing the process of FRET: spectral overlap between the emission of the donor and the absorption of the acceptor, distance between donor and acceptor, and the orientation factor (dipole-dipole interaction) (Partially reproduced in part with permission from reference 25. Copyright 2015 Springer).

On the other hand, the process of photoinduced electron transfer (PET) involves the transfer of electron from the donor to the acceptor, upon photoexcitation.[16] It is worth mentioning that the photoexcited species can either be a donor or an acceptor (**Figure 1.5a**).[16] The simplest form of a model system that shows photoinduced electron transfer is a dyad molecule (**Figure 1.5b**), in which a donor group is covalently linked to an acceptor through a rigid or flexible bridging unit. Photoexcitation of either donor or acceptor group of the dyad results in an electron transfer, leading to the formation of a radical cation of the donor and a radical anion of the acceptor.[16,26-29] The stabilization of the charge separated state, by avoiding the energy wasting back electron transfer process is crucial for the successful use of these dyad systems for energy conversion studies. Photoinduced electron transfer is one of the most important chemical processes in many biological, physical and chemical systems (both natural and artificial).[26-31]
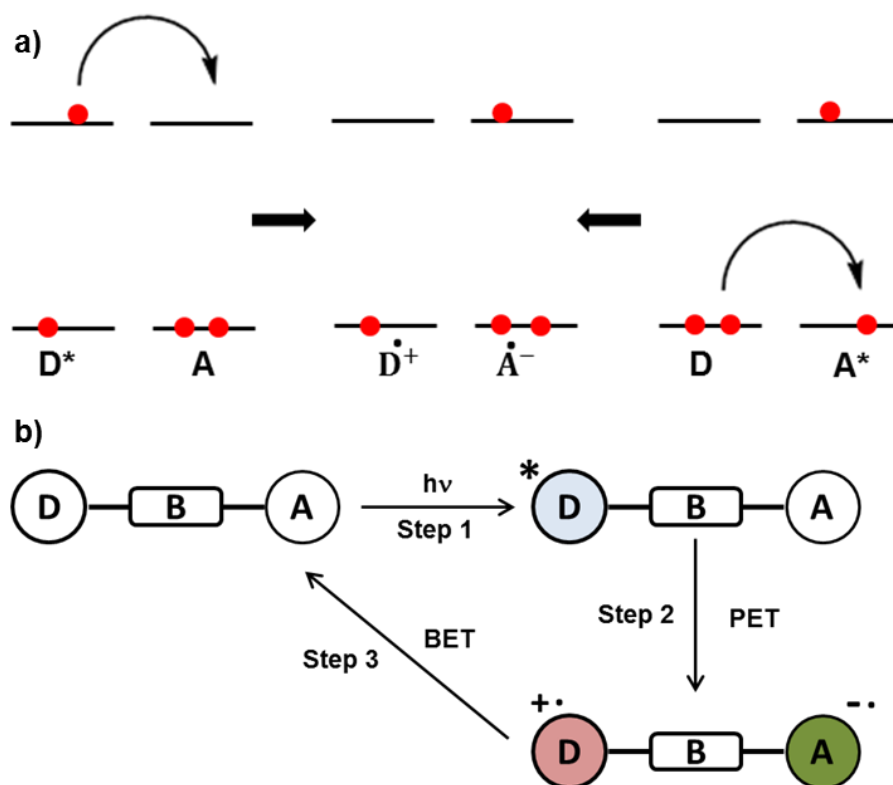
Figure 1.5: a) Schematic representation showing the process of photoinduced electron transfer, upon the photoexcitation of either donor or acceptor moieties. b) Schematic representation showing the model system for photoinduced electron transfer in a dyad system. The photoexcited donor molecules transfer the electron to the acceptor, thereby forming a charge separated complex. (Redrawn with permission from reference 26. Copyright 2015 Springer).

Quantum dot based donor-acceptor systems: Different classes of materials have been designed and developed to mimic the natural photosynthetic reaction center, including organic and inorganic molecules, polymers, and metal and semiconductor nanoparticles.[32-36] Among them, semiconductor nanoparticles or quantum dots (QDs) have achieved a special feat due to their unique size and shape-tunable optoelectronic properties such as broad absorption, narrow photoluminescence, large stoke shift, and high photostability.[37-39] All the unique properties of QDs emerge from the quantum confinement effect, when the size of the particle is below the Bohr excitonic radius (distance between a spatially separated electron and hole).[37-39] The quantum confinement leads to an increase in the band gap, and introduces discreteness in the continuum energy levels, in comparison to a bulk semiconductor (**Figure 1.6**).[37-39]
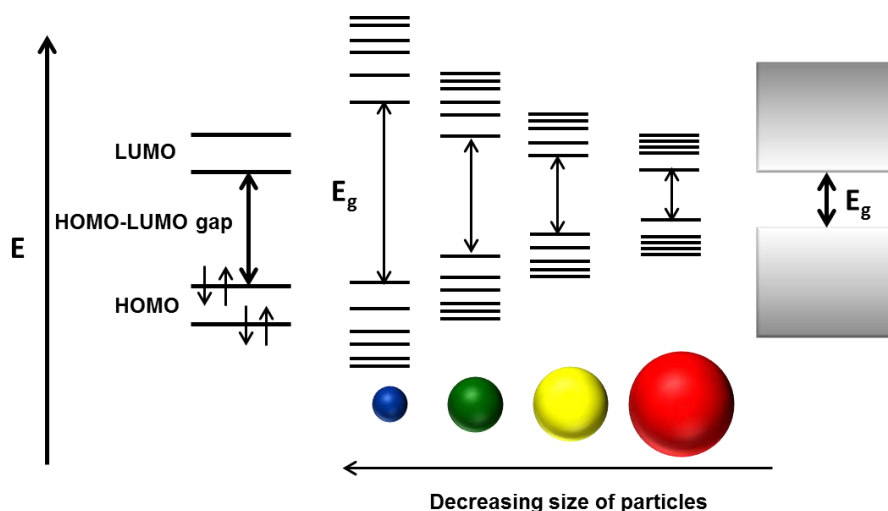
Figure 1.6: Schematic representation showing the effect of quantum confinement on tuning the optical properties in a size dependent manner, from molecule to bulk. (Redrawn from reference 37. Copyright 1990 Annual Reviews).

The band gap (E_g) of a QD is usually calculated using the Brus equation.[40]

$$E_g(QD) = E_g(bulk) + \frac{h^2}{8R^2}\left[\frac{1}{m_e} + \frac{1}{m_h}\right] - \frac{1.786e^2}{4\pi\epsilon_0\epsilon_r R^2}$$

Here, h is the Plank`s constant, R is the radius of the QD, m_e and m_h are the effective masses of electron and hole in the material, ϵ_0 is the permittivity of vacuum, and ϵ_r is the relative permittivity.

In general, most of the intriguing properties of a nanomaterial originate from its core. For instance, metallic cores like Ag, Au and Cu will impart plasmonic properties, semiconductor cores like CdSe, CdSe, PbTe etc. will impart photoluminescence properties, metals like Fe, Co, Ni, etc. will impart magnetic properties, and so on.[41] The initial era of research in the area of nanoscience was mostly focused on the core properties, and surface ligands were considered as a capping agent, which gives stability to the nanomaterials. Later, researchers have realized the enormous potential hidden in the surface ligands, which are much beyond a mere stabilizing agent. In fact, surface ligands have been found not only to improve the existing properties of nanomaterials, but also to impart new properties as well.[42-46] tuning the surface chemistry of nanomaterials, one can get different interactions into action, like H-bonding, electrostatic, π-π, hydrophobic, and hydrophilic interactions, which can play a decisive role in controlling the functions at the nanoscale (**Figure 1.7**).[42-46] Consequently, tuning the surface chemistry of nanomaterials has emerged as one of the active areas in modern nanoscience. Thus, one of the main focuses of the present Thesis is to study the effect

of surface ligands on the optical and electronic properties, charge recombination dynamics, energy, and electron transfer processes in QDs. Thus, the Chapter 1 gives a brief summary of how ligands on the surface of QD can control the interactions in a donor-acceptor system, and their impact on various photophysical processes.
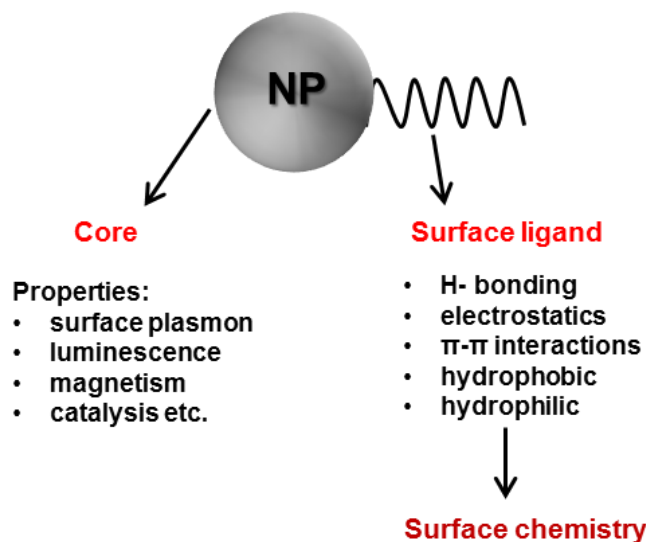
Figure 1.7: Schematic representation showing the general structure of nanoparticles and properties originating from the core and surface ligand.

1.2 Effect of surface ligand on light induced energy transfer

Energy transfer is a non-radiative process, where the photoexcited donor transfers its excess energy to an acceptor either through dipole-dipole interactions (Förster resonance energy transfer or, FRET) or by exchange mechanism (Dexter energy transfer).[16,47] The rate of FRET decays with $1/r^6$, where r is the distance between donor and acceptor; whereas the rate of Dexter energy transfer scales with e^{-2r}.[16,47] Thus, one of the main parameters governing the efficiency of energy transfer process is the distance between the donor and acceptor.[16,47] Ideally, a close proximity of donor and acceptor is desirable, and the ligands on the surface of QDs can dictate the outcome of this process.[48-50] In this direction, a wide range of ligand sets have been developed by the researchers based on proteins, peptides, nucleic acids, aliphatic and aromatic hydrocarbon chains, etc.[51-57] Mattoussi and co-workers have used the de novo polypeptides with variable lengths as a surface ligand, as well as a spacer in CdSe/ZnS QD - Cy-3 dye based donor-acceptor system.[55] Here, QDs played a dual role by providing its core as an energy donor, and its surface ligands as receptors for the adsorption of Cy-3 dyes. As theoretically predicted for FRET, a sixth power dependence of energy transfer efficiency on

donor-acceptor distance was observed by systematically varying the length of the polypeptides **(Figure 1.8)**.[55]
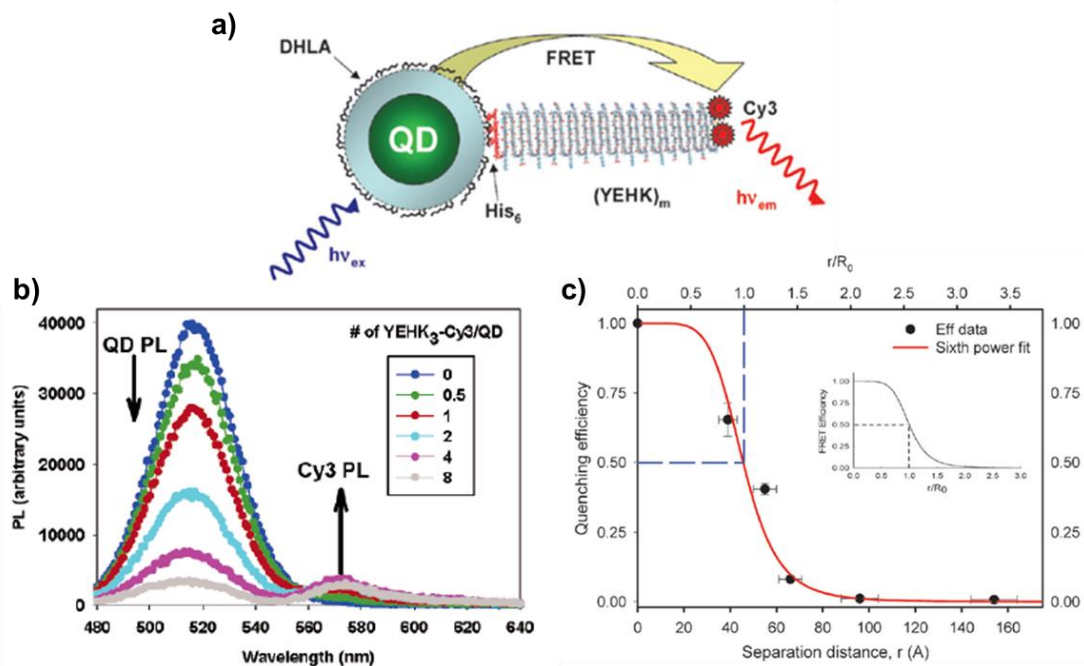
Figure 1.8: a) Schematic representation showing the QD-YEHK$_m$-Cy3 conjugate (m is the repeat units of peptide core). b) PL emission spectra of QD-YEHK$_3$-Cy3 conjugate with different ratios. c) A plot showing the PL quenching efficiency vs. distance, with the best fit using the Förster formalism. (Reproduced in part with permission from reference 55. Copyright 2006 American Chemical Society).

In another elegant work, Weiss and co-workers have designed a donor-acceptor system based on two different sizes of PbS QDs, functionalized with mercaptoalkanoic acid ligands of variable lengths (MAA; S^--$(CH_2)_{(n-1)}$-COO^-, n = 3-16).[57] In the absence of any external trigger, negligible FRET was observed in the QD-QD based donor-acceptor system. Interestingly, the addition of Zn^{2+} ions resulted in an efficient FRET from smaller to bigger sized QDs (E~86 %). The coordination ability of Zn^{2+} ions with carboxylic groups brings the donor-acceptor QDs close to each other, leading to an efficient FRET process (**Figure 1.9a**). **Figure 1.9b** shows the photoluminescence (PL) spectra of 12-mercaptoalkanoic acid functionalized QD mixture, before (solid black spectrum) and after (dashed black spectrum) the addition of 700 equivalents of Zn^{2+} ions. The blue and red spectra were generated by deconvolution, which corresponds to the individual contributions of the donor and the acceptor QDs, respectively. A bathochromic shift in the PL spectra of mixed QD solution was observed after the addition of Zn^{2+} ions. This confirms a decrease in the PL intensity of donor QDs, along with a simultaneous increase in the PL of acceptor QDs. Interestingly, no

appreciable changes were observed in the PL spectra upon crosslinking the donor and acceptor QDs independently, with Zn^{2+} ions. Upon decreasing the length of the ligand from n=16 to n= 3, the average interparticle distance decreased from 5.8 ± 0.3 nm to 3.7 ± 0.3 nm. Consequently, the rate of energy transfer increased from $\sim$150 ns^{-1} to $\sim$2 ns^{-1} (**Figure 1.9c**). Similar effect of ligand length on the FRET efficiency has been reported by Wu and co-workers in CdSe/ZnS QD – gold nanoparticle donor-acceptor system.[58]
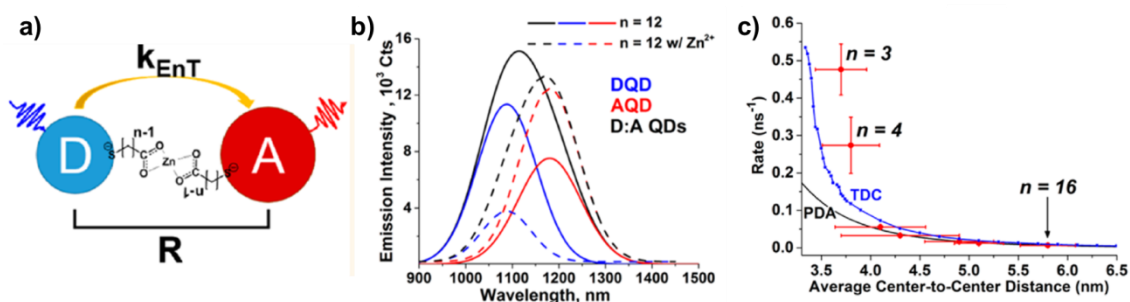
Figure 1.9: a) Schematic representation showing the energy transfer between different sizes of MAA capped PbS QDs, through COO$^-$ - Zn^{2+}- COO$^-$ bridging interaction. b) PL spectra of 2:1 ratio of donor and acceptor solution capped with 12-MAA ligands, before and after the addition of 700 equivalents of Zn^{2+} ions, at an excitation wavelength of 800 nm. c) A plot showing the rate of energy transfer vs. the donor-acceptor distance. (Reproduced in part with permission from reference 57. Copyright 2017 American Chemical Society).

Ligands, *can*, not just increase or decrease the rate of energy transfer, but *can* influence the nature of the quenching process itself. Tang and co-workers have studied the effect of anchoring groups of a ligand in controlling the nature of energy transfer between CdS QD donors and boron dipyrromethane dye acceptors.[59] Here, boron dipyrromethane dye was functionalized with amine and carboxylic acid groups, to control the interaction with the donor QDs. The carboxylic acid-functionalized acceptor dyes could attach itself to the multiple identical binding sites on the surface of QDs (**Figure 1.10a**). Accordingly, the PL of the QD donor was quenched by ~45 %, along with an enhancement in the acceptor emission by ~55 %, which confirms a moderate FRET from the donor QD to the dye acceptor (inset of **Figure 1.10b**). In contrast, both FRET as well as static quenching processes were observed, when amine-functionalized dyes were used as the acceptor. In the presence of amine-functionalized dyes, the PL of the donor was quenched by ~90 %, with a marginal enhancement in the acceptor emission (~10 %; **inset of Figure 1.10d**). Similarly, the PL lifetime of CdS QDs is significantly quenched in the presence of the amine-functionalized dye (**Figure 1.10e**). This contrasting behaviour was explained based on the existence of two sites available for the attachment of amine-functionalized dye on QDs. A bright site leading

to a normal FRET, and a dark site which will result in a charge transfer from the QDs through static interaction. On the other hand, acid-functionalized ligands bind to multiple identical sites on QDs, resulting in FRET as a sole quenching process.[59]
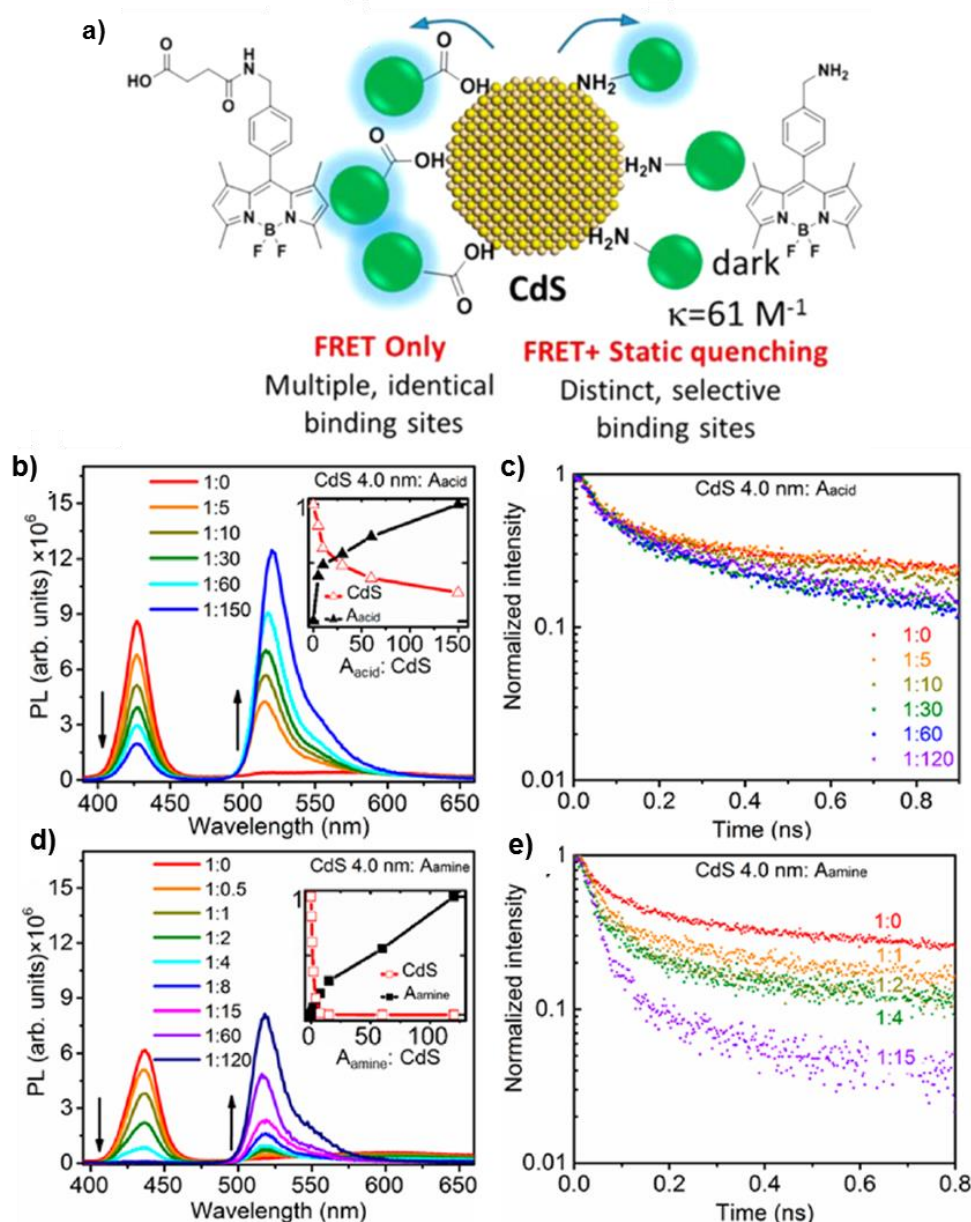
Figure 1.10: a) Schematic representation showing the energy transfer from CdS QD to dye boron dipyrromethane acceptors, linked through acid and amine groups. b,d) Spectral changes in the steady state PL, and c,e) corresponding time resolved spectra of CdS QDs, on the addition of varying amounts of acid and amine functionalized dye molecules. Insets show the corresponding decrease in the PL of CdS QD, and an increase in the emission of acid/amine functionalized dye molecules. (Reproduced in part with permission from reference 59. Copyright 2015 American Chemical Society).

Another report by Nyokong and co-workers revealed the effect of thiolated carboxylic acids on the efficiency of energy transfer in CdTe QD - aluminium phthalocyanines dye donor-acceptor system.[60] The CdTe QDs were functionalised with thioglycolic acid (TGA), mercaptopropionic acid (MPA), and L-cysteine (CYS) ligands. The trend in the efficiency of energy transfer followed the order CYS > MPA > TGA. The exact reason for the observed trend was not clearly understood, due to the additional effects of these ligands on the growth and crystallinity of QDs.[60] Another approach to achieve ligand directed energy transfer is to functionalize the QDs with photochromic ligands.[57] Photochromic dyes will undergo reversible transformation upon exposure to light, resulting in the switching between two photophysically distinct states.[61] Spiropyran and their derivatives are one of the most prominent and well-studied class of photochromic compounds.[61] Spiropyran exists in two forms: a closed spiro form and an open meso form, with their characteristic absorptions around 400 and 500-700 nm, respectively.[61,62] In principle, a photoregulated energy transfer process can be achieved by functionalizing a thiolated spiropyran on the surface of QDs. In normal light, negligible energy transfer will be observed from QD to spiropyran, due to the low spectral overlap between the PL of QD and absorption of the spiro isomer (~ 400 nm). Upon irradiation with UV light, the closed spiro form (SP) isomerizes to the open meso merrocyanine form (MC), and the absorption shifts in the range of 500-700 nm (**Figure 1.11a**). Consequently, a strong spectral overlap is established between the PL of QD and the absorption of the meso isomer, resulting in the switching ON of an efficient FRET process. This concept of photoregulated energy transfer was realized by Medintz and co-workers.[63]A photochromic BIPS (1′,3-dihydro-1′-(2-carboxyethyl)-3,3-dimethyl- 6-nitrospiro-[2H-1 benzopyran-2,2′-(2H)-indoline]) conjugated with maltose-binding protein (MBP) was functionalized on the surface of CdSe QDs. The isomerization of spyro to meso form resulted in a high spectral overlap integral value, thereby triggering an efficient FRET process from QD to the photochromic dyes (**Figure 1.11b,c**). Interestingly, the FRET process can be switched OFF by converting the meso form back to the closed spyro form, under visible light irradiation. This photoregulated switching between FRET ON and OFF states was achieved for many cycles, without any noticeable loss of efficiency (**Figure 1.11d**).[63] Similar FRET ON-OFF systems have been developed with other photochromic dyes like perfluorocyclopentene, dithienylethenes, oxazolylfulgides, and bismuth vanadate pigments.[64-66]
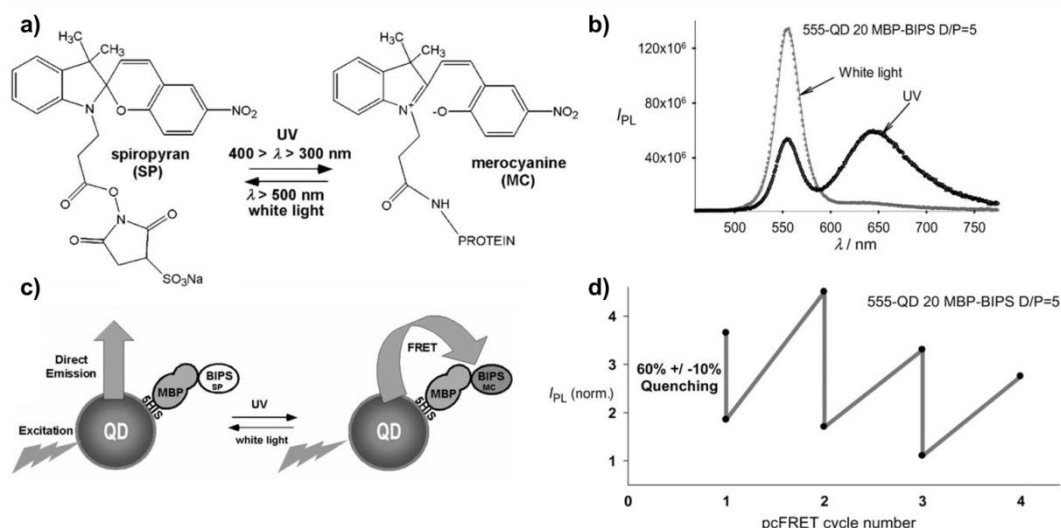
Figure 1.11: a) Structure of sulfo-NHS-BIPS in the SP (left) and MC (right) forms, after conjugation to a protein. b) PL spectra of QD-MBP-BIPS conjugate before and after illuminating with UV light. c) Schematic representation showing the conversion of SP form to MC form in BIPS, upon UV irradiation of QD-MBP-BIPS conjugate. d) Monitoring the QD luminescence during the photoconversion cycles. (Reproduced in part with permission from reference 63. Copyright 2015 American Chemical Society).

1.3 Effect of surface ligand on photoinduced electron transfer process

The process of photoinduced electron transfer (PET) involves the transfer of an electron from a donor to an acceptor, upon the excitation of either the donor or the acceptor.[16] The general outcome of a PET process is the formation of a non-luminescent complex, comprised of radical cation and radical anion species.[16] A fundamental understanding on the exciton dissociation and transfer (extraction of the charge carriers from the QD core) is the key for the successful design of QD based photovoltaic and photocatalytic systems.[67,68] The time scale of electron transfer should be much faster than the inherent PL lifetime, in order to extract the excitons efficiently out of the QD system.[67,68] Now, a surface ligand can either assist or block the transfer of excitons from the QDs, making the choice of ligands one of the crucial parts in the design of an efficient donor-acceptor system.[67,68] In a traditional approach, the distance between the donor and the acceptor is minimized by using short chain length ligands or bifunctional molecules to bridge the donor and the acceptor.[69-71] Recently, researchers have started to incorporate different interactions, emanating from the surface ligands, to enhance the rate of PET in donor-acceptor systems.[72-74] Kamat and co-workers were successful in improving the adsorption of CdSe QDs on TiO_2 films, by using a bifunctional 3-mercapto propionic acid (MPA) ligand as the linker.[72] The increase in the

adsorption constant directly translated into the enhancement of PET process in CdSe QD – TiO$_2$ donor- acceptor nanohybrid system. Later, Watson and co-workers studied the effect of chain length of mercaptoalkanoic acid (MAAs) based surface ligands, on the rate and efficiency of PET in CdS QD – TiO$_2$ donor- acceptor nanohybrid systems.[69] The thiol and carboxylic groups in the bifunctional ligands have a strong affinity towards the surfaces of QDs and TiO$_2$, respectively, leading to the formation of a strong donor-acceptor complex. The steady state and time resolved photophysical experiments reveal that the rate of electron transfer, from QD to TiO$_2$, increased as the length of the MAA ligand was decreased.[69] Not only the length but also the nature and electronic structure of the linker/ligand molecules can have an effect on the electron transfer properties.[70] Cánovas and co-workers have performed optical pump-probe terahertz spectroscopy measurements to study the electron transfer process in a QD donor-bridge-SnO$_2$ acceptor system, by tuning the electronic coupling strength of the linker molecules (**Figure 1.12a**).[71] The authors have used n-alkylene (SH−[CH$_2$]$_n$−COOH) and n-phenylene (SH−[C$_6$H$_4$]$_n$−COOH) molecular bridges in the system, where thiol and carboxylic groups can attach on to the QD and SnO$_2$ surfaces, respectively. It was demonstrated that the electron transfer occurred through a non-resonant quantum tunnelling with decay rates, β (tunnelling decay rate for a given barrier potential) of 0.94 for alkylene group, and 1.25 for phenylene group. A faster electron transfer process was observed with the aromatic phenylene bridges, when compared to aliphatic alkylene bridges. The molecular orbitals of alkylene linkers were localized on either ends of the bridge, with a large HOMO−LUMO gap. In contrast, the molecular orbitals of n-phenylene linkers delocalized across the entire molecule, which results in a decrease in the energy of LUMO, and thereby increasing the effective volume of the electronic wave function. This results in an increase in the spatial overlap between the donor (QD) and acceptor (TiO$_2$) moieties, resulting in an enhanced electron transfer in the case of phenylene bridges compared to alkylene bridges (**Figure 1.12b**).[71] Thus both the length and electronic structure of the ligand affects the PET process.
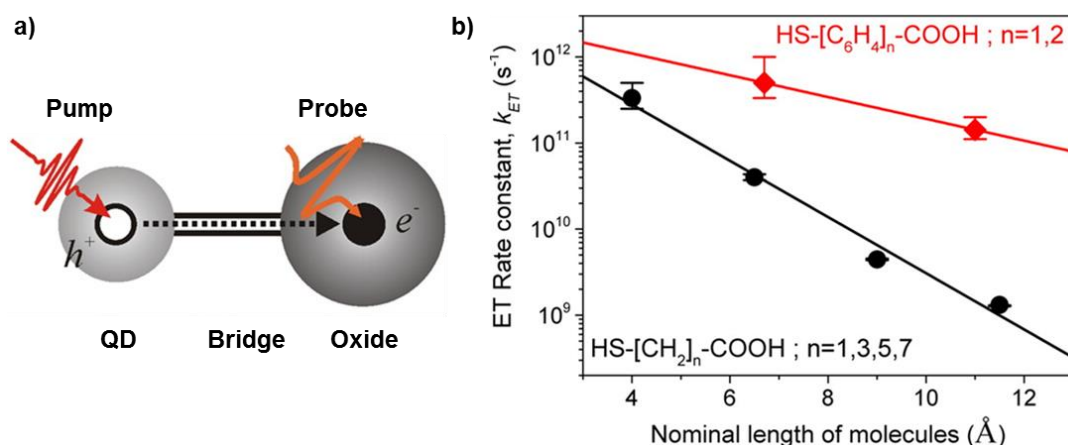
Figure 1.12: a) Schematic representation of a QD based donor-bridge-acceptor system. b) Plot showing the rate of electron transfer vs. length of linker molecules for n-alkylene (black dots) and n-phenylene (red dots) bridges. (Reproduced in part with permission from reference 71. Copyright 2013 American Chemical Society).

The nature of the binding/anchoring groups, constituting the surface ligands, is also known to influence the PET process. For instance, Kamat and co-workers have studied the influence of two commonly used binding groups on PET: thiol vs amine.[72] For this, the authors have decorated the surface of CdSe QDs with mercapto propionic acid (MPA) and β-alanine (β-Ala).[72] The thiol functional group creates carrier trapping sites on the surface of QDs, which hinders the electron transfer from QD to TiO_2. Whereas, QDs with amine-functionalized ligands (β-Ala) generates fewer trap states compared to thiols, which enhances the rate of PET in β-Ala functionalized QD-TiO_2 system (**Figure 1.13a**). On a side note, the electron transfer rate was always high when QDs were directly deposited on the TiO_2. This is due to the increase in the spatial overlap between the donor and acceptor states, as well as the formation of fewer trap sites (**Figure 1.13b**).[72]
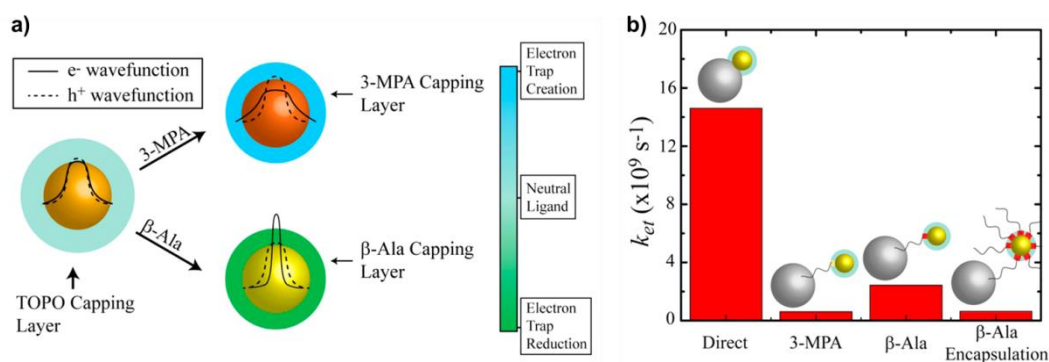
Figure 1.13: a) Schematic representation showing the effect of anchoring groups on the electron trap states in excited QDs. b) A bar diagram showing the effect of thiol and amine

15

functional groups on the rate of electron transfer. (Reproduced in part with permission from reference 72. Copyright 2011 American Chemical Society).

Another report from Wise and co-workers investigated the effect of anchoring groups on the acceptor moieties ($-SiX_3$, $-COOH$, $-PO_3H_2$, and $-SO_3Na$).[73] The donor-bridge-acceptor system comprised of PbS QD as the donor, TiO_2 as the acceptor, and linker molecule with different functional groups. As expected, an inverse dependence of the chain length of linker molecules was observed on the rate of PET process. Interestingly, the nature of anchoring groups had a dramatic influence on the PET process as well. The fastest PET rate was observed for the donor-acceptor system, where the linker molecule was anchored on the acceptor through sulfonate groups. Even though the exact mechanism was not discussed, the authors have attributed it to the ability of anchoring groups in modifying the density of states on the TiO_2 surface.[73] Further, Weiss and co-workers have used phenyl bis-(dithiocarbamate) (PBTC) as the linker molecule in zinc porphyrin (ZnP) - CdSe QD based donor-acceptor nanohybrid system.[74] In a control experiment, the QD acceptor was directly attached to the phorphyrin donor through the carboxylic groups on ZnP. The presence of PBTC linker improved the quantum yield of the PET process from ZnP to CdSe QD by a factor of ~4 (from 8 % to 38 %). The PBTC molecule links the ZnP and CdSe QD through the bifunctional dithiocarbamate group, by coordinating with the Cd^{2+} ions in the QD, and Zn metal centre in the ZnP (**Figure 1.14a,b**). The PBTC linker heled in increasing the binding affinity between CdSe QDs and ZnP, by an order of magnitude (from 1.0×10^5 M^{-1} to 1.0×10^6 M^{-1}). **Figure 1.14c** shows the transient absorption spectra of ZnP -PBTC- QD donor-bridge-acceptor system, by selectively exciting the ZnP at 700 nm. A steady increase in the QD ground state bleach was observed as the amount of PBTC linker was increased in the system (**Figure 1.14c**).[74]
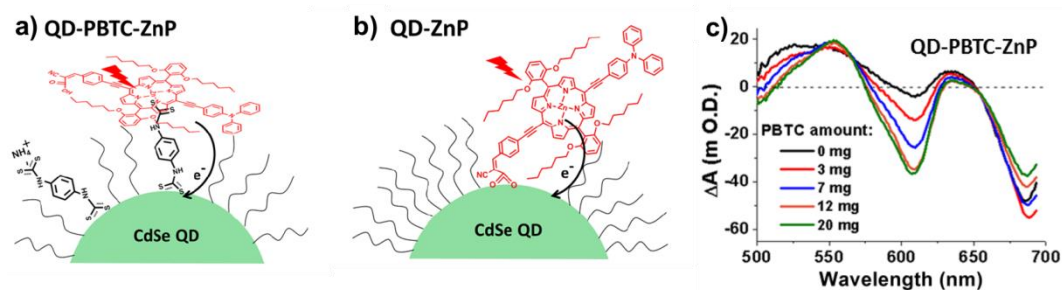
Figure 1.14: Schematic representation showing the electron transfer from ZnP to CdSe QD: through a) PBTC molecule, and b) carboxylic group of ZnP. c) Transient absorption spectra of QD-PBTC-ZnP mixture, where the QDs have been treated with different amounts of

PBTC ligands. (Reproduced in part with permission from reference 74. Copyright 2015 American Chemical Society).

All the above mentioned representative examples confirm a strong dependence of surface ligands, linkers, and anchoring groups on the dynamics and rate of energy and electron transfer processes in QD based donor-acceptor systems. Along with this, the surface ligands have the potency to transform the inherent property of a nanohybrid system. A representative example from the area of plasmonic nanoparticles is taken to demonstrate this particular unprecedented role of surface ligands in nanoscience. In one of the most revolutionary reports, Grzybowski and co-workers showed that the inherent conducting (electrical) property of metal nanoparticles can be transformed into a diode behaviour, with the use of appropriate surface ligands.[75] *In short, surface ligands can impart a semiconducting behaviour in a metallic system!*[75] For this, gold nanoparticles (AuNP) stabilized with positively charged N,N,N-trimethyl-(11-mercaptoundecyl) ammonium chloride (TMA) ligands surrounded by negative counter ions (Cl^-), and negatively charged 11-mercaptoundecanoic acid (MUA) surrounded by positive counter ions ($N(CH_3)_4^+$), were prepared (**Figure 1.15a**). Intermixing of mobile counter ions occurred, upon sandwiching the oppositely charged AuNP films: Cl^- ions migrated to MUA AuNP film, and $N(CH_3)_4^+$ ions migrated to TMA AuNP film. Thus, the mobile ions form a built-in electric field at the junction of AuNP films, similar to an electric double layer (**Figure 1.15b**). When the negative external potential was applied to the positively charged NP film, the mobile counter ions were pushed towards the interface. This increases the internal field at the junction, and as a result the conductivity decreases. When the bias was reversed, the mobile counter ions were pulled away from the interface, and the internal field at the junction was diminished, thereby increasing the conductivity. Thus, the metallic AuNP films exhibit a diode behaviour (**Figure 1.15c**), which is in stark contrast to the common ohmic behaviour.[75] This particular example has created a paradigm shift in the area of nanoscience, and revealed the power of surface ligands in not only improving, but also imparting newer properties at nanoscale.
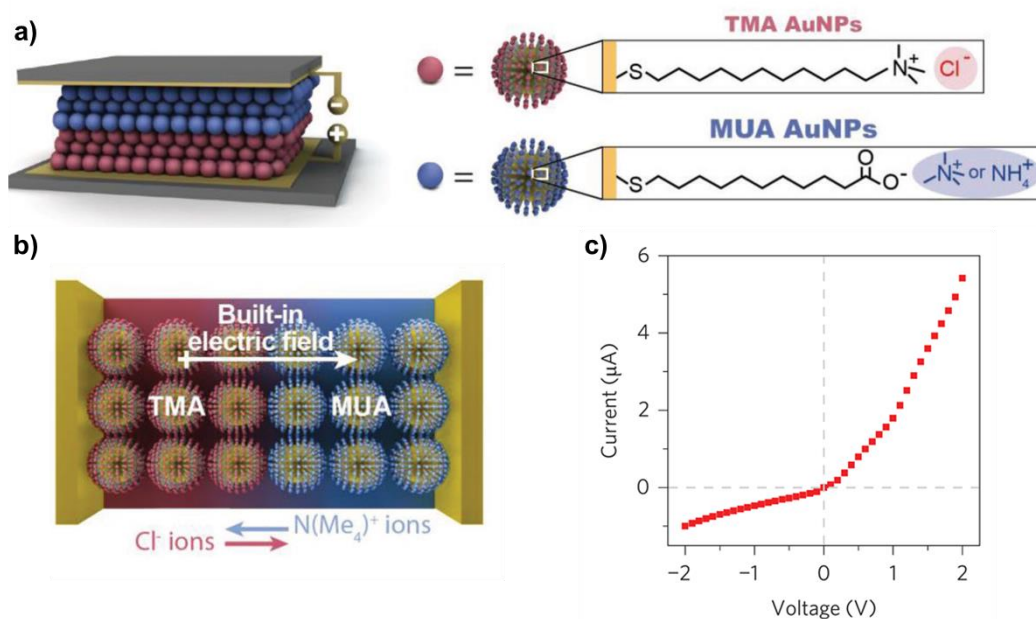
Figure 1.15: a) Schematic representation showing the formation of metal nanoparticle diode, by sandwiching layers of oppositely charged TMA and MUA AuNPs. b) Scheme showing the generation of an internal field at the interface by intermixing of counter ions. c) I–V characteristics showing the rectification of current in AuNP films. (Reproduced in part with permission from reference 75. Copyright 2016 Springer Nature).

1.4 Surface chemistry of metal and semiconductor nanoparticles

As mentioned in the previous sections, a smart of choice of surface ligands can be decisive in dictating the optoelectronic properties in metal and semiconductor nanomaterials.[76,77] Moreover, appropriate surface ligands can also introduce different interparticle interactions and forces into action.[42-46,78-81] Hence, it is crucial to develop protocols to functionalize the ligands of our choice on the surface of nanomaterials. This narrows down the discussion to an important topic: *surface chemistry – the art of ligand functionalization and engineering*. One of the key challenges in the area of surface chemistry is the ability to retain the inherent properties of the nanomaterials during the decoration of ligands of our choice. A thorough literature review reveals that the surface chemistry of QDs is less explored, in comparison to metal nanoparticles. For instance, all kinds of ligands have been functionalized on the surface of metal NPs, such as hydrophobic, hydrophilic, cationic, anionic, neutral, zwitterionic, and so on.[42-46,78-83] This clearly confirms that the surface of a metal NP is robust towards a wide range of functionalization. Whereas, the surface of a QD is highly sensitive to ligand functionalization, which restricts the choice of ligands that one can work with. The first choice of ligands for QDs are hydrophobic molecules such as trioctylphosphine/trioctylphosphine oxide (TOP/TOPO), long-chain alkylamines, and alkyl

thiols.[84- 89] Among hydrophilic ligands, most of the reports have used either anionic or neutral molecules, with a limited success with cationic molecules (**Figure 1.16**). It is worth mentioning that the attachment of cationic ligands on the QD surface of choice is still challenging, and one can easily loose its unique photoluminescent property in attempting to do so. Hence, there is a strong demand for the development of protocols for the functionalization of cationic ligands on the surface of QDs, so that the ligand directed optoelectronic studies can be extended to cationic QDs as well.
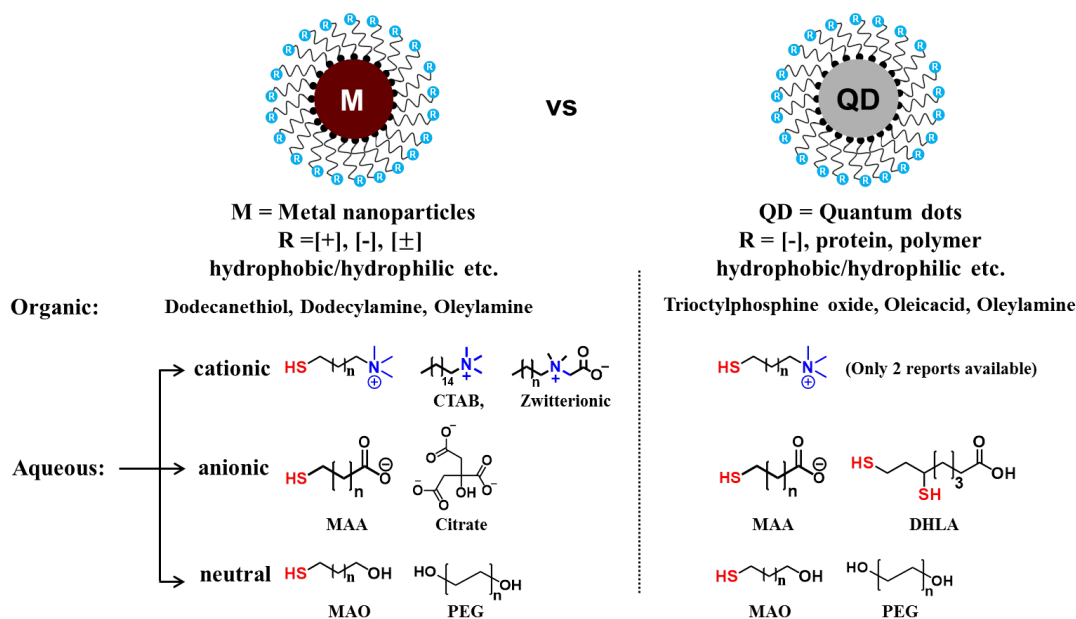
Figure 1.16: Schematic representation showing the comparison between the surface chemistries of metal and semiconductor nanoparticles.

1.5 Conclusions and Outline

Chapter 1 provides a brief summary of surface ligand directed energy and electron transfer processes in QD based nanohybrid systems. The representative examples presented here proves the power of surface ligands in not only improving, but also imparting newer properties at the nanoscale. Factors like length, electronic structure, and anchoring groups in surface ligands can influence the dynamics and rate of light harvesting in QD based nanohybrid systems. A thorough literature survey reveals the need for expanding the scope of surface chemistry in QDs, especially with cationic ligands. Thus, the main objective of the present Thesis is to expand the surface chemistry of QDs to permanently positively charged ligands, and realize the ligand directed photophysical studies in cationic QDs. Specifically, we have established the decisive role of electrostatic interactions, emanating from surface ligands, in dictating light induced energy and electron transfer processes in environmentally

friendly cationic QDs. Later, such ligand directed photophysical processes were explored in the area of QD photopatterning, which offers a fundamentally unique and cost-effective approach for the manufacturing of QD based display devices (**Figure 1.17**).
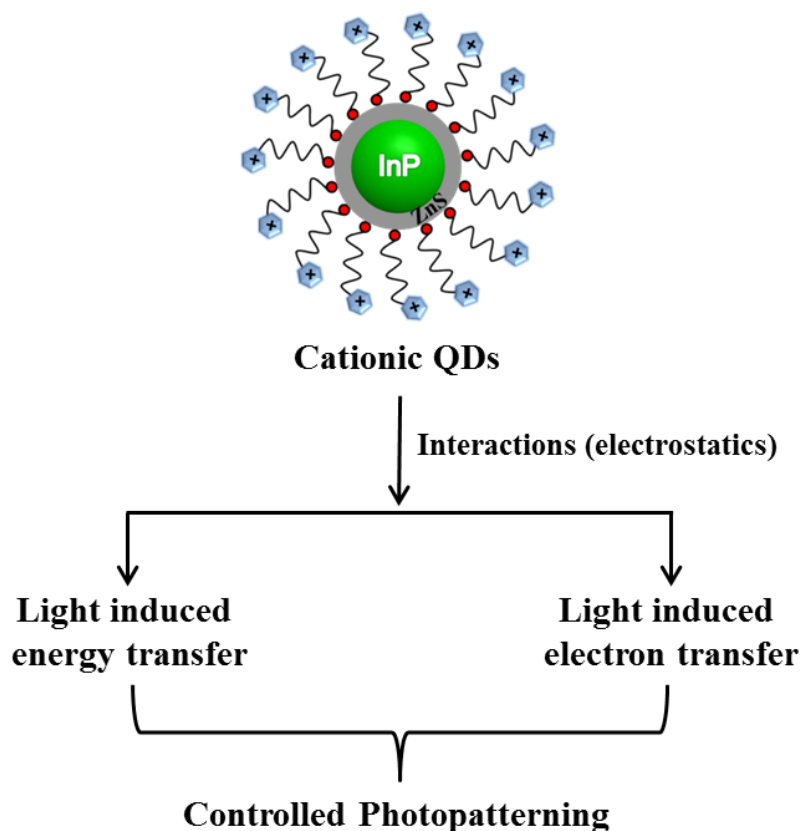
Figure 1.17: Schematic representation showing the main objective of the present Thesis: Surface ligand directed energy and electron transfer processes in cationic InP/ZnS QDs, and its exploration in QD photopatterning.

1.6: References

(1) Hertzog, M.; Wang, M.; Mony, J. Börjesson, K. Strong light–matter interactions: a new direction within chemistry *Chem. Soc. Rev.* **2019**, *48*, 937-961.

(2) Doytch, N.; Klein, Y. L. The Impact of Natural Disasters on Energy Consumption: An Analysis of Renewable and Nonrenewable Energy Demand in the Residential and Industrial Sectors. *Environ. Prog. Sustain. Energy* **2018**, *37*, 37–45.

(3) Gangwar, S. Energy Insecurity in India: Exploration of Renewable Energy Resource. *Adv. Electron. Electr. Eng.* **2013**, *3*, 1051–1056.

(4) Kamat, P. V. Meeting the Clean Energy Demand: Nanostructure Architectures for Solar Energy. *J. Phys. Chem. C* **2007**, *111*, 2834–2860.

(5) Owusu, P. A.; Asumadu-Sarkodie, S. A review of renewable energy sources,

sustainability issues and climate change mitigation. *Cogent Engineering*, **2016**. *3*, 1167990.

(6)   Shankleman, J.; Warren, H. Solar Power Will Kill Coal Faster Than You Think. https://www.bloomberg.com/news/articles/2017-06-15/solar-power-will-kill-coal-sooner-than-you-think June 15, **2017**.

(7)   Bredas, J. -L.; Sargent, E. H.; Scholes, G. D. Photovoltaic Concepts Inspired by Coherence Effects in Photosynthetic Systems. *Nat. Mater.* **2017**, *16*, 35– 44,

(8)   Light Management in New Photovoltaic Materials, S-Q Charts, https://www.lmpv.nl/sq/ July 22, **2020.**

(9)   Hall, D. O.; Rao, K. K. Photosynthesis. 6th Edition, Cambridge University Press, Cambridge, UK. **1999**.

(10)   Deisenhofer, B. J.; Michel, H. The Photosynthetic Reaction Center from the Purple Bacterium. *Angew. Chem., Int. Ed. Engl.* **1989**, *28*, 829–847.

(11)   Amarnath, K.; Bennett, D. I.; Schneider, A. R.; Fleming, G. R. Multiscale Model of Light Harvesting by Photosystem II in Plants. *Proc. Natl. Acad. Sci. U. S. A.* **2016**, *113*, 1156– 1161.

(12)   Shevela, D.; Björn, L. O. Govindjee Z-Scheme of Electron Transport in Photosynthesis, https://www.agrisera.com/en/blogg/agrisera-blog/2018/04/22/z-scheme-of-electron-transport-in-photosynthesis.html April 08, **2018**.

(13)   Mirkovic, T.; Ostroumov, E. E.; Anna, J. M.; van Grondelle, R.; Govindjee; Scholes, G. D. Light Absorption and Energy Transfer in the Antenna Complexes of Photosynthetic Organisms. *Chem. Rev.* **2017**, *117*, 249– 293.

(14)   Wasielewski, M. R. Photoinduced Electron Transfer in Supramolecular Systems for Artificial Photosynthesis. *Chem. Rev.* **1992**, *92*, 435–461.

(15)   Ishizaki, A.; Calhoun, T. R.; Schlau-Cohen, G. S.; Fleming, G. R. Quantum Coherence and Its Interplay with Protein Environments in Photosynthetic Electronic Energy Transfer. *Phys. Chem. Chem. Phys.* **2010**, *12*, 7319-7365.

(16)   Lakowicz, J. R. Principles of Fluorescence Spectroscopy, 3rd ed., Springer: New York, **1999**.

(17)   Stryer, L. Fluorescence Energy Transfer as a Spectroscopic Ruler. *Annu. Rev. Biochem.* **1978**, *47*, 819–846.

(18)   Scholes, G. D.; Andrews, D. L. Resonance Energy Transfer and Quantum Dots. *Phys. Rev. B: Condens. Matter Mater. Phys.* **2005**, *72*, 125331,

(19)   Clapp, A. R.; Medintz, I. L.; Mauro, J. M.; Fisher, B. R.; Bawendi, M. G.; Mattoussi,

H. Fluorescence Resonance Energy Transfer Between Quantum Dot Donors and Dye-Labeled Protein Acceptors. *J. Am. Chem. Soc.* **2004**, *126*, 301–310.

(20) Medintz, I. L.; Mattoussi, H. Quantum Dot-Based Resonance Energy Transfer and Its Growing Application in Biology. *Phys. Chem. Chem. Phys.* **2009**, *11*, 17–45.

(21) Funston, A. M.; Jasieniak, J. J.; Mulvaney, P. Complete Quenching of CdSe Nanocrystal Photoluminescence by Single Dye Molecules. *Adv. Mater.* **2008**, *20*, 4274–4280.

(22) Snee, P. T.; Somers, R. C.; Nair, G.; Zimmer, J. P.; Bawendi, M. G.; Nocera, D. G. A Ratiometric CdSe/ZnS Nanocrystal pH Sensor. J. Am. Chem. Soc. **2006**, 128, 13320-13321.

(23) Wang, C.; Weiss, E. A. Sub-Nanosecond Resonance Energy Transfer in the Near-Infrared within Self-Assembled Conjugates of PbS Quantum Dots and Cyanine Dye J-Aggregates. *J. Am. Chem. Soc.* **2016**, *138*, 9557–9564.

(24) He, C.; Weinberg, D. J.; Nepomnyashchii, A. B.; Lian, S.; Weiss, E. A. Control of the Redox Activity of PbS Quantum Dots by Tuning Electrostatic Interactions at the Quantum Dot/Solvent Interface. *J. Am. Chem. Soc.* **2016**, *138*, 8847–8854.

(25) Ishikawa-Ankerhold, H. C.; Ankerhold, R.; Drummen, G. P. Advanced Fluorescence Microscopy Techniques—FRAP, FLIP, FLAP, FRET and FLIM *Molecules* **2012**, *17*, 4047-4132.

(26) Praveen, V. K.; Ranjith, C.; Bandini, E. Assemblies : Versatile Materials for Excitation. *Chem. Soc. Rev.* **2014**, *43,* 4222–4242.

(27) Tvrdy, K.; Frantsuzov, P. A.; Kamat, P. V. Photoinduced Electron Transfer from Semiconductor Quantum Dots to Metal Oxide Nanoparticles. *Proc. Natl. Acad. Sci.* **2011**, *108*, 29–34.

(28) Lian, S.; Kodaimati, M. S.; Dolzhnikov, D. S.; Calzada, R.; Weiss, E. A. Powering a CO_2 Reduction Catalyst with Visible Light through Multiple Sub-Picosecond Electron Transfers from a Quantum Dot. *J. Am. Chem. Soc.* **2017**, *139*, 8931-8938.

(29) Shibu, E. S.; Sonoda, A.; Tao, Z.; Feng, Q.; Furube, A.; Masuo, S.; Wang, L.; Tamai, N.; Ishikawa, M.; Biju, V. Photofabrication of Fullerene-Shelled Quantum Dots Supramolecular Nanoparticles for Solar Energy Harvesting. *ACS Nano* **2012**, *6*, 1601-1608.

(30) Kärkäs, M. D.; Johnston, E. V.; Verho, O.; Akermark, B. Artificial Photosynthesis: From Nanosecond Electron Transfer to Catalytic Water Oxidation. *Acc. Chem. Res.* **2014**, *47*, 100–111.

(31) Kärkäs, M. D.; Verho, O.; Johnston, E. V.; Åkermark, B. Artificial Photosynthesis: Molecular Systems for Catalytic Water Oxidation. *Chem. Rev.* **2014**, *114*, 11863–12001.

(32) Sapsford, K. E.; Berti, L.; Medintz, I. L. Materials for Fluorescence Resonance Energy Transfer Analysis: Beyond Traditional Donor-Acceptor Combinations. *Angew. Chem. Int. Ed.* **2006**, *45*, 4562–4588.

(33) Zeng, Y.; Li, Y. Y.; Chen, J.; Yang, G.; Li, Y. Dendrimers: A Mimic Natural Light-Harvesting System. *Chem. - An Asian J.* **2010**, *5*, 992–1005.

(34) Ajayaghosh, A.; Praveen, V. K.; Vijayakumar, C. Organogels as Scaffolds for Excitation Energy Transfer and Light Harvesting. *Chem. Soc. Rev.* **2008**, *37*, 109–122.

(35) Murphy, C. J.; Coffer, J. L. Quantum Dots: A Primer. *Applied Spectroscopy*, **2002**, *56*, 16A-27A.

(36) Frischmann, P. D.; Mahata, K.; Würthner, F. Powering the Future of Molecular Artificial Photosynthesis with Light-Harvesting Metallosupramolecular Dye Assemblies. *Chem. Soc. Rev.* **2013**, *42*, 1847–1870.

(37) Bawendi, M. G.; Steigerwald, L. The quantum mechanics of larger semiconductor clusters (" QUANTUM DOTS "). *Annu. Rev. Phys. Chem.* **1990**, *4*, 477–496.

(38) Alivisatos, A. P. Semiconductor Clusters, Nanocrystals, and Quantum Dots. *Science*, **1996**, *271*, 933-937.

(39) Wu, X.; Liu, H.; Liu, J.; Haley, K. N.; Treadway, J. A.; Larson, J. P.; Ge, N.; Peale, F.; Bruchez, M. P. Immunofluorescent Labeling of Cancer Marker Her2 and Other Cellular Targets with Semiconductor Quantum Dots. *Nat. Biotechnol.* **2003**, *21*, 41-46.

(40) Brus, L. Electronic Wave Functions in Semiconductor Clusters: Experiment and Theory. *J. Phys. Chem.* **1986**, *90,* 2555-2560.

(41) Sperling, R. Surface Modification and Functionalization of Colloidal Nanoparticles, *Diss. Dr. rer. nat. Wiesbaden-Marburg-Lahn*, **2008**, *21*, 1451–1456.

(42) Saha, K.; Agasti, S. S.; Kim, C.; Li, X.; Rotello, V. M. Gold Nanoparticles in Chemical and Biological Sensing. *Chem. Rev.* **2012**, *112*, 2739−2779.

(43) Bishop, K. J. M.; Wilmer, C. E.; Soh, S.; Grzybowski, B. A. Nanoscale Forces and their uses in Self-Assembly. *Small* **2009**, *5,* 1600−1630

(44) Kalsin, A. M.; Kowalczyk, B.; Smoukov, S. K.; Klajn, R.; Grzybowski, B. A. Ionic-Like Behavior of Oppositely Charged Nanoparticles. *J. Am. Chem. Soc.* **2006**, *128*, 15046−15047.

(45) Pillai, P. P.; Huda, S.; Kowalczyk, B.; Grzybowski, B. A. Controlled pH Stability and Adjustable Cellular Uptake of Mixed Charge Nanoparticles. *J. Am. Chem. Soc.* **2013**, *135*, 6392−6395.

(46) Bishop, K. J. M.; Wilmer, C. E.; Soh, S.; Grzybowski, B. A. Nanoscale Forces and Their Uses in Self-Assembly. *Small* **2009**, *5*, 1600–1630.

(47) Förster, T. 10th Spiers Memorial Lecture. Transfer Mechanisms of Electronic Excitation. *Discuss. Faraday Soc.* **1959**, *27*, 7−17.

(48) Mork, A. J.; Weidman, M. C.; Prins, F.; Tisdale, W. A. Magnitude of the Förster Radius in Colloidal Quantum Dot Solids. *J. Phys. Chem. C* **2014,** *118*, 13920−13928.

(49) Oertel, D. C.; Bawendi, M. G.; Arango, A. C.; Bulović, V. Photodetectors based on treated CdSe Quantum-Dot Films. *Appl. Phys. Lett.* **2005**, *87*, 213505.

(50) Kagan, C. R.; Murray, C. B.; Bawendi, M. G. Long-range Resonance Transfer of Electronic Excitations in Close-packed CdSe Quantum-Dot Solids. *Phys. Rev. B: Condens. Matter Mater. Phys.* **1996**, *54*, 8633−8643.

(51) Lu, H.; Scho, O.; Woggon, U.; Niemeyer, C. M. Self-Assembled Donor Comprising Quantum Dots and Fluorescent Proteins for Long-Range Fluorescence Resonance Energy Transfer. *J. Am. Chem. Soc.* **2008**, 130, 4815-4827.

(52) Jou, A. F-J.; Lu, C-H.; Ou, Y-C.; Wang, S-S.; Hsu, A-L.; Willner, I.; Ho, J-A. A. Diagnosing the miR-141 Prostate Cancer Biomarker Using Nucleic acid-Functionalized CdSe/ZnS QDs and Telomerase. *Chem. Sci.,* **2015**, *6*, 659-665.

(53) Chou, K. F.; Dennis, A. M. Förster Resonance Energy Transfer between Quantum Dot Donors and Quantum Dot Acceptor. *Sensors*, **2015**, *15*, 13288-13325.

(54) Beane, G.; Boldt, K.; Kirkwood, N.; Mulvaney, P. Energy Transfer between Quantum Dots and Conjugated Dye Molecules. *J. Phys. Chem. C* **2014**, *118*, 18079−18086.

(55) Medintz, I. L.; Sapsford, K. E.; Clapp, A. R.; Pons, T.; Higashiya, S.; Welch, J. T.; Mattoussi, H.; Uni, V.; Boule, V.; Engineering, B. Designer Variable Repeat Length Polypeptides as Scaffolds for Surface Immobilization of Quantum Dots. *J. Phys. Chem. B* **2006**, *110*,10683–10690.

(56) Pons, T.; Medintz, I. L.; Sapsford, K. E.; Higashiya, S.; Grimes, A. F.; English, D. S.; Mattoussi, H.; On the Quenching of Semiconductor Quantum Dot Photoluminescence by Proximal Gold Nanoparticles. *Nano Lett.* **2007**, *7*, 3157-3164.

(57) Kodaimati, M. S.; Wang, C.; Chapman, C.; Schatz, G. C.; Weiss, E. A. Distance-Dependence of Interparticle Energy Transfer in the Near-Infrared within Electrostatic Assemblies of PbS Quantum Dots. *ACS Nano* **2017**, *11*, 5041−5050.

(58) Li, M.; Cushing, S. K.; Wang, Q.; Shi, X.; Hornak, L. A.; Hong, Z. Wu, N., Size-Dependent Energy Transfer between CdSe/ZnS Quantum Dots and Gold Nanoparticles. *J. Phys. Chem. Lett*, **2011,** 2, 2125-2129.

(59) Li, X.; Slyker, L. W.; Nichols, V. M.; Pau, G. S. H.; Bardeen, C. J.; Tang, M. L. Ligand Binding to Distinct Sites on Nanocrystals Affecting Energy and Charge Transfer. *J. Phys. Chem. Lett.* **2015**, *6*, 1709−1713.

(60) Idowu, M.; Chen, J. Y.; Nyokong, T. Photoinduced Energy Transfer between Water Soluble CdTe Quantum Dots and Aluminium Tetrasulfonated Phthalocyanine. *New J. Chem.* **2008**, *32*, 290−296.

(61) Klajn, R. Spiropyran-Based Dynamic Materials. *Chem. Soc. Rev*. **2014**, *43*, 148-184.

(62) Bahr, J. L.; Kodis, G.; Garza, L. De; Lin, S.; Moore, A. L.; Moore, T. A.; Gust, D. Photoswitched Singlet Energy Transfer in a Porphyrin - Spiropyran Dyad. *J. Am. Chem. Soc.* **2001**, *123*, 7124-7133.

(63) Medintz, I. L.; Trammell, S. A.; Mattoussi, H.; Mauro, J. M. Reversible Modulation of Quantum Dot Photoluminescence Using a Protein- Bound Photochromic Fluorescence Resonance Energy Transfer Acceptor. J. Am. Chem. Soc. **2004**, *126*, 30-31**.**

(64) Tücks, A.; Beck, H. P. The Photochromic Effect of Bismuth Vanadate Pigments. Part I: Synthesis, Characterization and Lightfastness of Pigment Coatings. *J. Solid State Chem.* **2005**, *178*, 1145-1156.

(65) Pu, S. Z.; Yang, T. S.; Xu, J. K.; Shen, L.; Li, G. Z.; Xiao, Q.; Chen, B. Syntheses and Optoelectronic Properties of Four Photochromic Dithienylethenes. *Tetrahedron* **2005**, *61*, 6623-6629.

(66) Matsushima, R.; Morikane, H.; Kohno, Y. Oxazolylfulgides as Yellow Photochromic Dyes. *Chem. Lett.* **2003**, *32*, 302-303.

(67) Zhang, Y.; Wu, G.; Liu, F.; Ding, C.; Zou, Z.; Shen, Q. Photoexcited Carrier Dynamics in Colloidal Quantum Dot Solar Cells: Insights into Individual Quantum Dots, Quantum Dot Solid Films and Devices. *Chem. Soc. Rev.* **2020**, *49*, 49-84.

(68) Knowles, K. E.; Peterson, M. D.; McPhail, M. R.; Weiss, E. A. Exciton Dissociation within Quantum Dot–Organic Complexes: Mechanisms, Use as a Probe of Interfacial Structure, and Applications. *J. Phys. Chem. C*, **2013**, *117*, 10229-10243.

(69) Dibbell, R. S.; Watson, D. F. Distance-Dependent Electron Transfer in Tethered Assemblies of CdS Quantum Dots and TiO_2 Nanoparticles. *J. Phys. Chem. C* **2009**, *113*, 3139−3149.

(70) Dibbell, R. S.; Youker, D. G.; Watson, D. F. Excited-State Electron Transfer from CdS Quantum Dots to TiO$_2$ Nanoparticles via Molecular Linkers with Phenylene Bridges. *J. Phys. Chem. C* **2009**, *113*, 18643−18651.

(71) Wang, H.; McNellis, E. R.; Kinge, S.; Bonn, M.; Cánovas, E. Tuning Electron Transfer Rates through Molecular Bridges in Quantum Dot Sensitized Oxides. *Nano Lett.* **2013**, *13*, 5311−5315.

(72) Pernik, D. R.; Tvrdy, K.; Radich, J. G.; Kamat, P. V. Tracking the Adsorption and Electron Injection Rates of CdSe Quantum Dots on TiO$_2$: Linked versus Direct Attachment. *J. Phys. Chem. C* **2011**, *115*, 13511−13519.

(73) Hyun, B. R.; Bartnik, A. C.; Sun, L. F.; Hanrath, T.; Wise, F. W. Control of Electron Transfer from Lead-Salt Nanocrystals to TiO2. *Nano Lett.* **2011**, *11*, 2126−2132.

(74) Jin, S.; Tagliazucchi, M.; Son, H.-J.; Harris, R. D.; Aruda, K. O.; Weinberg, D. J.; Nepomnyashchii, A. B.; Farha, O. K.; Hupp, J. T.; Weiss, E. A. Enhancement of the Yield of Photoinduced Charge Separation in Zinc Porphyrin−Quantum Dot Complexes by a Bis(dithiocarbamate) Linkage. *J. Phys. Chem. C* **2015**, *119*, 5195−5202.

(75) Yan, Y.; Warren, S. C.; Fuller, P.; Grzybowski, B. A. Chemoelectronic circuits based on metal nanoparticles. *Nat. Nanotechnol.* **2016**, *11*, 603-608.

(76) Ling, D.; Hackett, M. J.; Hyeon, T. Surface Ligands in Synthesis, Modification, Assembly and Biomedical Applications of Nanoparticles. *Nano Today* **2014**, *9*, 457-477.

(77) Boles, M. A.; Ling, D.; Hyeon, T.; Talapin, D. V. The Surface Science of Nanocrystals. *Nat. mat*. **2016,** 15, 141-153.

(78) Batista, C. A. S.; Larson, R. G.; Kotov, N. A. Nonadditivity of Nanoparticle Interactions. *Science* **2015**, *350*, 1242477−1242487.

(79) Walker, D. A.; Kowalczyk, B.; de la Cruz, M. O.; Grzybowski, B. A. Electrostatics at the Nanoscale. *Nanoscale* **2011**, *3*, 1316−1344.

(80) Luo, D.; Yan, C.; Wang, T. Interparticle Forces Underlying Nanoparticle Self-Assemblies. *Small* **2015**, *11*, 5984−6008.

(81) Min, Y.; Akbulut, M.; Kristiansen, K.; Golan, Y.; Israelachvili, J. The Role of Interparticle and External Forces in Nanoparticle Assembly. *Nat. Mater.* **2008**, *7*, 527−538.

(82) Albanese, A.; Tang, P. S.; Chan, W. C. W. The Effect of Nanoparticle Size, Shape, and Surface Chemistry on Biological Systems. *Annu. Rev. Biomed. Eng.,* **2012**, *14*, 1−16.

(83) Liu, X.; Li, H.; Jin, Q.; Ji, J. Surface Tailoring of Nanoparticles via Mixed-Charge Monolayers and their Biomedical Applications. *Small*, **2014**, *10*, 4230–4242.

(84) Zhou, J.; Liu, Y.; Tang, J.; Tang, W. Surface Ligands Engineering of Semiconductor Quantum Dots for Chemosensory and Biological Applications. *Mater. Today,* **2017**, *20*, 360–376.

(85) Albanese, A.; Tang, P. S.; Chan, W. C. W. The Effect of Nanoparticle Size, Shape, and Surface Chemistry on Biological Systems. *Annu. Rev. Biomed. Eng.,* **2012**, 14, 1-16.

(86) Schiffman, J. D.; Schiffman J. D.; Balakrishna, R. G., Quantum Dots as Fluorescent probes: Synthesis, Surface Chemistry, Energy Transfer Mechanisms, and Applications. *Sensors and Actuators B:* **2018**, *258*, 1191-1214.

(87) Nag, A.; Kovalenko, M. V.; Lee, J. S.; Liu, W.; Spokoyny, B.; Talapin, D. V. Metal-free inorganic ligands for colloidal nanocrystals: S^{2-}, HS^-, Se^{2-}, HSe^-, Te^{2-}, HTe^-, TeS_3^{2-}, OH^-, and NH_2^- as surface ligands. *J. Am. Chem. Soc.* **2011**, *133*, 27, 10612–10620.

(88) Hines, D. A.;. Kamat, P. V. Recent Advances in Quantum Dot Surface Chemistry. *ACS Appl. Mater. Interfaces* **2014**, *6*, 3041–3057.

(89) Bilan, R.; Fleury, F.; Nabiev, I.; Sukhanova, A., 2015. Quantum Dot Surface Chemistry and Functionalization for Cell Targeting and Imaging.

Chapter 2

Electrostatically Driven Förster Resonance Energy Transfer in Cationic InP/ZnS Quantum Dots
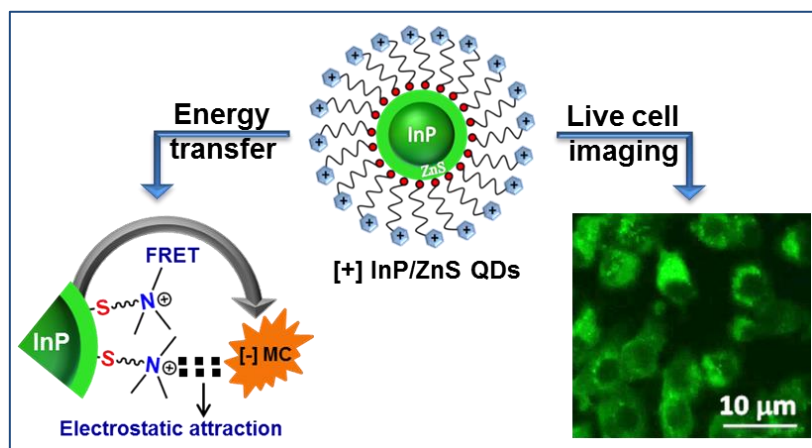
Devatha, G.; Roy, S.; Rao, A.; Mallick, A.; Basu, S.; Pillai, P. P.* Electrostatically Driven Resonance Energy Transfer in "Cationic" Biocompatible Indium Phosphide Quantum Dots. *Chem. Sci.* **2017**, *8*, 3879–3884.

2.1 Abstract

Indium Phosphide Quantum Dots (InP QDs) have emerged as an alternative to toxic metal ion based QDs in nanobiotechnology. The ability to generate cationic surface charge, without compromising stability and biocompatibility, is essential in realizing the full potential of InP QDs in biological applications. We have addressed this challenge by developing a place exchange protocol for the preparation of cationic InP/ZnS QDs. The quarternary ammonium group provides the much required permanent positive charge and stability to InP/ZnS QD in biofluids. The cationic InP/ZnS QDs retain ~80 % quantum yield with respect to parent QDs. The two important properties of QDs, namely bioimaging and light induced resonance energy transfer, are successfully demonstrated in cationic InP/ZnS QDs. The low cytotoxicity and stable photoluminescence of cationic InP/ZnS QDs inside cells make them ideal candidates as optical probes for cellular imaging. An efficient resonance energy transfer (E ~60 %) is observed, under physiological conditions, between the cationic InP/ZnS QD donor and anionic dye acceptor. A large bimolecular quenching constant along with a linear Stern-Volmer plot confirms the formation of a strong ground state complex between cationic InP/ZnS QD and anionic dye. Control experiments prove the role of electrostatic attraction in driving the light induced interactions, which can rightfully form the basis for future nanobio studies between cationic InP/ZnS QDs and anionic biomolecules.

2.2 Introduction

Electrostatic forces play a pivotal role in controlling the interactions between biomolecules and nanomaterials.[1-6] In this regard, cationic nanoparticles form an integral part of nanobiotechnology as they provide a complementary surface charge for binding with anionic biomolecules.[7-11] The unique size dependent luminescence properties of Quantum Dots (QDs) are an added advantage over metal nanoparticles in various biomedical applications like imaging, targeting and therapeutics.[12-19] One of the promising uses of QDs is in Förster Resonance Energy Transfer (FRET) based assays in monitoring various biomolecular processes including protein folding and sensing.[20-32] To achieve this goal, extensive research has been carried out to understand the energy transfer process in QDs based on Cd, Pb, Se, etc.[20-32] Mattoussi and co-workers used the luminescent CdSe/ZnS core/shell quantum dots as energy donors and a cyanine dye (Cy3) labelled maltose binding protein as energy acceptor, in FRET assay. The efficiency of FRET was controlled either by tuning the emission of QD or by altering the number of dye-labelled proteins immobilized on the QD (**Figure 2.1**).[20]
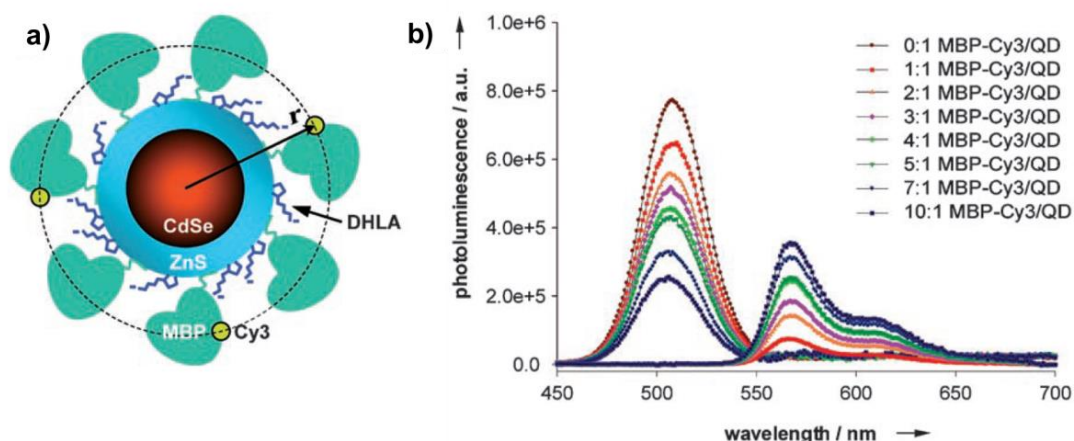
Figure 2.1: a) Schematic representation of a QD–protein–dye assembly. b) Evolution of the PL spectra obtained from titrating 510-nm emitting QDs with an increasing ratio, in QD–MBP–Cy3 assemblies (Reproduced in part with permission from reference 20. Copyright 2004 American Chemical Society).

In another elegant work, Nocera and co-workers have attached the pH sensitive squaraine dye on the QD surface via EDC coupling. The efficiency of FRET was modulated by varying the solution pH, and this was further used as a tool for chemical and biological sensing (**Figure 2.2**).[28]
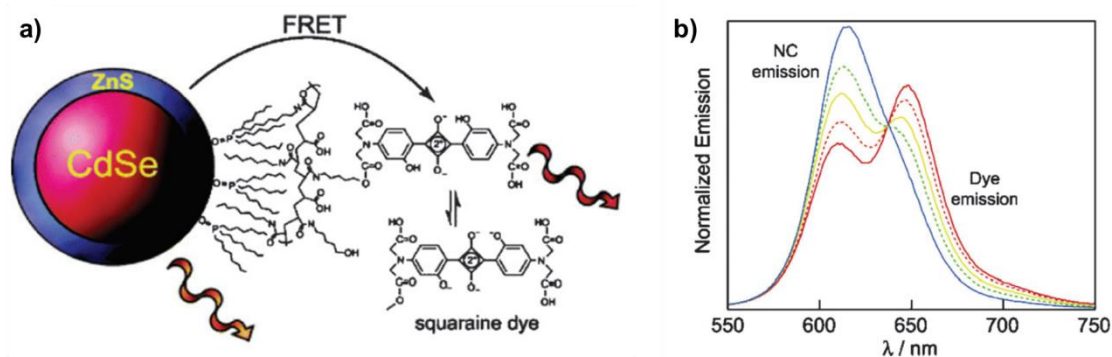
Figure 2.2: a) Schematic representation of a FRET based pH sensor constructed from CdSe–ZnS QD coupled to a pH-sensitive squaraine dye. b) Changes in the emission profile of a QD-squaraine dye conjugate as a function of pH (red 6.0; orange 7.0; yellow 8.0; green 9.0; and blue 10); samples were excited at 380 nm (Reproduced in part with permission from reference 28. Copyright 2006 American Chemical Society).

However, the increasing restrictions on the use of toxic metal ions have led to the search for environmentally friendly QDs possessing adequate biocompatibility and surface chemistries. InP QDs have emerged as an alternative due to their low toxicity and high tunability of emission in the near-infrared (NIR) region.[33-50] Recently, Thomas and co-workers have

showed that InP/ZnS QD is a versatile and environmentally friendly material for energy transfer applications, in both organic and aqueous solvents, by labelling with appropriate chromophoric dyes (**Figure 2.3**).[50]
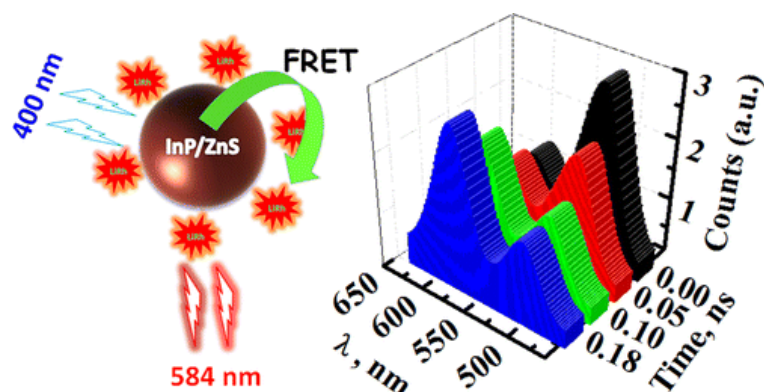
Figure 2.3: Schematic representation of resonance energy transfer process in InP/ZnS-dye complex, and the corresponding time resolved PL spectrum (Reproduced in part with permission from reference 50. Copyright 2014 American Chemical Society).

Another challenge in the area of QD, in general, is the lack of flexibility in tuning their surface chemistries. On top of this, the challenges associated with the synthesis of InP QDs[34,35] have mainly led to limited studies on their surface engineering,[49] especially those with a cationic surface charge. Apart from the fundamental perspective, the lack of ability to install a cationic surface charge on QDs can limit their use in various biological applications as well. A common strategy adopted in the literature to generate cationic charge is by functionalizing the anionic QDs with bifunctional biomolecules to impart a pH dependent cationic charge, which then facilitates the bio-nano interactions.[38-40,51-55] Among other problems, this strategy will increase the hydrodynamic diameter of nanohybrid systems beyond the limit of renal clearance.[15] Thus, it is always advantageous to have a permanent cationic ([+]) charge on QDs in the first place as it reduces the structural complexities. In fact, there are very few reports on cationic QDs that carry a permanent positive surface charge,[56-63] in comparison to metal nanoparticles.[64,65] Talapin and co-workers were successful in attaching an ionizable secondary amine on the surface of CdSe and CdTe QDs. However, the functionalization of these secondary amines on the surface of InP QDs was not achievable, because of the poor quantum efficiency of InP QDs.[56] Recently, Rotello and co-workers used a non-ionizable tertiary amine to prepare cationic CdSe QDs through two-step ligand exchange process (**Figure 2.4**).[57]
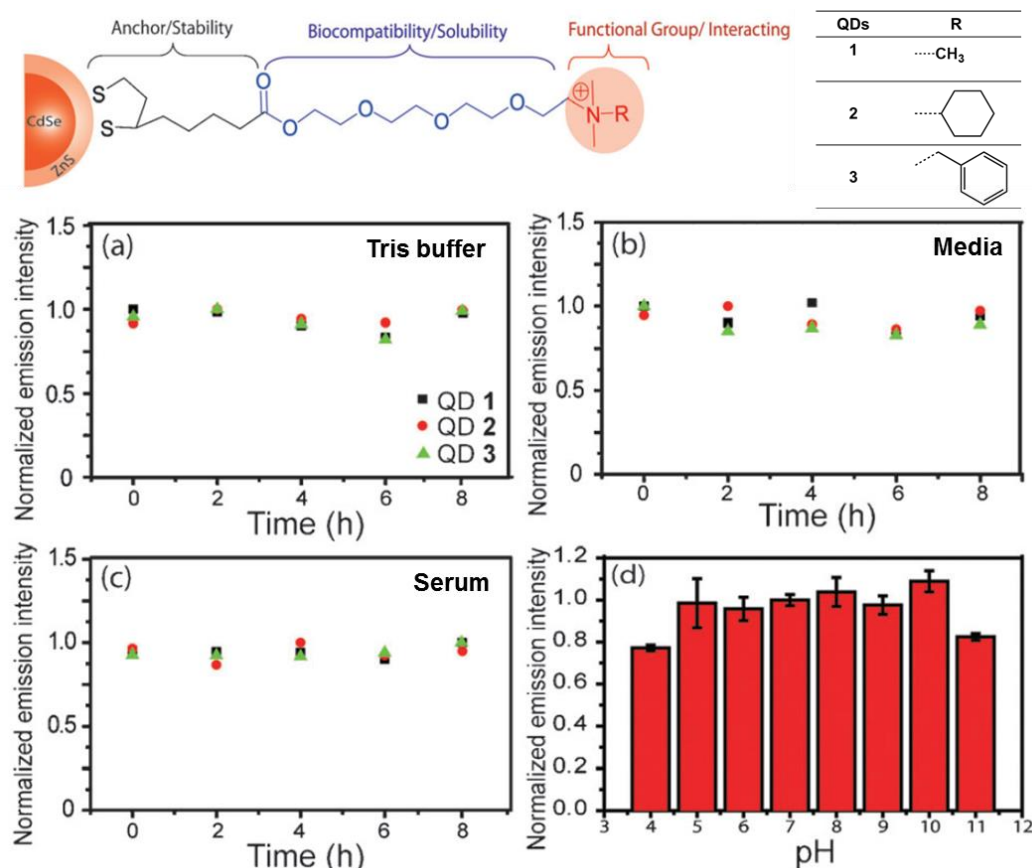
Figure 2.4: Design of dithiol cationic ligand: Stability of cationic CdSe/ZnS QDs in a) Tris buffer, b) cell culture media, and c) serum. d) PL of cationic CdSe/ZnS QDs QDs in different pH phosphate buffers after incubation for 6 h. (Reproduced in part with permission from reference 57. Copyright 2011 Royal Society of Chemistry).

Lack of availability of cationic InP QDs motivated us to develop a reproducible and robust protocol for achieving the same, and this forms the basis of this Chapter. Along with surface engineering, the ability of [+] InP/ZnS QDs to participate in energy transfer studies needs to be explored as well, to improve its potential in the area of light harvesting. Here, we address both the above mentioned issues and report an efficient light induced resonance energy transfer in [+] InP QDs under physiological conditions. A large bimolecular quenching constant along with a linear Stern-Volmer plot confirms the formation of a strong ground state complex between cationic InP/ZnS QDs and anionic dyes. The highlight of the present work was the use of electrostatic forces to control the light induced interactions, which can form the basis for future nanobio studies between [+] InP/ZnS QDs and [-] biomolecules. Moreover, the stable photoluminescence of [+] InP/ZnS QDs inside the cells, coupled with its low cytotoxicity, make them ideal candidates as optical probes for cellular imaging.

2.3 Experimental Section

2.3.1 Materials and Reagents:

Indium acetate, myristic acid (MA), octylamine, tetramethylammonium hydroxide (TMAOH) 25 % wt. in water, 11-mercaptoundecanoic acid (MUA), merocyanine-540 (MC) and 1, 1'-diethyl- 2, 2'-cyanine iodide (CY) were purchased from Sigma-Aldrich. Tris (trimethylsilyl phosphine) was purchased from Strem Chemicals. Dodecyl Amine (DDA), acetonitrile (ACN), DMEM media and 3-(4, 5-dimethylthiazol-2-yl)-2,5-diphenyltetrazolium bromide (MTT) were purchased from HiMedia. All the reagents were used as received without any further purification. N, N, N-trimethyl(11-mercaptoundecyl)ammonium chloride (TMA) was synthesized according to reported procedure.[66]

2.3.2 Synthesis of InP/ZnS quantum dots:

The synthesis was carried out by following the reported procedures.[50] Briefly, indium acetate (0.4 mmol, 0.112 g), myristic acid (1.54 mmol, 0.35 g), and 5 mL octadecene were loaded in a three-necked RB and heated to 120 $^{\circ}$C under N_2 atmosphere. The reaction mixture was evacuated for 30 min at 120 $^{\circ}$C, further raised to 200 $^{\circ}$C and a solution containing tris(trimethylsilyl phosphine; 0.2 mmol, 58 μL) and octylamine (2.4 mmol, 400 μL) in octadecene (1 mL) was injected. After desired crystal growth, the reaction was arrested by reducing the reaction temperature to 130 $^{\circ}$C. The InP QDs formed were further overcoated with ZnS in the same reaction vessel. An injection mixture containing diethylzinc (684 μL, 1 M solution in hexane) and hexamethyldisilathiane (128 μL) in 2 mL octadecene was added dropwise, under gentle stirring over a period of 30 min. After the addition is complete, the reaction mixture was raised to 200 $^{\circ}$C and stirring was continued for 2 h, resulting in the formation of core shell InP/ZnS QDs. The reaction mixture was then cooled to room temperature by adding 5 mL of cold toluene to arrest the growth of ZnS shell. The resultant InP/ZnS QDs were purified by precipitating with ethanol, and redispersed in chloroform. This step was repeated two times, and the purified QDs were dispersed in chloroform for further studies.

2.3.3 Preparation of water-soluble [+] InP/ZnS QDs:

The water-soluble [+] InP/ZnS QDs were prepared through a place exchange reaction. In a typical place exchange experiment, 5 mL of QDs solution in chloroform (1.6 μM) was mixed with 2 mL of TMA solution (25 mg per mL). The mixture was stirred for about 4 h leading to a complete phase transfer of QDs from the organic phase to the aqueous phase. The phase

transfer can be easily monitored by the color change of chloroform (orange to colorless) and water (colorless to orange) phases. The bifunctional TMA ligand helped in both QD surface functionalization (via thiol group) as well as in the phase transfer process (via quaternary ammonium group). The aqueous phase was carefully separated and precipitated with acetone to remove excess TMA ligands. This step was repeated two times. Finally, the cationic QDs were redispersed in deionized water for further studies. A similar procedure was adopted for the preparation of anionic [-] InP/ZnS QD by feeding a basic solution of 11-mercapto undecanoic acid as the ligand during the place exchange reaction.

2.3.4 Energy transfer experiments:

Energy transfer experiments were performed with different charged InP/ZnS QDs donors and dye acceptors. In a typical experiment, a 3 mL aqueous solution of charged InP/ZnS QDs was prepared such that the absorbance was ~0.1 at the excitation wavelength (400 nm, corresponding to a concentration of ~0.8 μM). Different aliquots of oppositely charged dyes were added sequentially to the QD solution and spectral changes were monitored by using Shimadzu UV-3600 and Fluorolog-3 (HORIBA Scientific) spectrofluorometers. The corresponding lifetime measurements were carried out in an IBH picosecond time correlated single photon counting (TCSPC) system, upon excitation with a 405 nm laser source. The fluorescence decay profiles were de-convoluted using IBH data station software version 2.1, and fitted with exponential decay, minimizing the χ^2 values.

2.3.5 Time resolved emission spectroscopy (TRES) experiment:

TRES measurement is an excellent technique to monitor the excited state dynamics of molecules and to identify multiple emissive species present in a given system. TRES experiment of [+] InP/ZnS::: MC complex was carried out by collecting the transient lifetime profiles in the spectral range of 450−690 nm, with an interval of 4 nm. Time resolved emission spectra were constructed by slicing the transient profiles obtained at each wavelength.

2.3.6 Fourier-transform infrared spectroscopy (FTIR):

FTIR studies in solid state using KBr disc were obtained using NICOLET 6700 FTIR spectrometer.

2.3.7 High resolution transmission electron microscope (HRTEM) studies:

A drop of [+] InP/ZnS solution was placed on a 400 mesh carbon-coated copper grid (Ted Pella, Inc.), at ambient conditions, and allowing the excess solvent to evaporate under air in dust free conditions. The samples were further dried under vacuum and imaged on a JEOL 200 kV high-resolution transmission electron microscope.

2.3.8 Zeta potential measurements:

An aqueous solution of [+] InP/ZnS QD (~0.8 μM) was used in zeta-potential (ζ) studies by using a Zetasizer Nano series, Nano-ZS90 (Malvern Instruments, U.K.), equipped with 655 nm laser. The error was calculated from three different measurements on three different samples.

ζ was determined by measuring the electrophoretic mobility and using Henry's equation[67] –

$$U_E = \frac{2\varepsilon\zeta f(\kappa_a)}{3\eta}$$

Where,

U_E = electrophoretic mobility

ζ = zeta potential

ε = dielectric constant

η = viscosity

$f(\kappa_a)$ = Henry's function

Smoluchowski's approximation was used to measure the zeta potential values of NPs.

2.3.9 MTT assay:

The cytotoxicity studies were performed on MCF-7 cell line using tetrazolium salt, 3,4,5-dimethylthiazol-2,5-diphenyltetrazolium bromide (MTT) assay.[68] MCF-7 cells were seeded in 96-well plate (in DMEM with 10% FBS, 1% penicillin and 10 μg/mL insulin) and incubated overnight in a 5 % CO_2 incubator at 37 °C for attachment. After achieving a confluence of ~85 %, the cells were incubated with different concentrations of QDs for ~24 h. Then 20 μL of MTT reagent (5 mg/mL) was added to each well and incubated for 4 h at 37 °C. The purple formazan crystals formed from the reduction of MTT by mitochondrial dehydrogenase enzyme were solubilized in 100 μL of DMSO. The absorbance of formazan crystals at 570 nm was measured using a micro plate reader (Varioskan Flash), and was representative of the number of viable cells per well. The absorbance from QD was negligible

in the concentration range studied. All samples were assayed in triplicate and the percent cell viability was calculated considering the untreated cells as 100% viable.

2.3.10 Confocal microscopy:

Confocal imaging was performed on a Zeiss LSM 710 microscope. MCF-7 cells were seeded (5×10^4 cells/dish) on a coverslip in a 6 well plate and incubated overnight in a 5 % CO_2 incubator at 37 °C. Next day, old media was removed and cells were washed with cold PBS, and ~10 nM [+] InP/ZnS QD solution was added to the cells and incubated for 4 h. Thereafter, cells were washed with PBS three times before taking the images. The excitation source used was ~400 nm laser.

2.4 Background of Förster Energy Transfer (FRET) formalism:

FRET is a non-radiative energy transfer between excited fluorescent donor and a ground state acceptor molecule. In FRET, the energy is transferred nonradiatively from donor to acceptor.[67] This process results from the dipole-dipole interactions and is thus strongly dependent on the distance between the donor and acceptor. It requires an appreciable spectral overlap between donor emission and acceptor absorption.

The rate of energy transfer for a D-A pair separated by a distance r can be expressed as[69]

$$k_T(r) = \frac{1}{\tau_D}\left(\frac{R_0}{r}\right)^6 \tag{1}$$

Where, R_0 is given by

$$R_0 = 0.2018\left(\frac{\phi_D\,\kappa^2\,J(\lambda)}{\eta^4}\right)^{1/6} A^0 \tag{2}$$

And

$$J(\lambda) = \int_0^\infty F_D(\lambda)\epsilon_A(\lambda)\lambda^4\,d\lambda \quad M^{-1}\,cm^{-1}\,nm^4 \tag{3}$$

Where, R_0 is the Förster distance at which the efficiency is 50 %, r is the distance between donor and acceptor, τ_D is the lifetime of donor in absence of the acceptor, ϕ_D is the quantum yield of the donor in absence of acceptor, κ^2 is the orientation factor for the dipoles, $J(\lambda)$ is the spectral overlap between the emission of donor and absorption of the acceptor, η is the refractive index of the medium. $F_D(\lambda)$ is the normalized fluorescence intensity of the donor at a particular wavelength, ϵ_A is the molar extinction coefficient of the acceptor.

The efficiency of FRET can be calculated from steady state emission and lifetime experiments.

From steady state emission quenching,[69]

$$E = 1 - \frac{F_{DA}}{F_D} \qquad (4)$$

From lifetime quenching studies, [69]

$$E = 1 - \frac{\tau_{DA}}{\tau_D} \qquad (5)$$

F_{DA}, τ_{DA} are the fluorescence intensity and lifetime of the donor in the presence of acceptor, and F_D, τ_D are the fluorescence intensity and lifetime of the donor in the absence of acceptor.

The nature of binding between the [+] InP/ZnS QD and [-] MC dyes was examined by Stern−Volmer analysis. The Stern−Volmer quenching constant was determined by the following equation.[69]

$$\frac{I_0}{I} = 1 + K_{SV}[Q] \qquad (6)$$

$$K_{SV} = k_q \tau_0 \qquad (7)$$

Where I_0 is the emission intensity of the donor [+] InP/ZnS QDs in the absence of the [-] MC dye, I is the emission intensity of donor in the presence of acceptor [-] MC, K_{SV} is the Stern-Volmer constant, [Q] is the concentration of the quencher [-] MC dye, k_q is the bimolecular quenching constant and τ_0 is the lifetime of donor [+] InP/ZnS QD in the absence of acceptor [-] MC dye.

The distance between donor and acceptor was calculated from the following equation:[69]

$$E = \frac{R_0^6}{R_0^6 + r^6} \qquad (8)$$

Here, E is the energy transfer efficiency calculated from the steady state experiments by using equation (4), R_0 is the Förster distance at which the efficiency is 50 % (calculated from equations (2) and (3)) and r is the distance between the donor and the acceptor.

2.5 Results and Discussion

2.5.1 Synthesis and characterization of cationic InP/ZnS QDs:

The InP/ZnS QD carrying a permanent positive charge was prepared by a place exchange method (**Figure 2.5**). The hydrophobic InP/ZnS QD capped with myristic acid (MA), having an average core diameter of 2.8 ± 0.8 nm, were synthesized by following the reported procedure.[50] The deep electronic trap states formed by the dangling bonds on the surface of QDs are accounted for the broad emission of InP/ZnS QDs (full width at half-maximum, fwhm ~70 nm).[48,50] This was further inferred by a moderate quantum yield of ~12 % for InP/ZnS QD in chloroform, matching the reported values.[50] The myristic acid on the surface of InP/ZnS QD was then replaced with (N,N,N-trimethyl(11-mercaptoundecyl)ammonium chloride, TMA, [+]) ligand to impart the water solubility and cationic surface charge. In a typical synthesis, 5 mL of InP/ZnS QD solution (1.5 µM) in chloroform was mixed with 2 mL of TMA solution in water (25 mg per mL). A constant stirring for ~4 h ensured a complete phase transfer of InP/ZnS QDs to the aqueous layer.

MA Capped InP/ZnS QD
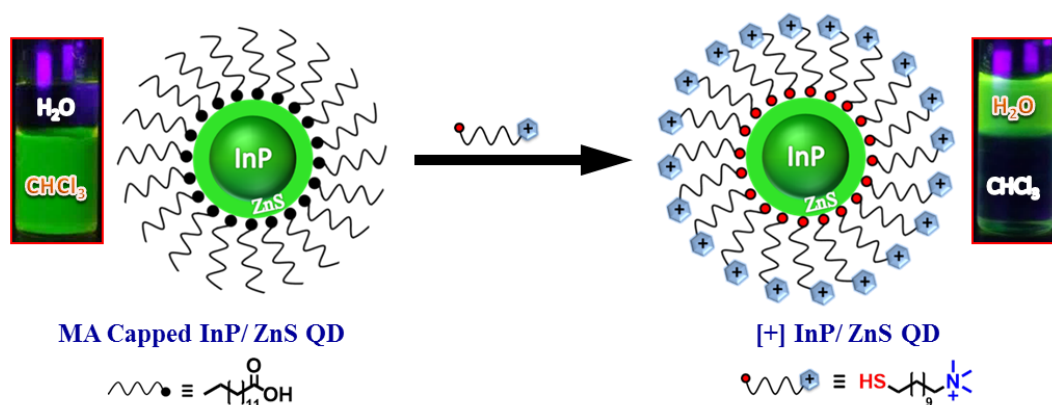
[+] InP/ZnS QD

Figure 2.5: Schematics for the synthesis of [+] InP/ZnS QD. Place exchange reaction between myristic acid capped InP/ZnS QD and [+] TMA ligand is represented. The photographs of the vials show the successful transfer of [+] InP/ZnS QD into aqueous layer.

The phase transfer process was followed by monitoring the color change of chloroform (orange to colorless) and water layers (colorless to orange). The aqueous layer was separated and precipitated with acetone to remove excess TMA ligands, and redispersed in deionized water for further studies. The bifunctional TMA ligand helped in both QD surface functionalization (via thiol group) as well as in the phase transfer process (via quarternary ammonium group). The [+] InP/ZnS QDs were well characterized using spectroscopic and microscopic techniques. The steady state studies revealed a negligible change in the

absorption and photoluminescence (PL) properties of [+] InP/ZnS QDs upon place exchange (**Figure 2.6a**). At the same time, the relative PL intensity and quantum yield calculations showed that the [+] InP/ZnS QDs retained ~80 % of its PL after the place exchange (Inset of **Figure 2.6a**). A decrease in PL is often observed in QDs upon water solubilization, which is attributed to the surface defects produced by thiol ligands.[70,71] The tri-exponential PL decay of InP/ZnS QDs was retained in the cationic form with an average lifetime of ~48 ns (**Figure 2.6b, and Table 2.1**). The high resolution transmission electron microscope (HRTEM) image shown in **Figure 2.6c** proves the size homogeneity and crystalline nature of [+] InP/ZnS QDs, with an interplanar distance of 0.287 nm corresponding to the zinc blende phase of bulk InP.[72] A zeta potential (ζ) value of $+52 \pm 2$ mV confirmed the successful functionalization of cationic TMA ligands on the surface of InP/ZnS QDs. The narrow charge distribution of ζ plot indicates that the [+] InP/ZnS QDs are well dispersed in aqueous medium (**Figure 2.6d**).
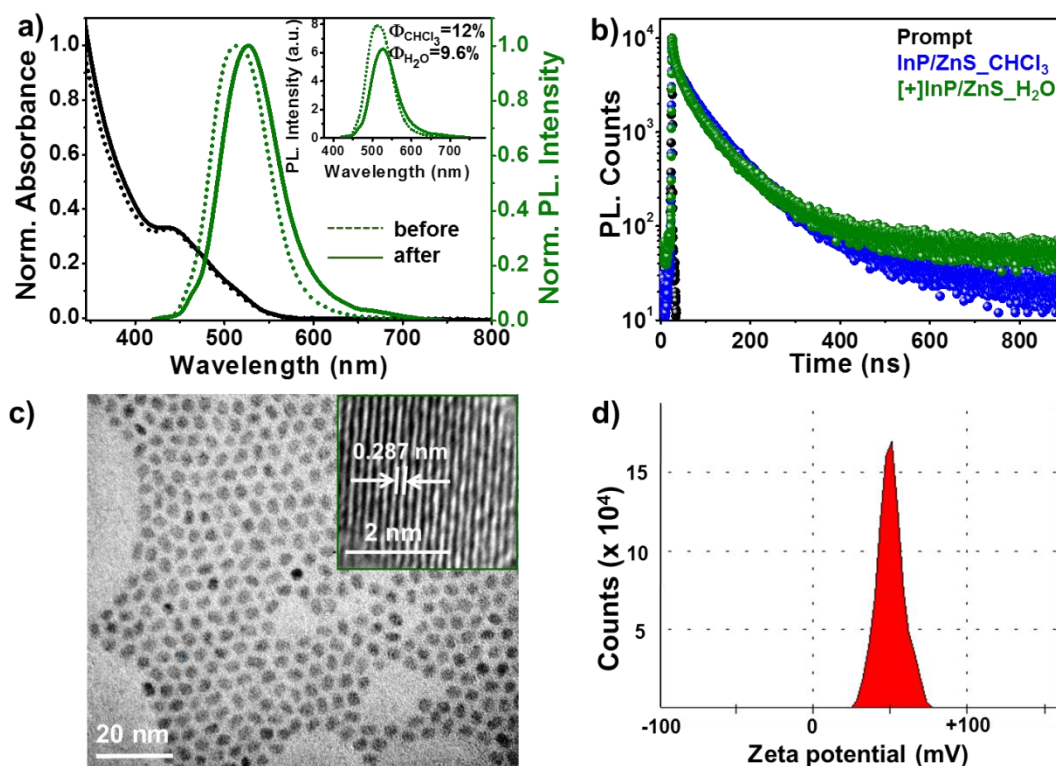
Figure 2.6: Spectroscopic and microscopic characterization of [+] InP/ZnS QDs. a) Normalized absorption and PL spectra of InP/ZnS QDs before and after place exchange reaction. The non-normalized PL spectra in the inset show that [+] InP/ZnS QD retained ~80 % of its PL after the place exchange. b) PL decay profiles of InP/ZnS QDs before and after the place exchange reaction. c) A representative HRTEM image of 2.8 ± 0.8 nm sized [+] InP/ZnS QD. The inset shows the lattice fringes with an interplanar distance of 0.287 nm, corresponding to the zinc blende phase of bulk InP.[72] d) A typical zeta potential plot (measured at pH ~7) confirming the cationic charge on the surface of InP/ZnS QDs.

Table 2.1: PL decay analysis of InP/ZnS QD in a time window of 1 μs.

Sample	τ_1 (ns)	a_1	τ_2 (ns)	a_2	τ_3 (ns)	a_3	Avg. τ (ns)	Chi. Sq
InP/ZnS_CHCl$_3$	1.29	0.66	43.75	0.26	112.6	0.08	71.25	1.15
TMA_InP/ZnS_H$_2$O	2.98	0.49	18.2	0.35	70.23	0.16	47.69	1.11

The absence of S-H stretching peak in the FTIR spectrum of [+] InP/ZnS QD further confirms that the TMA ligand is attached on the surface of InP/ZnS QDs via the thiol group[73] (**Figure 2.7**).
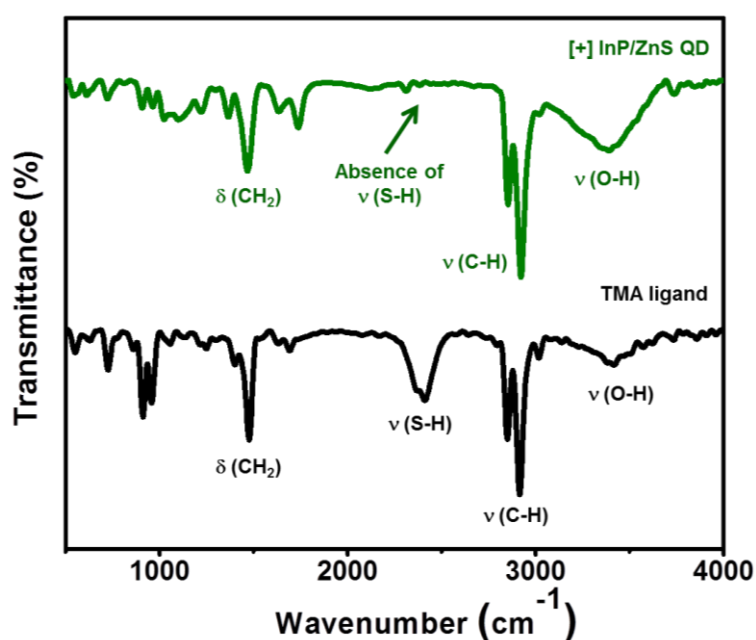
Figure 2.7: FTIR spectra of TMA ligand (black) and [+] InP/ZnS QD (green), along with the assignment of peaks.

2.5.2 Biocompatibility studies with [+] InP/ZnS QD:

In order to feature in biological applications, the [+] InP/ZnS QDs should satisfy the essential prerequisites of low cytotoxicity, and long-time stability in buffers and bio fluids. The colloidal stability of [+] InP/ZnS QDs was studied by monitoring their PL intensity for ~24 h, under various physiological conditions. **Figure 2.8** proves that the PL, and hence stability, of [+] InP/ZnS QDs is retained in PBS buffer, cell culture media, and a broad range of pH values. Further, the cytotoxicity of [+] InP/ZnS QDs was tested in MCF-7 cell line using the MTT assay (Details of cell viability studies are given in the Experimental Section). About 85 % of the cells were found to be alive after ~24 h of incubation with ~10 nM [+] InP/ZnS QDs

(**Figure 2.9**). The InP/ZnS QDs were found to be less cytotoxic than [+] CdSe/ZnS QDs, having a comparable size and surface charge (the Cd^{2+} ions leaked from the QD core are more toxic than In^{3+} ions, as reported previously[74,75]). The excellent stability and lower cytotoxicity of [+] InP/ZnS QDs paved their way as optical probes in cellular imaging studies. Live cell confocal imaging confirms the effective entry of [+] InP/ZnS QDs into MCF-7 cells (**Figure 2.10**).
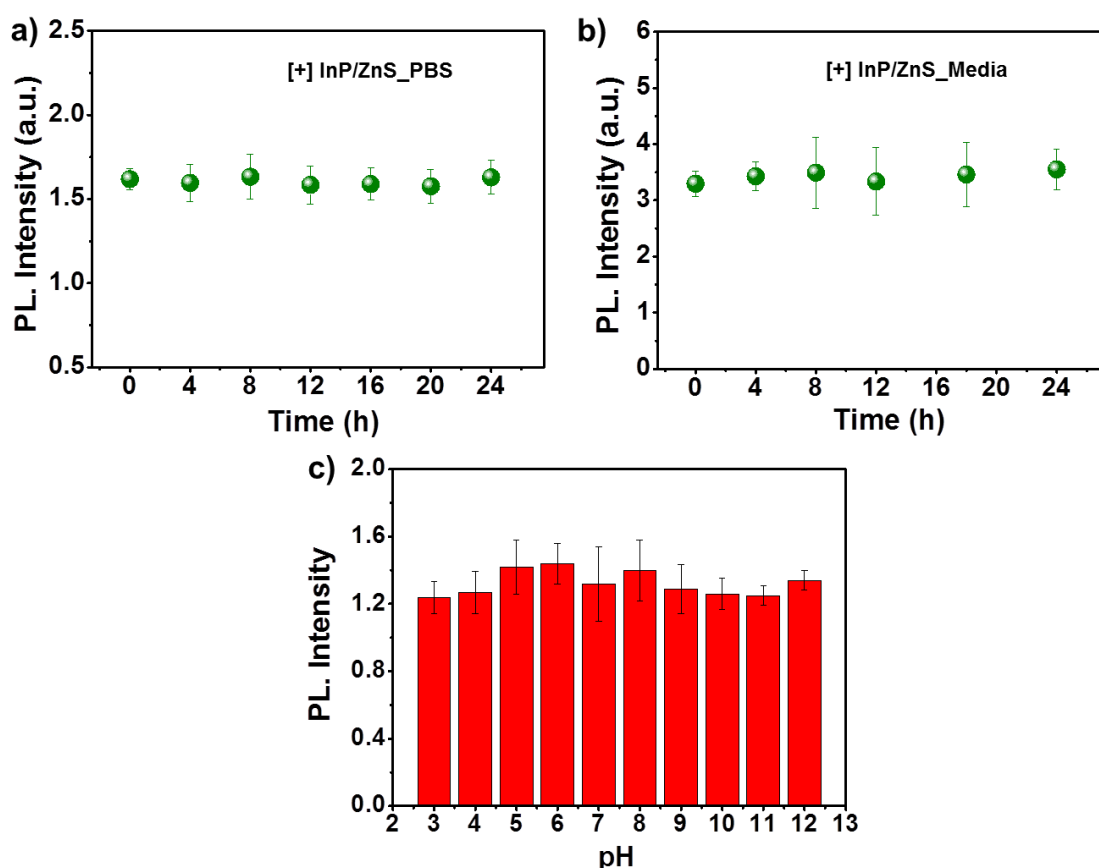
Figure 2.8: The persistence of PL, and hence stability, of [+] InP/ZnS QD in a) PBS, b) DMEM media (with 10 % FBS), and c) different pH values.

The subsistence of bright PL inside the cells, coupled with the low cytotoxicity, make [+] InP/ZnS QDs a practical alternative to toxic metal ion based QDs as optical probes for cellular imaging applications.
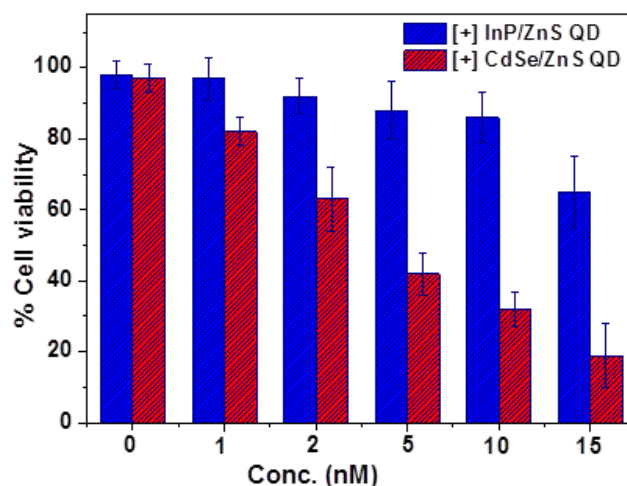
Figure 2.9: Biocompatibility of [+] InP/ZnS QDs. Viability of MCF-7 cells incubated with different concentrations of [+] InP/ZnS and [+] CdSe/ZnS QDs for 24 h.
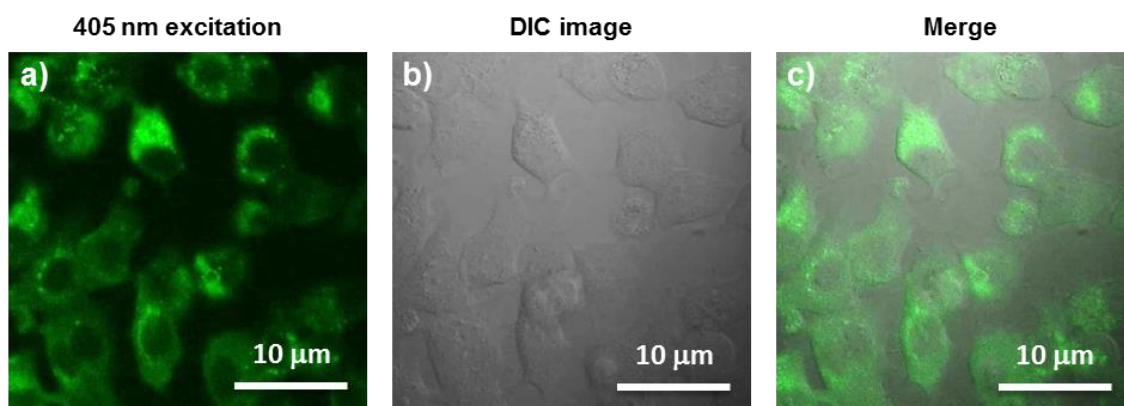
Figure 2.10: Fluorescent cell imaging by confocal microscopy of [+] InP/ZnS QD (10 nM) incubated with MCF-7 cells for 4 h: a) fluorescence, b) phase contrast (DIC), and c) merged images, upon excitation with 400 nm laser source.

2.5.3 Steady state resonance energy transfer studies:

Having established the protocol for the preparation of biocompatible [+] InP/ZnS QDs, our next focus was to utilize the cationic charge to drive the energy transfer to a complementary acceptor molecule. The idea here was to demonstrate a FRET based model study to prove the ability of [+] InP/ZnS QDs to indulge in electrostatically controlled interactions for future biological studies. In this view, merocyanine 540 dye (MC) was selected as the acceptor due to its anionic charge and excellent water solubility (**Figure 2.11**).[76] A high spectral overlap integral of 2.45×10^{15} $M^{-1}cm^{-1}nm^4$ assured that the [+] InP/ZnS QD and [-] MC dye forms an appropriate donor-acceptor pair for the energy transfer studies (**Figure 2.12a**).[69,77,78] An appreciable bathochromic shift of ~30 nm was observed in the absorption of MC dyes in the presence of [+] InP/ZnS QDs (**Figure 2.12b**).
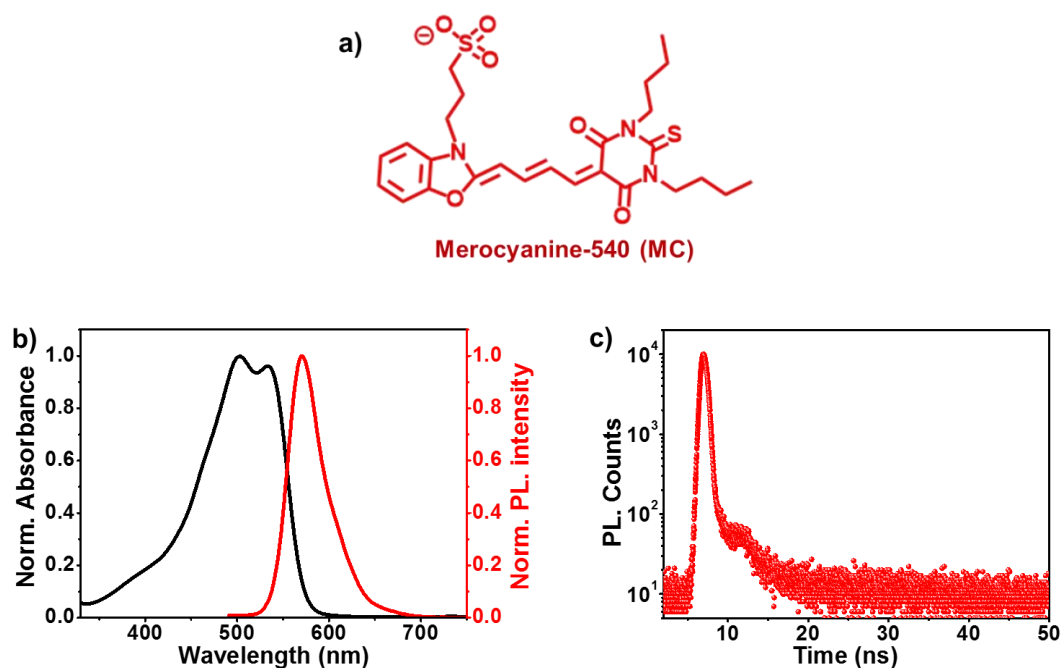
Figure 2.11: a) Chemical structure of merocyanine-540 (MC) dye. b) Normalized absorption (black curve) and PL (red curve) spectra of [-] MC dye in water. c) PL decay profile of [-] MC dye in water upon excitation with a 405 nm laser source.

The steady state PL experiments were performed by selectively exciting the [+] InP/ZnS QDs at 400 nm, wherein the acceptor absorption was minimal. A gradual decrease in the [+] InP/ZnS QD PL was observed upon successive addition of [-] MC dye, with a concomitant formation of a new band corresponding to the emission of MC dye (**Figure 2.12c**). The PL quenching of [+] InP/ZnS QD due to the direct excitation of the MC dye was ruled out by performing a control experiment, wherein the dye sample (~2 μM) was excited at 400 nm (**Figure 2.12d**). Moreover, the emission of MC dye was red shifted by ~13 nm in [+] InP/ZnS:::[-] MC complex (**Figure 2.12d**). The red shifts in both the absorption and emission of the dye in the presence of [+] InP/Zn QDs indicate a strong ground state interaction between the QD and dye.[23,50] This was confirmed by estimating the bimolecular quenching constant by combining the slope obtained from Stern-Volmer analysis and PL lifetime of the donor (Details are provided in the Experimental Section). The linear behaviour of Stern-Volmer plot (Slope = 6.52×10^5 M^{-1}, inset of **Figure 2.12c**) and large bimolecular quenching constant (1.36×10^{13} $M^{-1}s^{-1}$) proved that the interaction between the QD and the dye is predominantly static in nature.[69,77,78] The electrostatic attraction between the complementary charges on [+] InP/ZnS QD and [-] MC dye is responsible for the strong ground state interaction observed in [+] InP/ZnS:::[-] MC complex. The efficiency of energy transfer process was estimated to be ~60 %, which got saturated after ~2 μM addition of the acceptor.

43
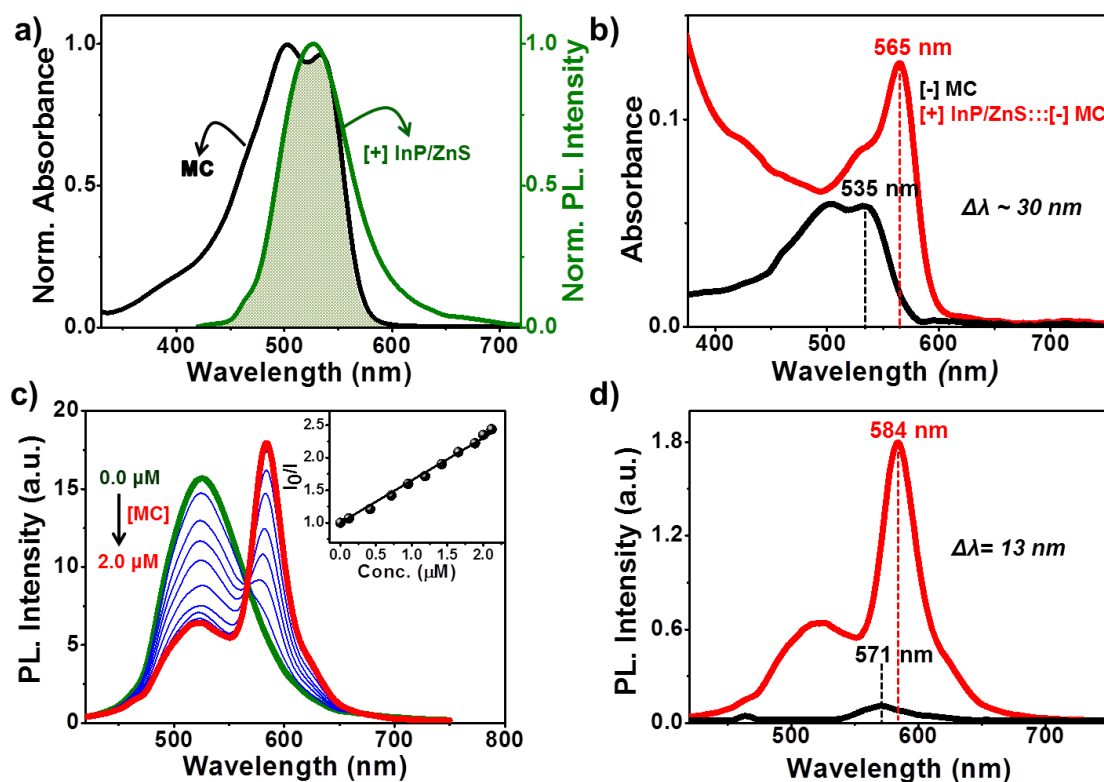
Figure 2.12: Steady state resonance energy transfer studies. a) Spectral overlap (shaded portion) between the PL of [+] InP/ZnS QD and absorption of [-] MC dye. b) A bathochromic shift of ~30 nm was observed in the absorption of MC dye upon complexation with [+] InP/ZnS QD. c) Spectral changes in the PL of [+] InP/ZnS QD on addition of varying concentrations of [-] MC dye. Inset is the Stern-Volmer plot showing the relative changes in the PL intensity of [+] InP/ZnS QD as a function of [-] MC dye concentration. d) PL spectra of [-] MC in the absence (black spectrum) and presence (red spectrum) of [+] InP/ZnS QD respectively. The emission of MC dye is red shifted by ~13 nm in InP/ZnS QD-MC dye complex.

2.5.4 Time resolved resonance energy transfer studies:

The process of resonance (nonradiative) energy transfer was followed by time resolved studies as well. The reduction in the average lifetime of [+] InP/ZnS QD from ~48 to ~17 ns, in the presence of MC dyes, confirms a resonance energy transfer process in [+] InP/ZnS:::[-] MC complex (**Figure 2.13a, and Table 2.2**).[50,69,77,78] An efficiency of ~62 % was estimated from PL lifetime quenching studies which are in close agreement with steady state experiments. Also, the rate of energy transfer from [+] InP/ZnS QD to [-] MC dye was estimated to be 3.02 x 10^7 s^{-1}. Various parameters involved in resonance energy transfer process between [+] InP/ZnS QD donor and [-] MC dye acceptor are summarized in **Table 2.4**. The ultimate proof for energy transfer process was obtained by observing the concomitant formation of the acceptor excited state, along with the donor decay. For this, the

PL decay was collected at the emission wavelengths of both donor and acceptor in a shorter time scale (time window of 50 ns). The [+] InP/ZnS:::[-] MC complex exhibited a rapid decay at ~525 nm with a concomitant growth of the acceptor emission (**Figure 2.13b, and Table 2.3**). The presence of a negative pre-exponential factor in the fast component of the acceptor emission corresponds to the formation of excited state of the MC dye (the growth time of MC emission was found to be ~250 ps). [50,69,77,78] Finally, time resolved emission spectroscopy (TRES) experiments were carried out to study the time dependent evolution of emission in [+] InP/ZnS:::[-] MC complex (Details of TRES studies are provided in Experimental Section). The emission spectrum constructed immediately after the laser irradiation showed a maximum around the donor InP/ZnS QDs (inset of **Figure 2.13b**). Interestingly, an emission maximum around the acceptor MC dye was observed when the TRES spectrum was constructed after a time delay of ~450 ps (inset of **Figure 2.13b**). The TRES studies conclude that the acceptor MC dye molecules get excited via a nonradiative energy transfer from the photoexcited [+] InP/ZnS QD donor, a typical of resonance energy transfer process.[50,69,77,78]
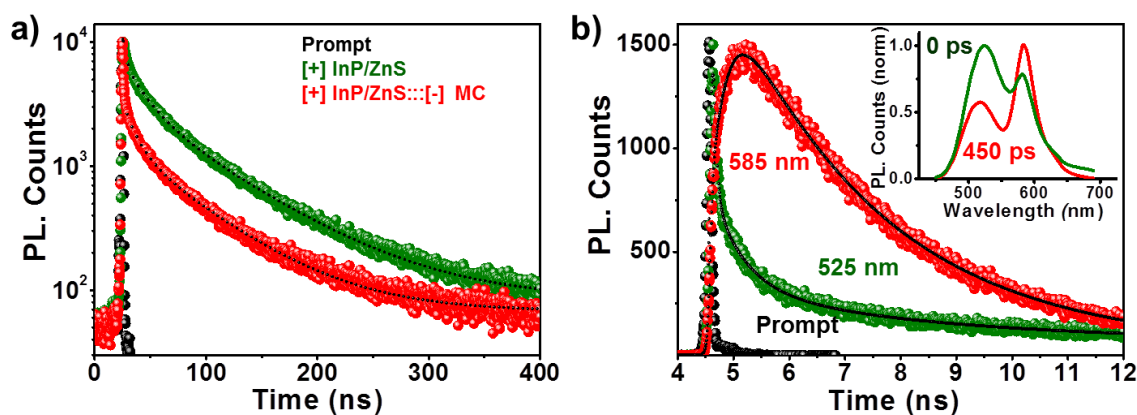
Figure 2.13: Time resolved energy transfer studies. a) PL decay profiles of [+] InP/ZnS QDs in the absence and presence of ~2 μM of [-] MC dye. b) PL decay profiles of [+] InP/ZnS:::[-] MC complex collected at the emission maxima of donor (525 nm) and acceptor (585 nm), at 50 ns time scale. Inset shows the TRES of [+] InP/ZnS:::[-] MC complex recorded immediately and after a time delay of 450 ps.

Table 2.2: PL decay analysis of [+] InP/ZnS QD in the absence and presence of [-] MC dye measured in a time window of 1 μs.

Sample	τ_1 (ns)	a_1	τ_2 (ns)	a_2	τ_3 (ns)	a_3	Avg. τ (ns)	Efficiency (%)
[+] InP/ZnS_H_2O	2.98	0.49	18.2	0.35	70.23	0.16	47.69	63.7
[+] InP/ZnS:::[-] MC (2 μM)	0.98	0.79	11.45	0.20	60.43	0.01	17.30	

Table 2.3: PL decay analysis of [+] InP/ZnS QD in the presence of [-] MC dye measured in a time window of 50 ns.

Sample	τ_1 (ns)	a_1	τ_2 (ns)	a_2	τ_3 (ns)	a_3	Chi. Sq
[+] InP/ZnS:::[-[MC @525 nm	2.58	0.15	0.53	0.79	24.2	0.05	1.16
[+] InP/ZnS:::[-] MC @585 nm	2.69	0.61	0.25	-0.36	12.8	0.03	1.14

2.5.5 Proof of electrostatically driven resonance energy transfer:

The role of electrostatics in resonance energy transfer in [+] InP/ZnS:::[-] MC complex was confirmed by performing independent control experiments.

<u>Control experiment # 1</u>

Electrostatic interactions are weakened in the presence of high salt concentration due to the screening of charges by the salts.[79] Accordingly, energy transfer studies were carried out in high salt concentration like phosphate buffered saline (PBS). An efficiency of ~32 % was obtained in PBS for the same concentration of MC dye (~2 μM) used in water. The screening of charges by salts weakens the electrostatic attraction between [+] InP/ZnS QDs and [-] MC dye, thereby lowering the efficiency. Interestingly, efficiency similar to that observed in water was obtained when the concentration of the acceptor dye in PBS was doubled (**Figure 2.14**).
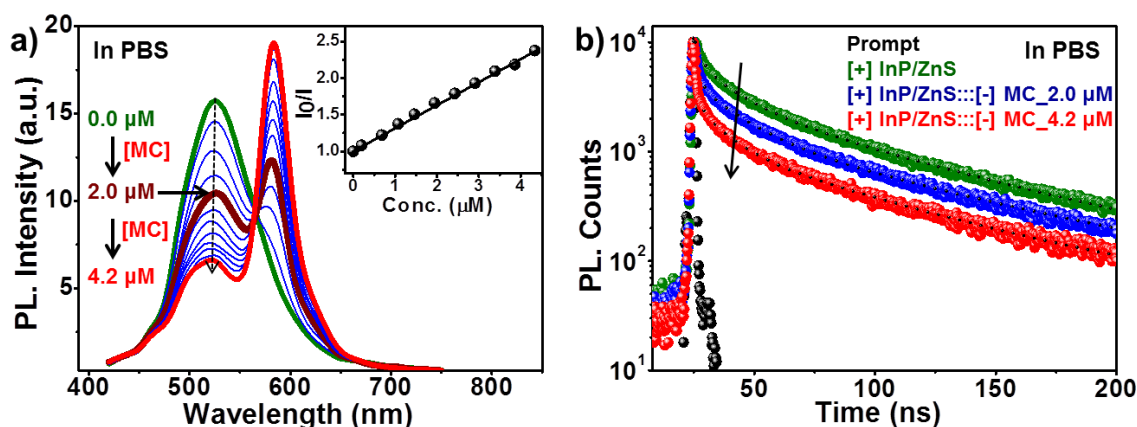
Figure 2.14: Proof of electrostatically driven resonance energy transfer. Changes in a) steady state and b) time resolved PL of [+] InP/ZnS QD on addition of [-] MC dye in PBS. Inset of a) is the Stern-Volmer plot of [+] InP/ZnS:::[-] MC complex in PBS.

Table 2.4: Energy transfer parameters for [+] InP/ZnS:::[-] MC system in water and PBS

Sample	$J(\lambda)$ $(M^{-1} cm^{-1} nm^4)$	R_0 (A)	E^a $(\%)$	E^b $(\%)$	r_0 (A)	$k_T(r)$ (s^{-1})
[+] InP/ZnS:::[-] MC @ H$_2$O	2.45×10^{15}	37.23	60.0	62.0	35.03	2.92×10^7
[+] InP/ZnS:::[-] MC _2.0 µM @ PBS	2.32×10^{15}	36.92	36.1	30.0	40.6	1.86×10^7
[+] InP/ZnS:::[-] MC _4.2 µM @ PBS	2.32×10^{15}	36.92	58.2	62.3	34.95	2.16×10^7

$J(\lambda)$ = Spectral overlap integral, R_0 = Förster distance, E^a = efficiency calculated from steady state data, E^b = efficiency calculated from lifetime analysis, r = distance between the Donor and acceptor, $k_T(r)$ = rate of energy transfer.

Control experiment # 2

Quenching experiments were performed between [+] InP/ZnS QD and a [+] cyanine acetate (CY) dye. A high spectral overlap integral of 1.56×10^{15} $M^{-1}cm^{-1}nm^4$ suggests that [+] InP/ZnS QDs and [+] CY dye can form a donor-acceptor pair (**Figure 2.15a**). However, the same charges on the surface of donor and acceptor prevented the formation of a complex, (**Figure 2.15b**) and no appreciable changes in both steady state and time resolved quenching experiments were observed (**Figure 2.15c,d**). This rules out the possibility of energy transfer between [+] InP/ZnS QDs and [+] CY.
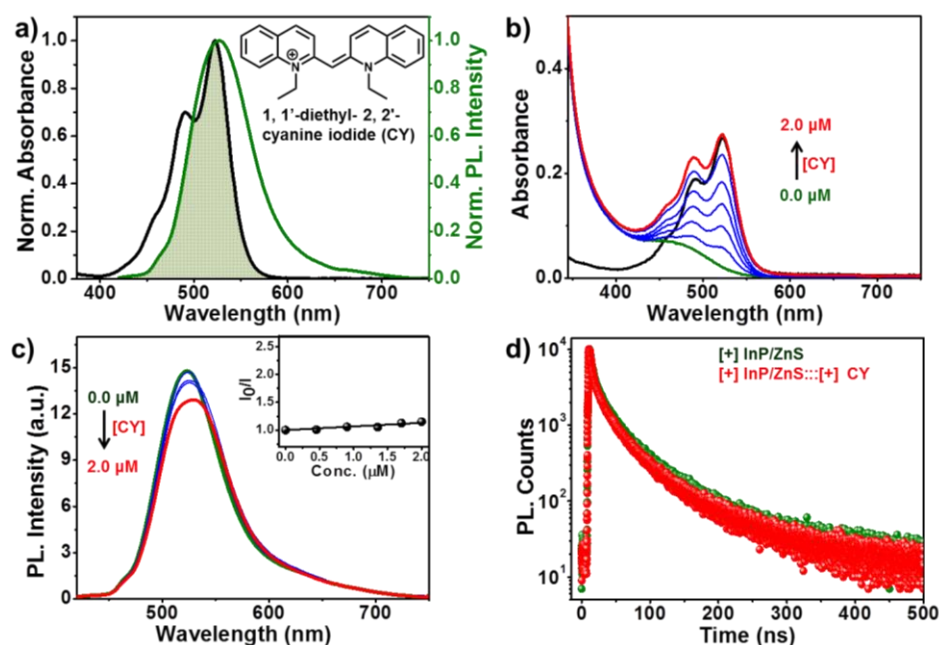
Figure 2.15: Proof of electrostatically driven resonance energy transfer a) Spectral overlap (shaded portion) between the PL of [+] InP/ZnS (green curve) and absorption of [+] CY (black curve). A large spectral overlap integral value of 1.56×10^{15} $M^{-1}cm^{-1}nm^4$ suggests that

[+] InP/ZnS QD and [+] CY dye form a good donor-acceptor pair. b) Absorption spectral changes of [+] InP/ZnS QD with increasing concentration of [+] CY dye. The absorption spectrum of [+] CY alone is shown as the black curve. The absence of red shift in the absorption of dye in the presence of QD rules out the formation of a strong ground state complex between [+] InP/ZnS QD and [+] CY dye. c) Steady state PL spectra of [+] InP/ZnS upon addition of varying concentrations of [+] CY dye. The inset shows the Stern-Volmer plot showing the negligible changes in the PL intensity of [+] InP/ZnS QD as a function of CY dye concentration. d) PL decay profiles of [+] InP/ZnS QDs in the absence (green decay) and presence (red decay) of ~2.0 μM [+] CY dye, upon excitation with a 405 nm laser.

A similar quenching experiment was performed with [-] InP/ZnS QD and [-] MC dye, which again proved the inability of similarly charged QD and dye to form a stable complex (**Figure 2.16**).
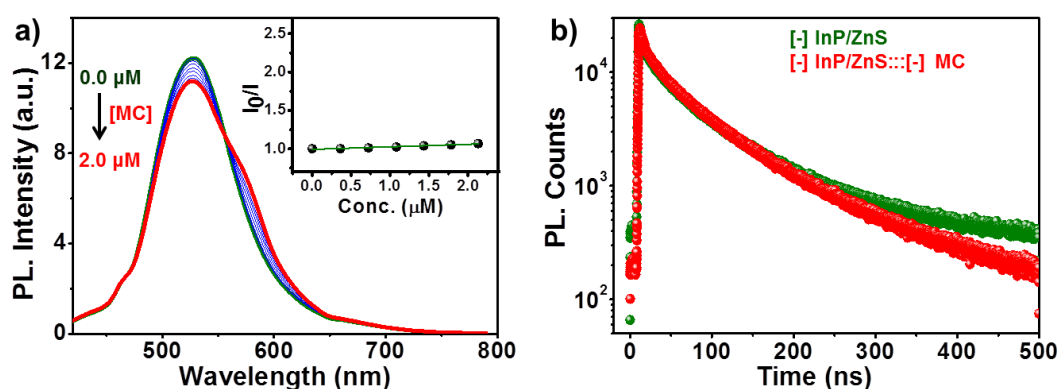
Figure 2.16: a) Steady state PL spectra of [-] InP/ZnS QD upon the addition of varying concentrations of [-] MC dye. Inset shows the corresponding Stern-Volmer plot. b) PL decay profiles of [-] InP/ZnS QD in the absence (green decay) and presence (red decay) of [-] MC (~2.0 μM), upon excitation with a 405 nm laser. All the steady state and time resolved experiments rules out the possibility of resonance energy transfer between [-] InP/ZnS QD and [-] MC dyes.

Finally, the stability studies of [+] InP/ZnS:::[-] MC complex in biofluids revealed the breaking of electrostatic attraction in the complex by the ions present in the medium (**Figure 2.17**). The dissociation of [+] InP/ZnS:::[-] MC complex was accompanied by a reduction in the energy transfer process, and the PL of donor InP/ZnS QD recovered with time. All these control experiments reiterate the role of electrostatic attraction in the formation of a strong ground state complex between [+] InP/ZnS QD and [-] MC dyes, leading to an efficient energy transfer process.
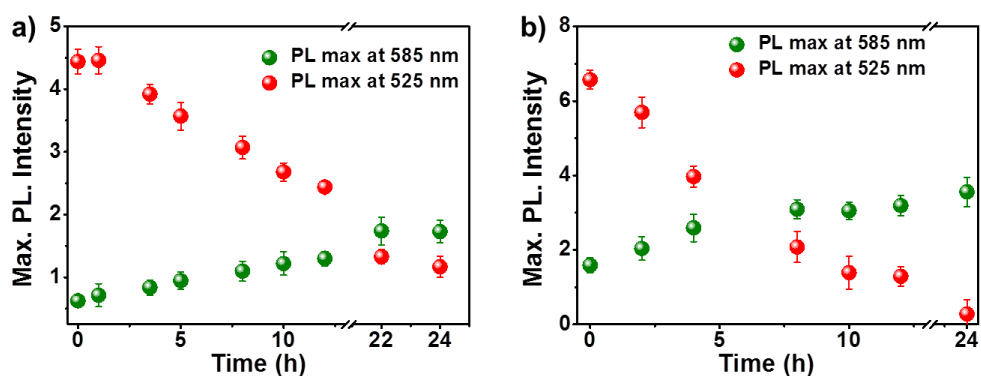
Figure 2.17: The variation of PL intensity of [+] InP/ZnS::: [-] MC complex in a) PBS and b) DMEM media (with 10 % FBS), monitored at the donor (green dots) and the acceptor emission (red dots) maxima.

Thus, the long ranged electrostatic field[64] helps in attracting more acceptor MC dyes towards the [+] InP/ZnS QD surface, thereby increasing the probability of resonance energy transfer.[80] The schematic representation of electrostatically driven resonance energy transfer studies in [+] InP/ZnS QD- [-] MC dye donor-accepotr system, under various conditions are shown in **Figure 2.18**.
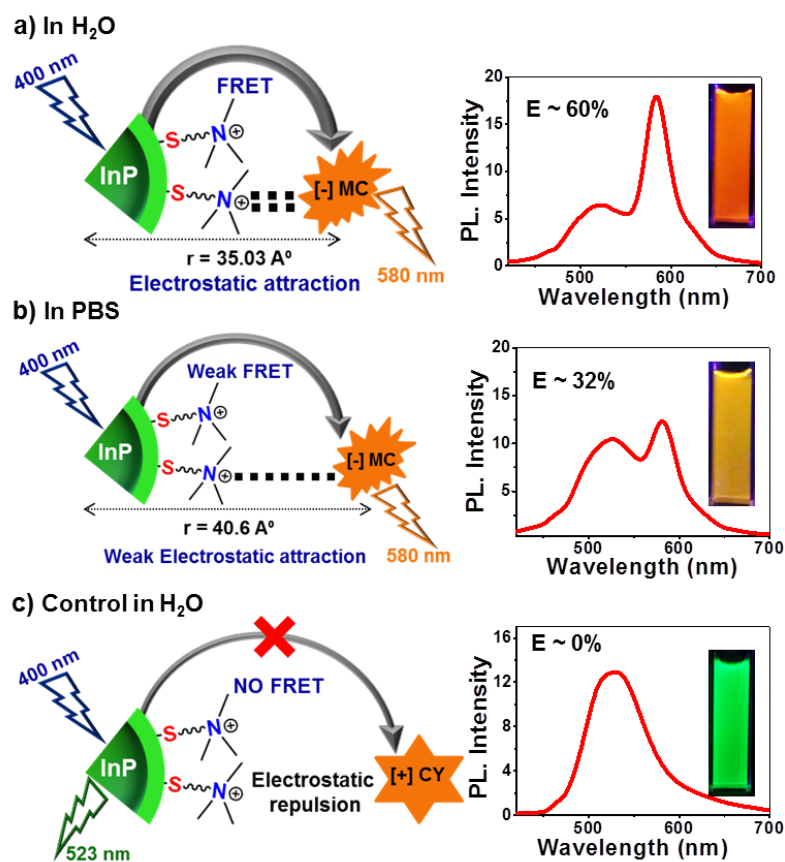
Figure 2.18: Electrostatically driven resonance energy transfer in [+] InP/ZnS QDs. a) efficient resonance energy transfer was observed between [+] InP/ZnS QDs and the [-] MC

dye in water. b) The presence of high concentration of salt in PBS screened the charges on the QDs and the dye, thereby decreasing the FRET efficiency. c) No appreciable energy transfer was observed when the charges on the donor and the acceptor were the same, confirming the role of electrostatics in FRET. The steady state PL plots and optical images of the samples corresponding to each of the three conditions are shown on the right. The concentration of [+] InP/ZnS QD and dyes was maintained at ~0.8 µM and ~2 µM respectively, in all of the three conditions.

2.5.6 Energy transfer in solid state:

Translating solution state studies into solid state is a crusial step towards designng artificial systems with configurable optoelectronic properties.[81] We have chosen glass cover slip as a substrate for the preparation of QD films. The cationic InP/ZnS QD films were prepared by drop casting ~200 µL of ~5 µM [+] InP/ZnS QD solution on a cover slip, and these films were characterized by standard spectroscopic techniques (**Figure 2.19**a). The steady state experiments showed negligible changes in the absorption, and a red shift of 15 nm in the emission maxima of [+] InP/ZnS QD films with respect to the solution state. This is because of the aggregation of QDs during the drying. The tri-exponential behaviour of [+] InP/ZnS QD was well retained in the films as well (**Figure 2.19b and Table 2.5**). The photographs of the [+] InP/ZnS QDs films under normal and UV light are shown in **Figures 2.19 c and d**.
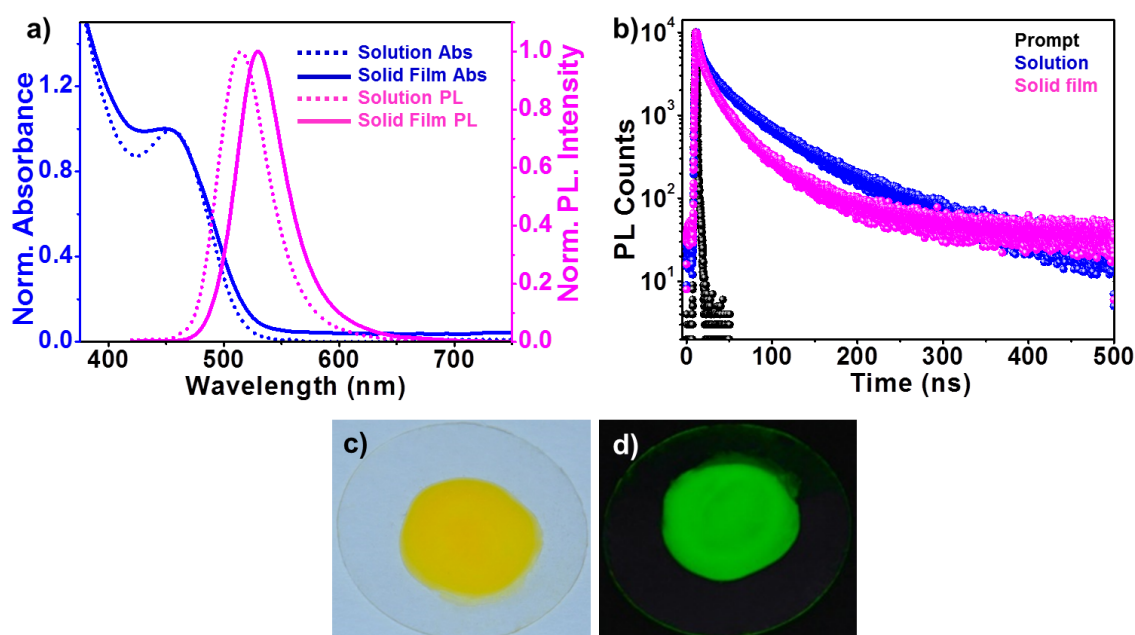
Figure 2.19: a) The normalized absorption and PL spectra of [+] InP/ZnS QDs in solution and solid film. b) Comparison of the PL decay profiles of [+] InP/ZnS QD in solution and solid film. c) Photographs of [+] InP/ZnS QD films under c) normal and d) UV light.

Table 2.5: PL decay analysis of InP/ZnS QD in solution and solid state in a time window of 500 ns.

Sample	τ_1 (ns)	a_1	τ_2 (ns)	a_2	τ_3 (ns)	a_3	Avg. τ (ns)	Chi. Sq
[+] InP/ZnS in solution	2.98	0.49	18.2	0.35	70.23	0.16	47.69	1.11
[+] InP/ZnS in solid film	4.69	0.52	21.54	0.21	72.56	0.27	57.63	1.13

In a typical energy transfer experiment in solid state, [+] InP/ZnS QD films were dipped in ~10 µM acetonitrile solution of [-] MC dye for ~3 h resulting in the diffusion and complexation of [-] MC dye with [+] InP/ZnS QD (**Figure 2.20a**). Finally the films were washed to remove the unbound or excess [-] MC dye. This entire processe was monitored using various spectroscopic techniques.
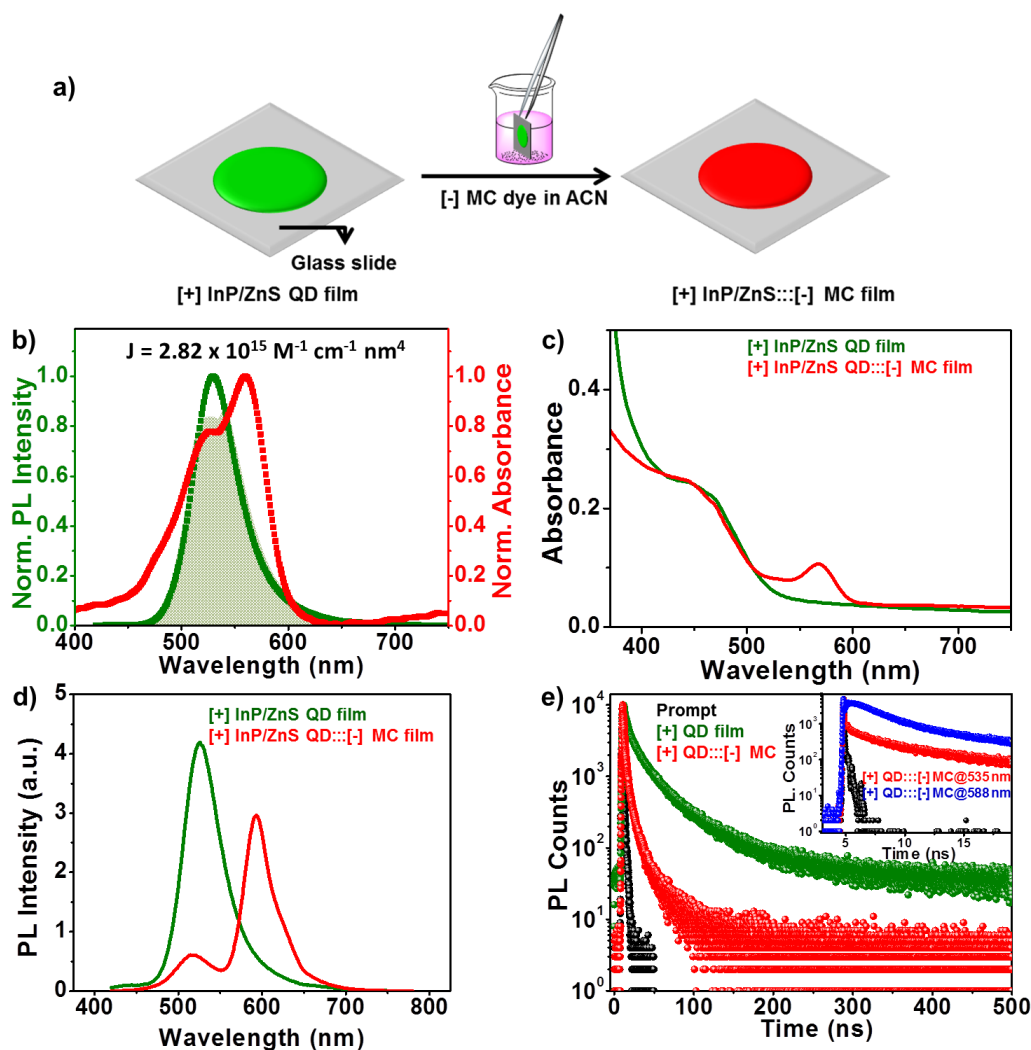
Figure 2.20: Energy transfer in solid film. a) Schematic representation of the preparation of [+] InP/ZnS:::[-] MC solid films. b) Spectral overlap (shaded portion) between the PL of [+]

InP/ZnS QD and the absorption of [-] MC dye. c) Absorption spectra of [+] InP/ZnS QD films before and after dipping in [-] MC dye solution. d) Changes in the steady state PL, and d) corresponding quenching in the PL decay profiles of the [+] InP/ZnS QD in the presence of [−] MC dye. Inset shows the PL decay profiles of [+] InP/ZnS:::[-] MC complex collected at the emission maxima of the donor (535 nm) and the acceptor (588 nm), in a 50 ns time scale.

Figure 2.20c shows the absorption spectra of [+] InP/ZnS QD films before and after dipping in [-] MC solution. The presence of the dye peak confirms the complexation of [-] MC dye with [+] InP/ZnS QD. A drastic decrease in the PL of [+] InP/ZnS QD was observed along with a simultaneous formation of a new band corresponding to the emission of [-] MC dye at 588 nm (**Figure 2.20d**). This indictes the process of energy transfer from [+] InP/ZnS QD to [-] MC dye in solid films. The efficiency of energy transfer process was estimated to be ~85 %. The reduction in the average PL lifetime of [+] InP/ZnS QD from ~57 to ~12 ns, confirms the resonance energy transfer process in [+] InP/ZnS:::[-] MC films (**Figure 2.20e and Table 2.6**). An efficiency of ~80 % was estimated from PL lifetime quenching studies which is in close agreement with steady state quenching results. Also, the rate of energy transfer was estimated to be ~7.59 x 10^7 s^{-1}. Intrestingly, we observed the negative pre-exponential factor corresponding to the formation of [-] MC excited state, in solid state as well (inset of **figure 2.20e and Table 2.7**). This is an ultimate proof for the energy transfer between [+] InP/ZnS and [-] MC dye in solid films. [50,69,77,78] The parameters involved in the energy transfer in [+] InP/ZnS:::[-] MC solid film are summarised in **Table 2.8**.

Table 2.6: PL decay analysis of [+] InP/ZnS QD solid films in the absence and presence of [-] MC dye, measured in a time window of 500 ns.

Sample	τ_1 (ns)	a_1	τ_2 (ns)	a_2	τ_3 (ns)	a_3	Avg. τ (ns)	Efficiency (%)
[+] InP/ZnS solid film	4.69	0.52	21.54	0.21	72.56	0.27	57.63	78.3
[+] InP/ZnS:::[-] MC solid film	1.52	0.78	9.66	0.13	21.14	0.09	12.46	

Table 2.7: PL decay analysis of [+] InP/ZnS QD solid films in the absence and presence of [-] MC dyes, measured in a time window of 50 ns.

Sample	τ_1 (ns)	a_1	τ_2 (ns)	a_2	τ_3 (ns)	a_3	Chi. Sq
[+] InP/ZnS:::[-[MC @535 nm	2.15	0.19	0.49	0.75	28.5	0.06	1.13
[+] InP/ZnS:::[-] MC @588 nm	2.48	0.65	0.31	-0.27	17.3	0.08	1.11

Table 2.8: Energy transfer parameters for [+] InP/ZnS:::[-] MC solid film.

Sample	$J(\lambda)$ (M^{-1} cm^{-1} nm^4)	R_0 (A)	E^a (%)	E^b (%)	r_0 (A)	$k_T(r)$ (s^{-1})
[+] InP/ZnS:::[-] MC solid film	2.82 x10^{15}	55.16	85.5	78.3	43.78	7.59 x 10^7

Thus, we have successfully translated the solution state energy transfer process into the solid state as well. The efiiciency of energy transfer was controlled by varying the concentration of [-] MC dye (**Fiure 2.21**), which can pave the way for future device level studies. The different luminescent colors of the thin films in **Figure 2.21** correspond to different FRET efficiencies between QD donor and dye acceptor. As the efficiency of FRET process increases, the luminescent color of the thin films will shift more towards the MC acceptor emission.
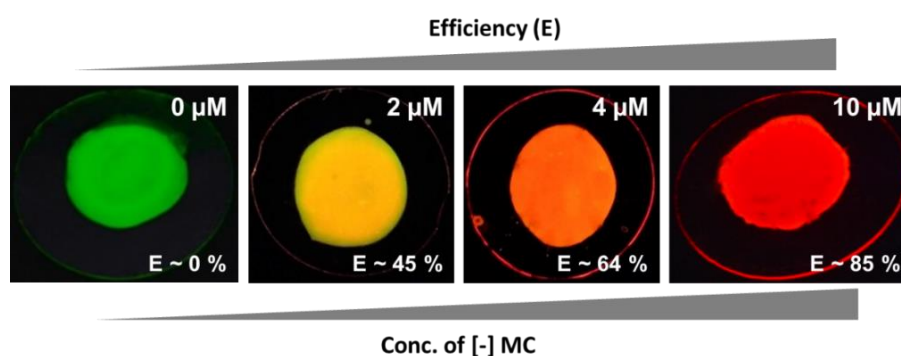
Figure 2.21: The photographs of [+] InP/ZnS QD films dipped in differnt concentrations of [-] MC dye for ~3 h.

Further, the effect of electrostatics in the solid films was monitored by performing control experiments with similarly charged donor-acceptor moieties (**Figure 2.22**). No noticeable presence of dye was observed in the absorption spectrum of QD films, after dipping in the dye solution. This confirms the lack of complexation between QD and dye, due to the

electrostatic repulsions between similarly charged donor and acceptor (**Figure 2.22b,e**). Also, no appreciable changes were observed in both steady state and lifetime experiments (**Figure 2.22c,f**). This clearly confirms the decisive role of electrostatics in driving an efficient resonance energy transfer in solid films as well.
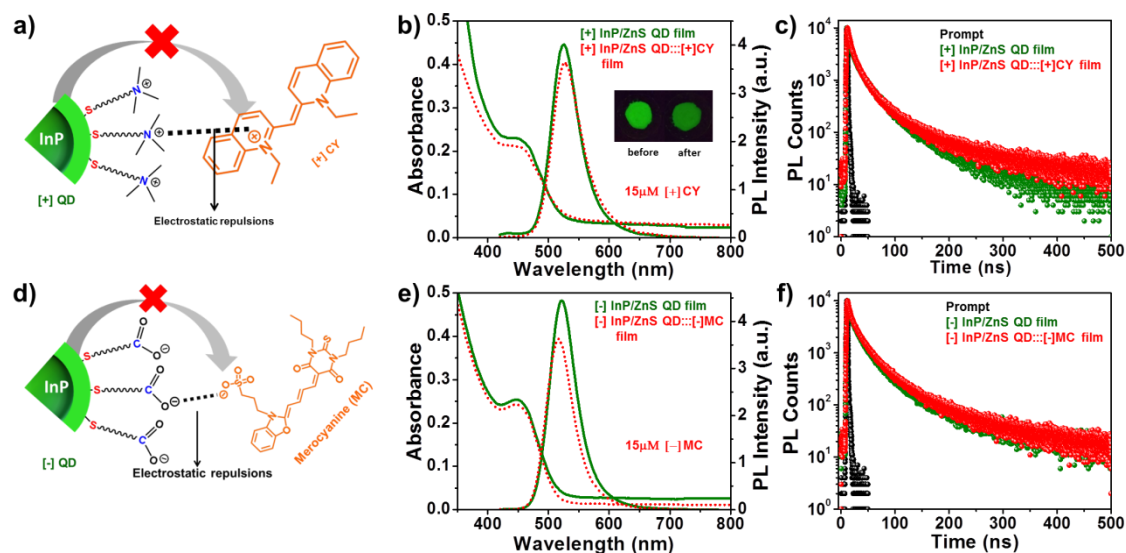
Figure 2.22: Proof for electrostatically driven energy transfer in solid films. a) Schematic representation of negligble energy transfer from [+] InP/ZnS QD to [+] CY dye. b) Absorption and PL of [+] InP/ZnS QD films before and after dipping in [+] CY solution for ~3 h. Inset shows the photographs of the [+] InP/ZnS QD film before and after dipping in the [+] CY solution. c) The corresponding PL decay profiles of [+] InP/ZnS QD films. d) Schematic representation of negligble energy transfer from [-] InP/ZnS QD to [-] MC dye. e) Absorption and PL of [-] InP/ZnS QD films before and after dipping in [-] MC solution for ~3 h, and f) the corresponding PL decay profiles.

2.6 Conclusions

In conclusion, our work introduces InP QD to the family of cationic nanoparticles as a practical alternative to toxic metal ion based QDs for future light harvesting and biological applications. The two important properties of QDs, namely bioimaging and resonance energy transfer, were successfully demonstrated in [+] InP/ZnS QDs. The low cytotoxicity and stable photoluminescence of [+] InP/ZnS QDs inside cells make them ideal candidates as optical probes for cellular imaging applications. An electrostatically driven efficient resonance energy transfer was observed between [+] InP/ZnS QD and [-] MC dye. A large bimolecular quenching constant along with a linear Stern-Volmer plot confirms the formation of a strong ground state complex between [+] InP/ZnS QD and [-] dye. Control experiments prove the role of

electrostatic attraction in driving the light induced processes, which can rightfully form the basis for future nanobio studies between cationic InP/ZnS QDs and anionic biomolecules. The process of electrostatically driven resonance energy transfer was successfully translated into solid state as well, which can pave the way for future device level applications. The dissociation of [+] InP/ZnS:::[-] MC complex under physiological conditions (**Figure 2.17**) has the potential to be thoughtfully translated into FRET based signaling and targeting of biomolecular processes.

2.7 Future Direction

In principle, the efficiency of FRET can be controlled by varying the distance or ratio between the donor and the acceptor. In this Chapter, we were able to control the efficiency of FRET using both the above mentioned strategies. In the solution state, the efficiency was controlled by varying the distance between the donor and the acceptor. This was achieved by increasing the ionic strength of the medium, which will screen the charges on the surface of QD and weaken the electrostatic interactions, thereby decreasing the FRET efficiency. On the other hand, the efficiency of FRET was controlled by varying the donor-acceptor ratio in the solid state. Here, different films corresponding to different donor-acceptor ratios were used to get different FRET efficient states. This can be a limitation for some solid state display studies, where the ideal way should be to vary the FRET efficiency in a single QD nanohybrid film. Obviously, this cannot be achieved by varying the distance between the donor and the acceptor, because of the restricted movement of components in the solid state. Hence, the only option is to develop strategies to control the donor-acceptor ratio in a single QD nanohybrid film, and this forms the basis of Chapter 3.

2.8 References

(1)   Bajaj, A.; Rana, S.; Miranda, O. R.; Yawe, J. C.; Jerry, D. J.; Bunz, U. H. F.; Rotello, V. M. Cell Surface-Based Differentiation of Cell Types and Cancer States Using a Gold Nanoparticle-GFP Based Sensing Array *Chem. Sci.,* **2010**, *1*, 134-138.

(2)   Nel, A. E.; Mädler, L.; Velegol, D.; Xia, T.; Hoek, E. M. V; Somasundaran, P.; Klaessig, F.; Castranova, V.; Thompson, M. Understanding Biophysicochemical Interactions at the Nano–bio Interface. *Nat. Mater.,* **2009**, *8*, 543-557.

(3)   Verma, A.; Stellacci, F. Effect of Surface Properties on Nanoparticle – Cell Interactions. *Small,* **2010**, *6*, 12-21.

(4)   Cho, E. C.; Au, L.; Zhang, Q.; Xia, Y. The Effects of Size, Shape, and Surface Functional Group of Gold Nanostructures on Their Adsorption and Internalization by Cells. *Small,* **2010, 6,** 517–522.

(5)   Albanese, A.; Tang, P. S.; Chan, W. C. W. The Effect of Nanoparticle Size, Shape, and Surface Chemistry on Biological Systems. *Annu. Rev. Biomed. Eng.,* **2012**, 14, 1-16.

(6)   Pillai, P. P.; Kowalczyk, B.; Kandere-grzybowska, K.; Borkowska, M.; Grzybowski, B. A. Engineering Gram Selectivity of Mixed-Charge Gold Nanoparticles by Tuning the Balance of Surface Charges. *Angew. Chem., Int. Ed.,* **2016**, *55*, 8610-8614.

(7)   Goodman, C. M.; McCusker, C. D.; Yilmaz, T.; Rotello, V. M. Toxicity of Gold Nanoparticles Functionalzied with Cationic and Anionic Side Chians. *Bioconju. Chem.* **2004**, *15*, 897–900.

(8)   Saha, K.; Bajaj, A.; Duncan, B.; Rotello, V. M. Beauty Is Skin Deep: A Surface Monolayer Perspective on Nanoparticle Interactions with Cells and Bio-Macromolecules. *Small* **2011**, *7*, 1903–1918.

(9)   Zhu, Z. -J; Yeh, Y. -C; Tang, R.; Yan, B.; Tamayo, J.; Vachet, R. W.; Rotello, V. M. Stability of Quantum Dots in Live Cells. *Nat. Chem.* **2011**, *3*, 963–968.

(10)   Ramos, J.; Forcada, J.; Hidalgo-Alvarez, R. Cationic Polymer Nanoparticles and Nanogels: From Synthesis to Biotechnological Applications. *Chem. Rev.* **2014**, *114*, 367–428.

(11)   Li, L.; Liu, J.; Yang, X.; Peng, Z.; Liu, W.; Xu, J.; Tang, J.; He, X.; Wang, K. Quantum Dot/methylene Blue FRET Mediated NIR Fluorescent Nanomicelles with Large Stokes Shift for Bioimaging. *Chem. Commun.* **2015**, *51*, 14357–14360.

(12)   Dubertret, B.; Skourides, P. D.; Norris, J.; Noireaux, V.; Brivanlou, A. H.; Libchaber, A. In Vivo Imaging of Quantum Dots Encapsulated in Phospholipid Micelles. *Science* **2002**, *298*, 1759–1762.

(13)   Gao, X.; Cui, Y.; Levenson, R. M.; Chung, L. W. K.; Nie, S. In Vivo Cancer Targeting and Imaging with Semiconductor Quantum Dots. *Nat. Biotechnol.* **2004**, *22*, 969–976.

(14)   Medintz, I. L.; Uyeda, H. T.; Goldman, E. R.; Mattoussi, H. Quantum Dot Bioconjugates for Imaging, Labelling and Sensing. *Nat. Mater.* **2005**, *4*, 435–446.

(15)   Choi, H. S.; Liu, W.; Misra, P.; Tanaka, E.; Zimmer, J. P.; Ipe, B. I.; Bawendi, M. G.; Frangioni, J. V. Renal Clearance of Quantum Dots. *Nat. Biotechnol.* **2007**, *25*, 1165–

1170.

(16) Liu, W.; Howarth, M.; Greytak, A. B.; Zheng, Y.; Nocera, D. G.; Ting, A. Y.; Bawendi, M. G. Compact Biocompatible Quantum Dots Functionalized for Cellular Imaging Compact Biocompatible Quantum Dots Functionalized for Cellular Imaging. *J. Am. Chem. Soc.* **2008**, *130*, 1274–1284.

(17) Biju, V.; Itoh, T.; Ishikawa, M. Delivering Quantum Dots to Cells: Bioconjugated Quantum Dots for Targeted and Nonspecific Extracellular and Intracellular Imaging. *Chem. Soc. Rev.* **2010**, *39*, 3031–3056.

(18) Shibu, E. S.; Sugino, S.; Ono, K.; Saito, H.; Nishioka, A.; Yamamura, S.; Sawada, M.; Nosaka, Y.; Biju, V. Singlet-Oxygen-Sensitizing near-Infrared-Fluorescent Multimodal Nanoparticles. *Angew. Chem. Int. Ed.* **2013**, *52*, 10559–10563.

(19) Wegner, K. D.; Hildebrandt, N. Quantum Dots: Bright and Versatile in Vitro and in Vivo Fluorescence Imaging Biosensors. *Chem. Soc. Rev.* **2015**, *44*, 4792–4834.

(20) Clapp, A. R.; Medintz, I. L.; Mauro, J. M.; Fisher, B. R.; Bawendi, M. G.; Mattoussi, H. Fluorescence Resonance Energy Transfer Between Quantum Dot Donors and Dye-Labeled Protein Acceptors. *J. Am. Chem. Soc.* **2004**, *126*, 301–310.

(21) Sapsford, K. E.; Berti, L.; Medintz, I. L. Materials for Fluorescence Resonance Energy Transfer Analysis: Beyond Traditional Donor-Acceptor Combinatio ns. *Angew. Chem. Int. Ed.* **2006***, 45,* 4562–4588.

(22) Funston, A. M.; Jasieniak, J. J.; Mulvaney, P. Complete Quenching of CdSe Nanocrystal Photoluminescence by Single Dye Molecules. *Adv. Mater.* **2008**, *20*, 4274–4280.

(23) Medintz, I. L.; Mattoussi, H. Quantum Dot-Based Resonance Energy Transfer and Its Growing Application in Biology. *Phys. Chem. Chem. Phys.* **2009**, *11*, 17–45.

(24) Lu, H.; Schöps, O.; Woggon, U.; Niemeyer, C. M.;. Self-Assembled Donor Comprising Quantum Dots and Fluorescent Proteins for Long-Range Fluorescence Resonance Energy Transfer. *J. Am. Chem. Soc.* **2008**, *130*, 4815-4827.

(25) Freeman, R.; Willner, B.; Willner, I. Integrated Biomolecule À Quantum Dot Hybrid Systems for Bioanalytical Applications. *J. Phys. Chem. Lett.* **2011**, *2*, 2667–2677.

(26) Biju, V.; Anas, A.; Akita, H.; Shibu, E. S.; Itoh, T.; Harashima, H.; Ishikawa, M. FRET from Quantum Dots to Photodecompose Undesired Acceptors and Report the Condensation and Decondensation of Plasmid DNA. *ACS Nano* **2012**, *6*, 3776–3788.

(27) Jou, A. F.; Lu, C.-H.; Ou, Y. -C.; Wang, S. -S; Hsu, S. -L.; Willner, I.; Ho, J. A.

Diagnosing the MiR-141 Prostate Cancer Biomarker Using Nucleic Acid-Functionalized CdSe / ZnS QDs and Telomerase. *Chem. Sci.* **2015**, *6*, 659-665.

(28) Snee, P. T.; Somers, R. C.; Nair, G.; Zimmer, J. P.; Bawendi, M. G.; Nocera, D. G. A Ratiometric CdSe/ZnS Nanocrystal pH Sensor. J. Am. Chem. Soc. **2006**, 128, 13320-13321.

(29) Wang, C.; Weiss, E. A. Sub-Nanosecond Resonance Energy Transfer in the Near-Infrared within Self-Assembled Conjugates of PbS Quantum Dots and Cyanine Dye J-Aggregates. *J. Am. Chem. Soc.* **2016**, *138*, 9557–9564.

(30) He, C.; Weinberg, D. J.; Nepomnyashchii, A. B.; Lian, S.; Weiss, E. A. Control of the Redox Activity of PbS Quantum Dots by Tuning Electrostatic Interactions at the Quantum Dot/Solvent Interface. *J. Am. Chem. Soc.* **2016**, *138*, 8847–8854.

(31) Hoffman, J. B.; Alam, R.; Kamat, P. V. Why Surface Chemistry Matters for QD–QD Resonance Energy Transfer. *ACS Energy Lett.* **2017**, *2*, 391–396.

(32) Micic, O.; Curtis, C. J.; Jones, K. M.; Sprague, J. R.; Nozik, A. J. Synthesis and Characterization of InP Quantum Dots. J. Phys. Chem. **1994**, 98, 4966–4969.

(33) Fu, H.; Zunger, A. InP Quantum Dots: Electronic Structure, Surface Effects, and the Redshifted Emission. *Phys. Rev. B* **1997**, *56*, 1496–1508.

(34) Talapin, D. V.; Gaponik, N.; Borchert, H.; Rogach, A. L.; Haase, M.; Weller, H. Etching of Colloidal InP Nanocrystals with Fluorides: Photochemical Nature of the Process Resulting in High Photoluminescence Efficiency. *J. Phys. Chem. B* **2002**, *106*, 12659–12663.

(35) Allen, P. M.; Walker, B. J.; Bawendi, M. G. Mechanistic Insights into the Formation of InP Quantum Dots. *Angew. Chemie., Int. Ed.* **2010**, *49*, 760–762.

(36) Harris, D. K.; Bawendi, M. G. Improved Precursor Chemistry for the Synthesis of III − V Quantum Dots. *J. Am. Chem. Soc.* **2012**, *134*, 20211–20213.

(37) Charron, G.; Stuchinskaya, T.; Edwards, D. R.; Russell, D. A.; Nann, T. Insights into the Mechanism of Quantum Dot-Sensitized Singlet Oxygen Production for Photodynamic Therapy. *J. Phys. Chem. C* **2012**, *116, 9334-9342.*

(38) Bharali, D. J.; Lucey, D. W.; Jayakumar, H.; Pudavar, H. E.; Prasad P. N. Folate Receptor Mediated Delivery of InP Quantum Dots for Bioimaging Using Confocal and Two-Photon Microscopy. *J. Am. Chem. Soc.* **2005***, 127, 11364-11371*

(39) Yong, K.-T.; Ding, H.; Roy, I.; Law, W.-C.; Bergey, E. J.; Maitra, A.; Prasad, P. N. Imaging Pancreatic Cancer Using Bioconjugated InP Quantum Dots. *ACS Nano* **2009**,

3, 502–510.

(40) Xu, G.; Zeng, S.; Zhang, B.; Swihart, M. T.; Yong, K. -T.; Prasad, P. N. New Generation Cadmium-Free Quantum Dots for Biophotonics and Nanomedicine. *Chem. Rev.* **2016**, *116*, 12234–12327.

(41) Li, L.; Reiss, P. One-Pot Synthesis of Highly Luminescent InP / ZnS Nanocrystals without Precursor Injetion *J. Am. Chem. Soc.* **2008**, *130*, 11588–11589.

(42) Nag, A.; Sarma, D. D. Solvothermal Synthesis of InP Quantum Dots. *J. Nanosci. Nanotechnol.* **2009**, *9*, 5633–5636.

(43) Huang, K.; Demadrille, R.; Silly, M. G.; Sirotti, F.; Reiss, P.; Renault, O. Internal Structure of InP/ZnS Nanocrystals Unraveled by High- Resolution Soft X-ray Photoelectron Spectroscopy *ACS Nano* **2010**, *4*, 4799–4805

(44) Chibli, H.; Carlini, L.; Park, S.; Dimitrijevic, N. M.; Nadeau, J. L. Cytotoxicity of InP/ZnS Quantum Dots Related to Reactive Oxygen Species Generation. *Nanoscale* **2011**, *3*, 2552–2559.

(45) Virieux, H.; Le Troedec, M.; Cros-Gagneux, A.; Ojo, W. -S.; Delpech, F.; Nayral, C.; Martinez, H.; Chaudret, B. InP/ZnS Nanocrystals: Coupling NMR and XPS for Fine Surface and Interface Description. *J. Am. Chem. Soc.* **2012**, *134*, 19701–19708.

(46) Gary, D. C.; Cossairt, B. M. The Role of Acid in Modulating Precursor Conversion in InP-QD Synthesis. *Chem. Mater.* **2013**, *25* , 2463-2469.

(47) Adam, S.; Talapin, D. V.; Borchert, H.; Lobo, A.; McGinley, C.; De Castro, A. R.; Haase, M.; Weller, H.; Möller, T. The Effect of Nanocrystal Surface Structure on the Luminescence Properties: Photoemission Study of HF-Etched InP Nanocrystals. *J. Chem. Phys.* **2005**, *123*, 084706.

(48) Xie, R.; Battaglia, D.; Peng, X. Colloidal InP Nanocrystals as Efficient Emitters Covering Blue to near-Infrared. *J. Am. Chem. Soc.* **2007**, *129*, 15432–15433.

(49) Cros-Gagneux, A.; Delpech, F.; Nayral, C.; Cornejo, A.; Coppel, Y.; Chaudret, B. Surface Chemistry of InP Quantum Dots: A Comprehensive Study. *J. Am. Chem. Soc.* **2010**, *132*, 18147–18157.

(50) Thomas, A.; Nair, P. V.; Thomas, K. G. InP Quantum Dots: An Environmentally Friendly Material with Resonance Energy Transfer Requisites. *J. Phys. Chem. C* **2014**, *118*, 3838–3845.

(51) Chan, W. C. W.; Nie, S. Quantum Dot Bioconjugates for Ultrasensitive Nonisotopic Detection. *Science.* **1998**, *281*, 2016–2018.

(52) Jaiswal, J. K.; Mattoussi, H.; Mauro, J. M.; Simon, S. M. Long-Term Multiple Color Imaging of Live Cells Using Quantum Dot Bioconjugates. *Nat. Biotechnol.* **2003**, *21*, 47–51.

(53) Alivisatos, P. The Use of Nanocrystals in Biological Detection. *Nat. Biotechnol.* **2004**, *22*, 47–52.

(54) Jamieson, T.; Bakhshi, R.; Petrova, D.; Pocock, R.; Imani, M.; Seifalian, A. M. Biological Applications of Quantum Dots. *Biomaterials* **2007**, *28*, 4717–4732.

(55) Wang, W.; Kapur, A.; Ji, X.; Safi, M.; Palui, G.; Palomo, V.; Dawson, P. E.; Mattoussi, H. Photoligation of an Amphiphilic Polymer with Mixed Coordination Provides Compact and Reactive Quantum Dots. *J. Am. Chem. Soc.* **2015**, *137*, 5438–5451.

(56) Talapin, D. V; Rogach, A. L.; Mekis, I.; Haubold, S.; Kornowski, A.; Haase, M.; Weller, H. Synthesis and Surface Modification of Amino-Stabilized CdSe , CdTe and InP Nanocrystals. Surfaces, A: *Colloids and Physicochemical and Engineering Aspect,* **2002**, *202*, 145–154.

(57) Yeh, Y.-C.; Patra, D.; Yan, B.; Saha, K.; Miranda, O. R.; Kim, C. K.; Rotello, V. M. Synthesis of Cationic Quantum Dots via a Two-Step Ligand Exchange Process. *Chem. Commun.* **2011**, *47*, 3069–3071.

(58) Yeh, Y.-C.; Saha, K.; Yan, B.; Miranda, O. R.; Yu, X.; Rotello, V. M. The Role of Ligand Coordination on the Cytotoxicity of Cationic Quantum Dots in HeLa Cells. *Nanoscale* **2013**, *5*, 12140–12143.

(59) Li, X.; Yeh, Y.-C.; Giri, K.; Mout, R.; Landis, R. F.; Prakash, Y. S.; Rotello, V. M. Control of Nanoparticle Penetration into Biofilms through Surface Design. *Chem. Commun.* **2015**, *51*, 282–285.

(60) Nakashima, T.; Kawai, T. Quantum Dots-Ionic Liquid Hybrids: Efficient Extraction of Cationic CdTe Nanocrystals into an Ionic Liquid. *Chem. Commun.* **2005**, 12, 1643–1645.

(61) Hayakawa, Y.; Nonoguchi, Y.; Wu, H.-P.; Diau, E. W.-G.; Nakashima, T.; Kawai, T. Rapid Preparation of Highly Luminescent CdTe Nanocrystals in an Ionic Liquid via a Microwave-Assisted Process. *J. Mater. Chem.* **2011**, *21*, 8849–8853.

(62) Taniguchi, Y.; Takishita, T.; Kawai, T.; Nakashima, T. End-to-End Self-Assembly of Semiconductor Nanorods in Water by Using an Amphiphilic Surface Design. *Angew. Chem. int. Ed.* **2016**, *55*, 2083–2086.

(63) Taniguchi, Y.; Yasue, K.; Kawai, T.; Nakashima, T. A Versatile Surface Design to

Disperse Nanoparticles in Ionic Liquids and Organic Solvents. *Chem. Lett.* **2016**, *45*, 898–900.

(64) Bishop, K. J. M.; Wilmer, C. E.; Soh, S.; Grzybowski, B. A. Nanoscale Forces and Their Uses in Self-Assembly. *Small* **2009**, *5*, 1600–1630.

(65) Rao, A.; Roy, S.; Unnikrishnan, M.; Bhosale, S. S.; Devatha, G.; Pillai, P. P. Regulation of Interparticle Forces Reveals Controlled Aggregation in Charged Nanoparticles. *Chem. Mater.* **2016**, *28*, 2348–2355.

(66) Tien, J.; Terfort, A.; Whitesides, G. M. Microfabrication through Electrostatic Self-Assembly. *Langmuir* **1997**, *13*, 5349–5355.

(67) Kaszuba, M.; Corbett, J.; Watson, F. M.; Jones, A. High-Concentration Zeta Potential Measurements Using Light-Scattering Techniques. Phil. Trans. R. Soc. A **2010**, *368*, 4439–4451.

(68) Freimoser, F. M.; Jakob, C. A.; Aebi, M.; Tuor, U. The MTT [3-(4,5-Dimethylthiazol-2-yl)-2,5-Diphenyltetrazolium Bromide] Assay Is a Fast and Reliable Method for Colorimetric Determination of Fungal Cell Densities. Appl. Environ. Microbiol. **1999**, *65*, 3727-3729.

(69) Lakowicz, J. R. Principles of Fluorescence Spectroscopy, 3rd ed., Springer: New York, **1999**.

(70) Breus, V. V.; Heyes, C. D.; Nienhaus, G. U. Quenching of CdSe-ZnS Core-Shell Quantum Dot Luminescence by Water-Soluble Thiolated Ligands. *J. Phys. Chem. C* **2007**, *111*, 18589–18594.

(71) Algar, W. R.; Krull, U. J. Luminescence and Stability of Aqueous Thioalkyl Acid Capped CdSe/ZnS Quantum Dots Correlated to Ligand Ionization. *ChemPhysChem* **2007**, *8*, 561–568.

(72) González-Araoz, M. P.; Sanchez-Ramirez, J. F.; Jiménez-Pérez, J. L.; Chigo-Anota, E.; Herrera-Pérez, J. L.; J. G. Mendoza-Alvarez, J. G. Negative Thermal Diffusivity Enhancement in Semiconductor Nanofluids. *Nat. Sci.* **2012**, *4*, 1022–1028.

(73) Santos, C. I. D. L.; Carvalho, M. S.; Raphael, E.; Dantas, C.; Ferrari, J. L.; Schiavon, M. A. Synthesis, Optical Characterization, and Size Distribution Determination by Curve Resolution Methods of Water-Soluble CdSe Quantum Dots. *Materials Research*, **2016**, *19*, 1407-1416.

(74) Derfus, A. M.; Chan, W. C. W.; Bhatia, S. N. Probing the Cytotoxicity of Semiconductor Quantum Dots. *Nano Lett.* **2004**, *4*, 11–18.

(75) Brunetti, V.; Chibli, H.; Fiammengo, R.; Galeone, A.; Malvindi, M. A.; Vecchio, G.; Cingolani, R.; Nadeau, J. L.; Pompa, P. P. InP/ZnS as a Safer Alternative to CdSe/ZnS Core/shell Quantum Dots: In Vitro and in Vivo Toxicity Assessment. *Nanoscale* **2013**, *5*, 307–317.

(76) Alarcón, E.; Aspée, a; González-Béjar, M.; Edwards, A. M.; Lissi, E.; Scaiano, J. C. Photobehavior of Merocyanine 540 Bound to Human Serum Albumin. *Photochem. Photobiol. Sci.* **2010**, *9*, 861–869.

(77) Förster, T. 10th Spiers Memorial Lecture. Transfer Mechanisms of Electronic Excitation. *Discuss. Faraday Soc.* **1959**, *27*, 7-17.

(78) Medintz, I. L.; Pons, T.; Susumu, K.; Boeneman, K.; Dennis, A. M.; Farrell, D.; Deschamps, J. R.; Melinger, J. S.; Bao, G.; Mattoussi, H. Resonance Energy Transfer between Luminescent Quantum Dots and Diverse Fluorescent Protein Acceptors. *J. Phys. Chem. C* **2009**, *113*, 18552–18561.

(79) Kastelic, M.; Kalyuzhnyi, Y. V; Hribar-Lee, B.; Dill, K. A.; Vlachy, V. Protein Aggregation in Salt Solutions. *Proc. Natl. Acad. Sci.* **2015**, *112*, 6766–6770.

(80) Berney, C.; Danuser, G. FRET or No FRET : A Quantitative Comparison. *Biophys. J.* **2003**, *84*, 3992–4010.

(81) Kholmicheva,N.; Moroz, P.; Eckard, H.; Jensen, G.; Mikhail, Z. Energy Transfer in Quantum Dot Solids. *ACS Energy Lett.* **2017**, *2*, 154−160.

(82) Peng, Z. A.; Peng, X. Formation of High-Quality CdTe, CdSe, and CdS Nanocrystals Using CdO as Precursor. *J. Am. Chem. Soc.* **2001**, *123*, 183–184.

(83) Reiss, P.; Protière, M.; Li, L. Core/Shell Semiconductor Nanocrystals. *small*, **2009**, *5*, 154-168.

2.9 Appendix

2.9.1 EDX analysis of [+] InP/ZnS QDs

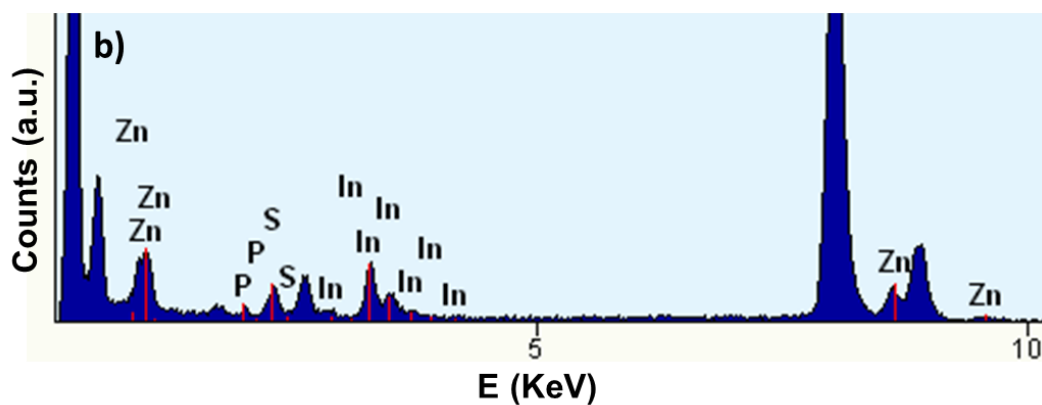**Figure 2.23:** EDX spectrum of [+] InP/ZnS QD studied during HRTEM analysis confirms the presence of In, P, Zn and S in the QDs.
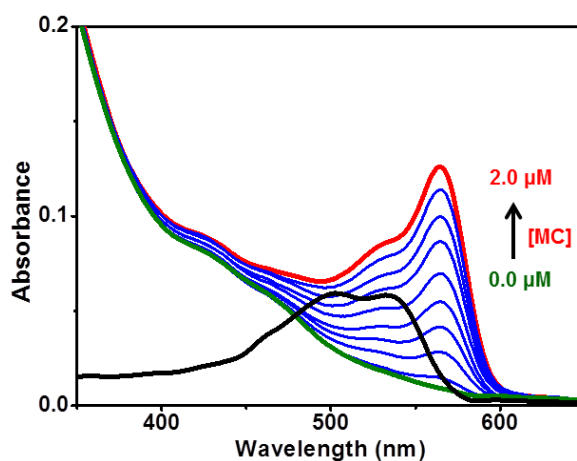

Figure 2.24: Absorption spectral changes of [+] InP/ZnS QD with increasing concentration of [-] MC dye. The absorption spectrum of [-] MC alone is shown as the black curve.
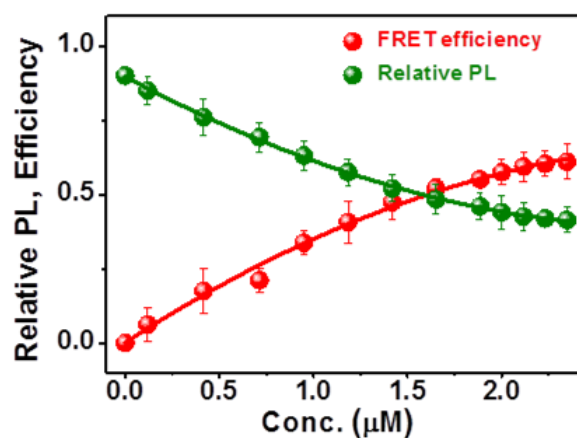
Figure 2.25: A plot showing the saturation of relative QD PL decay and FRET efficiency vs concentration of MC dye.
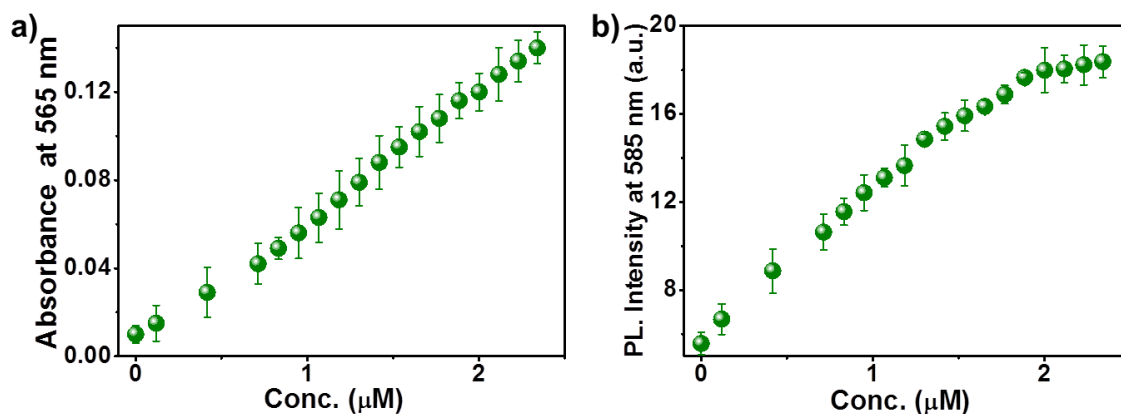
Figure 2.26: Variation in a) absorption (monitored at 565 nm) and b) PL (monitored at 585 nm) intensities of [+] InP/ZnS QD:::[-] MC complex with increasing concentration of [-] MC dyes are shown. The absorption intensity keeps on increasing with the addition of [-] MC dye to [+] InP/ZnS QD. Interestingly, the PL intensity got saturated after ~2 μM addition of [-] MC dyes, indicating that the MC dye is getting excited through a nonradiative energy transfer from InP/ZnS QDs.
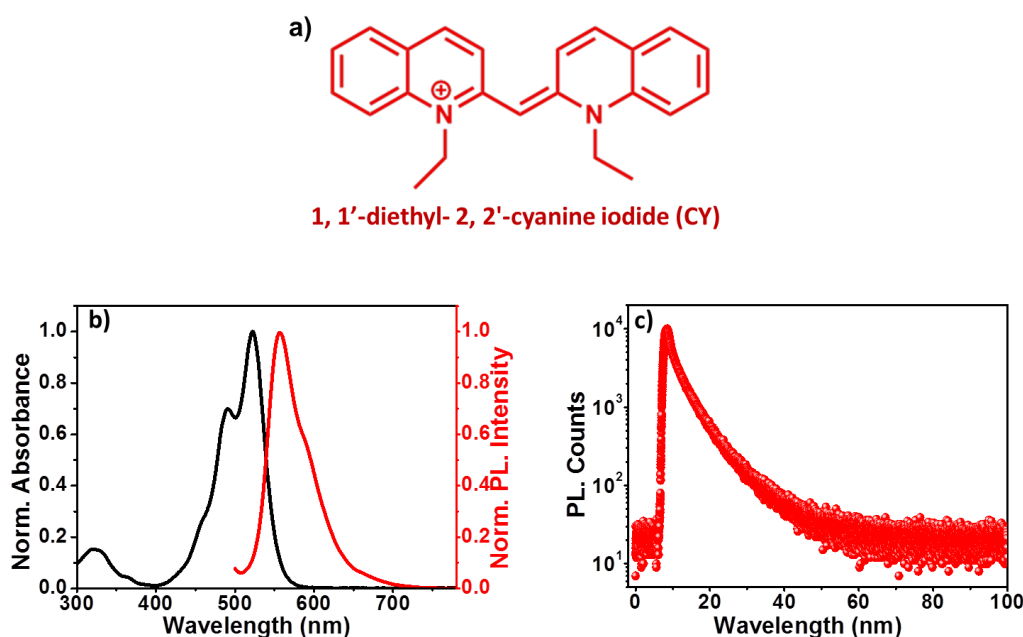
Figure 2.27: a) Chemical structure of 1, 1'-diethyl- 2, 2'-cyanine iodide dye (CY). b) Normalized absorption (black curve) and PL (red curve) spectra of [+] CY dye in water. c) PL decay profile of [+] CY dye in water upon excitation with a 405 nm laser source.

2.9.2 Synthesis of TOPO capped CdSe QDs

The synthesis was carried out by following the reported procedure.[82] Briefly, CdO (0.35 g, 0.26 mmol), dodecyl amine (3 mL), tetradecylphosphonic acid (0.21 g, 0.72 mmol), trioctyl phosphine oxide (1.35 g, 3.45 mmol) were loaded in a 50 mL of three-necked RB and heated to 100 ^{0}C under N_2 atmosphere. The temperature of the reaction mixture was further

increased to 300 ^{0}C to form a clear solution. The solution containing Se (0.032 g, 0.26 mmol) in 1 mL TOP was injected to the hot solution. After desired crystal growth, the reaction was arrested by reducing the reaction temperature to ambient conditions. The resultant QDs were purified two times by precipitation using excess ethanol and redispersing back in chloroform for further studies.

2.9.3 Synthesis of TOPO capped CdSe/ZnS QDs

A reaction mixture containing HDA, octadecene, and TOPO capped CdSe nanoparticles were heated to 100 ^{0}C in an inert atmosphere for 30 min. The mixture was further heated up to 150 ^{0}C, and an injection mixture containing calculated amount of (Et)$_2$Zn and HMDST in 2 mL of TOP was added dropwise, under gentle stirring. The temperature was further raised to 180 ^{0}C for 30 min. Then the reaction mixture was cooled to room temperature, and the resultant QDs were purified by precipitating with methanol, followed by centrifugation (3 times) and redispersed in chloroform.

2.9.4 Steady state absorption and PL of CdSe/ZnS QDs
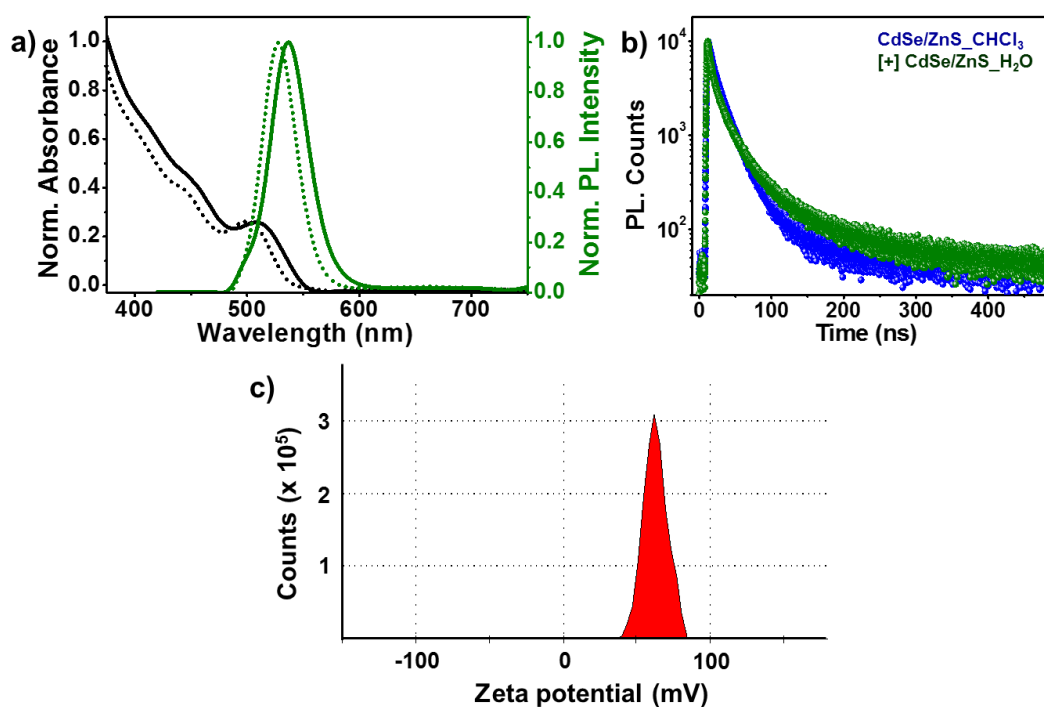
Figure 2.28: a) Normalized absorption (black spectrum) and PL (green spectrum) of CdSe/ZnS QD before (dotted spectrum) and after (solid spectrum) place exchange. b) PL decay profiles of CdSe/ZnS QD before (blue spectrum) and after (green spectrum) place exchange, upon 405 nm excitation. b) Zeta potential plot confirming the cationic charge on the surface of CdSe/ZnS QDs. A ζ of + 59.1 $\pm$ 2.7 was observed, and the error was calculated from three different measurements on three different samples.

The concentrations of the QDs were determined from the size and first excitonic peak using the following equations:

2.9.5 Calculation of concentration of [+] InP/ZnS QD:

The concentration was estimated from the optical absorption spectra of [+] InP/ZnS QD by using Beer -Lambert's law

$$A = \varepsilon C l \tag{9}$$

Here, A is the absorbance at first excitonic peak, ε is the molar extinction coefficient in L mol^{-1}cm^{-1}, C is the concentration, and l is the path length of the cuvette (1cm).

ε is calculated from following equation[83]

$$\varepsilon = 3046.1(D)^3 - 76532(D)^2 + (5.5137 \, X \, 10^5)(D) - (8.9839 \, X \, 10^5) \tag{10}$$

Here, D, the diameter of the [+] InP/ZnS QD was estimated to be 2.7 nm from the following equation[83]

$$D = (-3.7707 \, X \, 10^{-12})\lambda^5 + (1.0262 \, X \, 10^{-8})\lambda^4 - (1.0781 \, X \, 10^{-5})\lambda^3 +$$
$$(5.4550 \, X \, 10^{-3})\lambda^2 - (1.3122)\lambda + 119.9 \tag{11}$$

Here, λ is the wavelength at first excitonic peak in nm (440 nm). The ε was calculated to be 92347.1 L mol^{-1}cm^{-1}. Concentration of ~0.8 μM was obtained upon substituting the value of ε in equation (9) with OD of 0.074 at 440 nm.

2.9.6 Calculation of concentration of [+] CdSe/ZnS QD:

The diameter, D, of [+] CdSe/ZnS QD was estimated to be 2.5 nm from the following equation[83]

$$D = (1.6122 \, X \, 10^{-9})\lambda^4 - (2.6575 \, X \, 10^{-6})\lambda^3 + (1.6242 \, X \, 10^{-3})\lambda^2 - (0.4277)\lambda +$$
$$41.57 \tag{12}$$

Here, λ is the wavelength at first excitonic peak in nm (510 nm). The ε is calculated from following equation[83]

$$\varepsilon = 5857 \, (D)^{2.65} \tag{13}$$

The ε was calculated to be 66407.4 L mol^{-1}cm^{-1}. The concentration of [+] CdSe/ZnS QD was estimated by substituting the ε value in (9).
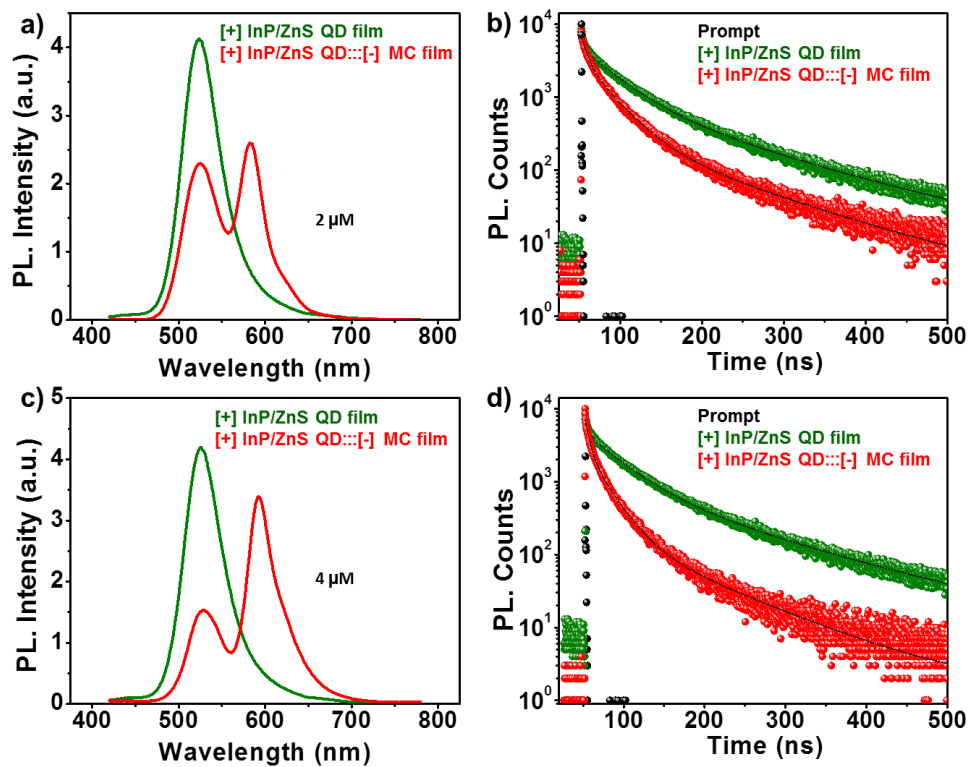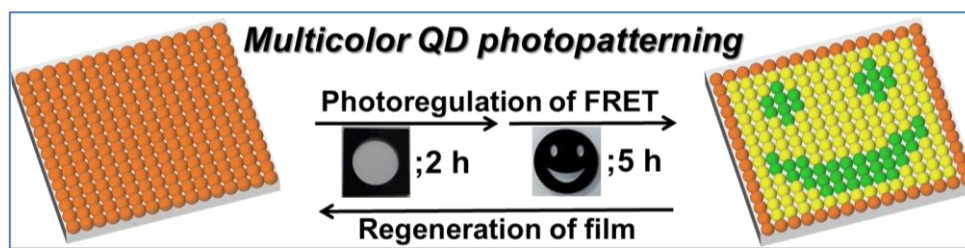
Figure 2.29: Changes in the steady state PL (a, c) and corresponding quenching in the PL decay profiles (b, d) of the [+] InP/ZnS QD in the presence of different concentrations of [−] MC dye in the solid film.

Chapter 3

FRET Assisted Multicolor Photopatterning from Single Quantum Dot Nanohybrid Films

3.1 Abstract

Precise patterning and localization of functional nanomaterials is the key step for miniaturization and building of optoelectronic devices. Present study utilises a robust methodology for the multicolor patterning of luminescent Indium Phosphide/Zinc Sulfide Quantum Dot (InP/ZnS QD) film, by taking the advantage of QD's superior photostability over organic dyes. The photoirradiation causes the controlled degradation of organic dye molecules and thereby, modulates the composition of donor-acceptor pair in the QD-dye nanohybrid film. Consequently the efficiency of Förster Resonance Energy Transfer (FRET) in QD − dye nanohybrid film is regulated between completely ON and OFF states, through a moderately efficient state. This led to the generation of multicolor luminescent patterns comprising of at least three distinct colors: orange (corresponding to FRET ON state, E_{FRET} ~85 %), yellow (corresponding to moderately FRET ON state, E_{FRET} ~50 %) and green (corresponding to FRET OFF state, $E_{FRET} = 0$ %). The photopatterns generated are recyclable over multiple cycles without any compromise of the color clarity, owing to the reversible switching between FRET ON and OFF states. The highlight of the present work is the use of a single QD nanohybrid system to create multicolor luminescent patterns; as opposed to the common practice of using different colored QDs. FRET assisted photopatterning of luminescent InP/ZnS QD films provides a fundamentally unique and cost effective approach for the manufacturing of luminescent optoelectronic devices.

3.2 Introduction

The creation of highly ordered multicolor luminescent patterns is an important step in the production of Quantum Dot (QD) based display devices.[1-8] Many patterning methodologies including direct deposition of QDs,[9,10] selective photon and e-beam irradiation of homogeneous QD film,[11,12] stamping,[13-16] ink-jet printing,[17,18] contact printing,[19-21] photolithographic lift-off,[22-24] and layer-by-layer assembly[25,26] have been developed in pursuit of achieving this goal. Kotov and Liz-Marzan's groups have used the photoactivation of citrate stabilized QDs to generate micron sized multicolor patterns. Upon irradiation, an increase in the luminescence and quantum yield of citrate capped CdSe/CdS QDs was observed. This was because of the smoothening of the surface of QDs in the presence of O_2, which decreases the surface trap states and defects **(Figure 3.1).**[27] Likewise, luminescent patterns of QDs with diffraction limited resolution were produced by Batteas and Coworkers through the photooxidation of surface bound ligands.[28]
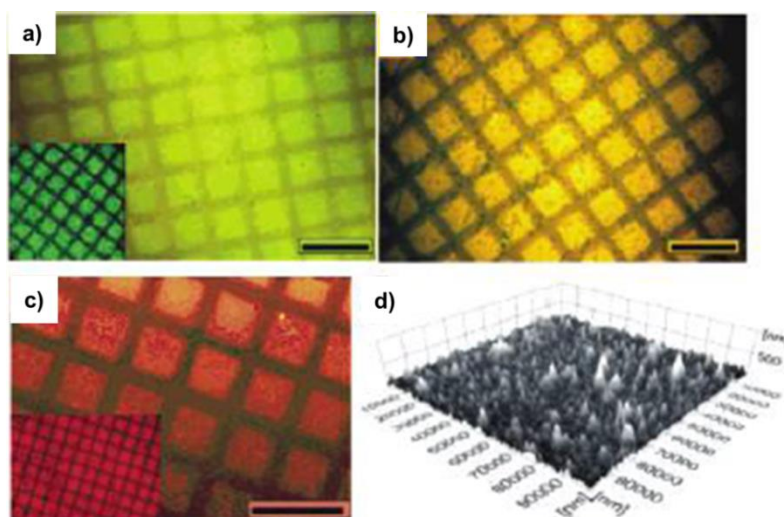
Figure 3.1: a-c) Fluorescence microscopy images of QD patterns generated through the photoactivation of different sizes of CdSe/CdS QDs, with a 200-mesh TEM grid as the photomask. Inset shows the corresponding confocal images. d) Topography image of the QD patterned film. Scale bar corresponds to 200 μm. (Reproduced in part with permission from reference 27. Copyright 2003 American Chemical Society).

Weiss and Coworkers were successful in generating micron sized single colored high contrast photopatterns, while preserving the original QD emission, through photodegradation of charge transfer quencher.[29] Tsukruk and Coworkers fabricated both positive and negative luminescent photopatterns by the intrinsic modification of QD emission upon exposure to light.[30] Rogers' group has generated the micron sized QD patterns using the protocol comprised of electrodynamic jet (E-jet) printing. This technique uses the electric field to eject the QD ink with a narrow width, and the resulting QD pattern shows uniform line thickness. The high resolution red and green QD patterns generated using this technique were used as an active layer in QD LEDs (**Figure 3.2**).[18]
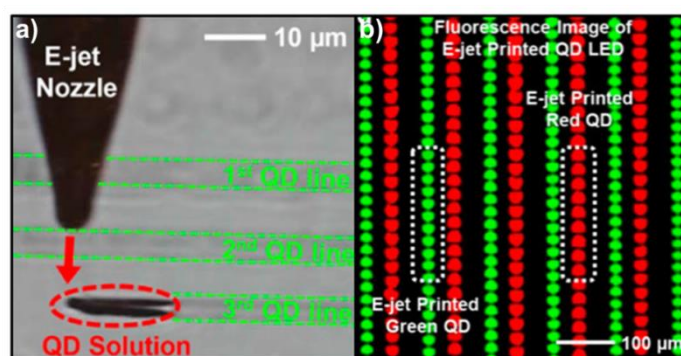
Figure 3.2: a) An optical microscope image captured during the E-jet printing process. b) Fluorescence images of E-jet printed luminescent patterns, where different sizes of QDs were used as the ink. (Reproduced in part with permission from reference 18. Copyright 2015 American Chemical Society).

Kim and Coworkers used an intaglio transfer-printing technique to generate high resolution QD arrays. This process employs an intaglio trench (stamping technique) to generate QD patterns with controlled and uniform pixel size. The difference in the surface energies between PDMS stamp and target substrate facilitated a ~100 % transfer yield, irrespective of the size and shape of the patterns (**Figure 3.3**).[31]
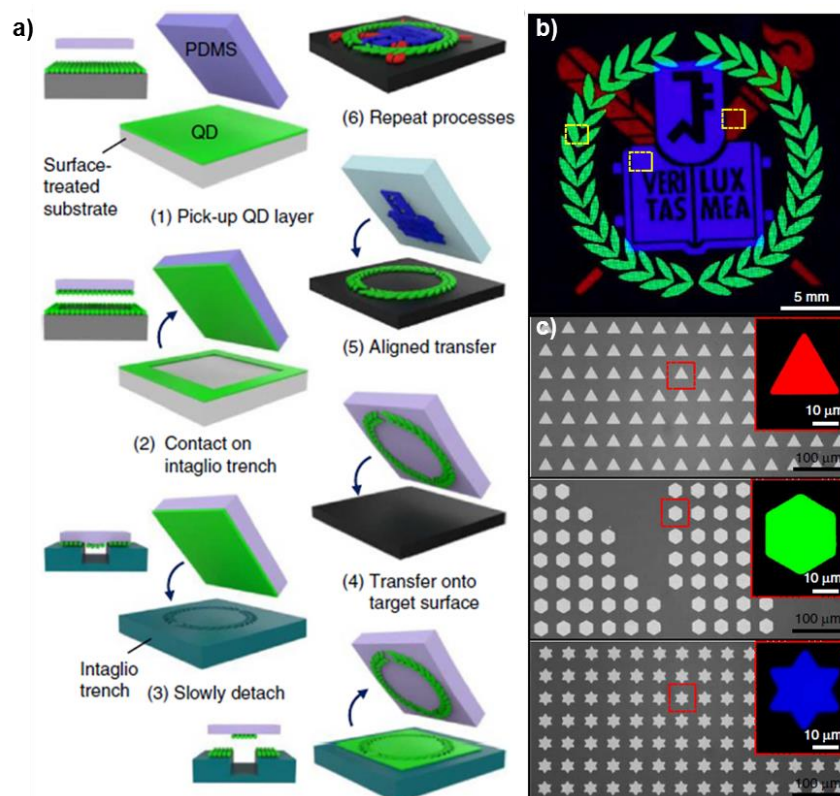
Figure 3.3: a) Schematic representation of intaglio transfer printing. b) The PL image of the multicolor QD patterns (RGB) via multiple aligned transfer printing. c) SEM and PL images (inset) of selected regions shown in panel 'b'. (Reproduced in part with permission from reference 31 Copyright 2015 Nature Publishing Group).

In another elegant work, Talapin and Coworkers have reported a direct optical lithography technique to create multicolor patterns of various nanomaterials stabilized with light responsive thiatriazole ligands. Here, the QDs were capped with photoactive ammonium 1,2,3,4-thiatriazole-5-thiolate ($NH_4CS_2N_3$), which were highly soluble in a mixture of dimethyl sulphoxide (DMSO) and dimethylformamide (DMF). An exposure of light, transforms the 1,2,3,4-thiatriazole-5-thiolate ($CS_2N_3^-$) to thiocyanate (SCN^-), making the QDs insoluble in DMF. Using this direct deposition methodology, the luminescent patterns were generated on rigid and flexible substrates by illuminating QDs films through a mask and then washing off the unexposed QDs with DMF (**Figure 3.4**).[10]
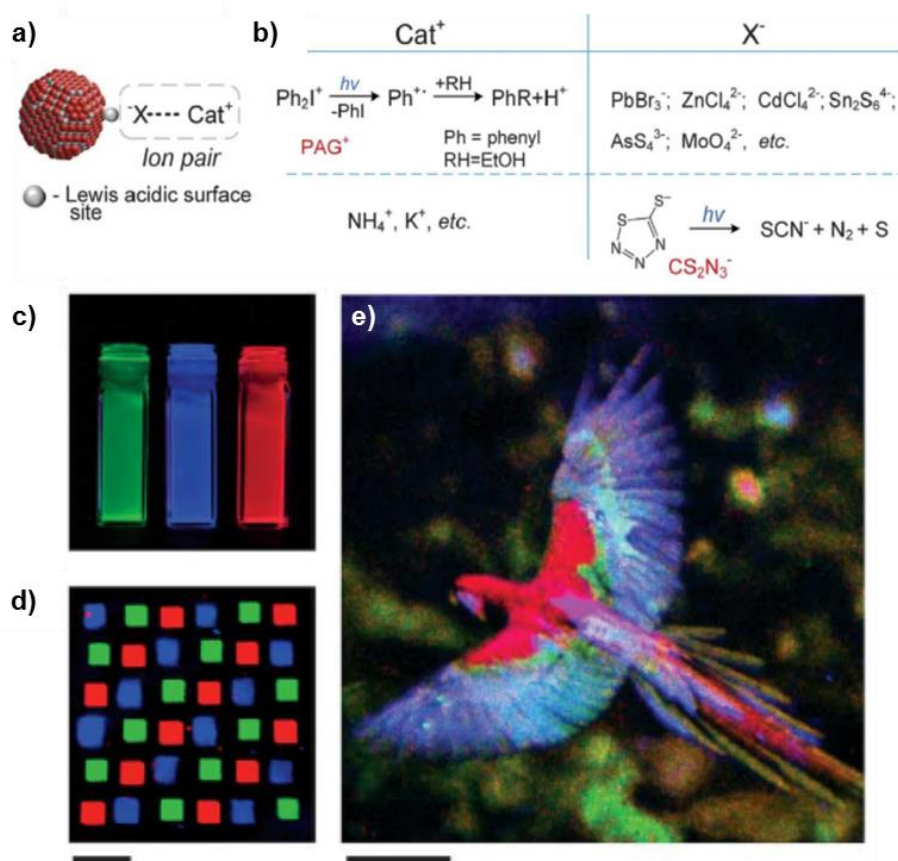
Figure 3.4: a) Schematic representation of nanoparticles functionalized with ion pair ligands. b) Two complementary approaches to achieve photosensitive inorganic ligands. Either cation (PAG$^+$) or anion (CS$_2$N$_3^-$) part of the ion-pair ligand can react with UV light. c) Photographs of red-emitting CdSe/ZnS, green-emitting InP/ZnS, and blue-emitting ZnSe/ZnS QDs capped with NH$_4$CS$_2$N$_3$ ligands dispersed in DMF, under UV light. d) Red, green and blue-emitting QDs patterns using photoactive NH$_4$CS$_2$N$_3$ ligands. e) A true color image containing ~8 × 105 RGB subpixels. Scale bar corresponds to 5 mm (Reproduced in part with permission from reference 10. Copyright 2017 American Association for the Advancement of Science).

In most of the previous examples of QD photopatterning, different sizes (colors) of QD samples were required to generate the multicolor patterns.[10,14-27,30-33] The advantage of our technique is the use of a single QD nanohybrid system, to create micron sized multicolor luminescent patterns. Our approach relies on the photoregulation of Förster Resonance Energy Transfer (FRET) efficiency in QD - dye donor-acceptor film. The phenomenon of FRET describes the mechanism of excitation energy transfer from a donor to an acceptor chromophore, through a nonradiative dipole–dipole coupling.[34-36] QDs have emerged as one of the integral part of modern FRET studies due to its direct impact in wide range of applications including optoelectronics, sensors, bio-imaging, DNA hybridization, protein folding and bio-assays.[37-44] In the present work, the superior photostability of the QDs over

organic dyes[45] was smartly used to form multicolor luminescent patterns in QD nanohybrid film. The photoirradiation causes the controlled degradation of acceptor organic dye molecules, and modulates the composition of donor-acceptor pair in the QD-dye nanohybrid film. Consequently the efficiency of FRET in QD − dye nanohybrid film was regulated between completely ON and OFF states, through a moderately efficient state (**Figure 3.5**). This led to the generation of multicolor luminescent patterns comprising of at least three distinctly different colors: orange (corresponding to an efficient FRET ON state, E_{FRET} ~85 %), yellow (corresponding to a moderately efficient FRET ON state, E_{FRET} ~50 %) and green (corresponding to a FRET OFF state, $E_{FRET} = 0$ %). Also, these luminescent photopattern films were reusable over multiple cycles without any compromise of the color clarity. Creation of well-organized patterns through the photoregulation of FRET is conceptually unique, and provides an alternate methodology for the manufacturing of luminescent nanocrystal based multicolor display devices.
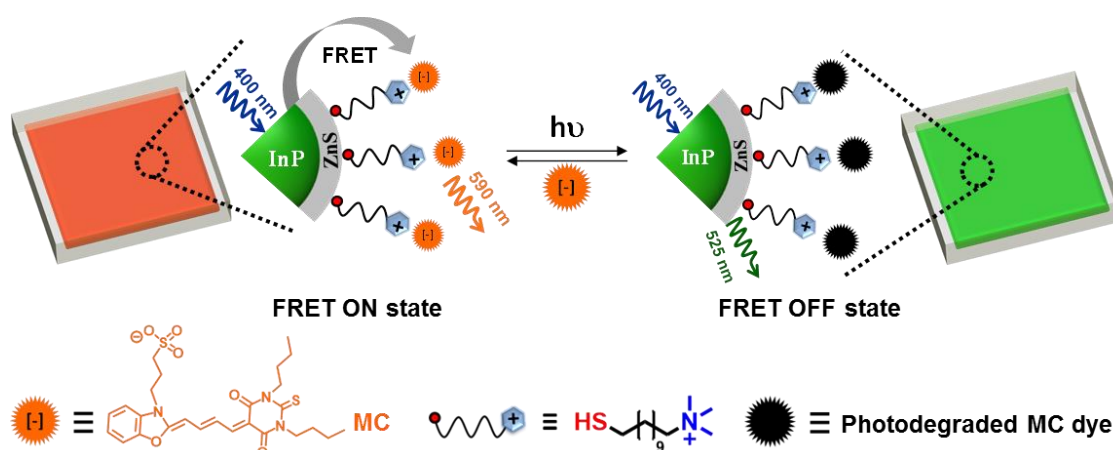
Figure 3.5: Schematic representation of photoassisted FRET ON-OFF process in [+] InP/ZnS QD:::[-] MC dye agarose film. The irradiation of QD:::dye agarose wet film resulted in the degradation of MC dyes, thereby switching OFF the FRET process. As a result the luminescence of agarose film changed from orange to green color (FRET ON to OFF states, respectively). Addition of fresh MC dyes to QD:::dye agarose film revives the donor-acceptor complexation, thereby switching back to FRET ON state.

3.3 Experimental Section

3.3.1 Materials and Reagents:

Indium acetate, myristic acid (MA), 1-octadecene (ODE), zinc stearate, dodecanethiol (DDT), merocyanine-540 (MC), agarose, isopropyl alcohol (IPA), polydimethylsiloxane (PDMS) were purchased from Sigma-Aldrich. Tris(trimethylsilyl)phosphine (P(TMS)$_3$) was purchased from Strem chemicals. All the reagents were used as received without any further purification. N,N,N-trimethyl(11-mercaptoundecyl)ammonium chloride (TMA) was synthesized according to a reported procedure.[46]

3.3.2 Synthesis of InP/ZnS quantum dots:

The protocol for the synthesis of InP/ZnS QDs was different from the one described in Chapter 2, in order to get QDs with higher quantum yield. We adopted a one-pot synthesis of InP/ZnS QDs with minor modifications.[47] Briefly, 0.2 mmol of indium acetate, 0.7 mmol of myristic acid and 6 mL of 1-octadecene were loaded in a three-necked flask and heated to 120 ^{o}C under N$_2$ atmosphere for 10 min, and evacuated for 1 h to obtain an optically clear solution. The reaction mixture was backfilled with N$_2$ and cool down to room temperature. Now a mixture of 0.2 mmol zinc stearate, 0.2 mmol DDT, 0.2 mmol P(TMS)$_3$, 3 mL of 1-octadecene were prepared under inert atmosphere and injected to the above solution, and the temperature was raised to 270 ^{o}C for 1 h. At around 60 ^{o}C, the reaction mixture starts becoming yellow which indicates the decomposition of P(TMS)$_3$ and start of reaction with Indium acetate to form InP core. The colour slowly changes from light yellow to dark orange with an increase in temperature, indicating the growth of QDs. When the temperature reaches ~230 ^{o}C, DDT starts decomposing leading to the formation of ZnS shell. Maintaining the reaction at 270 ^{o}C for 1 h ensures the formation of InP/ZnS QD. The reaction mixture was then cooled to room temperature by adding 5 mL of cold toluene to arrest the growth. The QDs were purified by precipitating with ethanol three times, and finally redispersing in chloroform for further studies. The quantum yield of InP/ZnS QD was estimated to be ~45 % with reference to Coumarin 153.

3.3.3 Preparation of water-stable [+] InP/ZnS QDs:

The water-stable [+] InP/ZnS QDs were prepared through a place exchange reaction, as mentioned in the Chapter 2.[48]

3.3.4 Preparation of wet and dry agarose films:

3.3.4.1 [+] InP/ZnS QD and [+] InP/ZnS:::[-] MC agarose wet film:

In a typical procedure, 30 mg of agarose 1.0 % (w/v) was mixed with ~3 mL [+] InP/ZnS QD solution (~5 μM). The mixture was then heated at 60 ^{o}C till the complete dissolution of agarose. The clear solution was then poured into a petri dish for film casting and cured for 1 h at room temperature. The [+] InP/ZnS QD agarose film was dipped in ~5 mL merocyanine-540 (MC) dye solution (~15 μM) for 3 h to get the [+] InP/ZnS QD:::[-] MC agarose wet film (QD:::dye agarose wet film).

3.3.4.2 [+] InP/ZnS QD:::[-] MC dry agarose film:

[+] InP/ZnS QD:::[-] MC dry agarose films were prepared by mixing the [+] InP/ZnS QD::: [-] MC complex with hot agarose solution (1.0 % w/v) and heating overnight at 50 ^{o}C. The films were thoroughly characterized using spectroscopic techniques to investigate the changes in the properties [+] InP/ZnS QD before and after the formation of films.

3.3.5 Energy transfer experiments in agarose film:

In a typical experiment, [+] InP/ZnS QD agarose film was dipped in a 15 μM of MC dye solution for ~3 h. Spectral changes were monitored by using Shimadzu UV-3600 and Fluorolog-3 (HORIBA Scientific) spectrofluoremeter. The corresponding PL lifetime measurements were carried out using Horiba DeltaFlex Time Correlated Single Photon Counting (TCSPC) system using a 405 nm Delta-diode as the excitation source.

3.3.6 Microscopy details:

QD:::dye agarose wet films were imaged on a Leica TCS SP8 two-photon microscope (Leica Microsystems Inc., Exton, PA) using water objective lens (40 X) and 800 nm laser excitation (Coherent Inc., Santa Clara, CA). The emission was collected simultaneously from two channels using 450-550 nm and 550-750 nm band-pass filters with non-descanned (NDD) PMT detector. Similarly, QD agarose wet film was imaged using 800 nm laser excitation, and emission was collected in the whole visible range of 450-750 nm. Lambda scanning was performed by scanning the films in the range of 450- 750 nm with 10 nm intervals. The PL spectrum was generated from the λ-stack of a particular area using Leica software. The 100 μm thick Z-stacks were acquired by scanning from the base to the top of the wet films with a spacing of 0.8 μm.

3.3.7 Photopatterning of QD:::dye agarose dry films:

All the photopatterning experiments were performed using QD:::dye agarose dry film with different masks. In a typical experiment, the mask was placed on top of the QD:::dye agarose film and exposed to ~5 h photoirradiation with 10 W green LED, at a distance of 2 cm from the film (incident power on the film was estimated to be ~6.5 mW/cm^2 using an optical power meter from Newport Model 842.PE). At the exposed regions, the dye molecules will be completely degraded displaying a green color under UV light, corresponding to emission of [+] InP/ZnS QD (E_{FRET} ~0 %). Whereas at the unexposed regions the QD:::dye complex will be preserved, displaying an orange color under UV light (E_{FRET} ~85 %). It is worth mentioning that the irradiation time was lowered to ~5 min using a 1 W green laser as the irradiation source (incident power on the film was estimated to be ~435 mW/cm^2).

3.3.8 Multicolor photopatterning:

Multicolor photopatterning was performed by controlling the extent of dye degradation by varying the time of irradiation. A prolonged ~5 h irradiation (as mentioned earlier) will cause a complete degradation of dye, thereby imparting a green color to the agarose film (corresponding to E_{FRET} ~0 %). Whereas, when the irradiation time was reduced to ~2 h, a distinct yellow color (corresponding to E_{FRET} ~50 %) was observed because of the partial degradation of the dye. The unexposed regions will always display an orange color corresponding to E_{FRET} ~85 %.

3.4 Results and Discussion

3.4.1 Photoregulation of FRET in QD:::dye agarose film:

We worked with a FRET donor-acceptor system comprising of environmentally friendly cationic Indium Phosphide/Zinc Sulfide core/shell ([+] InP/ZnS) QD and anionic merocyanine-540 ([-] MC) organic dye. An efficient FRET process in [+] InP/ZnS QD:::[-] MC dye nanohybrid system was previously demonstrated in the Chapter 2 in solution state.[48] The first and foremost step in the current photopatterning work was to translate the FRET process from solution state to thin films. Myristic acid capped green emitting InP/ZnS QD was prepared using modified literature reports.[47] The QD surface was then place exchanged with *N,N,N*-trimethyl (11-mercaptoundecyl)ammonium chloride (TMA) as per the place exchange protocol reported in Chapter 2, to impart the water stability and cationic surface charge.[48] The readily available and commonly used agarose was selected as the substrate for the thin film preparation. Wet agarose films of green emitting QD were prepared by

polymerizing them in the presence of [+] InP/ZnS QDs. The steady state and time resolved spectroscopic studies revealed that the photophysical properties of [+] InP/ZnS QD were well preserved in the wet agarose films (**Figure 3.6**). [+] InP/ZnS QD agarose wet film was then immersed in ~15 μM [-] MC dye solution for ~3 h, resulting in the diffusion and complexation of dye with QDs in the agarose film (**Figure 3.7**).
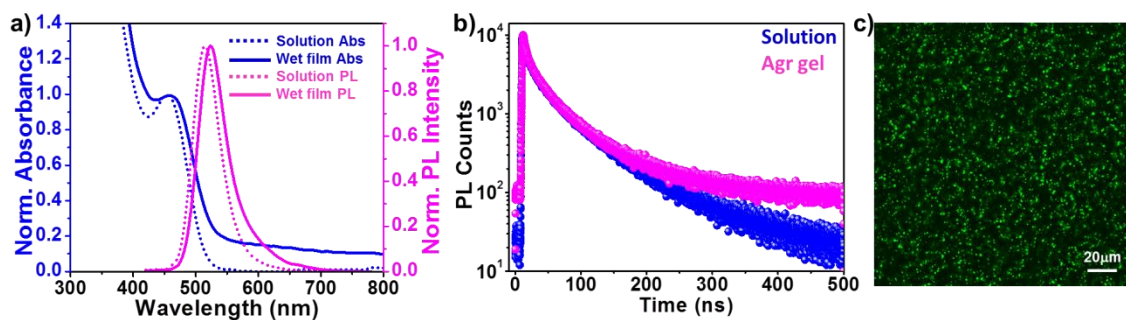
Figure 3.6: a) The normalized absorption and PL spectra of [+] InP/ZnS QD in solution and wet agarose film. b) The PL decay profiles of [+] InP/ZnS QD in both solution and wet agarose film. **c**) Two-photon PL image of [+] InP/ZnS QD agarose wet film, under 800 nm excitation collected in the entire visible range of 450-750 nm.
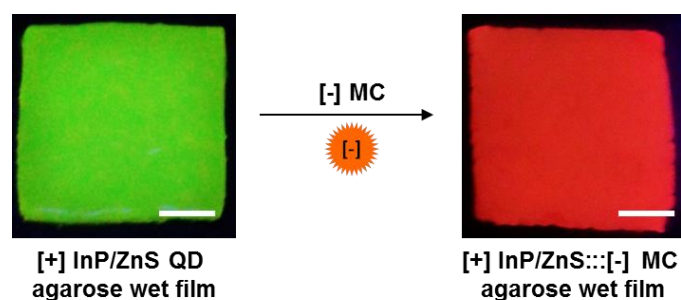
Figure 3.7: Preparation of [+] InP/ZnS:::[-] MC agarose wet films, by dipping the QD agarose film in the solution of ~15 μM MC dye for ~3 h. Scale bar corresponds to 1 cm.

These films will be referred to as QD:::dye agarose wet film throughout this Chapter. The process of FRET in QD:::dye agarose wet film was monitored using detailed spectroscopic (**Figure 3.8**) and optical microscopic techniques (**Figure 3.9**). The [+] InP/ZnS QD in the agarose film was selectively excited at 400 nm for steady state emission studies, wherein the MC dye absorption was minimal. A drastic quenching in the photoluminescence (PL) of [+] InP/ZnS QD was observed along with the concomitant formation of a new peak at ~590 nm (corresponding to the emission of [-] MC dye), through an isosbestic point (**Figure 3.8a**). This clearly indicates the process of resonance energy transfer from [+] InP/ZnS QD to [-] MC dye in the wet agarose film.[35,48-51] Time resolved PL studies showed a quenching in the

lifetime of [+] InP/ZnS QD from ~60 to ~15 ns, confirming the process of energy transfer in QD:::dye agarose wet film (**Figures 3.8b and Table 3.1**).[35,48-51] The efficiency and rate of energy transfer in QD:::dye agarose wet film were estimated to be ~75 % and ~4.7 x 10^7 s^{-1}, respectively (**Table 3.2**).
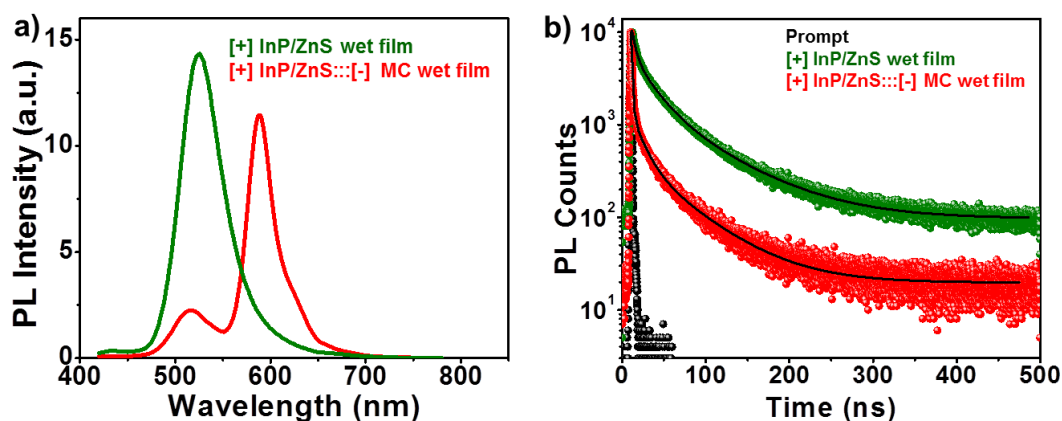
Figure 3.8: Photoregulation of FRET in QD:::dye agarose wet film. a) Variation in the steady state PL of [+] InP/ZnS QD in the presence of [-] MC dye, in QD-dye agarose wet film. b) PL decay profiles of [+] InP/ZnS QD agarose wet film in the absence (green decay) and presence (red decay) of [-] MC dye monitored at 525 nm, upon excitation with 405 nm laser source.

Table 3.1: PL decay analysis of [+] InP/ZnS QD agarose wet film in the presence of [-] MC dye measured in a time window of 500 ns.

Sample	τ_1 (ns)	a_1	τ_2 (ns)	a_2	τ_3 (ns)	a_3	Avg. τ (ns)	Efficiency (%)
[+] InP/ZnS agarose wet film	4.71	0.47	36.43	0.43	110.5	0.10	60.37	
[+] InP/ZnS:::[-] MC agarose wet film	1.01	0.56	12.71	0.32	22.6	0.12	15.23	74.76

Table 3.2: Energy transfer parameters for [+] InP/ZnS:::[-] MC agarose wet film.

Sample	$J(\lambda)$ (M^{-1} cm^{-1} nm^4)	R_0 (A)	E^a (%)	E^b (%)	r_0 (A)	$k_T(r)$ (s^{-1})
[+] InP/ZnS:::[-] MC agarose wet film	2.52 x 10^{15}	54.14	84.3	74.7	45.47	4.71 x 10^7

$J(\lambda)$ = Spectral overlap integral, R_0 = Förster distance, E^a = efficiency calculated from steady state, E^b = efficiency calculated from lifetime analysis, r = distance between the donor and acceptor, $k_T(r)$ = rate of energy transfer.

The two-photon confocal images were collected by selectively exciting QD at 800 nm. It is worth mentioning that [-] MC dye is two-photon inactive. 2D two-photon confocal images showed a weak emission from the [+] InP/ZnS QDs in the green channel (collected at 450-

550 nm), whereas a strong emission was observed in the red channel (collected at 550-750 nm), corresponding to the [-] MC dye emission. This once again confirms the process of resonance energy transfer from QD to MC dye (**Figures 3.9a,b**). Further, emission profiles constructed from the 2D two-photon confocal images were in agreement with the steady state data (**Figures 3.9d**). **Figures 3.9e,f** showed a uniform distribution of both [+] InP/ZnS QD and [-] MC dye throughout the agarose film.
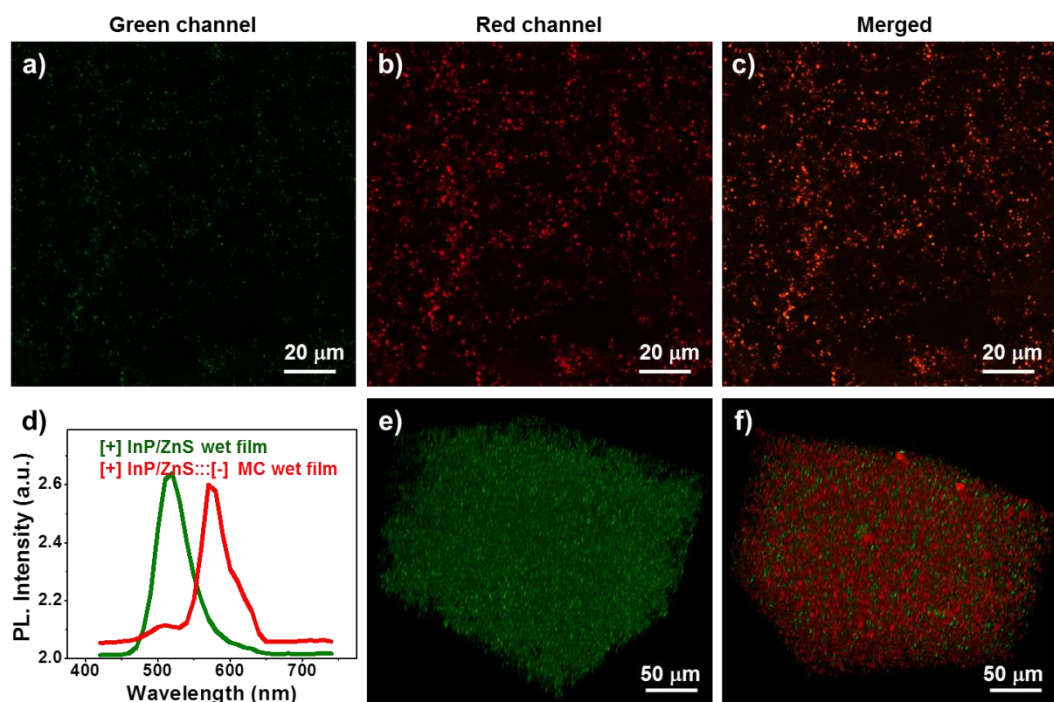
Figure 3.9: Two-photon PL images of [+] InP/ZnS agarose wet film dipped in a ~15 μM of [-] MC for ~3 h, collected at a) 450-550 nm wavelength range (QD donor emission range), b) 550-750 nm wavelength range ([-] MC acceptor emission range), and c) merged image. d) PL spectra (generated from lambda scanning) of [+] InP/ZnS QD (green solid line) and [+] InP/ZnS QD:::[-] MC (red solid line) agarose wet films. Z-stack 3D images of e) [+] InP/ZnS QD and f) [+] InP/ZnS:::[-] MC agarose wet films confirms the uniform distribution of both QD and dye in the film.

The process of energy transfer was observed uniformly throughout the agarose film due to the strong electrostatic attraction between oppositely charged InP/ZnS QD and MC dye. Control experiments performed between similarly charged [-] InP/ZnS QD and [-] MC dye show a lack of complexation, resulting in negligible FRET. This clearly confirms that a strong electrostatic attraction between the donor and acceptor components is essential for the creation of stable agarose film, and hence an efficient FRET (**Figures 3.10**).
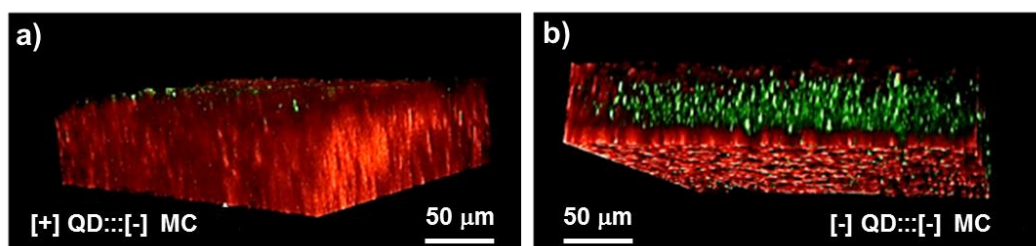
Figure 3.10: Z-stack 3D images of agarose wet films prepared by mixing a) oppositely charged [+] InP/ZnS and [-] MC, and b) similarly charged [-] InP/ZnS and [-] MC donor and acceptor complexes. The lack of uniform complexation in [-] InP/ZnS:::[-] MC agarose film confirms the role of electrostatic interactions in achieving an efficient FRET.

Next, systematic photoirradiation experiments were performed to selectively degrading the [-] MC dye for controlling the FRET, and thereby the emission color of QD:::dye agarose wet film. The PL of InP/ZnS QD gradually recovered back to its initial position (~525 nm), during the 5 h irradiation of the QD:::dye agarose wet film with a 10 W 530 nm light emitting diode (LED; **Figure 3.11**). The efficiency of FRET dropped down as a function of irradiation, and the emission color changed from orange to green (corresponding to FRET ON and OFF states, respectively). Addition of fresh [-] MC dyes to the photodegraded QD:::dye agarose wet film revives the donor-acceptor complexation, thereby switching back to the FRET ON state. This reversible switching between the FRET ON and OFF states was repeatable for multiple cycles.

Figure 3.11: PL spectral changes of QD:::dye agarose wet film upon continuous irradiation for ~5 h using a 10 W green LED. The emission of MC dye decreased and the PL of InP/ZnS QD recovered to its initial position (~525 nm).

3.4.2 FRET assisted luminescent photopatterning of QD:::dye agarose film:

Having photoregulated the process of FRET in QD:::dye agarose film, we then performed photopatterning experiments to generate luminescent patterns using masks of different dimensions and shapes. All the photopatterning experiments were performed using QD:::dye agarose d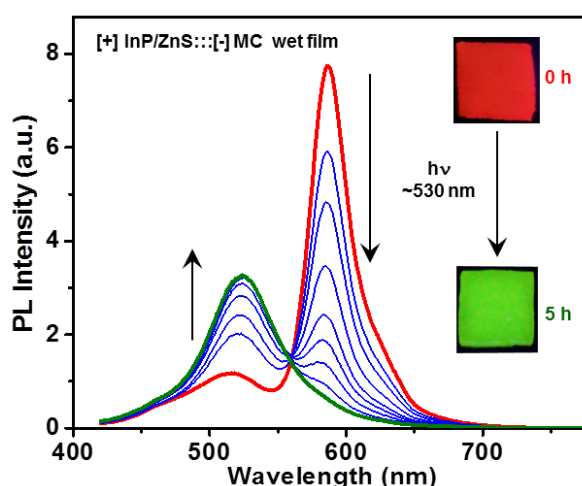ry film to get luminescent patterns (Details are provided in the Experimental Section). The underlying idea is that the MC dyes in the exposed regions in QD:::dye agarose film will photodegrade, leading to the recovery of green PL color corresponding to the FRET OFF state. On the other hand, the unexposed regions on the QD:::dye agarose film will exhibit the orange PL color corresponding to the FRET ON state (**Figure 3.12**). The continuous irradiation for 5 h using a commercially available 10 W green LED resulted in the complete degradation of MC dyes in QD:::dye agarose film (**Figure 3.11b**; incident power on the film was estimated to be ~6.5 mW/cm^2).

Figure 3.12: FRET assisted luminescent photopatterning of QD:::dye agarose film. a, b) PL images of QD:::dye agarose dry films before and after photoirradiation (using 'concentric ring' mask), with 10 W a green LED for ~5 h. Inset shows the corresponding images under normal light. Scale bar corresponds to 1 cm for all the images. All the PL images were recorded with an excitation wavelength of ~364 nm.

Representative examples for some of the PL images of photpatterned QD:::dye agarose film, using different masks, are shown in **Figure 3.13**. The effect of irradiation wavelength was observed to be marginal, as similar quality of photopatterns were obtained under green, blue and white LED irradiation, proving the flexibility of our methodology (**Figure 3.13e**).
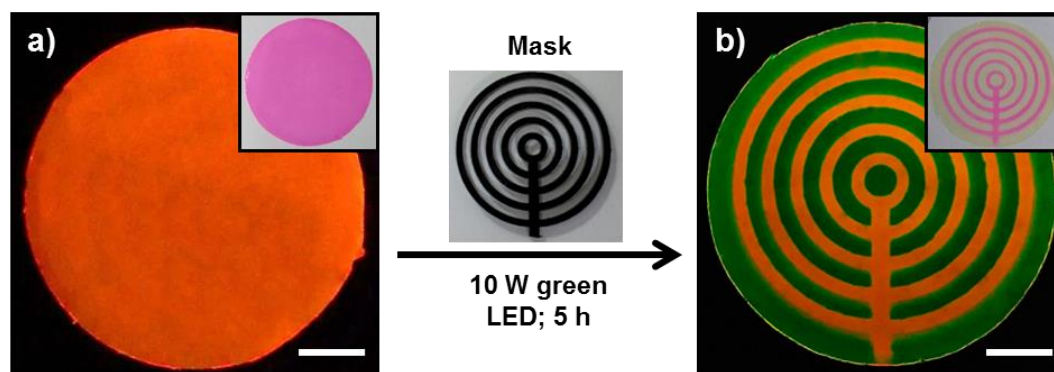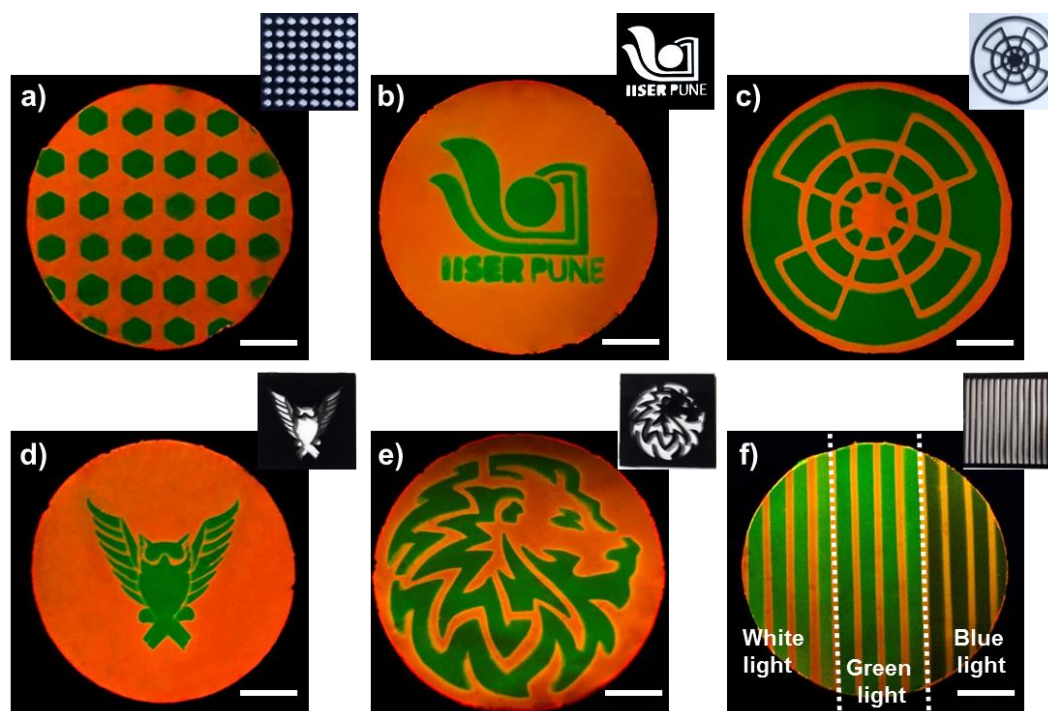
Figure 3.13: FRET assisted luminescent photopatterning of QD:::dye agarose film. a-e) PL images of QD:::dye agarose dry film photopatterned using masks of different shapes. f) PL image of QD:::dye agarose dry film showing marginal effect of irradiation wavelength on the color clarity of the photopatterns. The partitioned regions were separately and selectively irradiated for ~5 h with 10 W white, green and blue LEDs. Scale bar corresponds to 1 cm for all the images. All the PL images were recorded with an excitation wavelength of ~364 nm.

In our attempts to miniaturize the size of the photopatterns, we worked with masks of lower dimensions. For instance, we used an array of 1 mm holes to generate mm sized (**Figure 3.14a**), and 400 mesh commercial TEM grid to generate μm sized (~25 μm) luminescent patterns (**Figure 3.14b**). **Figure 3.14c** shows the intensity difference of orange color between the exposed and unexposed regions of the two-photon PL image generated with TEM mask. The emission profiles recorded using lambda scanning, during two-photon imaging from the orange and green patterned regions of **Figure 3.14b**, once again confirmed the FRET ON and OFF states, respectively (**Figure 3.14d**).
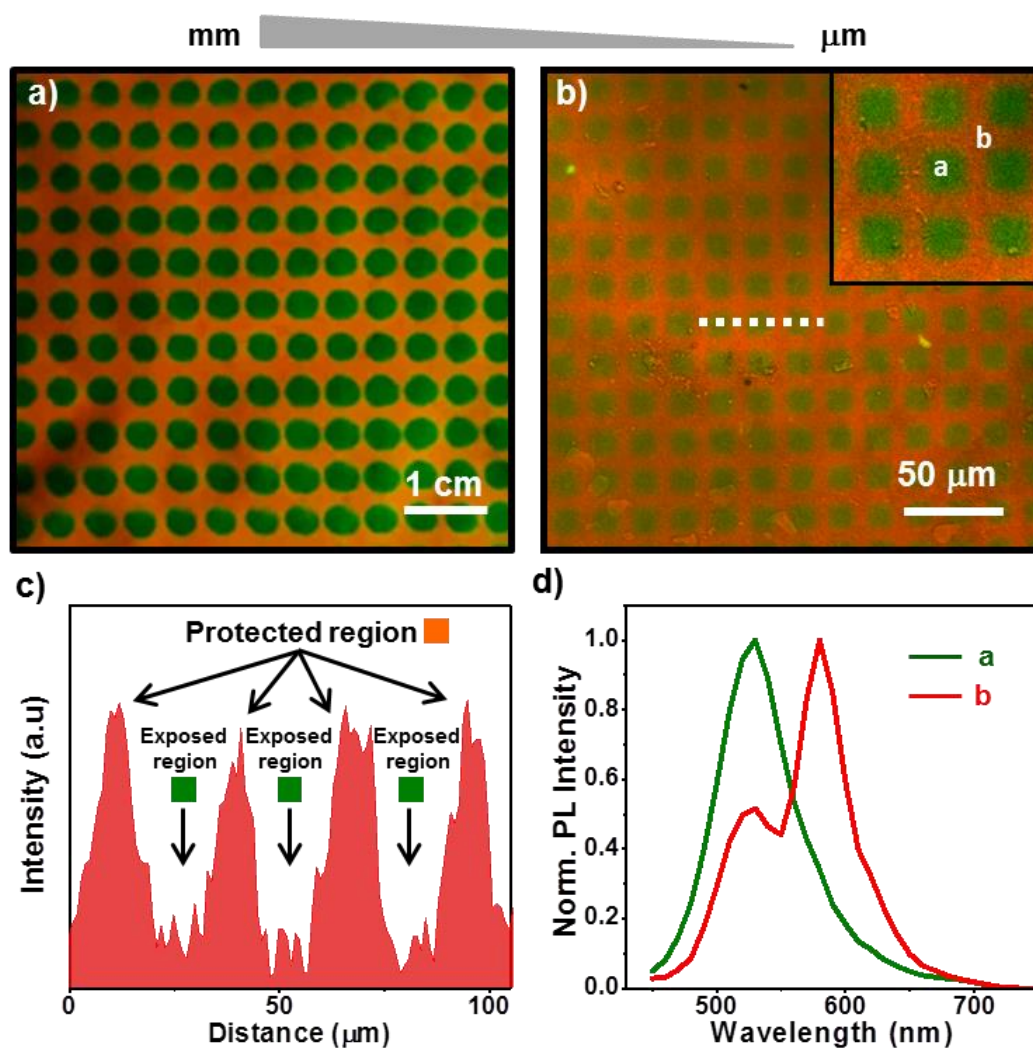
Figure 3.14: a) PL image of an array of ~1 mm holes, and b) two-photon PL image of ~25 µm s
quares created by the continuous irradiation of QD:::dye agarose film with a 10 W green LED for ~5 h. c) Intensity difference of orange color between the exposed and unexposed regions in the two-photon PL image 'b'. d) The emission profiles recorded using two-photon microscopy from the orange and green patterned regions in image 'b' confirms the FRET ON and OFF states, respectively. All the PL images were recorded with an excitation wavelength of ~364 nm.

Our FRET assisted photopatterning technique, in principle, can generate luminescent patterns with diffraction limited resolution using appropriate masks. For generality of our approach with respect to substrates, luminescent patterns of similar quality were created on other commonly used substrates like polydimethylsiloxane (PDMS) and glass slide (**Figure 3.15**).
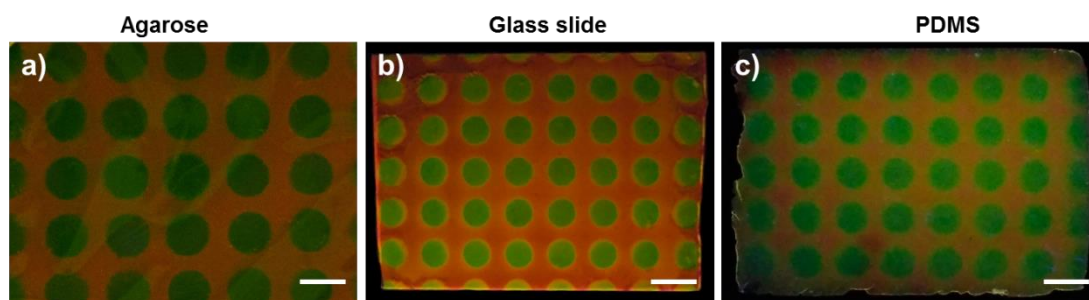
Figure 3.15: PL images of patterned QD:::dye films under UV light on a) agarose, b) glass slide, and c) PDMS substrates. Scale bar corresponds to 1 cm for all the images.

3.4.3 Multicolor luminescent photopatterns from a single QD nanohybrid system:

Next, we discuss about the most striking advantage and flexibility of our technique: creation of multicolor luminescent patterns from a single QD nanohybrid system. For this, the process of FRET in QD:::dye agarose film was fine-tuned to create a distinctly different third color. This was achieved by photodegrading the [-] MC dye acceptors, in a controlled way, in the QD:::dye agarose film. A continuous irradiation of QD:::dye agarose film for ~2 h imparted a yellow color to the exposed region, corresponding to a moderate FRET efficiency of ~50 % (**Figure 3.16a**); whereas ~5 h of continuous irradiation produced the green color as mentioned before. In order to demonstrate the multicolor patterning, the combination of green and yellow colors was chosen due to their clear visual contrast difference. Based on the time of photoirradiation, the process of FRET was fine-tuned between completely ON (orange colored region) and OFF (green colored region) states, along with a moderately efficient ON state (yellow colored region). Solid state PL studies were carried out at different patterned regions, and the coordinates calculated from CIE plot confirms the color purity of multicolor patterns generated (**Figures 3.16 b-d** and **Table 3.3**).
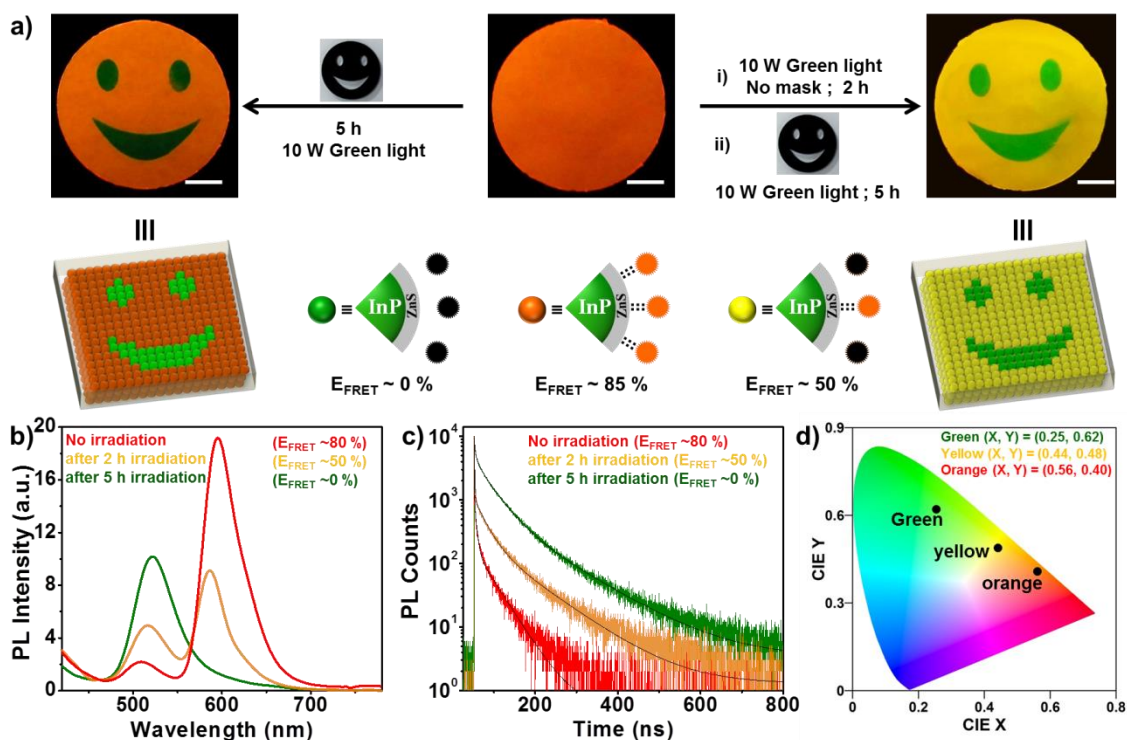
Figure 3.16: Creation of multicolor luminescent photopatterns from a single QD nanohybrid system. a) Generation of orange (left image) and yellow (right image) faced smiley images, by controlling the irradiation time. The yellow colored regions correspond to moderately efficient FRET state (~50 %), where the photodegradation of the MC dye was partial. Scale bar corresponds to 1 cm for all the images. b) Steady state PL spectra, and c) PL lifetime decay profiles from three different colored (green, yellow, orange) regions of QD:::dye films. d) The CIE plot showing the corresponding color coordinates. All the PL images were recorded with an excitation wavelength of ~364 nm.

Table 3.3: PL decay analysis at three different colored regions of QD:::dye film measured in a time window of 800 ns.

Sample	τ_1 (ns)	a_1	τ_2 (ns)	a_2	τ_3 (ns)	a_3	Avg. τ (ns)	Efficiency (%)
Green region	3.66	0.48	37.14	0.43	108.4	0.09	60.29	0.0
Yellow region	1.25	0.75	25.12	0.19	51.36	0.06	31.77	47.3
Red region	0.23	0.84	6.05	0.15	19.36	0.01	7.14	88.1

Figure 3.17 shows the representative examples of multicolor luminescent patterns created by the photoregulation of FRET using a single QD nanohybrid system. The procedure followed for the creation of multicolor smiley is described as follows (shown in **Figure 3.18**). First, the outer boundary of the smiley was masked and the rest of the QD:::dye agarose film was

exposed to ~2 h of irradiation. This imparted a uniform yellow color (corresponding to E_{FRET} ~50 %) throughout the QD:::dye agarose film, excluding the boundary (**Figure 3.18 b,f**). Second, the face and boundary of the smiley were masked, leaving the eyes and mouth exposed to continuous irradiation of ~5 h. This gave the green color (corresponding to E_{FRET} ~0 %) to eyes and mouth of the smiley, whereas the face of the smiley remained yellow colored (**Figure 3.18 c,g**).
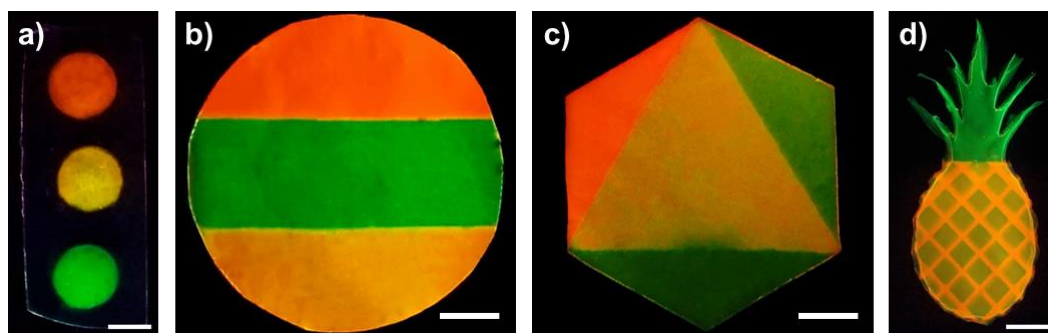
Figure 3.17: Creation of multicolor luminescent photopatterns from a single QD nanohybrid system. a-d) PL images of multicolor luminescent patterns on QD:::dye agarose dry film created by controlling the irradiation time. All these multicolor luminescent patterns were generated by the continuous irradiation with a 10 W green LED. All the PL images were recorded with an excitation wavelength of ~364 nm. Scale bar corresponds to 1 cm for all the images.

Similar sequential photoirradiation procedures were adopted for the creation of other multicolor patterns on QD:::dye agarose film. The FRET assisted photopatterning methodology demonstrated in this Chapter requires no major instrumentation or fabrication tools, and can be conveniently used universally for any luminescent nanocrystals, with high reproducibility.
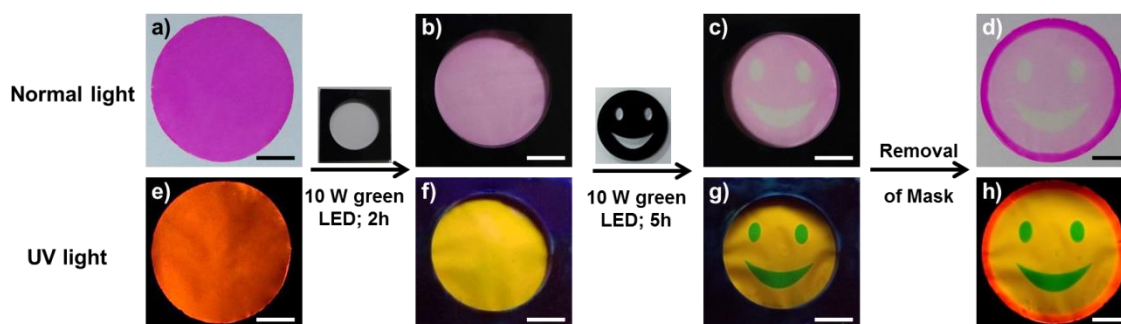
Figure 3.18: PL images of QD:::dye agarose film under normal and UV light a,e) before, b,f) after ~2 h irradiation (with mask) with 10 W green LED, and c,g) after ~5 h irradiation (using a mask of smiley) with 10 W green LED. d,h) Final photographs after the removal of mask. Scale bar corresponds to 1 cm for all the images. All the PL images were recorded with an excitation wavelength of ~364 nm.

Finally, the effect of incident power on irradiation time and reusability of QD:::dye agarose film are discussed. The time required for generating luminescent patterns was lowered to ~5 min using a 1 W green laser, which once again confirms the adaptability of our strategy for practical applications (incident power on the film was estimated to be ~435 mW/cm^2). Multiple exposures were required to generate larger sized patterns due to the smaller beam diameter of the laser (~0.5 cm; **Figure 3.19**). The irradiation time used in the present work was similar to other photopatterning techniques reported in the literature (**Table 3.4**).
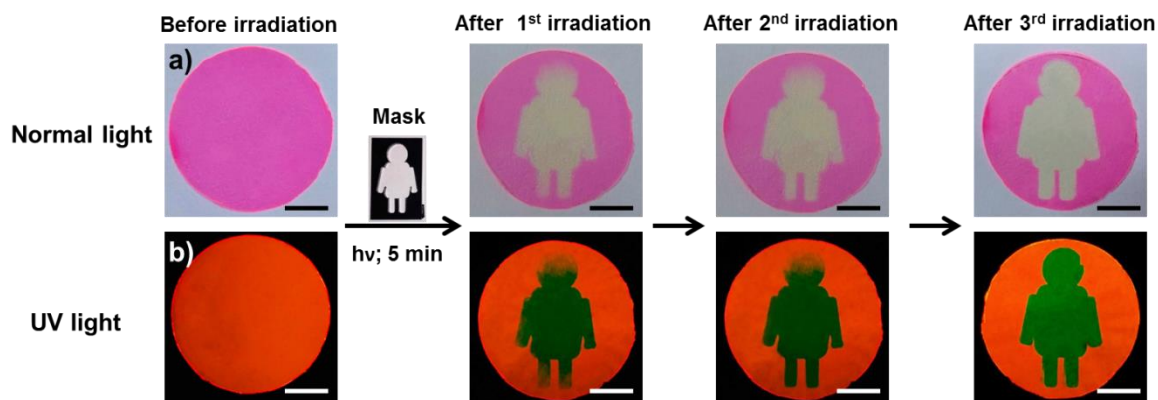
Figure 3.19: PL images of QD:::dye agarose films before and after photoirradiation with 1 W green laser for 5 min, with multiple irradiation, under a) normal and b) UV light. Scale bar corresponds to 1 cm for all the images. All the PL images were recorded with an excitation wavelength of ~364 nm.

The luminescent patterns generated were found to be reusable for many cycles. The luminescent orange color was completely recovered by replenishing the photodegraded [-] MC dye with fresh dye solution. The same QD:::dye agarose film was further irradiated to rewrite the features without any compromise of the color clarity. We have reused the QD:::dye agarose film for 5 cycles, and in one example a negative pattern was generated to prove that the reused film can be used for patterning different features as well (**Figure 3.20**). In this particular example, background of the reused QD:::dye agarose film was selectively irradiated to switch OFF the FRET (green color), while the masked regions retained the FRET ON state (orange color).
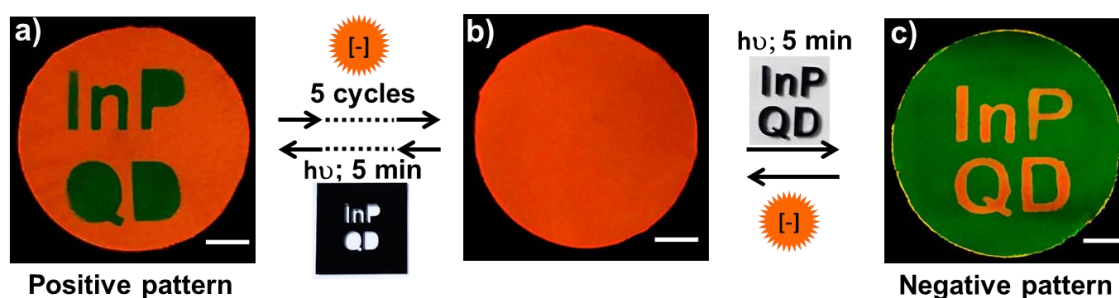
Figure 3.20: Reusable FRET assisted luminescent photopatterning of QD:::dye agarose film. a) A PL image of QD:::dye agarose film using the mask of InP QD. b) The photopatterned QD:::dye agarose film was immersed in fresh MC dye solution to regenerate the donor-acceptor complexation, thereby switching back to FRET ON state. The reused QD:::dye agarose film was further irradiated to pattern the features without any compromise of color clarity or film stability. c) PL image of a negative pattern on the reused QD:::dye agarose film (after 5 cycles). All the patterns were generated by irradiating the films with 1 W green laser for 5 min, and the PL images were recorded with an excitation wavelength of ~364 nm. Scale bar corresponds to 1 cm for all the images.

Table 3.4: Comparison of time of irradiation with literature reports for QD photopatterning.

Sl. No	System	Source of light irradiation	Time of irradiation	Reference
1	CdSe/CdS core/shell nanocrystal	60 W table lamp (Intensity 4.7 mW)	~72 h	*J. Am. Chem. Soc.* **2003,** *125,* 2830-2831
2	CdSe@CdS@ZnS QD and Polyviologen	UV illumination (367 nm, Power 0.014 mW/cm^2)	~24 h	*Adv. Mater.* **2012**, *24*, 3617–3621
3	CdSe/ZnS, and CdSe/Cd$_{1-x}$ Zn$_x$ Se$_{1-y}$ S$_y$ QD	20 W Hg vapor short arc lamp	~45 min	*Adv. Optical Mater.* **2016,** *4,* 608–619
4	CdSe/CdS/ZnS (Core/Shell/Shell) QD	Blue light (470 nm, Power 11mW/cm^2)	~5 h	*J. Am. Chem. Soc.* **2017**, *139*, 7603−7615
5	CdSe/ZnS, InP/ZnS and ZnSe/ZnS QD	UV light (254 nm, Power 6.3 mW/cm^2)	~20 s	*Science* **2017,** *357*, 385–388
6	InP/ZnS QD and Merocyanine-540 (MC)	10 W Green light (530 nm, Power 6.5 mW/cm^2	~5 h	*ACS Energy Lett.* **2019**, 4, 1710−1716
		1 W green laser (532 nm, 435 mW/Cm^2)	~5 min	(Present work)

3.5 Conclusions

In summary, a simple yet robust technique for the fabrication of reusable multicolor luminescent photopatterns of QD films was demonstrated. Our methodology requires only a single QD nanohybrid system for the creation of multicolor luminescent patterns (at least three distinctly different colors). This is in stark contrast to the existing techniques where different sized QDs were required to achieve different luminescent colors. The composition of donor-acceptor pair in the QD-dye nanohybrid film was controllably varied by the selective photodegradation of the dye molecules. Consequently, the FRET process in QD – dye nanohybrid film was regulated between completely ON (orange colored luminescence) and OFF (green colored luminescence) states, through a moderately efficient state (yellow colored luminescence). The FRET controlled photopatterning presented here provides a fundamentally unique and cost effective strategy for the fabrication of high contrast multicolor luminescence display devices from a single QD nanohybrid system. A close examination of luminescent patterns reveals that the surface of QDs are differently exposed at different parts of the photopatterned QD:::dye agarose film. Specifically, the green and orange colored regions on QD:::dye agarose film corresponds to [+] InP/ZnS QD and [+] InP/ZnS QD:::[-] MC dye complex, respectively. One could, in principle, address these patterned QD surfaces differently and use them for spatially selective QD functions like metal ion reduction/deposition, LED and micro/nanoelectrode fabrication, sensing etc.

3.6 Future Direction

In this Chapter, we have successfully generated multicolor (at least three distinct colors) luminescent patterns from a single QD nanohybrid film, by the photoregulation of FRET process. One of the limitations of the present methodology is the lack of generation of a black non-luminescent region, which forms the integral part of many images. As demonstrated by Weiss and co-workers, the photoregulation of electron transfer process in a QD-dye donor-acceptor system can generate black non-luminescent regions, corresponding to electron transfer OFF state.[30] Thus, the incorporation and photoregulation of both electron and energy transfer processes in a single QD nanohybrid system should, in principle, generate a combination of black and high-contrast multicolor luminescent patterns. However, establishing a fine interplay between photoinduced electron and energy transfer processes in a single QD nanohybrid system is fundamentally challenging, and this forms the basis of Chapter 4.

3.7 References

(1)   Choi, M. K.; Yang, J.; Hyeon, T.; Kim, D. -H. Flexible Quantum Dot Light-Emitting Diodes for next-Generation Displays. *npj Flex. Electron.* **2018**, *2*, 1–14.

(2)   Kim, T. -H.; Cho, K. -S.; Lee, E. K.; Lee, S. J.; Chae, J.; Kim, J. W.; Kim, D. H.; Kwon, J.-Y.; Amaratunga, G.; Lee, S. Y.; Choi, B. L.; Kuk, Y.; Kim, J. M.; kim, K. Full-Colour Quantum Dot Displays Fabricated by Transfer Printing. *Nat. Photonics* **2011**, *5*, 176-182.

(3)   Jun, S.; Jang, E.; Park, J.; Kim, J. Photopatterned Semiconductor Nanocrystals and Their Electroluminescence from Hybrid Light-Emitting Devices. *Langmuir* **2006**, *22*, 2407–2410.

(4)   Lin, C. H.; Zeng, Q.; Lafalce, E.; Yu, S.; Smith, M. J.; Yoon, Y. J.; Chang, Y.; Jiang, Y.; Lin, Z.; Vardeny, Z. V.; Tsukruk, V. V. Large-Area Lasing and Multicolor Perovskite Quantum Dot Patterns. *Adv. Opt. Mater.* **2018**, *6*, 1800474.

(5)   Zhu, S.; Meng, Q.; Wang, L.; Zhang, J.; Song, Y.; Jin, H.; Zhang, K.; Sun, H.; Wang, H.; Yang, B. Highly Photoluminescent Carbon Dots for Multicolor Patterning , Sensors , and Bioimaging. *Angew. Chem. Int. Ed.* **2013**, *52*, 3953–3957.

(6)   Chen, X.; Rogach, A. L.; Talapin, D. V; Fuchs, H.; Chi, L. Hierarchical Luminescence Patterning Based on Multiscaled Self-Assembly. *J. Am. Chem. Soc.* **2006**, *128*, 9592–9593.

(7)   Paik, T.; Yun, H.; Fleury, B.; Hong, S.-H.; Jo, P. S.; Wu, Y.; Oh, S.-J.; Cargnello, M.; Yang, H.; Murray, C. B.; Kagan, C. R. Hierarchical Materials Design by Pattern Transfer Printing of Self- Assembled Binary Nanocrystal Superlattices. *Nano Lett.* **2017**, *17*, 1387–1394.

(8)   Liu, M.; Voznyy, O.; Sabatini, R.; García de Arquer, F. P.; Munir, R.; Balawi, A. H.; Lan, X.; Fan, F.; Walters, G.; Kirmani, A. R.; Hoogland, S.; Laquai, F.; Amassian, A.; Sargent, E. H. Hybrid Organic–inorganic Inks Flatten the Energy Landscape in Colloidal Quantum Dot Solids. *Nat. Mater.* **2016**, *16*, 258-263.

(9)   Babayan, Y.; Barton, J. E.; Greyson, E. C.; Odom, T. W. Templated and Hierarchical Assembly of CdSe/ZnS Quantum Dots. *Adv. Mater.* **2004**, *16*, 1341–1345.

(10)   Wang, Y.; Fedin, I.; Zhang, H.; Talapin, D. V. Direct Optical Lithography of Functional Inorganic Nanomaterials. *Science* **2017**, *357*, 385–388.

(11)   Nandwana, V.; Subramani, C.; Yeh, Y.-C.; Yang, B.; Dickert, S.; Barnes, M. D.; Tuominen, M. T.; Rotello, V. M. Direct Patterning of Quantum Dot

Nanostructuresviaelectron Beam Lithography. *J. Mater. Chem.* **2011**, *21*, 16859–16862.

(12) Palankar, R.; Medvedev, N.; Rong, A.; Delcea, M. Fabrication of Quantum Dot Microarrays Using Electron Beam Lithography for Applications in Analyte Sensing and Cellular Dynamics. *ACS Nano* **2013**, *7*, 4617–4628.

(13) Malak, S. T.; Liang, G.; Thevamaran, R.; Yoon, Y. J.; Smith, M. J.; Jung, J.; Lin, C. H.; Lin, Z.; Thomas, E. L.; Tsukruk, V. V. High-Resolution Quantum Dot Photopatterning via Interference Lithography Assisted Microstamping. *J. Phys. Chem. C* **2017**, *121*, 13370–13380.

(14) Kim, B. H.; Nam, S.; Oh, N.; Cho, S.-Y.; Yu, K. J.; Lee, C. H.; Zhang, J.; Deshpande, K.; Trefonas, P.; Kim, J.-H.; Lee, J.; Shin, J. H. ; Yu, Y.; Lim, J. B.; Won, S. M.; Cho, Y. K.; Kim, N. H.; Seo, K. J.; Lee, H.; Kim, T.-I.; Shim, M.; Rogers, J. A. Multilayer Transfer Printing for Pixelated, Multicolor Quantum Dot Light-Emitting Diodes. *ACS Nano* **2016**, *10*, 4920–4925.

(15) Nguyen, D. T.; Freitag, M.; Körsgen, M.; Lamping, S.; Rühling, A.; Schäfer, A. H.; Siekman, M. H.; Arlinghaus, H. F.; van der Wiel, W. G.; Glorius, Ravoo, B. J. Versatile Micropatterns of N-Heterocyclic Carbenes on Gold Surfaces: Increased Thermal and Pattern Stability with Enhanced Conductivity. *Angew. Chemie. Int. Ed.* **2018**, *57*, 11465–11469.

(16) Roling, O.; De Bruycker, K.; Vonhören, B.; Stricker, L.; Körsgen, M.; Arlinghaus, H. F.; Ravoo, B. J.; Du Prez, F. E. Rewritable Polymer Brush Micropatterns Grafted by Triazolinedione Click Chemistry. *Angew. Chemie. Int. Ed.* **2015**, *54* (44), 13126–13129.

(17) Wu, S.; Liu, B.; Su, X.; Zhang, S. Structural Color Patterns on Paper Fabricated by Inkjet Printer and Their Application in Anticounterfeiting. *J. Phys. Chem. Lett.* **2017**, *8*, 2835–2841.

(18) Kim, B. H.; Onses, M. S.; Lim, J. B.; Nam, S.; Oh, N.; Kim, H.; Yu, K. J.; Lee, J. W.; Kim, J.-H.; Kang, S.-K.; Lee, C.-H.; Lee, J.; Shin, J. H.; Kim, N. H.; Leal, C.; Shim, M.; Rogers, J. A. High-Resolution Patterns of Quantum Dots Formed by Electrohydrodynamic Jet Printing for Light-Emitting Diodes. *Nano Lett.* **2015**, *15*, 969–973.

(19) Kim, L.; Anikeeva, P. O.; Coe-Sullivan, S. A.; Steckel, J. S.; Bawendi, M. G.; Bulović, V. Contact Printing of Quantum Dot Light-Emitting Devices. *Nano Lett.* **2008**, *8*, 4513–4517.

(20) Keum, H.; Jiang, Y.; Park, J. K.; Flanagan, J. C.; Shim, M.; Kim, S. Photoresist Contact

Patterning of Quantum Dot Films. *ACS Nano* **2018**, *12*, 10024–10031.

(21) Porter, L. A.; Choi, H. C.; Schmeltzer, J. M.; Ribbe, A. E.; Elliott, L. C. C.; Buriak, J. M. Electroless Nanoparticle Film Deposition Compatible with Photolithography, Microcontact Printing, and Dip-Pen Nanolithography Patterning Technologies. *Nano Lett.* **2002**, *2*, 1369–1372.

(22) Park, J.-S.; Kyhm, J.; Kim, H. H.; Jeong, S.; Kang, J.; Lee, S.; Lee, K.-T.; Park, K.; Barange, N.; Han, J.; Song, J. D.; Choi, W. K.; Han, I. K. Alternative Patterning Process for Realization of Large-Area, Full-Color, Active Quantum Dot Display. *Nano Lett.* **2016**, *16*, 6946–6953.

(23) Gopal, A.; Hoshino, K.; Zhang, X. Photolithographic Patterning of Subwavelength Top Emitting Colloidal Quantum Dot Based Inorganic Light Emitting Diodes on Silicon. *Appl. Phys. Lett.* **2010**, *96*, 131109.

(24) Xie, W.; Gomes, R.; Aubert, T.; Bisschop, S.; Zhu, Y.; Hens, Z.; Brainis, E.; Van Thourhout, D. Nanoscale and Single-Dot Patterning of Colloidal Quantum Dots. *Nano Lett.* **2015**, *15*, 7481–7487.

(25) Bae, W. K.; Kwak, J.; Lim, J.; Lee, D.; Nam, M. K.; Char, K.; Lee, C.; Lee, S. Multicolored Light-Emitting Diodes Based on All-Quantum-Dot Multilayer Films Using Layer-by-Layer Assembly Method. *Nano Lett.* **2010**, *10*, 2368–2373.

(26) Lin, Y. -W.; Tseng, W. -L.; Chang, H. -T. Using a Layer-by-Layer Assembly Technique to Fabricate Multicolored-Light-Emitting Films of CdSe@CdS and CdTe Quantum Dots. *Adv. Mater.* **2006**, *18*, 1381–1386.

(27) Wang, Y.; Tang, Z.; Correa-Duarte, M. A.; Liz-Marzán, L. M.; Kotov, N. A. Multicolor Luminescence Patterning by Photoactivation of Semiconductor Nanoparticle Films. *J. Am. Chem. Soc.* **2003**, *125*, 2830–2831.

(28) Chen, J.; Chan, Y.-H.; Yang, T.; Wark, S. E.; Son, D. H.; Batteas, J. D. Spatially Selective Optical Tuning of Quantum Dot Thin Film Luminescence. *J. Am. Chem. Soc.* **2009**, *131*, 18204–18205.

(29) Tagliazucchi, M.; Amin, V. A.; Schneebeli, S. T.; Stoddart, J. F.; Weiss, E. A. High-Contrast Photopatterning of Photoluminescence within Quantum Dot Films through Degradation of a Charge-Transfer Quencher. *Adv. Mater.* **2012**, *24*, 3617–3621.

(30) Malak, S. T.; Jung, J.; Yoon, Y. J.; Smith, M. J.; Lin, C. H.; Lin, Z.; Tsukruk, V. V. Large-Area Multicolor Emissive Patterns of Quantum Dot-Polymer Films via Targeted Recovery of Emission Signature. *Adv. Opt. Mater.* **2016**, *4*, 608–619.

(31) Choi, M. K.; Yang, J.; Kang, K.; Kim, D. C.; Choi, C.; Park, C.; Kim, S. J.; Chae, S. I.;

Kim, T. -H.; Kim, J. H.; Hyeon, T.; Kim, D. –H. Wearable Red–green–blue Quantum Dot Light-Emitting Diode Array Using High-Resolution Intaglio Transfer Printing. *Nat. Commun.* **2015**, *6*, 1–8.

(32) Shin, S. -H.; Hwang, B.; Zhao, Z. -J.; Jeon, S. H.; Jung, J.; Lee, J. -H.; Ju, B. -K.; Jeong, J.-H. Transparent Displays Utilizing Nanopatterned Quantum Dot Films. *Sci. Rep.* **2018**, *8*, 2463.

(33) Jung, S.; Park, J.; Bang, J.; Kim, J. -Y.; Kim, C.; Jeon, Y.; Lee, S. H.; Jin, H.; Choi, S.; Kim, B.; Lee, W. J.; Pack, C. -G.; Lee, J. -B.; Lee, N. K.; Kim, S. Light-Induced Fluorescence Modulation of Quantum Dot-Crystal Violet Conjugates: Stochastic Off–On–Off Cycles for Multicolor Patterning and Super-Resolution. *J. Am. Chem. Soc.* **2017**, *139*, 7603–7615.

(34) Förster, T. 10th Spiers Memorial Lecture. Transfer Mechanisms of Electronic Excitation. *Discuss. Faraday Soc.* **1959**, *27*, 7–17.

(35) Lakowicz, J. R. Principles of Fluorescence Spectroscopy, 3rd ed., Springer: New York **1999**.

(36) V. Biju, A. Anas, H. Akita, E. S. Shibu, T. Itoh, H. Harashima, M. Ishikawa, M. FRET from Quantum Dots to Photodecompose Undesired Acceptors and Report the Condensation and Decondensation of Plasmid DNA. *ACS Nano* **2012**, *6*, 3776-3788.

(37) Clapp, A. R.; Medintz, I. L.; Mauro, J. M.; Fisher, B. R.; Bawendi, M. G.; Mattoussi, H. Fluorescence Resonance Energy Transfer between Quantum Dot Donors and Dye-Labeled Protein Acceptors. *J. Am. Chem. Soc.* **2004**, *126*, 301–310.

(38) Sapsford, K. E.; Berti, L.; Medintz, I. L. Materials for Fluorescence Resonance Energy Transfer Analysis: Beyond Traditional Donor-Acceptor Combinations. *Angew. Chem. Int. Ed.* **2006**, *45*, 4562–4588.

(39) Funston, A. M.; Jasieniak, J. J.; Mulvaney, P. Complete Quenching of CdSe Nanocrystal Photoluminescence by Single Dye Molecules. *Adv. Mater.* **2008**, *20*, 4274–4280.

(40) Medintz, I. L.; Mattoussi, H. Quantum Dot-Based Resonance Energy Transfer and Its Growing Application in Biology. *Phys. Chem. Chem. Phys.* **2009**, *11*, 17–45.

(41) Hoffman, J. B.; Choi, H.; Kamat, P. V. Size-Dependent Energy Transfer Pathways in CdSe Quantum Dot–Squaraine Light-Harvesting Assemblies: Förster versus Dexter. *J. Phys. Chem. C* **2014**, *118*, 18453–18461.

(42) Hoffman, J. B.; Alam, R.; Kamat, P. V. Why Surface Chemistry Matters for QD-QD Resonance Energy Transfer. *ACS Energy Lett.* **2017**, *2*, 391–396.

(43) Kholmicheva, N.; Moroz, P.; Eckard, H.; Jensen, G.; Zamkov, M. Energy Transfer in Quantum Dot Solids. *ACS Energy Lett.* **2017**, *2*, 154–160.

(44) Kodaimati, M. S.; Wang, C.; Chapman, C.; Schatz, G. C.; Weiss, E. A. The Distance-Dependence of Inter-Particle Energy Transfer in the Near-Infrared within Electrostatic Assemblies of PbS Quantum Dots, *ACS Nano* **2017**, *11*, 5041-5050.

(45) Wu, X.; Liu, H.; Liu, J.; Haley, K. N.; Treadway, J. A.; Larson, J. P.; Ge, N.; Peale, F.; Bruchez, M. P. Immunofluorescent Labeling of Cancer Marker Her2 and Other Cellular Targets with Semiconductor Quantum Dots. *Nat. Biotechnol.* **2003**, *21*, 41-46.

(46) Tien, J.; Terfort, A.; Whitesides, G. M. Microfabrication through Electrostatic Self-Assembly. *Langmuir* **1997**, *13*, 5349–5355.

(47) Li, L.; Reiss, P. One-Pot Synthesis of Highly Luminescent InP/ZnS Nanocrystals without Precursor Injection. *J. Am. Chem. Soc.* **2008**, *130*, 11588–11589.

(48) Devatha, G.; Roy, S.; Rao, A.; Mallick, A.; Basu, S.; Pillai, P. P. Electrostatically Driven Resonance Energy Transfer in "Cationic" Biocompatible Indium Phosphide Quantum Dots. *Chem. Sci.* **2017**, *8*, 3879–3884.

(49) Thomas, A.; Nair, P. V.; Thomas, K. G. InP Quantum Dots: An Environmentally Friendly Material with Resonance Energy Transfer Requisites. *J. Phys. Chem. C* **2014**, *118*, 3838–3845.

(50) Thirunavukkuarasu, S.; George, A.; Thomas, A.; Thomas, A.; Vijayan, V.; Thomas, K. G. InP Quantum Dots: Probing the Active Domain of Tau Peptide Using Energy Transfer. *J. Phys. Chem. C* **2018**, *122*, 14168–14176.

(51) Medintz, I. L.; Pons, T.; Susumu, K.; Boeneman, K.; Dennis, A. M.; Farrell, D.; Deschamps, J. R.; Melinger, J. S.; Bao, G.; Mattoussi, H. Resonance Energy Transfer between Luminescent Quantum Dots and Diverse Fluorescent Protein Acceptors. *J. Phys. Chem. C* **2009**, *113*, 18552–18561.

3.8 Appendix
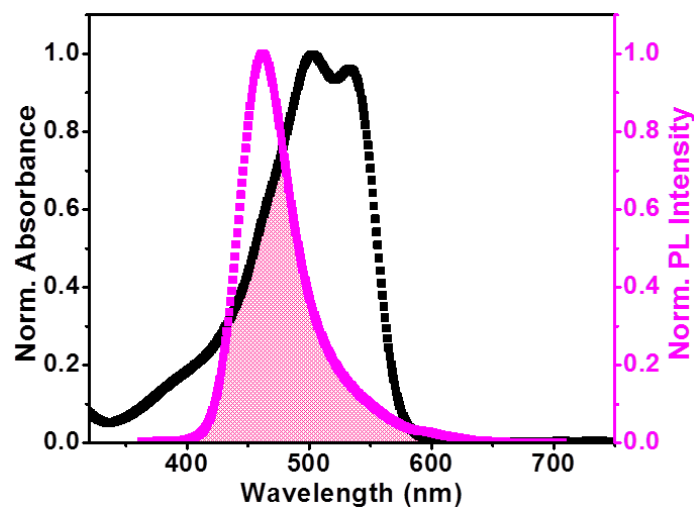
Figure 3.21: Spectral overlap (shaded portion) between the PL of [+] InP/ZnS agarose wet film and the absorption of [-] MC dye.

3.81 Real time monitoring of FRET in [+] InP/ZnS:::[-] MC agarose film:

Real time FRET was monitored using two-photon fluorescence microscopy. In a typical experiment, [+] InP/ZnS QD agarose wet film was dipped in ~3 mL of ~15 μM [-] MC solution. The fluorescence images were collected from two different channels using 450-550 nm and 550-750 nm band-pass filters, with non-descanned (NDD) PMT detector, for upto 3 h with 10 min of interval.

Figure 3.22: Two-photon PL images of [+] InP/ZnS QD agarose wet film at 0 h and 3 h after dipping in [-] MC solution. The PL images collected through a,d) green channel (QD

emission) b,e) red channel (MC emission), and c,f) merged images from green and red channels.

3.8.2 Role of electrostatics:

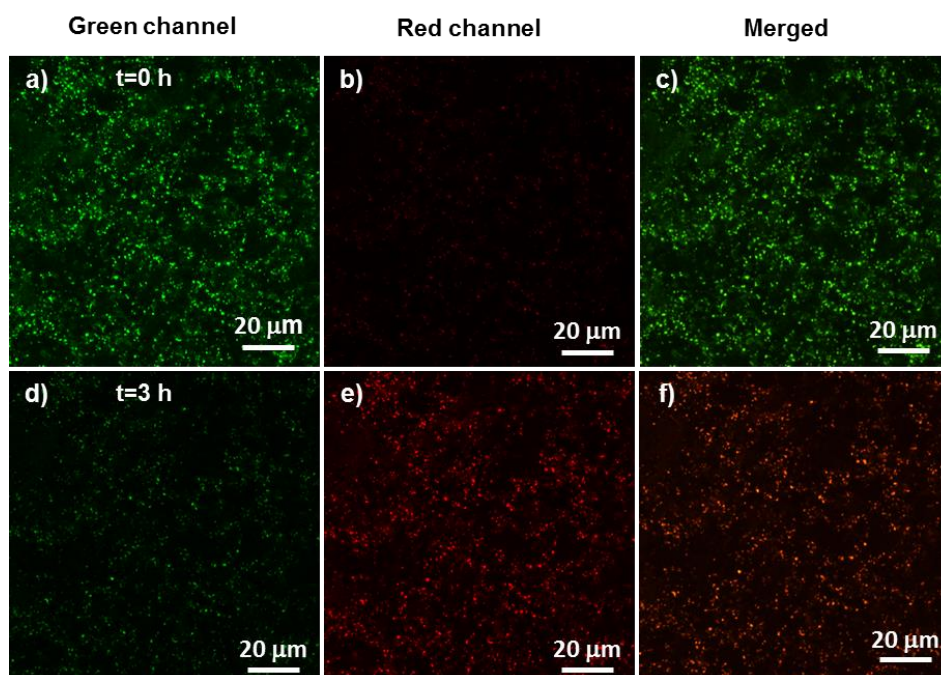We have performed control experiments to check the effect of electrostatics in FRET assisted photopatterning. For this, FRET studies between similarly charged [-] InP/ZnS QD and [-] MC dye were performed. As reported previously, no noticeable FRET was observed upon addition of ~2 μM [-] MC dye to ~0.89 μM [-] InP/ZnS QD in solution state.[48] Whereas, at a very high concentration of ~20 μM [-] MC dye, a signature of FRET was observed from both steady state and time resolved PL studies. However, the [-] InP/ZnS:::[-] MC complex was breaking within ~5 min, and no signature of FRET was observed after ~5 min. Moreover, no red-shift in the absorption of [-] MC dye was observed in the presence of [-] InP/ZnS QD, as shown in the **Figure 3.23**. All these studies confirm that [-] InP/ZnS QD and [-] MC dye fail to form a stable complex.
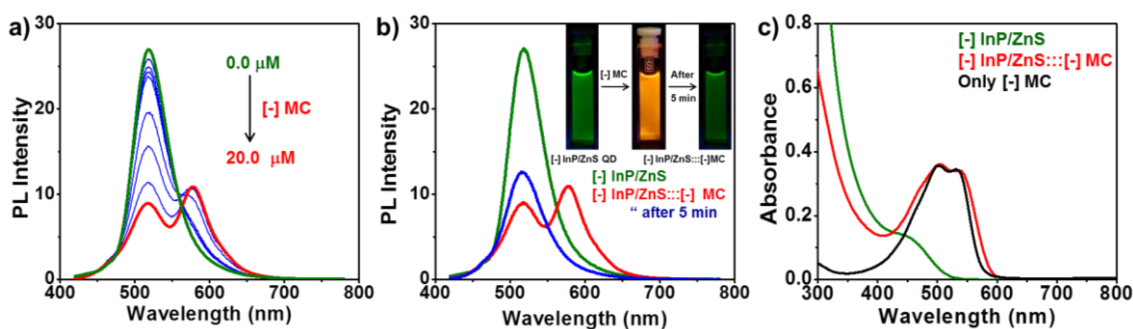
Figure 3.23: a) Spectral changes in the PL of [-] InP/ZnS QD on addition of varying concentrations of [-] MC dye, in solution state. b) Breaking of [-] InP/ZnS QD:::[-] MC complex with time. c) Absorption spectra of [-] MC in the absence (black spectrum) and presence (red spectrum) of [-] InP/ZnS QD respectively.

Alternately, we tried to perform the complexation by immersing the agarose film of [-] InP/ZnS QD in ~20 μM of [-] MC dye solution. The rationale is that appreciable complexation may take place in solid films by the diffusion of MC dyes though the pores of the agarose film. However, as shown in the **Figure 3.10**, we still failed to observe any noticeable complexation between [-] InP/ZnS QD and [-] MC dye in solid agarose film. These studies clearly confirm that a strong electrostatic attraction between the donor and acceptor is essential for an efficient FRET, and thereby the creation of stable photopatterns, .
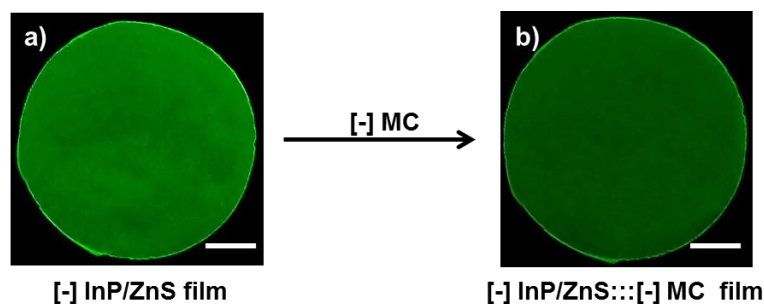
Figure 3.24: PL images of InP/ZnS QD agarose film before and after immersion in ~20 μM of [-] MC dye solution. Scale bar corresponds to 1 cm.

3.8.3 Degradation of dye upon irradiation:

The [-] MC agarose wet film was prepared by mixing 0.2 mL of ~15 μM [-] MC dye with hot agarose solution (1 % w/v) followed by curing for 1h. This [-] MC wet agarose film was further irradiated with 10 W green LED, and the absorption and emission changes were monitored up to ~5 h at different time intervals. A complete quenching in both absorption and emission clearly proves the degradation of dye molecules upon irradiation.
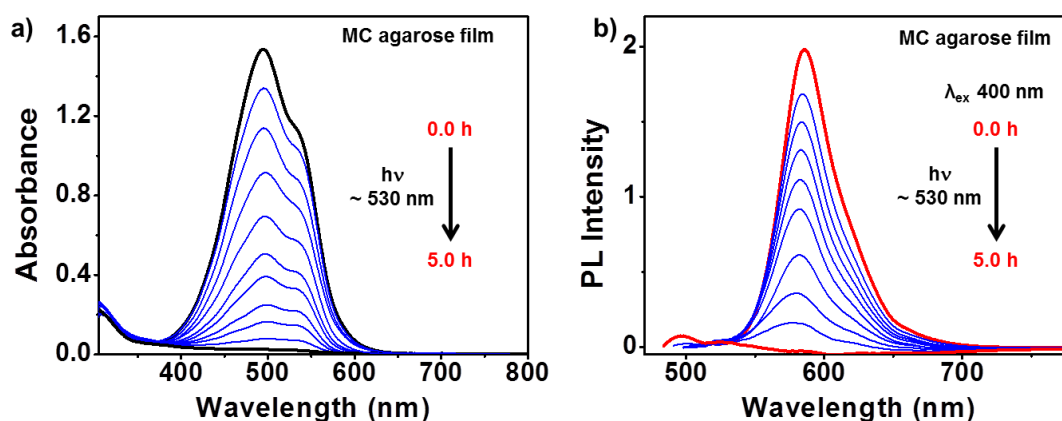
Figure 3.25: a) Absorption and b) PL spectral changes in [-] MC dye agarose film upon irradiation with a 10 W green LED for ~5 h.

3.8.4 Photopatterning on [+] InP/ZnS:::[-] MC agarose films:
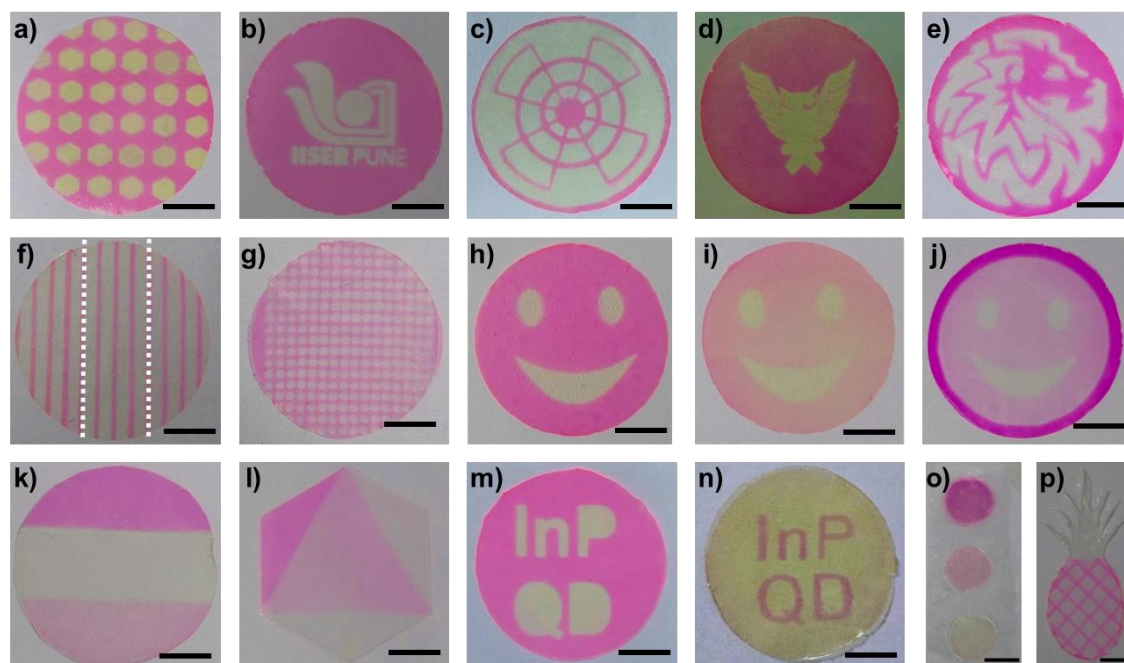
Figure 3.23: Optical images of QD:::dye agarose films after photoirradiation using different masks with a 10 W green LED for ~5 h, under normal light. The corresponding PL images are already mentioned in the Results and Discussion section of Chapter 3. The scale bar corresponds to 1 cm for all the images.

Chapter 4

Multicolor Luminescent Patterning via Photoregulation of Electron and Energy Transfer Processes in Quantum Dots
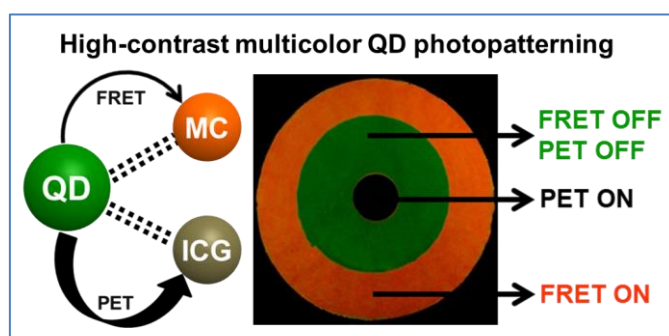
This Chapter is adapted with permission from the following paper. Copyright permission has been taken from American Chemical Society for the entire paper

4.1 Abstract

Ability to create high-contrast multicolor luminescent patterns is essential to realize the full potential of quantum dots (QDs) in display technologies. The idea of using a non-emissive state (black background) is adopted in the present work to enhance the color contrast of QD based photopatterns. This is achieved at a multicolor level by the photoregulation of electron and energy transfer processes in a donor-acceptor-acceptor triad film, comprising of one QD donor and two dye acceptors. The dominance of photoinduced electron transfer over energy transfer process generates a non-luminescent QD nanohybrid film, which provides the black background for multicolor patterning. The superior photostability of QDs over organic dyes is used for the photoregulation of electron and energy transfer processes in the nanohybrid film. A selective photodegradation of electron acceptor dye triggered the onset of energy transfer process, thereby imparting a luminescent color to the QD nanohybrid film. Further, a controlled photoregulation of energy transfer process paved the way for multicolor luminescent patterning. The idea of selective and sequential photoregulation of electron and energy transfer processes generated three distinct luminescent colors (orange, yellow, and green) on a non-emissive black background. Apart from enhancing the color contrast, our approach offers the option of creating luminescent images that have inherent black regions, at a multicolor level.

4.2 Introduction

Unique size dependent optical properties of Quantum Dots (QDs) have rendered their use in various light harvesting studies.[1-17] Among them, one of the emerging applications is in the area of display technologies,[18-23] which rely on strategies to precisely localize and pattern these luminescent QDs. Some of the promising approaches include selective photoactivation,[24-30] layer-by-layer assembly,[31,32] ink-jet, contact printing,[33-38] stamping, and photolithographic lift-off,[39-42] and so on. In general, the photopatterning based techniques have evolved as an attractive option due to its ease and robustness in creating luminescent QD patterns at micro and macroscopic levels.[24-30] For instance, a spatially controlled photoetching of surface ligands created highly luminescent QD patterns, with a high signal-to-noise ratio.[24] A conceptually unique approach based on the photo-triggering of surface ligands has been reported to directly deposit QDs, for creating luminescent patterns.[28] Likewise, Chi and Coworkers were able to generate hierarchical luminescent patterns based

on self-assembly of CdSe QDs. First, the green emitting stripes were prepared by self-assembling the 2-(4,4-difluoro- 5-methyl-4-bora-3a,4a-diaza-s-indacene-3-dodecanoyl)-1-hexadecanoyl-sn-glycero-3 phosphocholine (BODIPY) through Langmuir-Blodgett technique. Next, a drop of red-emitting CdSe QDs solution was added on the green emitting stripes. Finally, the mask was placed and irradiated with light, leading to the selective photo bleaching of the BODIPY dyes over CdSe QDs (**Figure 4.1**).
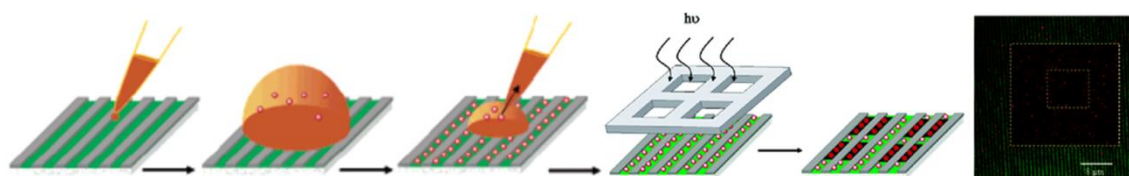
Figure 4.1: Schematic representation for the generation of hierarchical luminescent patterns prepared by the photobleaching of CdSe-BODIPY QD-dye aggregates. (Reproduced in part with permission from reference 19 Copyright 2006 American Chemical Society).

Kim's group has generated a large-area, full-color QD display patterns using a transfer printing process, where the QDs were spin coated on a substrate (PDMS), and quickly transferred to a target substrate using structured stamp. Noticeably, the amount of vacancies and cracks drastically reduced in the QD patterns using this technique (**Figure 4.2**).
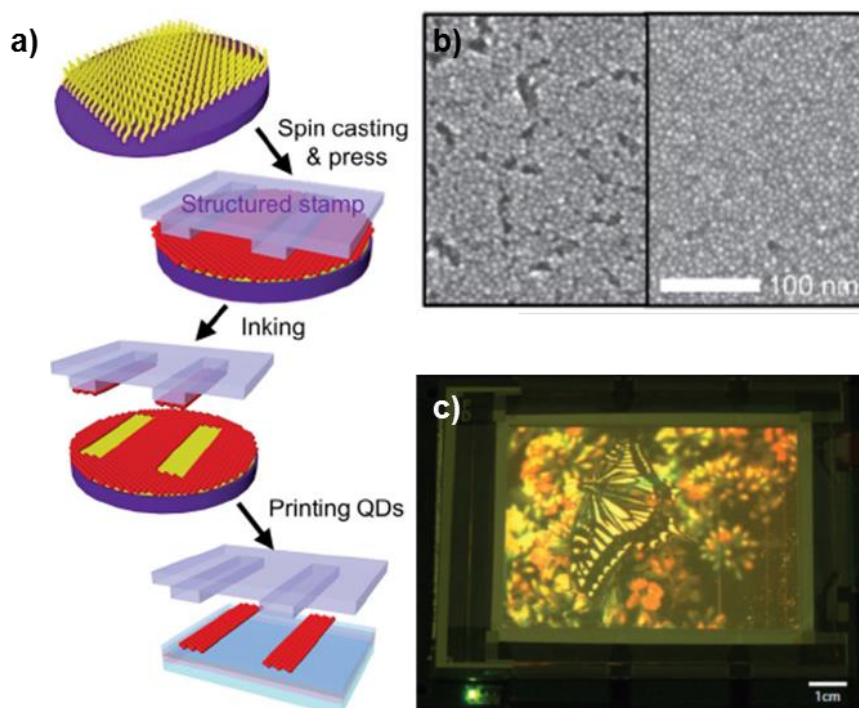
Figure 4.2: a) Schematic representation of pick-and-release transfer printing using a structured stamp. b) SEM image of QD patterns before (left) and after (right) transfer printing. c) Electroluminescence image of a four-inch full-color QD display. (Reproduced in part with permission from reference 21 Copyright 2011 Nature Publishing Group).

Tsukruk and Coworkers employed a collective and selective luminescence recovery strategies to generate high-resolution multicolor photopatterns using mixtures of different QDs.[26] In this strategy, both decay and recovery of QD emission were used to create high contrast multicolor luminescent photopatterns. A film comprised of QDs and polymer was first exposed to light to minimize the emission of QD. A photomask was placed on the film to protect the specific areas from the direct exposure of light. Next, the film was irradiated with light, which allowed recovery of QD PL in the exposed areas of the film (**Figure 4.3**).
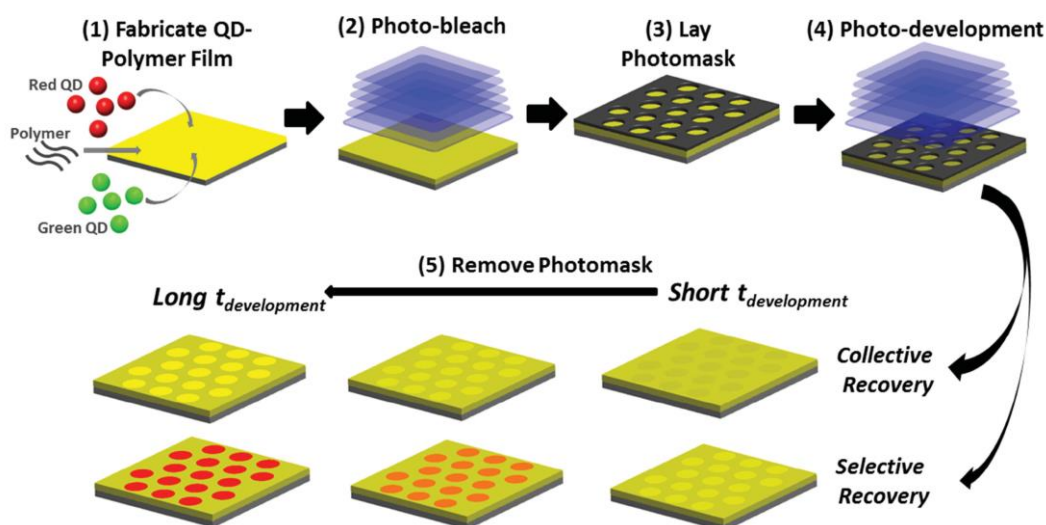
Figure 4.3: Schematic representation to generate high-resolution multicolor QD photopatterns using collective and selective recovery method. (Reproduced in part with permission from reference 26 Copyright 2016 John Wiley and Sons).

Another notable method relies on the spatial regulation of photophysical processes in QD-dye nanohybrid systems,[27,30] which exploits the superior photostability of QDs over organic dyes.[19] For example, the photoinduced electron transfer process in CdSe/ZnS QD and polyviologen (PV) donor-acceptor system was switched-OFF by the selective photodegradation of the PV dye, resulting in the revival of QD luminescence.[27] It is worth mentioning that the presence of a non-luminescent black background (corresponding to the photoinduced electron transfer-ON state) enhanced the contrast of the singly colored QD based luminescent patterns (**Figure 4.4**). However, this approach, like most of the others, is limited with the need for different sizes of QDs to generate multicolor luminescent patterns.[24-29,31-42] In Chapter 3 we have overcome this challenge by spatially degrading the acceptor molecules to photoregulate another key photophysical process, namely energy transfer, in a QD-dye donor-acceptor system.[30]
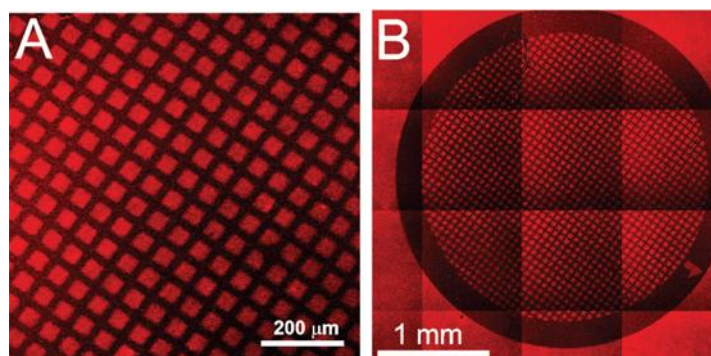
Figure 4.4: a and b) Confocal microscope image of a photopattern generated by the irradiation of UV light on a CdSe/ZnS QD-PV dye donor-acceptor system, with TEM-grid as a photomask, at two different magnifications. (Reproduced in part with permission from reference 27 Copyright 2012 John Wiley and Sons).

The photoregulation of Förster resonance energy transfer (FRET) efficiencies led to the creation of multicolor luminescent patterns from a single QD nanohybrid film (at least 3 distinct colors were created).[30] However, the interference from the background luminescence can affect the contrast of the multicolor patterns formed. Despite achieving enormous progress, the field of QD photopatterning will benefit from a reliable strategy that can enhance the contrast of multicolor luminescent patterns at a single film level. In principle, the incorporation of a non-luminescent black region can help in enhancing the contrast of multicolor patterns. To accomplish this, the key challenge will be to realize as well as regulate both photoinduced electron and energy transfer processes in a single QD nanohybrid system, and this forms the basis of the present work.

High-contrast multicolor luminescent patterns were created by incorporating, and selectively photoregulating electron and energy transfer processes in a single QD nanohybrid system (**Figure 4.5**). For this, agarose thin films of one donor - two acceptors based triad system was developed, which comprised of indium phosphide/zinc sulfide core/shell (InP/ZnS) QD as the donor, indocyanine green (ICG) as the electron acceptor and merocyanine-540 (MC) as the energy acceptor. The strong electrostatic attractions between positively charged donor QD and negatively charged acceptor dyes was the driving force for the formation of a stable [-] ICG dye:::[+] InP/ZnS QD:::[-] MC dye complex. Likewise, the repulsion between similarly charged [-] MC and [-] ICG dyes led to negligible photophysical interactions between the two acceptor moieties. The process of photoinduced electron transfer (PET) from QD to ICG dye was found to be dominant in [-] ICG dye:::[+] InP/ZnS QD:::[-] MC dye complex, which generated a non-luminescent black agarose film. A selective and spatial photodegradation of

ICG dyes triggered the switching-OFF of the photoinduced electron transfer process in the QD nanohybrid film, resulting in the onset of FRET between InP/ZnS QD and MC dye. Consequently, orange colored luminescent patterns were formed on the QD nanohybrid agarose film, along with non-luminescent black regions. Further, multicolor patterns containing yellow and green luminescent regions were created by the partial and complete photodegradation of energy acceptor dyes, respectively. Thus, the coupling of photoinduced electron and energy transfer processes, in a single QD nanohybrid agarose film, led to the creation of multicolor luminescent patterns on a non-luminescent background. Along with enhancing the color contrast, our approach expands the scope of QD photopatterning towards creating luminescent images that have inherent black regions, at a multicolor level.
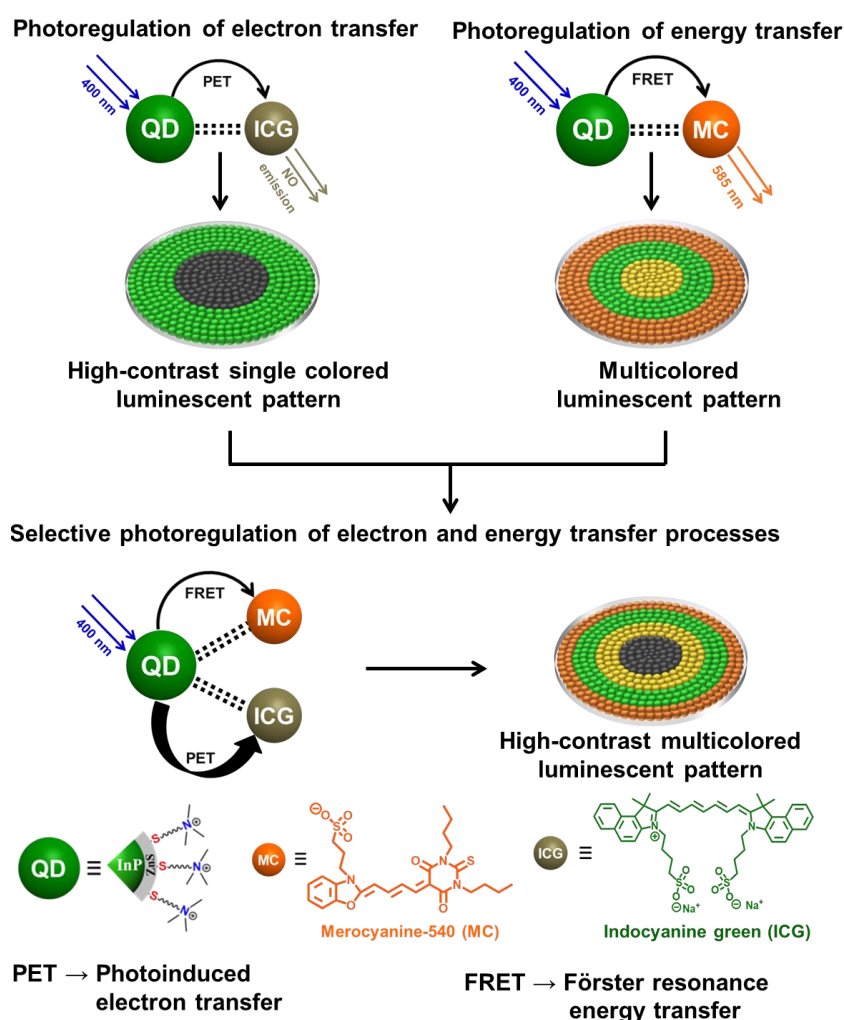

Figure 4.5: Schematic representation for the photoregulation of energy and electron transfer processes in a single QD nanohybrid film, for creating high-contrast multicolor luminescent patterns. The color contrast was improved by incorporating a non-luminescent black region (due to photoinduced electron transfer) in multicolor luminescent patterns (due to energy transfer).

4.3 Experimental Section

4.3.1 Materials and Methods:

Indium acetate (In(Ac)$_3$), myristic acid (MA), 1-octadecene (ODE), zinc stearate (Zn(St)$_2$), 1-dodecanethiol (DDT), merocyanine-540 ([-] MC), indocyanine green ([-] ICG), agarose, 11-mercaptoundecanoic acid ([-]), tetramethylammonium hydroxide (TMAOH) 25 % wt. in water isopropyl alcohol (IPA) were purchased from Sigma-Aldrich. Tris (trimethylsilyl) phosphine (P(TMS)$_3$) was purchased from Strem Chemicals. All the reagents were used as received without any further purification. N,N,N-Trimethyl(11-mercaptoundecyl)ammonium chloride ([+]) was synthesized according to a reported procedure.[43]

4.3.2 Synthesis of InP/ZnS quantum dots:

The InP/ZnS QDs were prepared through a one-pot synthesis, as mentioned in Chapter 3.[30]

4.3.3 Preparation of water-stable InP/ZnS QDs:

The water-stable [+] InP/ZnS and [-] InP/ZnS QDs were prepared through a place exchange reaction, as mentioned in the Chapter 2.[44]

4.3.4 Photoinduced electron transfer experiments:

In a typical experiment, ~3 mL solution of [+] InP/ZnS QD with an optical density of ~0.1 (at the excitation wavelength of 400 nm; ~0.6 μM[44]) was taken in a 4-sided quartz cuvette. With the QDs acting as donors, aliquots of acceptor dye molecules (ICG) were sequentially added to the QD solution, followed by 15 min purging with Ar after each addition. Spectral changes were monitored using Shimadzu UV-3600 and Fluorolog-3 (HORIBA Scientific) spectrofluorimeter. The corresponding lifetime measurements were carried out in a HORIBA Delta Flex Time-Correlated Single Photon Counting system using a 405 nm laser source. The fluorescence decay profiles were fitted with tri-exponential functions with minimum χ^2 value. A similar procedure was adopted for the temperature dependent studies where the samples were equilibrated for ~5 min at the set temperature before the measurement, with a tolerance range of 0.5 ^{0}C. The time resolved studies in agarose films were performed in the solid-state mode (front phase collection mode).

4.3.5 Preparation of agarose films:

[-] ICG dye:::[+] InP/ZnS QD:::[-] MC dye dry agarose films were prepared by mixing [-] ICG dye:::[+] InP/ZnS QD::: [-] MC dye complex with hot agarose solution (1.0 % w/v), and heating overnight at 50 ^{0}C. The films were thoroughly characterized using spectroscopic

techniques to monitor the changes in the properties of [+] InP/ZnS QD before and after the formation of films. Similar procedures were followed for the preparation of agarose films of [+] InP/ZnS QD:::[-] MC dye, [+] InP/ZnS QD, [-] MC dye, [-] ICG dye and [-] ICG dye:::[-] MC dye. The concentrations of QD, MC and ICG in agarose films were ~5, ~15, ~25 μM, respectively.

4.3.6 Photopatterning of [-] ICG dye:::[+] InP/ZnS QD:::[-] MC dye agarose films:

The QD nanohybrid agarose films were irradiated with a 10 W 730 nm light emitting diode (LED) for ~6 h, placed at a distance of ~2 cm from the film, to selectively degrade the ICG dye (incident power on the film was estimated to be ~98 mW/cm^2 using an optical power meter from Newport Model 842.PE). Similarly, a 10 W 530 nm LED was used to degrade the MC dye in QD nano hybrid film (incident power on the film was estimated to be ~54 mW/cm^2). MC dyes were completely and partially degraded upon irradiation for ~5 h and ~2 h, respectively. All the photoluminescence images were recorded with an excitation wavelength of ~364 nm.

4.3.7 Calculation of rate and efficiency of photoinduced electron transfer process:

The rate (k_{PET}) and efficiency (E) of the photoinduced electron transfer from [+] InP/ZnS QD (donor) to ICG dye (acceptor) was calculated using the following expressions.[45]

$$k_{PET} = \frac{1}{\tau} - \frac{1}{\tau_0} \quad \text{and} \quad E = 1 - \frac{\tau}{\tau_0}$$

Where τ, τ_0 are the average lifetime of InP/ZnS QDs in the presence and absence of ICG dye, respectively.

4.3.8 Optimization of concentrations of [+] InP/ZnS QD, MC and ICG dyes in the triad nanohybrid system:

The present work aims at realizing high-contrast multicolor luminescent patterns through the photoregulation of both electron and energy transfer processes, in a single QD-dye nanohybrid film. Here, attaining maximum efficiencies for both photoinduced electron and energy transfer processes was crucial in developing highly luminescent and high-contrast patterns, respectively. With this in mind, we optimized the relative ratio of the three components InP/ZnS QD, ICG and MC dyes in the triad system. The relative ratio was first optimized in solution state, and then extended to thin agarose film. The concentration of InP/ZnS QD was fixed at ~0.6 μM (3 mL), and small aliquots of MC dye (5 μL of ~0.4 mM) were added, until a maximum energy transfer was achieved (this was reflected by the

saturation of MC dye absorption peak at 588 nm). Energy transfer efficiency got saturated upon the addition of ~2 μM of MC dye, which was similar to our previous study.[44] To this QD:::MC dyad solution, we added small aliquots of ICG dye (~5 μL of ~1.5 mM) until a complete quenching of the steady state photoluminescence was obtained (corresponding to maximum electron transfer state). The final concentrations of the InP/ZnS QD, MC, and ICG dye in solution state studies were ~0.6 μM, ~2 μM, and ~18 μM respectively.

It was crucial to use excess amounts of QD and MC dye in agarose films, so that the generated luminescent photopatterns can be clearly visible under the excitation of 3W 364 nm lamp. For this, we used ~8 times excess of InP/ZnS QD (~5 μM) and MC dye (~15 μM), as compared to the solution state studies. Similar concentrations of InP/ZnS QD and MC dye were used in our previous study as well, to create highly luminescent photopatterns.[30] To this QD:::MC dyad agarose film, we added various concentrations of ICG dye until a completely non-luminescent agarose film was obtained. This state was achieved after the addition of 25 μM of ICG dye. Thus, the final concentrations of InP/ZnS QD, MC, and ICG dyes in the triad agarose film were ~5 μM, ~15 μM, and ~25 μM, respectively.

4.4 Results and Discussion

4.4.1 Design of QD based one donor – two acceptors triad system:

Green emitting InP/ZnS QD was chosen as the donor component, based on the previous reports on their use as efficient donors in both photoinduced electron and energy transfer processes.[44,46-48] One of the major challenges in the present work was the selection of electron and energy acceptor components. The organic fluorophores have to meet the following four conditions to qualify as acceptors for the triad system.

(i)   The two acceptors should selectively and independently participate in photoinduced electron and energy transfer processes with InP/ZnS QD.

(ii)   The process of photoinduced electron transfer should dominate the energy transfer to generate a non-luminescent complex, which can act as the black background for further photopatterning.

(iii)   There should be minimal overlap between the absorption spectra of the two acceptors, so that the electron acceptor can be selectively photodegraded.

(iv) There should be negligible photophysical interactions between the electron and energy acceptors.

Based on our previous experience on light harvesting with QD-dye nanohybrids, merocyanine-540 (MC) and indocyanine green (ICG) dyes were found to satisfy all the above conditions to qualify as efficient energy and electron acceptors, respectively (**Figure 4.5**).[44,49] A similar net surface charge and minimal overlap between the absorptions of MC and ICG dyes resulted in negligible photophysical interactions between the two acceptor dyes (**Figure 4.6**).
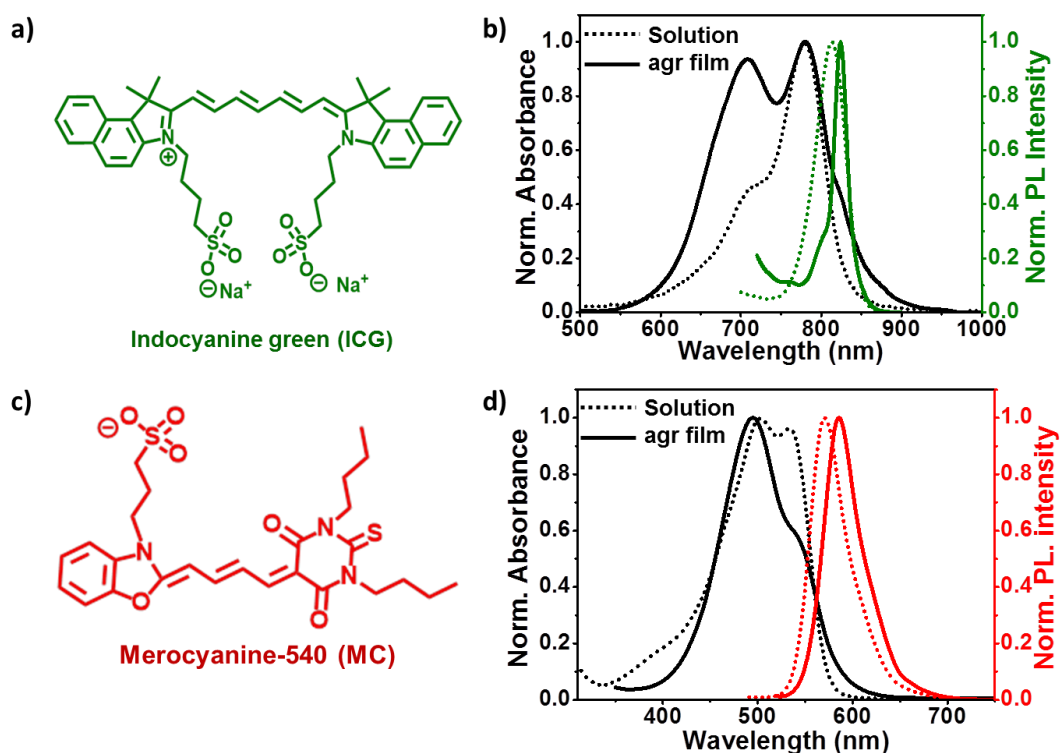
Figure 4.6: a,c) Chemical structures of indocyanine green (ICG) and merocyanine-540 (MC) dyes, respectively. b,d) Normalized absorption and PL spectra of [-] ICG and [-] MC dyes in solution and agarose films, respectively.

4.4.2 Electron transfer in [+] InP/ZnS QD:::[-] ICG dye donor-acceptor system:

The ability of [+] InP/ZnS QD and [-] MC dye to participate in an efficient FRET process has already been reported in both solution and solid states in the Chapters 2 and 3.[30,44] Next, the potency of [-] ICG dye to act as an efficient electron acceptor was tested in solution state. A previously reported place exchange protocol was followed to prepare green emitting [+] InP/ZnS QD.[44] Myristic acid ligands were replaced with N,N,N-trimethyl(11-mercaptoundecyl)ammonium chloride ([+]) ligands to impart water solubility and permanent

cationic charge on the surface of InP/ZnS QD. The energy level positions of [+] InP/ZnS QD and [-] ICG dye[50] revealed that the photoinduced electron transfer from QD to dye is thermodynamically favorable (ΔG = -20 kJ mol^{-1}; **Figure 4.7**).

Figure 4.7: Energy levels of [+] InP/ZnS QD and [-] ICG dye against vacuum, estimated from a combination of absorption and cyclic voltammetry studies.

Systematic photophysical studies were performed by titrating an aqueous solution of [+] InP/ZnS QD (3 mL of ~0.6 µM) with small aliquots of [-] ICG dye (5 µL of ~1.5 mM), under inert conditions. A bat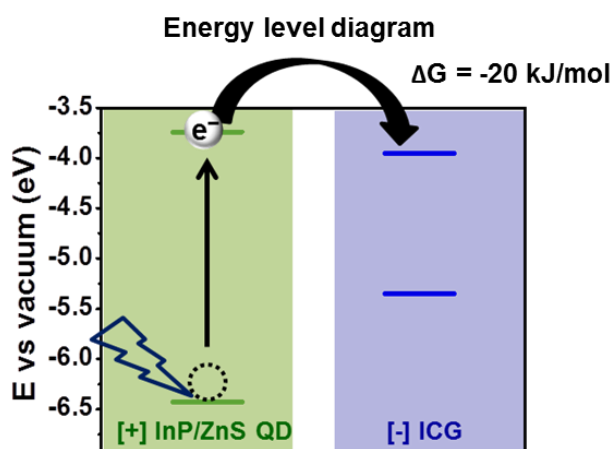hochromic shift of ~26 nm was observed in the absorption of ICG dye in the presence of QD, indicating a strong ground state interaction in [+] InP/ZnS QD:::[-] ICG dye complex (**Figure 4.8a**).[45,51-56] The steady state photoluminescence (PL) studies were performed by selectively exciting the InP/ZnS QD at 400 nm, where the absorption of ICG dye was minimal. A steady and continuous decrease in the PL of InP/ZnS QD was observed upon the addition of ICG dye, without the emergence of any new emission peak (**Figure 4.8b**). The non-linear nature of the Stern–Volmer plot indicates the presence of both static and dynamic components in the PL quenching of QD in [+] InP/ZnS QD:::[-] ICG dye complex (inset of **Figure 4.8b**).[45,51] The PL quenching efficiency was estimated to be ~97 %, which got saturated after the addition of ~18 µM of ICG dye (**Figure 4.8c**; E = 1-I/I$_0$;[45] where I and I$_0$ are PL intensities of donor in the presence and absence of acceptor). The quenching of QD in [+] InP/ZnS QD:::[-] ICG dye complex was further confirmed using time resolved PL studies, where the average lifetime of [+] InP/ZnS QD decreased from ~64.5 to ~1.4 ns (**Figures 4.8d**, **and Table 4.1**). The PL quenching efficiency was estimated to be ~98 %, which is in close agreement with steady state results (E = 1-τ/τ_0;[45] where τ and τ_0 are average lifetimes of donor in the presence and absence of acceptor). Consistent PL quenching and formation of a non-luminescent complex, observed in both steady state and time resolved

studies, strongly indicates the possibility of photoinduced electron transfer from QD to dye in [+] InP/ZnS QD:::[-] ICG dye complex.
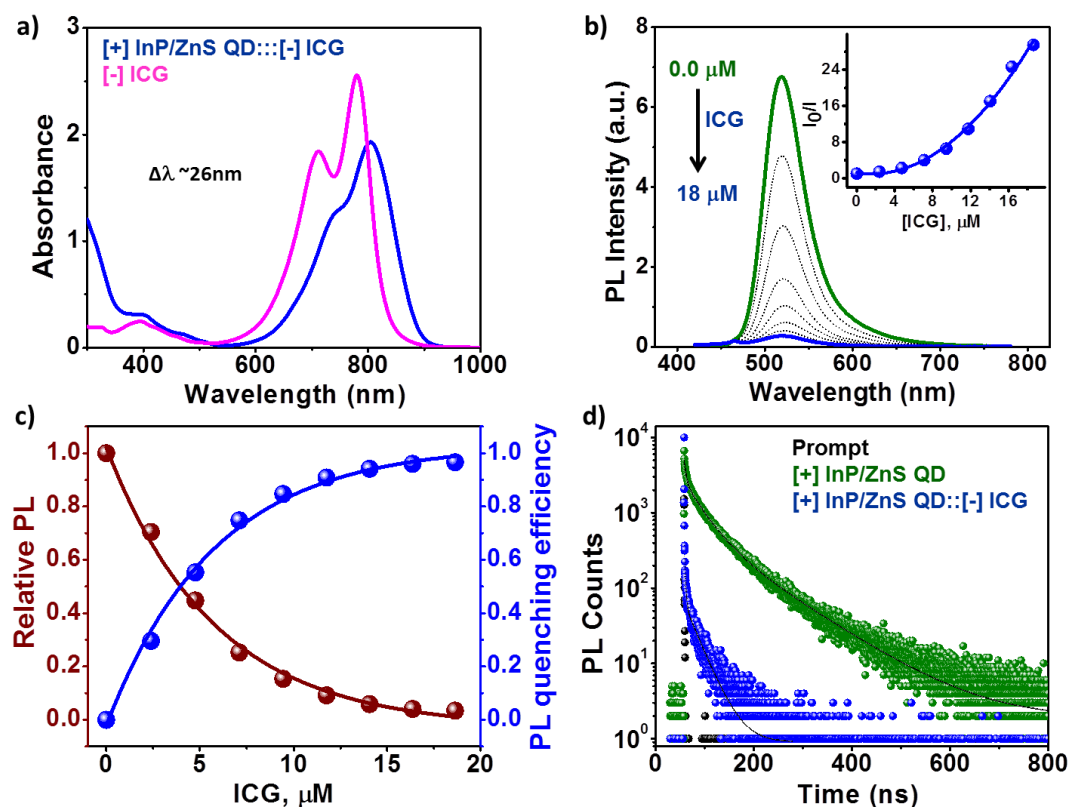
Figure 4.8: PL quenching studies in [+] InP/ZnS QD:::[-] ICG dye nanohybrid in solution state. a) The absorption spectra of [-] ICG dye in the absence and presence of [+] InP/ZnS QD. b) Spectral changes in the PL of [+] InP/ZnS QDs upon sequential addition of [-] ICG dye. The inset shows the corresponding Stern–Volmer plot. c) A plot showing the saturation in relative QD PL and quenching efficiency vs the concentration of the ICG dye. d) The PL lifetime decay profiles of [+] InP/ZnS QD in the absence and presence of [-] ICG dye, collected at the QD emission of 520 nm.

Table 4.1: PL decay analysis of [+] InP/ZnS QD in the presence of [-] ICG dye measured in a time window of 800 ns.

Sample	τ_1 (ns)	a_1	τ_2 (ns)	a_2	τ_3 (ns)	a_3	Avg. τ (ns)	Efficiency (%)
[+] InP/ZnS_H$_2$O	4.02	0.45	36.19	0.41	101.7	0.14	64.51	97.8
[+] InP/ZnS ::: [-] ICG_H$_2$O	0.12	0.98	3.53	0.02			1.41	

The process of photoinduced electron transfer involves the transfer of an electron from photoexcited donor to a ground state acceptor, resulting in the formation of a charged transfer complex.[45] The stability and formation of the charge transfer complex will depend on the

solvent polarity and temperature of the medium.[57-63] Thus, systematic studies by varying these two parameters are commonly performed to prove the photoinduced electron transfer (PET) process in a donor-acceptor system.[49,57-63] The concentration of acceptor ICG dye was maintained at ~11 µM (instead of ~18 µM) to see an appreciable effect of solvent polarity and temperature on the PL quenching. In the present work, the effect of solvent polarity on the PL quenching of QD was studied by decreasing the dielectric constant of the medium from ~78 to ~41 (for H_2O and 0.7:0.3 v/v $CH_3CN:H_2O$ at 293 K, respectively[58]). The steady state experiments revealed that the efficiency of QD PL quenching by ICG dye was lowered to ~67 % in $CH_3CN:H_2O$ mixture (**Figures 4.9a,b**). A similar trend was also observed in the PL lifetime quenching studies as well (**Figures 4.9c,d** and **Table 4.2**; E_{H_2O} ~80 % vs $E_{CH_3CN:H_2O}$ ~40 %).
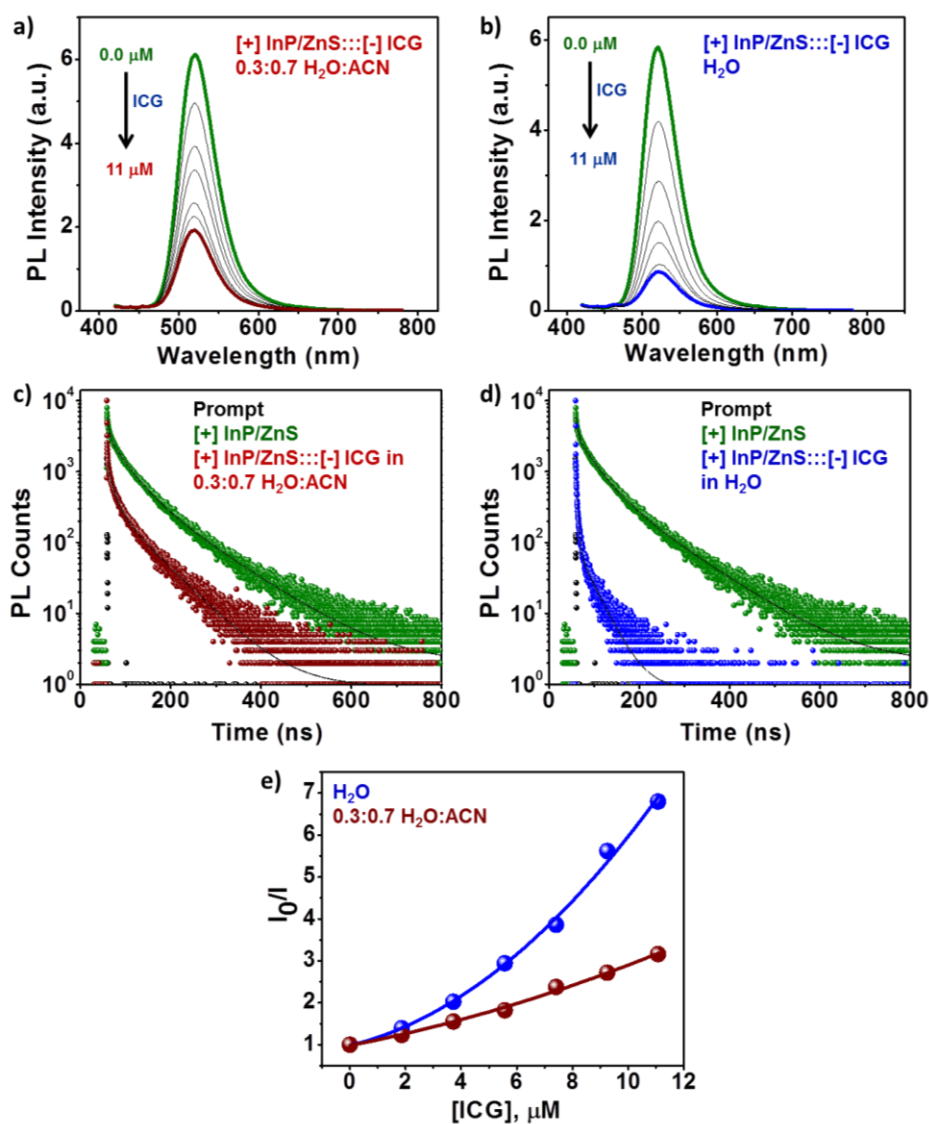

Figure 4.9: Proof for photoinduced electron transfer process in [+] InP/ZnS QD:::[-] ICG dye complex. Steady state PL spectral changes of [+] InP/ZnS QD upon addition of ~11 µM [-]

ICG dye in a) 0.7:0.3 v/v $CH_3CN:H_2O$ and (b) H_2O. PL decay profiles of [+] InP/ZnS QD in the absence and presence of ~11 µM [-] ICG in c) 0.7:0.3 v/v $CH_3CN:H_2O$, and d) H_2O. e) Stern-Volmer plot showing the relative changes in the PL intensity of [+] InP/ZnS QD as a function of [-] ICG dye concentration in both 0.7:0.3 v/v $CH_3CN:H_2O$ (brown curve) and H_2O (blue curve). The concentration of acceptor ICG dye was maintained at ~11 µM (instead of ~18 µM) to see an appreciable effect of solvent polarity on the PL quenching.

As a result, the rate of quenching ($k_{PET} = 1/\tau - 1/\tau_0$) was observed to be lower in $CH_3CN:H_2O$ mixture compared to H_2O ($k_{PET} = $ ~1.03 x 10^7 s^{-1} and ~6.42 x 10^7 s^{-1} in $CH_3CN:H_2O$ mixture and H_2O, respectively). The rationale being that the charge transfer complex formed is more stabilized in a polar solvent compared to a non-polar medium, thereby enhancing the efficiency of photoinduced electron transfer.[57-60]

Table 4.2: PL decay analysis of [+] InP/ZnS QD in the presence of [-] ICG dye in different solvents measured in a time window of 800 ns.

Sample	τ_1 (ns)	a_1	τ_2 (ns)	a_2	τ_3 (ns)	a_3	Avg. τ (ns)	Efficiency (%)
[+] InP/ZnS_H_2O	4.02	0.45	36.19	0.41	101.7	0.14	64.51	
[+] InP/ZnS ::: [-] ICG_H_2O	0.39	0.88	4.72	0.11	35.64	0.01	12.54	80.5
[+] InP/ZnS ::: [-] ICG_0.3:0.7 H_2O:ACN	0.94	0.72	13.4	0.21	61.24	0.07	38.6	40.1

Next, systematic PL quenching studies were performed by increasing the temperature from 288 K to 328 K. Both steady state and time resolved experiments showed an enhancement in the efficiency and rate of PL quenching in [+] InP/ZnS QD:::[-] ICG dye complex, with an increase in temperature (**Figure 4.10 and Table 4.3**). For instance, k_{PET} increased from ~1.32 x 10^7 s^{-1} to ~369 x 10^7 s^{-1}, as the temperature was raised from 288 K to 328 K, respectively. A rise in temperature helps in overcoming the activation barrier, thereby increasing the rate of photoinduced electron transfer process.[61-63] The non-linear nature of the Stern–Volmer plot was maintained at all the temperatures (**Figure 4.11a**). Thus, both solvent polarity and temperature dependent studies confirm that the PL quenching observed in [+] InP/ZnS QD:::[-] ICG dye complex was due to an efficient photoinduced electron transfer from InP/ZnS QD to ICG dye. Further, a linear form of lnk_{PET} vs. 1/T plot indicates that the photoinduced electron transfer in [+] InP/ZnS QD:::[-] ICG dye follows an Arrhenius behavior, and is in accordance with the Marcus theory (**Figure 4.11b**).[64,65] Accordingly, the photoinduced electron transfer process was modeled using the expression $k_{ET} = k_{el}\nu$ exp(-

$\Delta G^{\ddagger}/k_B T$), where $\Delta G^{\ddagger}$ is the Gibbs free energy of activation, k_{el} is the electronic transmission coefficient, ν is the frequency of nuclear motion over the barrier, T is the temperature in kelvin, and k_B is the Boltzmann constant.[64,65] A linear regression of the plot gives $\Delta G^{\ddagger}$ =108.55 kJ mol^{-1} for the photoinduced electron transfer process in [+] InP/ZnS QD:::[-] ICG dye complex.

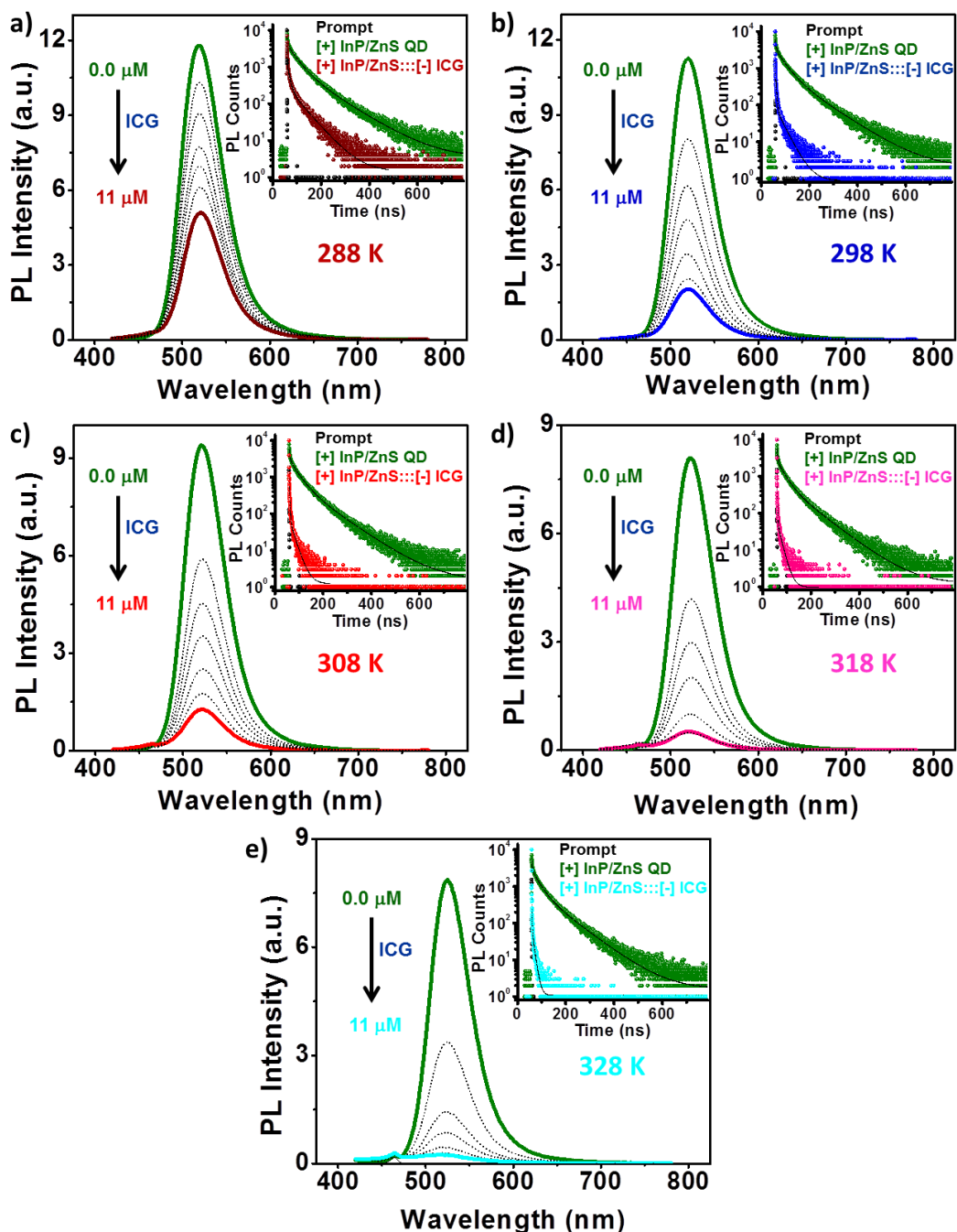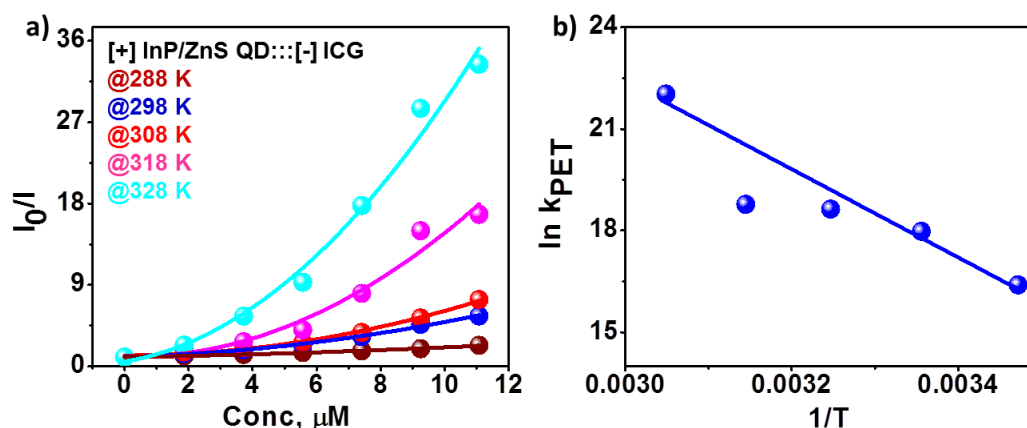**Figure 4.10:** Steady state PL quenching of [+] InP/ZnS QD by ~11 μM [-] ICG dye at a) 288 K, b) 298 K, c) 308 K, d) 318 K, and e) 328 K in H_2O. Inset shows the corresponding PL lifetime decay profiles.

Table 4.3: PL decay analysis of [+] InP/ZnS QD in the presence of [-] ICG dye at different temperatures measured in a time window of 800 ns.

Sample	τ_1 (ns)	a_1	τ_2 (ns)	a_2	τ_3 (ns)	a_3	Avg. τ (ns)	Efficiency (%)
[+] InP/ZnS_H$_2$O	4.02	0.45	36.19	0.41	101.7	0.14	64.51	
[+] InP/ZnS ::: [-] ICG_288 K	1.22	0.73	9.57	0.21	57.92	0.06	34.75	46.1
[+] InP/ZnS ::: [-] ICG_298 K	0.39	0.88	4.72	0.11	35.64	0.01	12.54	80.5
[+] InP/ZnS ::: [-] ICG_308 K	0.23	0.88	2.24	0.11	20.36	0.01	7.19	88.8
[+] InP/ZnS ::: [-] ICG_318 K	0.18	0.9	1.64	0.09	16.53	0.01	6.32	90.2
[+] InP/ZnS ::: [-] ICG_328 K	0.13	0.98	1.08	0.02	-	-	0.26	99.3

Figure 4.11: a) The Stern−Volmer plots constructed from steady state PL quenching studies of [+] InP/ZnS QD:::[-] ICG dye complex at different temperatures. b) Variation in the photoinduced electron transfer rate, k_{PET}, as a function of temperature in [+] InP/ZnS QD:::[-] ICG dye complex.

4.4.3 Coupling of photoinduced electron and energy transfer processes in single QD nanohybrid system:

Our next objective was to couple both photoinduced electron and energy transfer processes in [-] ICG dye:::[+] InP/ZnS QD:::[-] MC dye triad complex. The compatibility of ICG and MC dye to participate in selective photoinduced electron and energy transfer processes with InP/ZnS QD was first optimized in solution state. Systematic photophysical studies were performed by titrating an aqueous solution of [+] InP/ZnS QD with small aliquots of [-] MC and [-] ICG dye, under inert conditions (Details are provided in the Experimental Section). Bathochromic shifts of ~35 nm and ~26 nm were observed in the absorption spectra MC and

ICG dyes, respectively, in the presence of [+] InP/ZnS QDs (**Figure 4.12a**). This indicates that both the dyes have a strong ground state interaction and complexation with [+] InP/ZnS QDs. On addition of ~2 μM of MC dye to the 3 mL solution of ~0.6 μM [+] InP/ZnS QDs, we observed a quenching in the QD PL along with the formation of new peak at 588 nm corresponding to emission of [-] MC dye (due to FRET; **Figure 4.12b**). A complete quenching in the PL of both [+] InP/ZnS QD and [-] MC dye was observed in the presence of ~18 μM [-] ICG dye, with formation of no new PL peak (**Figure 4.12b**). This indicates that the elecron transfer is dominating over the energy transfer process in [-] ICG dye:::[+] InP/ZnS QD:::[-] MC dye triad complex. Similar PL quenching results were observed in time resolved studies as well. Thus, the quenching in the PL decay of QD in [-] ICG dye:::[+] InP/ZnS QD:::[-] MC dye triad complex indicates the dominance of photoinduced electron transfer process (**Figure 4.12c and Table 4.4**).
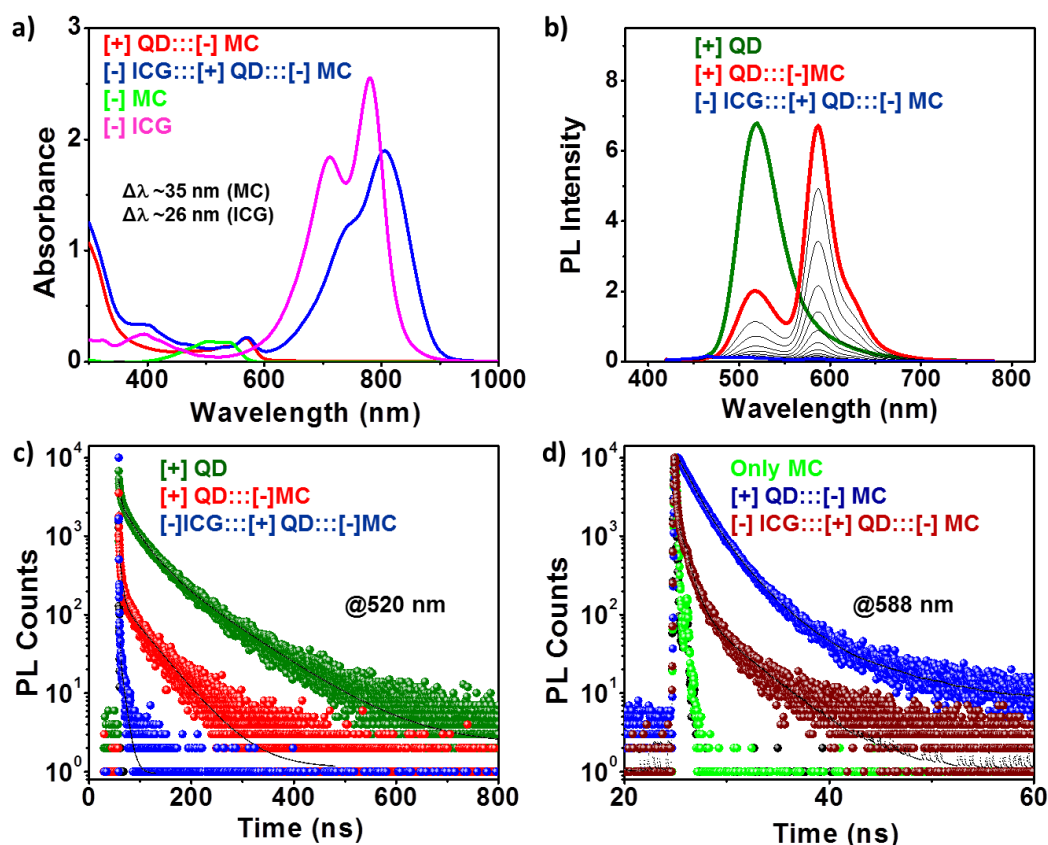
Figure 4.12: Coupling of photoinduced electron and energy transfer processes in [-] ICG:::[+] InP/ZnS QD:::[-] MC complex in solution. a) The absorption spectra of solutions of [+] InP/ZnS:::[-] MC dyad, [-] ICG:::[+] InP/ZnS:::[-] MC triad, [-] MC and [-] ICG. The concentrations of InP/ZnS QD, MC and ICG were ~0.6, ~2, ~18 μM, respectively. b) Steady state PL spectra of various complex solutions. The PL of [+] InP/ZnS:::[-] MC dyad solution (due to FRET) gradually decreased upon the addition of ICG dye, and finally became non-luminescent after the addition of ~18 μM ICG dye. c) The PL decay profiles of [+] InP/ZnS

QD in the absence (green decay), presence of MC dye (red decay) and presence of ICG dye (blue decay), collected at 520 nm. d) The PL decay profiles collected at 588 nm in [+] InP/ZnS:::[-] MC (blue decay) and [-] ICG:::[+] InP/ZnS:::[-] MC (brown decay) solutions.

It is worth mentioning that an efficient FRET was observed in [+] InP/ZnS:::[-] MC dyad solution, as previously reported by our group.[44] This was further proved by the observation that the PL lifetime of MC dye is increased in [+] InP/ZnS:::[-] MC (blue decay in **Figure 4.12d and Table 4.5**). However, the incorporation of ICG dye into the [+] InP/ZnS:::[-] MC solution interrupts the interaction between QD and MC dye, and selectively triggers the photoinduced electron transfer process between QD and ICG dye (brown decay in **Figure 4.12d and Table 4.5**). This clearly confirms that the process of photoinduced electron transfer from QD to ICG dye is dominating in [-] ICG dye:::[+] InP/ZnS QD:::[-] MC dye complex.

Table 4.4: Solution state PL decay analysis of [-] InP/ZnS QD in [-] ICG:::[+] InP/ZnS QD:::[-] MC and [+] InP/ZnS QD:::[-] MC complexes, in a time window of 800 ns. The decay was collected at 520 nm.

Sample	τ_1 (ns)	a_1	τ_2 (ns)	a_2	τ_3 (ns)	a_3	Avg. τ (ns)	Efficiency (%)
[+] InP/ZnS_H_2O	4.02	0.45	36.19	0.41	101.7	0.14	64.51	
[+] InP/ZnS :::[-] MC	1.01	0.76	19.8	0.18	41.91	0.06	25.80	60.1
[-] ICG::: [+] InP/ZnS :::[-] MC	0.10	0.98	2.05	0.01			0.43	98.6

Table 4.5: Solution state PL decay analysis of MC dye in [-] ICG:::[+] InP/ZnS QD:::[-] MC and [+] InP/ZnS QD:::[-] MC complexes, in a time window of 100 ns. The decay was collected at 588 nm.

Sample	τ_1 (ns)	a_1	τ_2 (ns)	a_2	τ_3 (ns)	a_3
[+] InP/ZnS :::[-] MC@ 588 nm	3.05	0.69	0.5	-0.28	11.5	0.03
[-] ICG:::[+] InP/ZnS :::[-] MC@ 588 nm	0.05	0.86	0.74	0.13	6.5	0.01

Next, to create high contrast luminescent patterns, the solution state photoinduced electron and energy transfer studies have to be successfully translated to solid state. For this, agarose was selected as a solid substrate to prepare thin films of [-] ICG dye:::[+] InP/ZnS QD:::[-] MC dye triad complex, by mixing the individual components with hot agarose solution.

Likewise, the thin films of [+] InP/ZnS QD:::[-] MC dye, [+] InP/ZnS QD, [-] MC dye, [-] ICG dye and [-] ICG dye:::[-] MC dye were also prepared (Details are provided in Experimental Section). Bathochromic shifts of ~28 nm and ~23 nm were observed in the absorption spectra of [-] MC and [-] ICG dyes, in the [-] ICG dye:::[+] InP/ZnS QD:::[-] MC dye agarose film respectively (**Figure 4.13a**). This indicates a strong ground state interaction and complexation between [+] InP/ZnS QD and the two dyes, in the agarose film.[45, 51-56] All the PL studies on agarose films were performed by selectively exciting the InP/ZnS QD at 400 nm, where both MC and ICG dyes have negligible absorption. The steady state PL experiments showed negligible luminescence from [-] ICG dye:::[+] InP/ZnS QD:::[-] MC dye agarose film, indicating the dominance of photoinduced electron transfer process from InP/ZnS QD to ICG dye (**Figure 4.13b**). Similarly, the time resolved PL studies revealed a drastic quenching of the QD PL lifetime from ~63 to ~0.36 ns in [-] ICG dye:::[+] InP/ZnS QD:::[-] MC dye agarose film (**Figure 4.13c and Tables 4.6**).
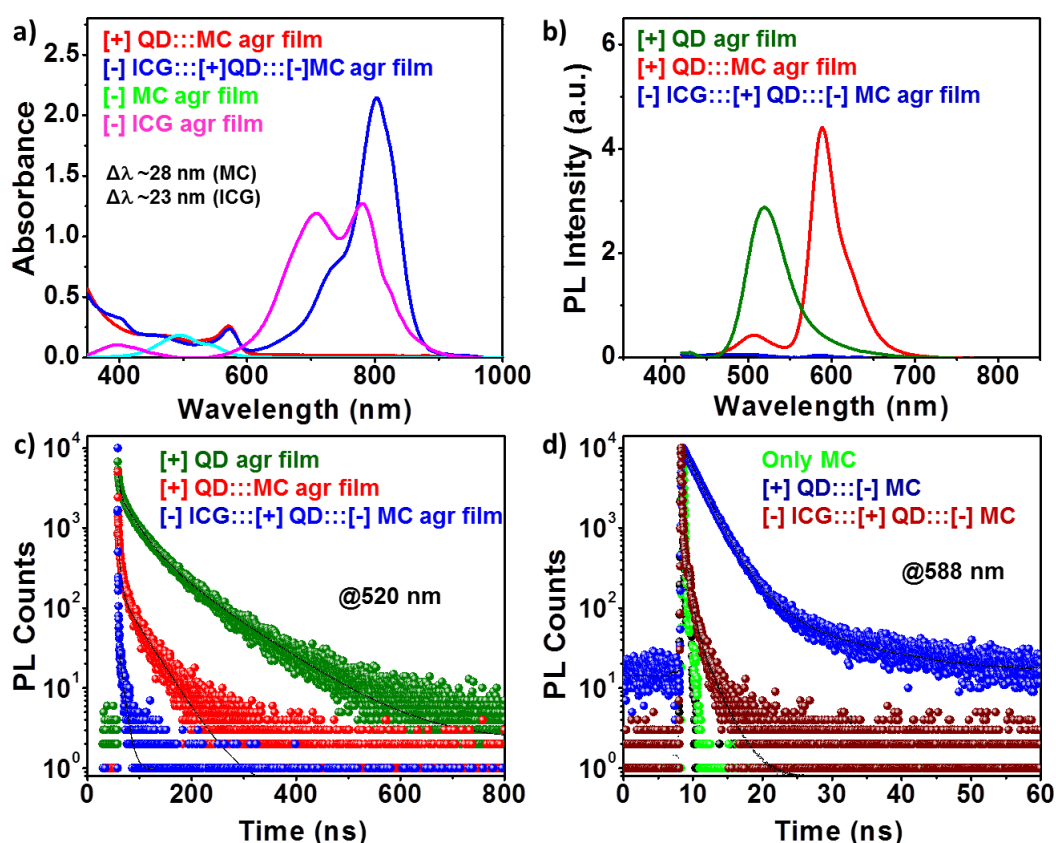
Figure 4.13: Coupling of photoinduced electron and energy transfer processes in [-] ICG dye:::[+] InP/ZnS QD:::[-] MC dye triad in agarose film. a) The absorption spectra of [+] InP/ZnS:::[-] MC dyad, [-] ICG:::[+] InP/ZnS:::[-] MC triad, [-] MC and [-] ICG agarose films. b) Steady state PL spectra of different agarose films. Negligible PL was observed in [-] ICG dye:::[+] InP/ZnS QD:::[-] MC dye agarose film (blue curve). c) The PL decay profiles of InP/ZnS QD collected at 520 nm in the absence (green decay), presence of MC dye (red

decay), and presence of both MC and ICG dyes (blue decay). d) The PL decay profiles of MC collected at 588 nm in [+] InP/ZnS QD:::[-] MC dye (blue decay) and [-] ICG dye:::[+] InP/ZnS QD:::[-] MC dye agarose films (brown decay). The concentrations of InP/ZnS QD, MC and ICG dyes in agarose films were ~5, ~15, ~25 μM, respectively.

It is worth mentioning that an efficient FRET was observed in the [+] InP/ZnS :::[-] MC dyad agarose film, as shown in Chapter 3. As a result, the PL lifetime of the MC dyes was higher in the [+] InP/ZnS QD:::[-] MC agarose film (**Figure 4.13d and Table 4.7**). However, the incorporation of ICG dye into the [+] InP/ZnS QD:::[-] MC dyad interrupts the interaction between QD and MC dye, in both solution and agarose film, and thereby selectively triggering the photoinduced electron transfer process between QD and ICG dye. The rate of photoinduced electron transfer was estimated to be ~25 times greater than the rate of energy transfer process in [-] ICG dye:::[+] InP/ZnS QD:::[-] MC dye agarose film (k_{PET} = 2.7 x 10^9 s^{-1} and k_{FRET} = 1.05 x 10^8 s^{-1}). All these studies confirm that the process of photoinduced electron transfer from QD to ICG dye is dominating over the FRET between QD and MC dye, in [-] ICG dye:::[+] InP/ZnS QD:::[-] MC dye agarose film as well. Thus, a non-luminescent black agarose film was generated by complexing [+] InP/ZnS QD with [-] MC and [-] ICG dyes. All the key parameters for photoinduced electron transfer process in [+] InP/ZnS QD:::[-] ICG dye dyad and [-] ICG dye:::[+] InP/ZnS QD:::[-] MC dye triad systems are summarized in **Table 4.8**.

Table 4.6: PL decay analysis of [-] InP/ZnS QD in [-] ICG:::[+] InP/ZnS QD:::[-] MC triad and [+] InP/ZnS QD:::[-] MC dyad agarose films, in a time window of 800 ns. The decay was collected at 520 nm.

Sample	τ_1 (ns)	a_1	τ_2 (ns)	a_2	τ_3 (ns)	a_3	Avg. τ (ns)	Efficiency (%)
[+] InP/ZnS_H_2O	3.25	0.48	31.57	0.38	98.51	0.14	63.71	
[+] InP/ZnS :::[-] MC	0.34	0.86	4.85	0.11	16.36	0.03	8.13	87.2
[-] ICG::: [+] InP/ZnS :::[-] MC	0.12	0.99	1.90	0.01			0.36	99.4

Table 4.7: PL decay analysis of MC dye in [-] ICG:::[+] InP/ZnS QD:::[-] MC triad and [+] InP/ZnS QD:::[-] MC dyad agarose films, in a time window of 100 ns. The decay was collected at 588 nm.

Sample	τ_1 (ns)	a_1	τ_2 (ns)	a_2	τ_3 (ns)	a_3
[+] InP/ZnS :::[-] MC@ 588 nm	2.38	0.71	0.28	-0.27	9.5	0.05
[-] ICG:::[+] InP/ZnS :::[-] MC@ 588 nm	0.03	0.97	0.57	0.02	1.26	0.01

Table 4.8: Table summarizing various photoinduced electron transfer parameters in [+] InP/ZnS QD:::[-] ICG dye dyad and [-] ICG dye:::[+] InP/ZnS QD:::[-] MC dye triad complexes, under different experimental conditions.

[+] InP/ZnS QD:::[-] ICG dye complex (dyad)	Solvent Polarity[a]		Temperature (K)[a]					[-] ICG dye:::[+] InP/ZnS QD:::[-] MC dye complex (triad)	
	H_2O (ε ~78)	0.7:0.3 v/v CH_3CN: H_2O (ε ~41)	288	298	308	318	328	Solution (H_2O)	Agarose film
PL quenching efficiency (Steady state)[b]	81 %	67 %	43 %	81 %	86 %	94 %	97 %	99 %	99 %
PL quenching efficiency (Lifetime)[c]	80 %	40 %	46 %	80 %	88 %	90 %	99 %	98 %	99 %
Rate of photoinduced electron transfer (k_{PET})[d] ($\times 10^7$ s^{-1})	6.42	1.03	1.32	6.42	12.3	14.2	369	230	270

[a]The concentration of acceptor ICG dye was maintained at ~11 μM (instead of ~18 μM) to see an appreciable effect of solvent polarity and temperature on the PL quenching of InP/ZnS

QD. [b]E = 1-I/I_0; where I and I_0 are PL intensities of donor in the presence and absence of acceptor. [c]E = 1-τ/τ_0; where τ and τ_0 are average lifetimes of donor in the presence and absence of acceptor. [d]k_{PET} =1/τ - 1/τ_0.

Interestingly, no notable signs of interactions were observed between MC and ICG in agarose films (**Figure 4.14;** most probably due to the electrostatic repulsions), thereby justifying the selection of these two dyes in the QD based triad system.
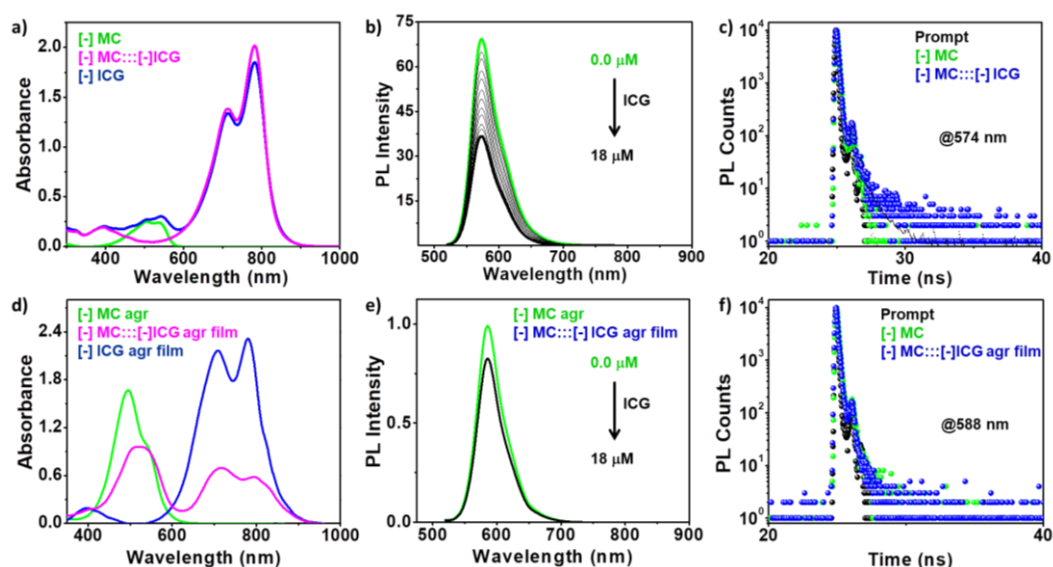

Figure 4.14: a,d) Absorption of mixture of [-] MC and [-] ICG dyes in solution and agarose film, respectively. b,e) Relative changes in the steady state PL spectra of [-] MC dye upon addition of ~18 μM of [-] ICG dye in solution and agarose film, respectively. c,f) Time resolved PL decay profiles collected at the PL wavelength of [-] MC dye in the absence (green decay) and presence (blue decay) of [-] ICG dye in solution and agarose film, respectively.

4.4.4 Creation of high-contrast multicolor luminescent patterns:

An efficient photoinduced electron transfer process from QD to ICG dyes resulted in a non-luminescent black [-] ICG dye:::[+] InP/ZnS QD:::[-] MC dye agarose film, under ~364 nm excitation. Next, photopatterning experiments were performed on the triad agarose film to create high-contrast multicolor luminescent patterns (**Figure 4.15a**). As mentioned earlier, the presence of ICG dye was suppressing the FRET between InP/ZnS QD and MC dye. Thus, in principle, a selective photodegradation of ICG dye will restore the efficient FRET in [-] ICG dye:::[+] InP/ZnS QD:::[-] MC dye agarose film. Accordingly, the agarose film was irradiated with a 10 W 730 nm light emitting diode (LED) for ~6 h. This resulted in the complete and selective degradation of ICG dye (**Figure 4.15b**), thereby switching-OFF the photoinduced electron transfer process in [-] ICG dye:::[+] InP/ZnS QD:::[-] MC dye agarose

film. This triggered the onset of FRET process, and an orange luminescent color was developed on the agarose film, corresponding to the PL of MC dye (E_{FRET} ~87 %, **Table 4.6**). Further, multicolor luminescent patterns were created by photodegrading the FRET acceptor (MC dye) using a 10 W 530 nm LED for ~5 h (**Figure 4.15c**). Consequently, a green luminescent color was developed on the complex agarose film, corresponding to FRET-OFF state (E_{FRET} = 0 %). The PL photographs of complex agarose films under UV light, at different stages of irradiation are showed in **Figure 4.15d**.
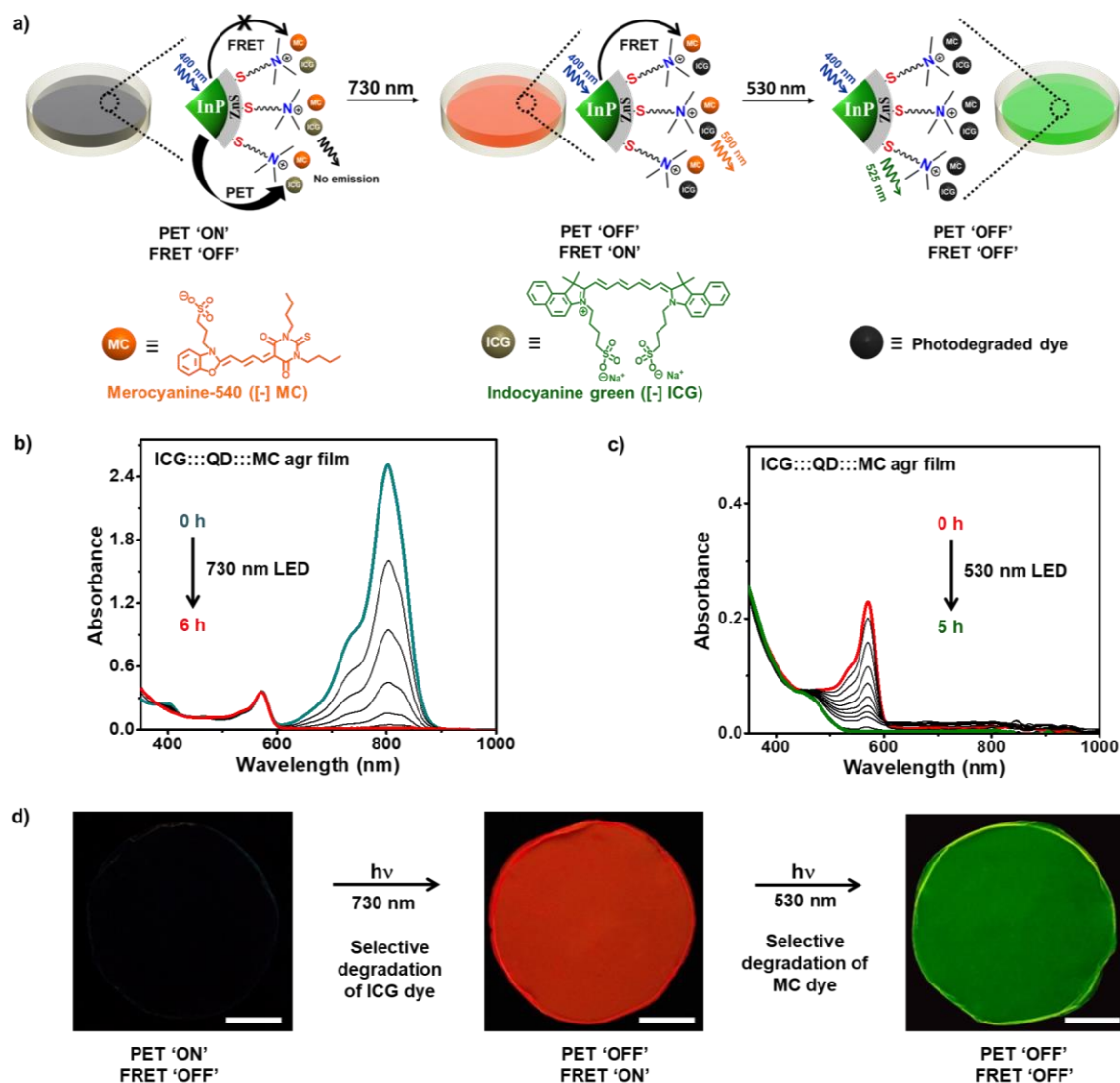

Figure 4.15: Selective photoregulation of energy and electron transfer processes in [-] ICG dye:::[+] InP/ZnS QD:::[-] MC dye agarose film. a) Schematic representation showing the sequential photodegradation of ICG and MC dyes, leading to the switching-OFF of the photoinduced electron and energy transfer processes, respectively. Absorption spectral changes in [-] ICG dye:::[+] InP/ZnS QD:::[-] MC dye agarose film upon sequential irradiation with b)10 W 730 nm and c) 530 nm LEDs, for photodegrading ICG and MC dyes, respectively. d) Corresponding PL photographs of [-] ICG dye:::[+] InP/ZnS QD:::[-] MC

dye agarose films, under UV light, at different stages of irradiation. The scale bar corresponds to 1 cm for all images.

The ability to selectively degrade the acceptor dyes was further explored in a spatially controlled fashion to create high-contrast multicolor luminescent patterns, on a single QD nanohybrid agarose film. In one example, the center of the agarose film was masked against irradiation to retain the black region corresponding to the photoinduced electron transfer-ON state. The rest of the agarose film was irradiated with a 730 nm LED for ~6 h to selectively photodegrade the ICG dyes, thereby switching-ON the FRET between InP/ZnS QD and MC dyes. This imparted an orange colored luminescence to rest of the agarose film (**Figure 4.16a**). Finally, selected portion of the orange region was irradiated with a 530 nm LED for ~5 h to degrade the MC dyes, and create a green colored luminescent pattern on the agarose film (corresponding to FRET-OFF state). Thus, concentric rings comprising of two different colors, and one black region was developed using the selective photoregulation of electron and energy transfer processes in a single QD nanohybrid agarose film (**Figure 4.16a**). Thus, the incorporation of a non-luminescent black region improved the contrast of the multicolor luminescent patterns. Likewise, a variety of high-contrast multicolor luminescent patterns were created using different photomasks (**Figures 4.16b-e**). A controlled photodegradation of MC dyes, for ~2 h, resulted in a moderately efficient FRET state (E_{FRET} ~50 %),[30] which created yellow colored patterns on the complex agarose film (**Figures 4.16c,d**).
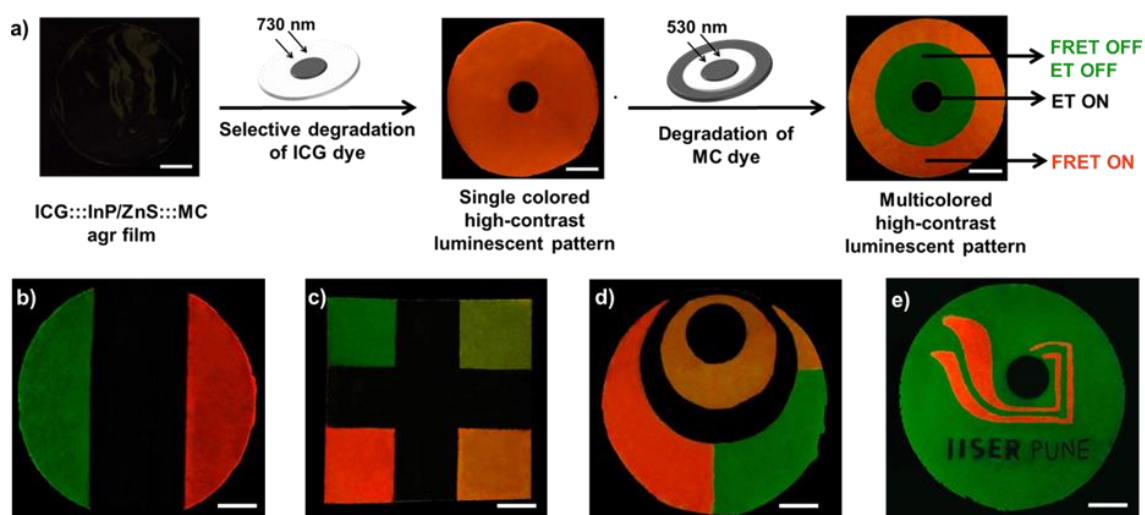

Figure 4.16: High-contrast luminescent patterns from a single QD nanohybrid film. a) Photopatterning of [-] ICG dye:::[+] InP/ZnS QD:::[-] MC dye agarose film, by the sequential irradiation with 730 nm and 530 nm LEDs, to create high-contrast multicolor luminescent patterns. b-e) A few examples of PL images of high-contrast multicolor luminescent patterns

created by our approach of selective photoregulation of electron and energy transfer processes, using different photomasks. The yellow luminescent regions in panel 'c' and 'd' were created by the partial degradation of MC dye (moderately FRET-ON state[30]). The scale bar corresponds to 1 cm for all images.

Thus, the idea of selective and sequential photoregulation of electron and energy transfer processes helped in enhancing the contrast of multicolor luminescent patterns on a single QD nanohybrid agarose film: black (corresponding to photoinduced electron transfer-ON state), orange and yellow (corresponding to FRET-ON states with maximum and moderate efficiencies, respectively), and green (corresponding to photoinduced electron transfer-OFF and FRET-OFF states).

4.5 Conclusions

In conclusion, efficient photoinduced electron and energy transfer processes were coupled in a single QD nanohybrid system in solution and agarose thin film states. This was realized through a single donor – two acceptors based triad system comprising of InP/ZnS QD as donor, ICG dye as the electron acceptor and MC dye as the FRET acceptor. The strong electrostatic attraction between oppositely charged QD donor and dye acceptors resulted in the formation of a stable [-] ICG dye:::[+] InP/ZnS QD:::[-] MC dye triad complex. The domination of photoinduced electron transfer process from InP/ZnS QD to ICG dye produced a non-luminescent black complex agarose film. The superior photostability of QDs over organic dyes was explored to create high-contrast multicolor luminescent patterns. The selective photodegradation of ICG dye triggered the switching ON of FRET process from InP/ZnS QD to MC dye, resulting in the creation of orange colored luminescent patterns. Further, partial and complete photodegradation of MC dye created yellow and green luminescent patterns, corresponding to moderately FRET ON and OFF states, respectively. Thus, a selective and sequential photoregulation of electron and energy transfer processes in a single QD nanohybrid agarose film led to the creation of multicolor luminescent patterns on a non-luminescent black background. The ability to achieve a fine interplay between photoinduced electron and energy transfer processes in a single QD based nanohybrid system is fundamentally intriguing, and can have potential impact on other light harvesting applications as well.

4.6 Future Direction

The main focus of the present Thesis was to regulate photophysical processes in a single QD nanohybrid system to create high-contrast multicolor luminescent patterns. An obvious next step would be to expand this concept for the generation of entire VIBGYOR colored patterns, using appropriate single donor-multiple acceptor systems (long range FRET pairs). Moreover, a closer examination of luminescent patterns reveals that the surface of QDs are differently exposed at different parts of the photopatterned QD:::dye agarose film. Specifically, the green and orange colored regions on QD:::dye agarose film corresponds to [+] InP/ZnS QD and [+] InP/ZnS QD:::[-] MC dye complex, respectively. One could, in principle, address these patterned QD surfaces differently and use them for spatially selective QD functions like metal ion reduction/deposition, LED and micro/nanoelectrode fabrication, sensing etc.

4.7 References

(1)   Kamat, P. V. Quantum Dot Solar Cells. The Next Big Thing in Photovoltaics. *J. Phys. Chem. Lett.* **2013**, *4*, 908-918.

(2)   Zhang, J. Z. Semiconductor Nanostructures for Energy and Biomedical Applications. *J. Phys. Chem. Lett.* **2013,** *4,* 2975−2976.

(3)   Wheeler, D. A.; Zhang, J. Z. Exciton Dynamics in Semiconductor Nanocrystals. *Adv. Mater.* **2013,** *25,* 2878-2896.

(4)   Zhong, H.; Bai, Z.; Zou, B. Tuning the Luminescence Properties of Colloidal I–III–VI Semiconductor Nanocrystals for Optoelectronics and Biotechnology Applications. *J. Phys. Chem. Lett.* **2012,** *3,* 3167-3175.

(5)   Kamat, P. V. Quantum Dot Solar Cells . Semiconductor Nanocrystals as Light Harvesters. *J. Phys. Chem. C* **2008,** *112,* 18737–18753.

(6)   Guzelturk, B.; Demir, H. V. Organic–Inorganic Composites of Semiconductor Nanocrystals for Efficient Excitonics. *J. Phys. Chem. Lett.* **2015**, 6, 2206-2215.

(7)   Ji, X.; Wang, W.; Mattoussi, H. Controlling the Spectroscopic Properties of Quantum Dots via Energy Transfer and Charge Transfer Interactions : Concepts and Applications. *Nano Today* **2016**, *11*, 98-121.

(8)   Moroz, P.; Jin, Z.; Sugiyama, Y.; Lara, D. A.; Razgoniaeva, N.; Yang, M.; Kholmicheva, N.; Khon, D.; Mattoussi, H.; Zamkov, M. The Competition of Charge and Energy Transfer Processes in Donor - Acceptor Fluorescence Pairs : Calibrating the

Spectroscopic Ruler . *ACS Nano* **2018**, *12*, 5657-5665.

(9) Dutta, S. K.; Mehetor, S. K.; Pradhan, N. Metal Semiconductor Heterostructures for Photocatalytic Conversion of Light Energy. *J. Phys. Chem. Lett.* **2015**, *6*, 936-944.

(10) Sarkar, S.; Bose, R.; Jana, S.; Jana, N. R.; Pradhan, N. Doped Semiconductor Nanocrystals and Organic Dyes: An Efficient and Greener FRET System. *J. Phys. Chem. Lett.* **2010**, *1*, 636-640.

(11) Lee, J.; Govorov, A. O.; Kotov, N. A. Bioconjugated Superstructures of CdTe Nanowires and Nanoparticles : Multistep Cascade Förster Resonance Energy Transfer and Energy Channeling. *Nano Lett.* **2005**, *5*, 2063-2069.

(12) Yan, J.; Feng, W.; Kim, J.-Y.; Lu, J.; Kumar, P.; Mu, Z.; Wu, X.; Mao, X.; Kotov, N. A. Self-Assembly of Chiral Nanoparticles into Semiconductor Helices with Tunable near-Infrared Optical Activity. *Chem. Mater.* **2020**, *32*, 476-488.

(13) Lian, S.; Kodaimati, M. S.; Dolzhnikov, D. S.; Calzada, R.; Weiss, E. A. Powering a CO_2 Reduction Catalyst with Visible Light through Multiple Sub-Picosecond Electron Transfers from a Quantum Dot. *J. Am. Chem. Soc.* **2017**, *139*, 8931-8938.

(14) Shibu, E. S.; Sonoda, A.; Tao, Z.; Feng, Q.; Furube, A.; Masuo, S.; Wang, L.; Tamai, N.; Ishikawa, M.; Biju, V. Ph

(15) otofabrication of Fullerene-Shelled Quantum Dots Supramolecular Nanoparticles for Solar Energy Harvesting. *ACS Nano* **2012**, *6*, 1601-1608.

(16) Thomas, E. M.; Ghimire, S.; Kohara, R.; Anil, A. N.; Yuyama, K.; Takano, Y.; Thomas, K. G.; Biju, V. P. Blinking Suppression in Highly-Excited CdSe / ZnS Quantum Dots by Electron Transfer under Large Positive Gibbs (Free) Energy Change. *ACS Nano* **2018**, *12*, 9060-9069.

(17) Taniguchi Y.; Sazali, M. A. B.; Kobayashi, Y.; Arai, N.; Kawai, T.; Nakashima, T. Programmed Self-Assembly of Branched Nanocrystals with an Amphiphilic Surface Pattern. *ACS Nano* **2017***, 11,* 9312-9320.

(18) Nakashima, T.; Shigekawa, K.; Katao S.;, Asanoma, F.; Kawai, T. Solvation of Quantum Dots in 1-Alkyl-1-Methylpyrrolidinium Ionic Liquids: Toward Stably Luminescent Composites. *Sci. Technol. Adv. Mater.* **2020**, *21*, 187–194.

(19) Choi, M. K.; Yang, J.; Hyeon, T.; Kim, D.-H. Flexible Quantum Dot Light-Emitting Diodes for next-Generation Displays. *npj Flex. Electron.* **2018**, *2*, 1-14.

(20) Chen, X.; Rogach, A. L.; Talapin, D. V; Fuchs, H.; Chi, L. Hierarchical Luminescence Patterning Based on Multiscaled Self-Assembly. *J. Am. Chem. Soc.* **2006**, *128*, 9592–9593.

(21) Lin, C. H.; Zeng, Q.; Lafalce, E.; Yu, S.; Smith, M. J.; Yoon, Y. J.; Chang, Y.; Jiang, Y.; Lin, Z.; Vardeny, Z. V.; Tsukruk, V. V. Large- Area Lasing and Multicolor Perovskite Quantum Dot Patterns. *Adv.Opt. Mater.* **2018**, *6*, 1800474.

(22) Kim, T.-H.; Cho, K.-S.; Lee, E. K.; Lee, S. J.; Chae, J.; Kim, J. W.; Kim, D. H.; Kwon, J.-Y.; Amaratunga, G.; Lee, S. Y.; Choi, B. L.; Kuk, Y.; Kim, J. M.; Kim, K. Full-Colour Quantum Dot Displays Fabricated by Transfer Printing. *Nat. Photonics* **2011**, *5*, 176-182.

(23) Smith, M.; Malak, S. T.; Jung, J.; Yoon, Y. J.; Lin, C. H.; Kim, S.; Lee, M. K.; Ma, R.; White, T. J.; Bunning, T. J.; Lin, Z.; Tsukruk, V. V. Robust , Uniform , and Highly Emissive Quantum Dot- Polymer Films and Patterns Using Thiol-Ene Chemistry. *ACS Appl. Mater. Interfaces*, **2017**, *9*, 17435-17448.

(24) Ma, R.; Gordon, D.; Yushin, G.; Tsukruk, V. V. Robust and Flexible Micropatterned Electrodes and Micro-Supercapacitors in Graphene – Silk Biopapers. *Adv. Mater. Interfaces*, **2018**, *5*, 1801203.

(25) Wang, Y.; Tang, Z.; Correa-Duarte, M. A.; Liz-Marzán, L. M.; Kotov, N. A. Multicolor Luminescence Patterning by Photoactivation of Semiconductor Nanoparticle Films. *J. Am. Chem. Soc.* **2003**, *125*, 2830–2831.

(26) Chen, J.; Chan, Y.-H.; Yang, T.; Wark, S. E.; Son, D. H.; Batteas, J. D. Spatially Selective Optical Tuning of Quantum Dot Thin Film Luminescence. *J. Am. Chem. Soc.* **2009**, *131*, 18204–18205.

(27) Malak, S. T.; Jung, J.; Yoon, Y. J.; Smith, M. J.; Lin, C. H.; Lin, Z.; Tsukruk, V. V. Large-Area Multicolor Emissive Patterns of Quantum Dot-Polymer Films via Targeted Recovery of Emission Signature. *Adv. Opt. Mater.* **2016**, *4*, 608–619.

(28) Tagliazucchi, M.; Amin, V. A.; Schneebeli, S. T.; Stoddart, J. F.; Weiss, E. A. High-Contrast Photopatterning of Photoluminescence within Quantum Dot Films through Degradation of a Charge-Transfer Quencher. *Adv. Mater.* **2012**, *24*, 3617–3621.

(29) Wang, Y.; Fedin, I.; Zhang, H.; Talapin, D. V. Direct Optical Lithography of Functional Inorganic Nanomaterials. *Science* **2017**, *357*, 385–388.

(30) Jung, S.; Park, J.; Bang, J.; Kim, J.-Y.; Kim, C.; Jeon, Y.; Lee, S. H.; Jin, H.; Choi, S.; Kim, B.; Lee, W. J.; Pack, C.-G.; Lee, J.-B.; Lee, N. K.; Kim, S. Light-Induced Fluorescence Modulation of Quantum Dot-Crystal Violet Conjugates: Stochastic Off–On–Off Cycles for Multicolor Patterning and Super-Resolution. *J. Am. Chem. Soc.* **2017**, *139*, 7603–7615.

(31) Devatha, G.; Rao, A.; Roy S.; Pillai, P. P. Förster Resonance Energy Transfer

Regulated Multicolor Photopatterning from Single Quantum Dot Nanohybrid Films. *ACS Energy Lett.* **2019**, *4*, 1710–1716.

(32) Bae, W. K.; Kwak, J.; Lim, J.; Lee, D.; Nam, M. K.; Char, K.; Lee, C.; Lee, S. Multicolored Light-Emitting Diodes Based on All-Quantum-Dot Multilayer Films Using Layer-by-Layer Assembly Method. *Nano Lett.* **2010**, *10*, 2368–2373.

(33) Lin, Y. -W.; Tseng, W. -L.; Chang, H. -T. Using a Layer-by-Layer Assembly Technique to Fabricate Multicolored-Light-Emitting Films of CdSe@CdS and CdTe Quantum Dots. *Adv. Mater.* **2006**, *18*, 1381–1386.

(34) Kim, B. H.; Onses, M. S.; Lim, J. B.; Nam, S.; Oh, N.; Kim, H.; Yu, K. J.; Lee, J. W.; Kim, J.-H.; Kang, S.-K.; Lee, C.-H.; Lee, J.; Shin, J. H.; Kim, N. H.; Leal, C.; Shim, M.; Rogers, J. A. High-Resolution Patterns of Quantum Dots Formed by Electrohydrodynamic Jet Printing for Light-Emitting Diodes. *Nano Lett.* **2015**, *15*, 969–973.

(35) Kim, L.; Anikeeva, P. O.; Coe-Sullivan, S. A.; Steckel, J. S.; Bawendi, M. G.; Bulović, V. Contact Printing of Quantum Dot Light-Emitting Devices. *Nano Lett.* **2008**, *8*, 4513–4517.

(36) Keum, H.; Jiang, Y.; Park, J. K.; Flanagan, J. C.; Shim, M.; Kim, S. Photoresist Contact Patterning of Quantum Dot Films. *ACS Nano* **2018**, *12*, 10024–10031.

(37) Porter, L. A.; Choi, H. C.; Schmeltzer, J. M.; Ribbe, A. E.; Elliott, L. C. C.; Buriak, J. M. Electroless Nanoparticle Film Deposition Compatible with Photolithography, Microcontact Printing, and Dip-Pen Nanolithography Patterning Technologies. *Nano Lett.* **2002**, *2*, 1369–1372.

(38) Prins, F.; Sumitro, A.; Weidman, M. C.; Tisdale, W. A. Spatially Resolved Energy Transfer in Patterned Colloidal Quantum Dot Heterostructures. *ACS Appl. Mater. Interfaces* **2014**, *6*, 3111−3114.

(39) Cho, H.; Kwak, J.; Lim, J.; Park, M.; Lee, D.; Bae, K.; Kim, Y. S.; Char, K.; Lee, S.; Lee, C. Soft Contact Transplanted Nanocrystal Quantum Dots for Light-Emitting Diodes : Effect of Surface Energy on Device Performance. *ACS Appl. Mater. Interfaces* **2015**, 7, 10828-10833.

(40) Malak, S. T.; Liang, G.; Thevamaran, R.; Yoon, Y. J.; Smith, M. J.; Jung, J.; Lin, C. H.; Lin, Z.; Thomas, E. L.; Tsukruk, V. V. High-Resolution Quantum Dot Photopatterning via Interference Lithography Assisted Microstamping. *J. Phys. Chem. C* **2017**, *121*, 13370–13380.

(41) Kim, B. H.; Nam, S.; Oh, N.; Cho, S.-Y.; Yu, K. J.; Lee, C. H.; Zhang, J.; Deshpande,

K.; Trefonas, P.; Kim, J.-H.; Lee, J.; Shin, J. H. ; Yu, Y.; Lim, J. B.; Won, S. M.; Cho, Y. K.; Kim, N. H.; Seo, K. J.; Lee, H.; Kim, T.-I.; Shim, M.; Rogers, J. A. Multilayer Transfer Printing for Pixelated, Multicolor Quantum Dot Light-Emitting Diodes. *ACS Nano* **2016**, *10*, 4920–4925.

(42) Park, J.-S.; Kyhm, J.; Kim, H. H.; Jeong, S.; Kang, J.; Lee, S.; Lee, K.-T.; Park, K.; Barange, N.; Han, J.; Song, J. D.; Choi, W. K.; Han, I. K. Alternative Patterning Process for Realization of Large-Area, Full-Color, Active Quantum Dot Display. *Nano Lett.* **2016**, *16*, 6946–6953.

(43) Gopal, A.; Hoshino, K.; Zhang, X. Photolithographic Patterning of Subwavelength Top Emitting Colloidal Quantum Dot Based Inorganic Light Emitting Diodes on Silicon. *Appl. Phys. Lett.* **2010**, *96*, 131109.

(44) Tien, J.; Terfort, A.; Whitesides, G. M. Microfabrication through Electrostatic Self-Assembly. *Langmuir* **1997**, *13*, 5349–5355.

(45) Devatha, G.; Roy, S.; Rao, A.; Mallick, A.; Basu, S.; Pillai, P. P. Electrostatically Driven Resonance Energy Transfer in "Cationic" Biocompatible Indium Phosphide Quantum Dots. *Chem. Sci.* **2017**, *8*, 3879–3884.

(46) Lakowicz, J. R. Principles of Fluorescence Spectroscopy, 3rd ed., Springer: New York **1999**.

(47) Thomas, A.; Nair, P. V.; Thomas, K. G. InP Quantum Dots: An Environmentally Friendly Material with Resonance Energy Transfer Requisites. *J. Phys. Chem. C* **2014**, *118*, 3838–3845.

(48) Thomas, A.; Sandeep, K.; Somasundaran, S. M.; Thomas, K. G. How Trap States Affect Charge Carrier Dynamics of CdSe and InP Quantum Dots: Visualization through Complexation with Viologen. *ACS Energy Lett.* **2018**, *3*, 2368-2375.

(49) Thirunavukkuarasu, S.; George, A.; Thomas, A.; Thomas, A.; Vijayan, V.; Thomas, K. G. InP Quantum Dots: Probing the Active Domain of Tau Peptide Using Energy Transfer. *J. Phys. Chem. C* **2018**, *122*, 14168–14176.

(50) Xavier, J. A. M.; Devatha, G.; Roy, S.; Rao, A.; Pillai, P. P. Electrostatically Regulated Photoinduced Electron Transfer in "Cationic" Eco-friendly $CuInS_2$/ZnS Quantum Dots in Water. *J. Mater. Chem. A* **2018**, *6*, 22248-22255.

(51) Barros, T. C.; Toma, S. H.; Toma, H. E.; Bastos, E. L.; Baptista, M. S. Polymethine Cyanine Dyes in β-Cyclodextrin Solution: Multiple Equilibria and Chemical Oxidation. *J. Phys. Org. Chem.* **2010**, *23*, 893–903.

(52) Förster, T. 10th Spiers Memorial Lecture. Transfer Mechanisms of Electronic

Excitation. *Discuss. Faraday Soc.* **1959**, *27*, 7–17.

(53) Medintz, I. L.; Pons, T.; Susumu, K.; Boeneman, K.; Dennis, A. M.; Farrell, D.; Deschamps, J. R.; Melinger, J. S.; Bao, G.; Mattoussi, H. Resonance Energy Transfer between Luminescent Quantum Dots and Diverse Fluorescent Protein Acceptors. *J. Phys. Chem. C* **2009**, *113*, 18552–18561.

(54) Aldeek, F.; Ji, X.; Mattoussi, H. Quenching of Quantum Dot Emission by Fluorescent Gold Clusters: What It Does and Does Not Share with the Förster Formalism. *J. Phys. Chem. C* **2013**, *117*, 15429-15437.

(55) Clapp, A. R.; Medintz, I. L.; Mattoussi, H. Förster Resonance Energy Transfer Investigations using Quantum-Dot Fluorophores. *ChemPhysChem* **2006**, *7*, 47-57.

(56) Funston, A. M.; Jasieniak, J. J.; Mulvaney, P. Complete Quenching of CdSe Nanocrystal Photoluminescence by Single Dye Molecules. *Adv. Mater.* **2008**, *20*, 4274–4280.

(57) Collison, C. J.; Donnell, M. J.; Alexander, J. L. Complexation between Rhodamine 101 and Single-Walled Carbon Nanotubes Indicative of Solvent-Nanotube Interaction Strength. *J. Phys. Chem. C* **2008**, *112*, 15144–15150.

(58) Fukuzumi, S.; Ohkubo, K.; Suenobu, T.; Kato, K.; Fujitsuka, M.; Ito, O. Photoalkylation of 10-Alkylacridinium Ion via a Charge-Shift Type of Photoinduced Electron Transfer Controlled by Solvent Polarity. *J. Am. Chem. Soc.* **2001**, *123*, 8459–8467.

(59) Moreau, C.; Douhéret, G. Thermodynamic and Physical Behaviour of Water + Acetonitrile Mixtures. Dielectric Properties. *J. Chem. Thermodyn.* **1976**, *8*, 403–410.

(60) Heitele, H.; Finckh, P.; Weeren, S.; Poellinger, F.; Michel-Beyerle, M. E. Solvent Polarity Effects on Intramolecular Electron Transfer. 1. Energetic Aspects. *J. Phys. Chem.* **1989**, *93*, 5173–5179.

(61) Pramod, P.; Sudeep, P. K.; Thomas, K. G.; Kamat, P. V. Photochemistry of Ruthenium Trisbipyridine Functionalized on Gold Nanoparticles. *J. Phys. Chem. B* **2006**, *110*, 20737–20741.

(62) Venturoli, G.; Drepper, F.; Williams, J. C.; Allen, J. P.; Lin, X.; Mathis, P. Effects of Temperature and ΔG^0 on Electron Transfer from Cytochrome c_2 to the Photosynthetic Reaction Center of the Purple Bacterium Rhodobacter Sphaeroides. *Biophys. J.* **1998**, *74*, 3226–3240.

(63) Jortner, J. Temperature Dependent Activation Energy for Electron Transfer between

Biological Molecules. *J. Chem. Phys.* **1976**, *64*, 4860–4867.

(64) Tafen, D. N.; Prezhdo, O. V. Size and Temperature Dependence of Electron Transfer between CdSe Quantum Dots and a TiO$_2$ Nanobelt. *J. Phys. Chem. C* **2015**, *119*, 5639–5647.

(65) Marcus, R. A.; Sutin, N. Electron Transfers in Chemistry and Biology. *Biochim. Biophys. Acta* **1985**, *811*, 265–322.

(66) Tvrdy, K.; Frantsuzov, P. A.; Kamat, P. V. Photoinduced Electron Transfer from Semiconductor Quantum Dots to Metal Oxide Nanoparticles. *Proc. Natl. Acad. Sci.* **2011**, *108*, 29–34.

(67) Kastelic, M.; Kalyuzhnyi, Y. V; Hribar-Lee, B.; Dill, K. A.; Vlachy, V. Protein Aggregation in Salt Solutions. *Proc. Natl. Acad. Sci.* **2015**, *112*, 6766–6770.

4.8 Appendix

4.8.1 Proof for electrostatically driven photoinduced electron transfer:

Control experiment # 1

Photoinduced electron transfer studies between [+] InP/ZnS QD and [-] ICG dye in PBS:

Control experiments were carried out with [+] InP/ZnS QD as a donor and [-] ICG dye as an acceptor in a high salt concentration (1X PBS). Electrostatic interactions are weakened in the presence of high salt concentration due to the screening of charges by the salts.[66] This increases the distance between donor and acceptor, thereby decreasing the quenching efficiency.
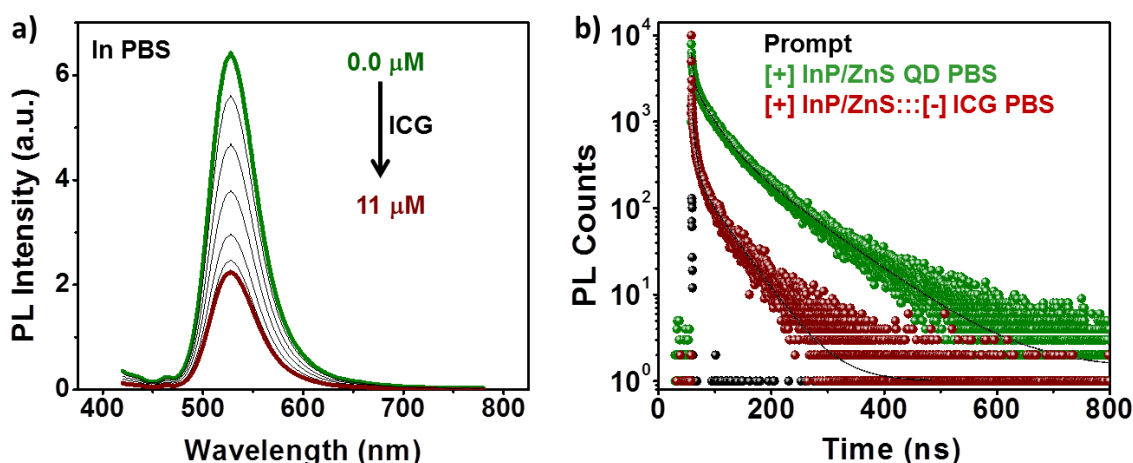
Figure 4.17: a) Spectral changes in the PL of [+] InP/ZnS QD on the addition of [-] ICG dye. b) PL decay profiles of [+] InP/ZnS in the absence (green decay) and presence of ~11 μM (brown decay) of [-] ICG, upon excitation with a 405 nm laser source.

Table 4.9: PL decay analysis of [+] InP/ZnS QD in the presence of [-] ICG dye in PBS in a time window of 800 ns.

Sample	τ_1 (ns)	a_1	τ_2 (ns)	a_2	τ_3 (ns)	a_3	Avg. τ (ns)	Efficiency (%)
[+] InP/ZnS_PBS	3.07	0.59	28.79	0.30	92.51	0.11	57.97	
[+] InP/ZnS :::[-] ICG_PBS	0.28	0.91	5.38	0.07	46.93	0.01	21.26	63.3

Control experiment # 2

Control experiments were carried out with similarly charged [-] InP/ZnS QD as a donor and [-] ICG dye as an acceptor. The electrostatic repulsion between the donor-acceptor is expected to prevent the complex formation, thereby decreasing the probability of photoinduced electron transfer process.
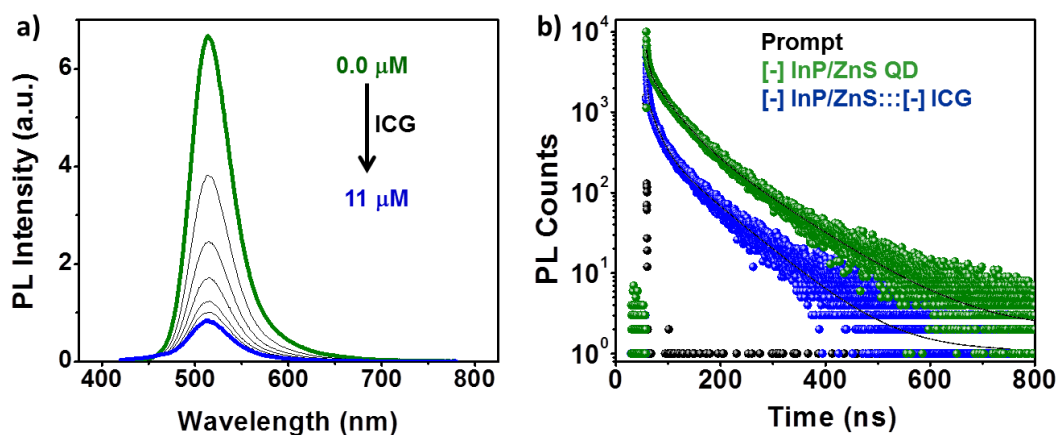

Figure 4.18: a) Steady state PL spectra of [-] InP/ZnS upon addition of varying concentrations of [-] ICG dye. b) PL decay profiles of [-] InP/ZnS in the absence (green decay) and presence (blue decay) of ~11 μM [-] ICG dye, upon excitation with a 405 nm laser. One positive charge on [-] ICG dye can still participate in a weak electrostatic attraction with [-] InP/ZnS QD, which can lead to low PL quenching.

Table 4.10: PL decay analysis of [-] InP/ZnS QD in the presence of [-] ICG dye in a time window of 800 ns.

Sample	τ_1 (ns)	a_1	τ_2 (ns)	a_2	τ_3 (ns)	a_3	Avg. τ (ns)	Efficiency (%)
[-] InP/ZnS_H$_2$O	3.80	0.42	36.85	0.43	104.22	0.15	67.09	26.4
[-] InP/ZnS ::: [-] ICG_H$_2$O	1.54	0.72	17.40	0.21	79.78	0.07	49.36	

Table 4.11: Table summarizing the PL quenching and photoinduced electron transfer parameters in [+] InP/ZnS QD donor:::[-] ICG dye acceptor nanohybrid (in water and PBS) and [-] InP/ZnS QD donor:::[-] ICG dye acceptor nanohybrid in water.

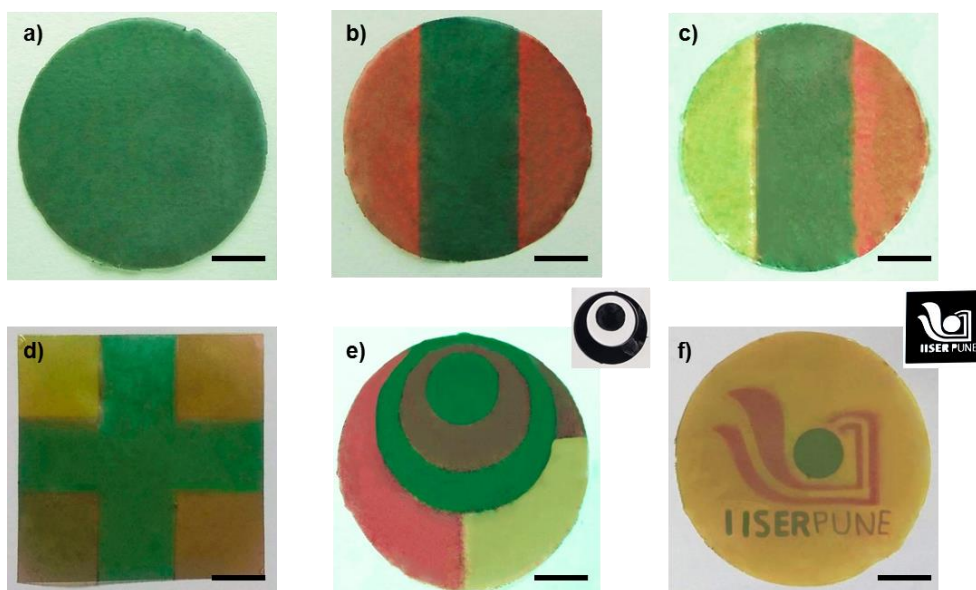| System	[+] InP/ZnS:::[-] ICG		[-] InP/ZnS:::[-] ICG
	H$_2$O	PBS	H$_2$O
PL quenching Efficiency (Steady State)	81%	65%	87%
PL quenching Efficiency (Lifetime)	80%	63%	26%
Rate of photoinduced electron transfer (k_{PET})	6.42×10^7 s^{-1}	2.97×10^7 s^{-1}	5.35×10^6 s^{-1}

4.8.2 Photopatterning on [-] ICG dye:::[+] InP/ZnS QD:::[-] MC dye agarose film:

Figure 4.18: Optical images of [-] ICG dye:::[+] InP/ZnS QD:::[-] MC dye agarose films after photoirradiation using appropriate masks with 10 W 730 for ~6h and 10 W green LED for ~5 h, under normal light. The corresponding PL images are provided in the Results and Discussion Section of Chapter 4. The scale bar corresponds to 1 cm for all the images.

List of Publications

Included in Thesis

1. **<u>Devatha, G</u>**.; Roy, S.; Rao, A; Mallick, A.; Basu, S.; Pillai, P. P.* Electrostatically Driven Resonance Energy Transfer in "Cationic" Biocompatible Indium Phosphide Quantum Dots. *Chem. Sci.* **2017**, *8*, 3879-3884.

2. **<u>Devatha, G</u>**.; Rao, A; Roy, S.; Pillai, P. P.* Förster Resonance Energy Transfer Regulated Multicolor Photopatterning from Single Quantum Dot Nanohybrid Films. *ACS Energy. Lett*. 2019, *4*, 1710-1716.

3. **<u>Devatha, G</u>**.; Rao, A; Roy, S.; Pillai, P. P.* Multicolor Luminescent Patterning via Photoregulation of Electron and Energy Transfer Processes in Quantum Dots. *J. Phys. Chem. Lett.* **2020**, *11*, 4099–4106.

Not Included in Thesis

1. Rao, A.; Roy, S.; Unnikrishnan, M.; Bhosale, S. S.; **<u>Devatha, G</u>**.; Pillai, P. P.* Regulation of Interparticle Forces Reveals Controlled Aggregation in Charged Nanoparticles. *Chem. Mater.* **2016**, *28*, 2348-2355.

2. Roy, S.; Rao, A; **<u>Devatha, G.</u>**; Pillai, P. P.* Revealing the Role of Electrostatics in Gold-Nanoparticle-Catalyzed Reduction of Charged Substrates. *ACS Catal*. **2017**, *7*, 7141-7145.

3. Mududli, S.; Pandey, P.; **<u>Devatha, G.</u>**; Babar, R.; Kothari, T. M. D. C.; Kabir, M.;* Pillai, P. P.;* Ogale, S. B.* Photoluminescence Quenching in Self-Assembled CsPbBr3 Quantum Dots on Few-Layer Black Phosphorous Sheets. *Angew. Chem. Int. Ed.* **2018**, *57*, 7682-7686.

4. Xavier, J. A. M., **<u>Devatha, G.,</u>** Roy, S., Rao, A., Pillai, P. P., Electrostatically Regulated Photoinduced Electron Transfer in Cationic Eco-friendly CuInS$_2$/ZnS Quantum Dots in Water. J. Mater. Chem. A 2018, 6, 22248-22245. (**‡equal contribution**)

5. Roy, S., Roy, S., Rao, A., **<u>Devatha, G</u>**., Pillai P. P., Precise Nanoparticle − Reactant Interaction Outplays Ligand Poisoning in Visible-Light Photocatalysis. *Chem. Mater.* **2018**, *30*, 8415-8419.

6. Chakraborty, I.; Roy, S.; **<u>Devatha, G</u>**.; Rao, A.; Pillai, P. P., InP/ZnS Quantum Dots as Efficient Visible-Light Photocatalysts for Redox and Carbon-Carbon Coupling Reaction. *Chem. Mater.* **2019**, *31*, 2258-2262.

7. Rao, A.; Kumar, G. S.; Roy, S.; Rajesh, A. T.; **Devatha, G**.; Pillai, P. P. Turn-On Selectivity in Inherently Nonselective Gold Nanoparticles for Pb^{2+} Detection by Preferential Breaking of Interparticle Interactions. *ACS Appl. Nano Mater.* **2019**, 2, 5625-5633.

8. Roy, P.; **<u>Devatha, G.</u>**; Roy, S.; Rao, A.; Pillai, P. P. Electrostatically Driven Resonance Energy Transfer in an All-Quantum Dot Based Donor-Acceptor System. *J. Phys. Chem. Lett.* **2020**, *11*, 5354-5360.

Conferences attended

1. Presented a poster titled *"Electrostatically Driven Energy Transfer in Biocompatible InP Quantum Dots :Towards Live Cell Imaging"* in **International Conference on Nanoscience and Technology (ICONSAT)** held at **Indian Institute of Science Education and Research (IISER) Pune** in March 2016.

2. Presented a poster titled *"Electrostatically Driven Resonance Energy Transfer in "Cationic" Biocompatible Indium Phosphide Quantum Dots"* in **Chemical Research Society of India (CRSI) Symposium in Chemistry (NSC-21)** held at **Indian Institute of Chemical Technology (IICT),** Hyderabad in July 2017

3. Presented a poster titled *"Electrostatically Driven Resonance Energy Transfer in "Cationic" Biocompatible Indium Phosphide Quantum Dots"* in International Conference on Advanced Nanomaterials and Nanotechnology, (ICANN), held at Indian Institute of Technology Guwahati (IITG) in December, 2017.

4. Gave a talk titled "*Surface Ligand Controlled Quantum Dot Photophysics to Write with Light*" in Chemsymphoria (in-house Symposium) at **IISER Pune** in July 2018.

RightsLink

🏠 Home | ❓ Help | ▬ Email Support | 👤 Gayathri Devatha ⌄

ACS Publications
Most Trusted. Most Cited. Most Read.

Designer Variable Repeat Length Polypeptides as Scaffolds for Surface Immobilization of Quantum Dots

Author: Igor L. Medintz, Kim E. Sapsford, Aaron R. Clapp, et al

Publication: The Journal of Physical Chemistry B

Publisher: American Chemical Society

Date: Jun 1, 2006

Copyright © 2006, American Chemical Society

PERMISSION/LICENSE IS GRANTED FOR YOUR ORDER AT NO CHARGE

This type of permission/license, instead of the standard Terms & Conditions, is sent to you because no fee is being charged for your order. Please note the following:

- Permission is granted for your request in both print and electronic formats, and translations.
- If figures and/or tables were requested, they may be adapted or used in part.
- Please print this page for your records and send a copy of it to your publisher/graduate school.
- Appropriate credit for the requested material should be given as follows: "Reprinted (adapted) with permission from (COMPLETE REFERENCE CITATION). Copyright (YEAR) American Chemical Society." Insert appropriate information in place of the capitalized words.
- One-time permission is granted only for the use specified in your request. No additional uses are granted (such as derivative works or other editions). For any other uses, please submit a new request.
- If credit is given to another source for the material you requested, permission must be obtained from that source.

BACK   CLOSE WINDOW

137

RightsLink

🏠 Home   ❓ Help   ▬ Email Support   👤 Gayathri Devatha ⌄

ACS Publications
Most Trusted. Most Cited. Most Read.

Ligand Binding to Distinct Sites on Nanocrystals Affecting Energy and Charge Transfer

Author: Xin Li, Lydia W. Slyker, Valerie M. Nichols, et al

Publication: Journal of Physical Chemistry Letters

Publisher: American Chemical Society

Date: May 1, 2015

Copyright © 2015, American Chemical Society

138

RightsLink

Home　Help　Email Support　Gayathri Devatha ⌄

Reversible Modulation of Quantum Dot Photoluminescence Using a Protein- Bound Photochromic Fluorescence Resonance Energy Transfer Acceptor

ACS Publications
Most Trusted. Most Cited. Most Read.

Author: Igor L. Medintz, Scott A. Trammell, Hedi Mattoussi, et al

Publication: Journal of the American Chemical Society

Publisher: American Chemical Society

Date: Jan 1, 2004

Copyright © 2004, American Chemical Society

PERMISSION/LICENSE IS GRANTED FOR YOUR ORDER AT NO CHARGE

This type of permission/license, instead of the standard Terms & Conditions, is sent to you because no fee is being charged for your order. Please note the following:

- Permission is granted for your request in both print and electronic formats, and translations.
- If figures and/or tables were requested, they may be adapted or used in part.
- Please print this page for your records and send a copy of it to your publisher/graduate school.
- Appropriate credit for the requested material should be given as follows: "Reprinted (adapted) with permission from (COMPLETE REFERENCE CITATION). Copyright (YEAR) American Chemical Society." Insert appropriate information in place of the capitalized words.
- One-time permission is granted only for the use specified in your request. No additional uses are granted (such as derivative works or other editions). For any other uses, please submit a new request.
If credit is given to another source for the material you requested, permission must be obtained from that source.

BACK　　　　　　　　　　　　　　　　　　　　　　　　　　　　CLOSE WINDOW

RightsLink

🏠 Home   ❓ Help   ▬ Email Support   👤 Gayathri Devatha ▾

ACS Publications
Most Trusted. Most Cited. Most Read.

Tuning Electron Transfer Rates through Molecular Bridges in Quantum Dot Sensitized Oxides

Author: Hai Wang, Erik R. McNellis, Sachin Kinge, et al

Publication: Nano Letters

Publisher: American Chemical Society

Date: Nov 1, 2013

Copyright © 2013, American Chemical Society

PERMISSION/LICENSE IS GRANTED FOR YOUR ORDER AT NO CHARGE

This type of permission/license, instead of the standard Terms & Conditions, is sent to you because no fee is being charged for your order. Please note the following:

- Permission is granted for your request in both print and electronic formats, and translations.
- If figures and/or tables were requested, they may be adapted or used in part.
- Please print this page for your records and send a copy of it to your publisher/graduate school.
- Appropriate credit for the requested material should be given as follows: "Reprinted (adapted) with permission from (COMPLETE REFERENCE CITATION). Copyright (YEAR) American Chemical Society." Insert appropriate information in place of the capitalized words.
- One-time permission is granted only for the use specified in your request. No additional uses are granted (such as derivative works or other editions). For any other uses, please submit a new request.
- If credit is given to another source for the material you requested, permission must be obtained from that source.

BACK   CLOSE WINDOW

RightsLink

Home | Help | Email Support | Gayathri Devatha ⌄

ACS Publications
Most Trusted. Most Cited. Most Read.

Tracking the Adsorption and Electron Injection Rates of CdSe Quantum Dots on TiO2: Linked versus Direct Attachment

Author: Douglas R. Pernik, Kevin Tvrdy, James G. Radich, et al

Publication: The Journal of Physical Chemistry C

Publisher: American Chemical Society

Date: Jul 1, 2011

Copyright © 2011, American Chemical Society

BACK   CLOSE WINDOW

RightsLink

ACS Publications
Most Trusted. Most Cited. Most Read.

Enhancement of the Yield of Photoinduced Charge Separation in Zinc Porphyrin–Quantum Dot Complexes by a Bis(dithiocarbamate) Linkage

Author: Shengye Jin, Mario Tagliazucchi, Ho-Jin Son, et al

Publication: The Journal of Physical Chemistry C

Publisher: American Chemical Society

Date: Mar 1, 2015

Copyright © 2015, American Chemical Society

PERMISSION/LICENSE IS GRANTED FOR YOUR ORDER AT NO CHARGE

This type of permission/license, instead of the standard Terms & Conditions, is sent to you because no fee is being charged for your order. Please note the following:

- Permission is granted for your request in both print and electronic formats, and translations.
- If figures and/or tables were requested, they may be adapted or used in part.
- Please print this page for your records and send a copy of it to your publisher/graduate school.
- Appropriate credit for the requested material should be given as follows: "Reprinted (adapted) with permission from (COMPLETE REFERENCE CITATION). Copyright (YEAR) American Chemical Society." Insert appropriate information in place of the capitalized words.
- One-time permission is granted only for the use specified in your request. No additional uses are granted (such as derivative works or other editions). For any other uses, please submit a new request.
If credit is given to another source for the material you requested, permission must be obtained from that source.

BACK   CLOSE WINDOW

142

RightsLink

Home   Help   Email Support   Gayathri Devatha ∨

SPRINGER NATURE

Chemoelectronic circuits based on metal nanoparticles

Author: Yong Yan et al

Publication: Nature Nanotechnology

Publisher: Springer Nature

Date: Mar 14, 2016

Copyright © 2016, Springer Nature

Review Order

Please review the order details and the associated terms and conditions.

Licensed Content

Licensed Content Publisher	Springer Nature
Licensed Content Publication	Nature Nanotechnology
Licensed Content Title	Chemoelectronic circuits based on metal nanoparticles
Licensed Content Author	Yong Yan et al
Licensed Content Date	Mar 14, 2016

Order Details

Type of Use	Thesis/Dissertation
Requestor type	academic/university or research institute
Format	print and electronic
Portion	figures/tables/illustrations
Number of figures/tables/illustrations	1
High-res required	yes
Will you be translating?	no
Circulation/distribution	1 - 29
Author of this Springer Nature content	no

About Your Work

Title	Surface Ligand Controlled Photophysics and Photopatterning with InP/ZnS Quantum Dots
Institution name	Indian Institute of Science Education and Research, Pune
Expected presentation date	Oct 2020

Additional Data

Portions	Figure 1.15

Requestor Location

Requestor Location	Ms. Gayathri Devatha IISER pune Pune, other 411008 India Attn: Ms. Gayathri Devatha

Tax Details

Price

Total	170.20 USD

☑ I agree to these terms and conditions.

☐ I understand this license is for reuse only and that no content is provided.

Customer Code(if supplied) [ ]

Apply Code

Total: 170.20 USD

BACK   DECLINE   HOLD QUOTE   CHOOSE PAYMENT

143

RightsLink

ACS Publications
Most trusted. Most cited. Most read.

Fluorescence Resonance Energy Transfer Between Quantum Dot Donors and Dye-Labeled Protein Acceptors

Author: Aaron R. Clapp, Igor L. Medintz, J. Matthew Mauro, et al

Publication: Journal of the American Chemical Society

Publisher: American Chemical Society

Date: Jan 1, 2004

Copyright © 2004, American Chemical Society

144

RightsLink

AC5 Publications
Most Trusted. Most Cited. Most Read.

A Ratiometric CdSe/ZnS Nanocrystal pH Sensor

Author: Preston T. Snee, Rebecca C. Somers, Gautham Nair, et al

Publication: Journal of the American Chemical Society

Publisher: American Chemical Society

Date: Oct 1, 2006

Copyright © 2006, American Chemical Society

PERMISSION/LICENSE IS GRANTED FOR YOUR ORDER AT NO CHARGE

BACK   CLOSE WINDOW

RightsLink

Home | Help | Email Support | Gayathri Devatha ⌄

ACS Publications
Most Trusted. Most Cited. Most Read.

InP Quantum Dots: An Environmentally Friendly Material with Resonance Energy Transfer Requisites

Author: Anoop Thomas, Pratheesh V. Nair, K. George Thomas

Publication: The Journal of Physical Chemistry C

Publisher: American Chemical Society

Date: Feb 1, 2014

Copyright © 2014, American Chemical Society

PERMISSION/LICENSE IS GRANTED FOR YOUR ORDER AT NO CHARGE

This type of permission/license, instead of the standard Terms & Conditions, is sent to you because no fee is being charged for your order. Please note the following:

- Permission is granted for your request in both print and electronic formats, and translations.
- If figures and/or tables were requested, they may be adapted or used in part.
- Please print this page for your records and send a copy of it to your publisher/graduate school.
- Appropriate credit for the requested material should be given as follows: "Reprinted (adapted) with permission from (COMPLETE REFERENCE CITATION). Copyright (YEAR) American Chemical Society." Insert appropriate information in place of the capitalized words.
- One-time permission is granted only for the use specified in your request. No additional uses are granted (such as derivative works or other editions). For any other uses, please submit a new request.
- If credit is given to another source for the material you requested, permission must be obtained from that source.

BACK   CLOSE WINDOW

146

Copyright Clearance Center **Marketplace™**

< Return to search

SHOPPING CART Empty this cart

Currency   **USD** ▼

1. Chemical communications ✏   0.00 USD

ISSN	1364-548X	**Publisher**	ROYAL SOCIETY OF CHEMISTRY
Type of Use	Republish in a thesis/dissertation	**Portion**	Image/photo/illustration

LICENSED CONTENT

Publication Title	Chemical communications	**Country**	United Kingdom of Great Britain and Northern Ireland
Author/Editor	Royal Society of Chemistry (Great Britain)	**Rightsholder**	Royal Society of Chemistry
Date	01/01/1996	**Publication Type**	e-Journal
Language	English		

REQUEST DETAILS

Portion Type	Image/photo/illustration	**Distribution**	Worldwide
Number of images / photos / illustrations	01	**Translation**	Original language of publication
Format (select all that apply)	Print	**Copies for the disabled?**	No
Who will republish the content?	Academic institution	**Minor editing privileges?**	No
Duration of Use	Current edition and up to 15 years	**Incidental promotional use?**	Yes
Lifetime Unit Quantity	Up to 499	**Currency**	USD
Rights Requested	Main product		

NEW WORK DETAILS

Title	Surface Ligand Controlled Photophysics and Photopatterning with InP/ZnS Quantum Dots	**Institution name**	Indian Institute of Science Education and Research, Pune
		Expected presentation date	2020-10-30
Instructor name	Dr. Pramod Pillai		

ADDITIONAL DETAILS

147

RightsLink

ACS Publications
Most Trusted. Most Cited. Most Read.

Förster Resonance Energy Transfer Regulated Multicolor Photopatterning from Single Quantum Dot Nanohybrid Films

Author: Gayathri Devatha, Anish Rao, Soumendu Roy, et al

Publication: ACS Energy Letters

Publisher: American Chemical Society

Date: Jul 1, 2019

Copyright © 2019, American Chemical Society

PERMISSION/LICENSE IS GRANTED FOR YOUR ORDER AT NO CHARGE

This type of permission/license, instead of the standard Terms & Conditions, is sent to you because no fee is being charged for your order. Please note the following:

- Permission is granted for your request in both print and electronic formats, and translations.
- If figures and/or tables were requested, they may be adapted or used in part.
- Please print this page for your records and send a copy of it to your publisher/graduate school.
- Appropriate credit for the requested material should be given as follows: "Reprinted (adapted) with permission from (COMPLETE REFERENCE CITATION). Copyright (YEAR) American Chemical Society." Insert appropriate information in place of the capitalized words.
- One-time permission is granted only for the use specified in your request. No additional uses are granted (such as derivative works or other editions). For any other uses, please submit a new request.

BACK   CLOSE WINDOW

RightsLink

🏠 Home   ❓ Help   ✉ Email Support   👤 Gayathri Devatha ⌄

ACS Publications
Most Trusted. Most Cited. Most Read.

Multicolor Luminescence Patterning by Photoactivation of Semiconductor Nanoparticle Films

Author: Ying Wang, Zhiyong Tang, Miguel A. Correa-Duarte, et al

Publication: Journal of the American Chemical Society

Publisher: American Chemical Society

Date: Mar 1, 2003

Copyright © 2003, American Chemical Society

PERMISSION/LICENSE IS GRANTED FOR YOUR ORDER AT NO CHARGE

This type of permission/license, instead of the standard Terms & Conditions, is sent to you because no fee is being charged for your order. Please note the following:

- Permission is granted for your request in both print and electronic formats, and translations.
- If figures and/or tables were requested, they may be adapted or used in part.
- Please print this page for your records and send a copy of it to your publisher/graduate school.
- Appropriate credit for the requested material should be given as follows: "Reprinted (adapted) with permission from (COMPLETE REFERENCE CITATION). Copyright (YEAR) American Chemical Society." Insert appropriate information in place of the capitalized words.
- One-time permission is granted only for the use specified in your request. No additional uses are granted (such as derivative works or other editions). For any other uses, please submit a new request.
- If credit is given to another source for the material you requested, permission must be obtained from that source.

BACK   CLOSE WINDOW

RightsLink

SPRINGER NATURE

Wearable red–green–blue quantum dot light-emitting diode array using high-resolution intaglio transfer printing

Author: Moon Kee Choi et al

Publication: Nature Communications

Publisher: Springer Nature

Date: May 14, 2015

Copyright © 2015, Springer Nature

Creative Commons

THE AMERICAN ASSOCIATION FOR THE ADVANCEMENT OF SCIENCE LICENSE
TERMS AND CONDITIONS

Jul 28, 2020

This Agreement between Ms. Gayathri Devatha ("You") and The American Association for
the Advancement of Science ("The American Association for the Advancement of Science")
consists of your license details and the terms and conditions provided by The American
Association for the Advancement of Science and Copyright Clearance Center.

License Number	4877920254236
License date	Jul 28, 2020
Licensed Content Publisher	The American Association for the Advancement of Science
Licensed Content Publication	Science
Licensed Content Title	Direct optical lithography of functional inorganic nanomaterials
Licensed Content Author	Yuanyuan Wang,Igor Fedin,Hao Zhang,Dmitri V. Talapin
Licensed Content Date	Jul 28, 2017
Licensed Content Volume	357
Licensed Content Issue	6349
Volume number	357
Issue number	6349
Type of Use	Thesis / Dissertation

151

RightsLink

Home   Help   Email Support   Gayathri Devatha ⌄

ACS Publications
Most Trusted. Most Cited. Most Read.

Multicolor Luminescent Patterning via Photoregulation of Electron and Energy Transfer Processes in Quantum Dots

Author: Gayathri Devatha, Pradyut Roy, Anish Rao, et al

Publication: Journal of Physical Chemistry Letters

Publisher: American Chemical Society

Date: May 1, 2020

Copyright © 2020, American Chemical Society

PERMISSION/LICENSE IS GRANTED FOR YOUR ORDER AT NO CHARGE

This type of permission/license, instead of the standard Terms & Conditions, is sent to you because no fee is being charged for your order. Please note the following:

- Permission is granted for your request in both print and electronic formats, and translations.
- If figures and/or tables were requested, they may be adapted or used in part.
- Please print this page for your records and send a copy of it to your publisher/graduate school.
- Appropriate credit for the requested material should be given as follows: "Reprinted (adapted) with permission from (COMPLETE REFERENCE CITATION). Copyright (YEAR) American Chemical Society." Insert appropriate information in place of the capitalized words.
- One-time permission is granted only for the use specified in your request. No additional uses are granted (such as derivative works or other editions). For any other uses, please submit a new request.

BACK   CLOSE WINDOW

152

ACS Publications
Most Trusted. Most Cited. Most Read.

Hierarchical Luminescence Patterning Based on Multiscaled Self-Assembly

Author: Xiaodong Chen, Andrey L. Rogach, Dmitri V. Talapin, et al

Publication: Journal of the American Chemical Society

Publisher: American Chemical Society

Date: Aug 1, 2006

Copyright © 2006, American Chemical Society

SPRINGER NATURE LICENSE
TERMS AND CONDITIONS

Jul 28, 2020

This Agreement between Ms. Gayathri Devatha ("You") and Springer Nature ("Springer Nature") consists of your license details and the terms and conditions provided by Springer Nature and Copyright Clearance Center.

License Number	4877921115477
License date	Jul 28, 2020
Licensed Content Publisher	Springer Nature
Licensed Content Publication	Nature Photonics
Licensed Content Title	Full-colour quantum dot displays fabricated by transfer printing
Licensed Content Author	Tae-Ho Kim et al
Licensed Content Date	Feb 20, 2011
Type of Use	Thesis/Dissertation
Requestor type	academic/university or research institute
Format	print and electronic
Portion	figures/tables/illustrations
Number of figures/tables/illustrations	1
High-res required	no

154

JOHN WILEY AND SONS LICENSE
TERMS AND CONDITIONS

Jul 28, 2020

This Agreement between Ms. Gayathri Devatha ("You") and John Wiley and Sons ("John Wiley and Sons") consists of your license details and the terms and conditions provided by John Wiley and Sons and Copyright Clearance Center.

License Number 4877940593723

License date Jul 28, 2020

Licensed Content Publisher John Wiley and Sons

Licensed Content Publication Advanced Optical Materials

Licensed Content Title Large-Area Multicolor Emissive Patterns of Quantum Dot–Polymer Films via Targeted Recovery of Emission Signature

Licensed Content Author Vladimir V. Tsukruk, Zhiqun Lin, Chun Hao Lin, et al

Licensed Content Date Jan 11, 2016

Licensed Content Volume 4

Licensed Content Issue 4

Licensed Content Pages 12

Type of use Dissertation/Thesis

Requestor type University/Academic

155

JOHN WILEY AND SONS LICENSE
TERMS AND CONDITIONS

Jul 28, 2020

This Agreement between Ms. Gayathri Devatha ("You") and John Wiley and Sons ("John Wiley and Sons") consists of your license details and the terms and conditions provided by John Wiley and Sons and Copyright Clearance Center.

License Number	4877940481460
License date	Jul 28, 2020
Licensed Content Publisher	John Wiley and Sons
Licensed Content Publication	Advanced Materials
Licensed Content Title	High-Contrast Photopatterning of Photoluminescence within Quantum Dot Films through Degradation of a Charge-Transfer Quencher
Licensed Content Author	Mario Tagliazucchi, Victor A. Amin, Severin T. Schneebeli, et al
Licensed Content Date	Jun 8, 2012
Licensed Content Volume	24
Licensed Content Issue	27
Licensed Content Pages	5

156